Mathematical modelling of blood glucose dynamics in normal and impaired glucose tolerance

by

Manuel Max Werner Eichenlaub

Thesis

Submitted to the University of Warwick

for the degree of

Doctor of Philosophy

School of Engineering

October 2020

Contents

i

List of Tables

List of Figures

Acknowledgments

This work would not have been possible without the support, guidance and patience from my supervisors, Drs. Natasha Khovanova and John Hattersley. I am especially thankful that they allowed me the freedom to explore the topic of metabolic modelling in diabetes according my own interest and develop the project into new directions.

I also am indebted to all the staff at the Human Metabolism Research Unit, especially Mrs Alison Campbell, for their help in conducting my experimental study. Furthermore, I would like to thank all volunteers who sacrificed their time and participated in my study. I would also like to thank Mrs Ludmilla Pessanha and Prof. Carel le Roux from the University College Dublin and Dr Andrew White from the Arden Tissue Bank at UHCW for the preparation and analysis of my blood samples. Furthermore, I am thankful to Prof. Mike Chappell for providing a crucial dataset used in this work.

Special thanks are directed towards all my colleagues from the Warwick Engineering in Biomedicine group for all the engaging discussions on the topic of mathematical modelling, but more importantly for making me feel welcome and at home in a to me foreign country.

Lastly, I would like to thank my family and especially my parents for their continuing support at home and abroad.

Declarations

This thesis is submitted to the University of Warwick in support of my application for the degree of Doctor of Philosophy. It has been composed by myself and has not been submitted in any previous application for any degree.

Results of this research have been disseminated in two publications and at four conferences as below

Publications

M. Eichenlaub, J. Hattersley, N. Khovanova (2019): "A Minimal Model Approach for the Description of Postprandial Glucose Responses from Glucose Sensor Data in Diabetes Mellitus". In: 2019 41st Annual International Conference of the IEEE Engineering in Medicine and Biology Society (EMBC), Berlin, 23-27 July 2019, p. 265-268

M. Eichenlaub, J. Hattersley, N. Khovanova (2019): "A Model Describing the Multiphasic Dynamics of Mixed Meal Glucose Responses in Healthy Subjects". In: World Congress on Medical Physics and Biomedical Engineering 2018. IFMBE Proceedings, vol 68/1

Presentations and posters

Poster presentation: M. Eichenlaub, J. Hattersley, N. Khovanova: "Modelling of glucose dynamics and estimation of insulin sensitivity from glucose data only", 19th Annual Diabetes Technology Meeting, Bethesda, Maryland, USA, 2019

Poster presentation: M. Eichenlaub, J. Hattersley, N. Khovanova: "Quantifying Insulin Sensitivity without Insulin: Is it possible ? ", BioMedEng19 Conference, Imperial College London, UK, 2019

Oral presentation: M. Eichenlaub, J. Hattersley, N. Khovanova: "Modelling of glucose dynamics and estimation of insulin sensitivity from glucose data only", 41st Annual International Conference of the IEEE Engineering in Medicine and Biology Society (EMBC), Berlin, Germany, 2019

Oral presentation: M. Eichenlaub, J. Hattersley, N. Khovanova: "A Model Describing the Multiphasic Dynamics of Mixed Meal Glucose Responses in Healthy Subjects", World Congress on Medical Physics and Biomedical Engineering, Prague, Czech Republic, 2018

Abstract

Type 2 diabetes mellitus and its preliminary stages are characterised by chronically elevated blood glucose levels, particularly after food intake. Assessing the postprandial glucose metabolism is, therefore, crucial to facilitate appropriate treatment strategies such as dietary interventions. This thesis develops mathematical models for the description of glucose profiles in response to food intake using glucose data alone. These glucose-only models thereby overcome the necessity of measuring insulin which is laborious and unreliable, thus enabling their widespread use in clinical practice. The main purpose of the developed models is the extraction of information on insulin sensitivity and meal-related glucose appearance, both of which have a significant influence on the postprandial glucose response. The extracted information is validated against the results from the established oral minimal model requiring both glucose and insulin data for identification. For both oral minimal and glucose-only models, this work proposes a novel input function for the description of the meal-related glucose appearance. This new function is fully differentiable and more suitable for modelling consecutive meal responses on the same day in comparison to the conventional but highly impractical piecewise-linear function. The models are identified from both a literature dataset and a dataset collected during an experimental study designed and conducted in the context of this work. The latter includes subjects with normal glucose tolerance, prediabetes and type 2 diabetes mellitus and features the use of continuous glucose monitoring. The model identification procedure is carried out using a variational Bayesian technique, which offers an efficient method for the probabilistic treatment of the parameter estimation task. The results demonstrate that the developed glucose-only models can be used to infer information on insulin sensitivity as they contain a parameter highly correlated to the insulin sensitivity inferred from the established oral minimal model. Furthermore, it is shown that the glucose appearance profiles inferred from the glucose-only models allow the same interpretation of trends in glucose appearance with respect meal composition as the oral minimal model. Using the information on insulin sen-

sitivity and glucose appearance, the developed models could thus support healthcare professionals in designing effective treatment strategies such as dietary interventions and monitor the disease progression from prediabetes to type 2 diabetes.

Abbreviations

BG	blood glucose
T1DM	type 1 diabetes mellitus
T2DM	type 2 diabetes mellitus
Pre-DM	prediabetes
NGT	normal glucose tolerance
CGM	continuous glucose monitoring
CHO	carbohydrate
HbA1c	glycated haemoglobin
OGTT	oral glucose tolerance test
IS	insulin sensitivity
HEC	hyperinsulinemic euglycaemic clamp
IVGTT	intravenous glucose tolerance test
GA	meal-related rate of glucose appearance
SMBG	self-monitoring of blood glucose
ISF	interstitial fluid
OMM	oral minimal model of glucose dynamics
ODE	ordinary differential equation
ORC	observability rank criterion
PDF	probability density function
MCMC	Markov Chain Monte Carlo
SMC	sequential Monte Carlo
VB	variational Bayesian
MEM	mixed-effects modelling
CV	coefficient of variation
BMA	Bayesian model averaging
AUC	area under the curve

MTT	mixed-meal tolerance test
RMSE	root mean squared error
GOM	glucose-only model

Chapter 1

Introduction

1.1 Overview

Glucose is the main source of energy for the human body. In a healthy person, its concentration in the blood is maintained within a very narrow range by a complex control system. One of the key components in this system is a hormone called insulin. Any impairment to its action or production typically lead to abnormally high blood glucose (BG) levels, which is the main characteristic of a group of diseases referred to as diabetes mellitus. One specific subgroup called type 1 diabetes mellitus (T1DM) is caused by a lack of insulin production and treated with the lifelong administration of external insulin. The largest share of patients, however, belong to the subgroup of type 2 diabetes mellitus (T2DM), where a combination of impaired insulin action and production causes the glycaemic derangement. This disorder typically develops over the course of several years with earlier stages known as prediabetes (Pre-DM). In the UK alone, over three million people are living with T2DM and the number of people affected by Pre-DM and T2DM is steadily growing. If BG levels are not controlled within a healthy range, the resulting complications can have a large impact on a person's wellbeing and society as a whole [1]. Due to its increasing prevalence and the sheer amount of people affected, this thesis will specifically focus on T2DM.

The treatment for all types of diabetes including T2DM, has the goal of maintaining BG levels in a healthy range to avoid short and long-term complications. In T2DM this can be achieved by pharmacological interventions accompanied by lifestyle modifications in the form of recommendations on diet and physical activity. Changes in lifestyle are particularly effective in people with Pre-DM, as they can significantly delay

or even prevent the progression to T2DM [1–3]. One shortcoming of current treatment strategies is that the majority of pharmacological treatments are most effective in resolving basal hyperglycaemia, i.e. escalated levels of glucose in the fasted state [4]. However, in better controlled T2DM patients, the overall glycaemic state is mainly determined by hyperglycaemia in the fed (postprandial) state [5]. This limitation calls for more treatments specifically targeting postprandial hyperglycaemia, such as dietary interventions [4, 6], requiring appropriate tools to accurately assess the postprandial glucose metabolism in clinical practice.

Due to its importance in the context of diabetes, glucose metabolism has been the subject of research across several disciplines. One of these disciplines is the field of dynamical systems modelling. It has greatly contributed to the knowledge and understanding of glucose metabolism by providing the necessary tools to address its inherent complexity [7]. This complexity is manifested by several nonlinear and time-varying effects present within and across all levels of physiology (e.g. cellular, organ, whole body). The general modelling approach approximates the real system by formulating a set of simplified mathematical rules and constraints, called the mathematical model. The degree of simplification and therefore the scale of the model is mainly determined by the purpose of the modelling task. Generally speaking, models can be used to describe, predict, interpret or explain different aspects of glucose metabolism that would be difficult or even impossible to measure directly [8].

In the context of glucose metabolism it is common to distinguish models according to their intended use into minimal and maximal models [7], also referred to as clinical and non-clinical models [9]. As the name suggests, maximal or non-clinical models provide a fine-grained description of all relevant parts of the glucoregulatory system and are developed for simulation purposes without the intention of describing measured data. The term minimal-type model is specific to the field of glucose dynamics modelling and was coined by Cobelli et al. [7] to describe more coarse-grained models that contain less detail and aim for a parsimonious description of the system's functionality. The key feature discriminating them from maximal models is that they are strongly informed and subsequently validated by the collection of experimental data in a clinical context such as a diagnostic test. This allows the clinical interpretation of the collected data and increases the understanding of the individual system [7, 9].

In this thesis, we will adopt a minimal-type modelling approach aiming to be relevant

in clinical applications and focus on postprandial glucose metabolism, i.e. the metabolic response to food intake. This approach to modelling allows individual inference of the meal-related appearance of glucose in the bloodstream and the quantification of insulin action on glucose metabolism. Both of these quantities have a significant influence on the postprandial glucose response and thus determine the extent of postprandial hyperglycaemia. Information on these quantities is thus of high clinical relevance and can be applied to accurately characterise postprandial glucose metabolism, the demand for which has been highlighted earlier. The so developed methods can support healthcare professionals in designing effective treatment strategies such as dietary interventions or the monitoring of disease progression from Pre-DM to T2DM.

1.2   Problem statement

Over the past decades, minimal-type models have become increasingly sophisticated. This development has been mainly driven by the steady improvement in experimental techniques, allowing researchers to capture a growing amount of physiological processes, leading to increased model complexity without sacrificing the connection to experimental data [7]. This trend started by only measuring glucose and insulin concentrations [10] and led to the use of traced glucose, i.e. molecules of glucose containing radioactive isotopes of either carbon or hydrogen [11]. Other models have been developed to study brain glucose metabolism and are based on data from magnetic resonance imaging [12]. The current practice in the development of minimal-type models for the description of the postprandial glucose metabolism in normal glucose tolerance (NGT) and T2DM is to utilise at least glucose and insulin data [7, 13, 14]. This is a very active field of research and has greatly contributed to the general understanding of the underlying metabolic processes responsible for the loss of glycaemic control in the context of T2DM [7].

Despite this progress, the application of any of the proposed models in clinical practice, i.e. for the diagnosis or treatment of individuals, has yet to be seen. While minimal-type models can theoretically be used for this purpose, the lack of clinical application is mostly attributed to the large effort associated with insulin data collection for model and parameter identification. This makes current minimal models unsuitable for widespread use in clinical practice because the measurement of insulin concentrations

is dependant on venous blood sampling, which can be expensive and unreliable due to missing standardisation in measurement techniques. The determination of insulin levels is thus not part of any clinical routine in the diagnosis or treatment of T2DM [15] and impossible outside a clinical setting. In contrast to that, the techniques for the reliable and straightforward collection of glucose data, even outside the hospital, have steadily improved. This has led to a persistent increase in the amount of glucose data available to healthcare professionals. Especially important for this development has been the improved accuracy and reduced cost of devices for continuous glucose monitoring (CGM), commonly utilised in research and increasingly used in the management of T2DM [16–18].

Apart from the dependence on insulin data, a further weakness of current minimal-type models is that they are mainly developed for the description of glucose responses to a single, isolated meal from a fasted state, often consisting of pure carbohydrates [7, 9]. This form of meal consumption is, however, unrepresentative of the behaviour occurring in everyday life, making it desirable to have models capable of describing glucose responses under more realistic conditions. These conditions mean that the meals contain additional macronutrients such as fat and protein, have varying composition and are consumed at different times of the day.

To overcome the described weaknesses of minimal-type models, this thesis will be concerned with the development and validation of models that can be identified by only measuring glucose profiles capturing a variety of meal responses under realistic conditions. The exclusive use of glucose data is already a common feature of minimal-type models for T1DM or advanced stages of T2DM, where no or very little endogenous insulin is produced. In these cases, the vast majority of insulin is administered externally, meaning that crucial and easily attainable data on insulin action can be used during model identification [14, 19]. In contrast, the models developed in this thesis will focus on the NGT, Pre-DM and a non-insulin dependent T2DM state, where no insulin is administered externally. This lack of data on insulin action poses an additional challenge from a modelling perspective as it greatly reduces the amount of available information during the modelling process. However, it also gives the models greater potential for application because the majority of T2DM patients, about 70 % according to Wilke et al. [20], are not treated with insulin.

A comparatively small number of glucose-only models for the description of glucose

profiles in NGT and T2DM subjects have already been published. One subset of these models is formulated in such a way that their states and parameters are difficult to interpret physiologically [21–25]. Other models have a physiological interpretation, but their application to real data has been limited to a few subjects and they yielded a poor description of the data [26, 27]. A detailed review of these models will be given in Chapter 6.

Within the overall modelling approach, the process of model identification is of crucial importance. It involves a structural identifiability analysis, the estimation of parameters and the comparison between models if multiple candidates are considered. Due to the use of a minimal amount of data, the choice of the most appropriate approach for model identification is important. In terms of the parameter estimation problem, the vast majority of existing glucose-only modelling approaches employ a frequentist approach [21–23, 26, 27], meaning that it is assumed that every parameter can be represented by a single value. This makes it difficult to incorporate prior knowledge into the parameter estimation which is essential when a minimal amount of data are used. It also hinders the quantification of the uncertainty associated with the estimated parameters and model states. In contrast, Bayesian approaches assume the parameters to be random variables [8]. These methods overcome the previously described weaknesses of frequentist approaches and are most suitable when a minimal amount of data are available. They additionally provide a comprehensive framework to combine the results of multiple model candidates into a single set of estimates.

1.3 Aim and objectives

The aim of this thesis is to develop minimal-type models for the description of post-prandial glucose responses in NGT, Pre-DM and T2DM subjects that can be identified from glucose data only. The key novelty of the utilised approach is that the model development and validation will be greatly informed by comparison with established, physiologically-based models using glucose and insulin data. This ensures that resulting glucose-only models are physiologically interpretable and can describe the glucose dynamics with similar accuracy, overcoming the weaknesses of current glucose-only modelling approaches. It will also ensure that the extracted, clinically relevant information on insulin sensitivity and the meal-related appearance of glucose is valid. The overall

aim of this thesis can be divided into the following objectives, splitting the modelling process into several parts.

The first objective is to procure suitable datasets for model development and identification, fulfilling several requirements. The datasets should: (1) contain both glucose and insulin data, (2) record multiple meal responses on the same day from meals of varying composition and (3) contain data from subjects with varying degrees of glycaemic control. A dataset from the literature fulfilling criteria (1) and (2) was available but did not include data from subjects with Pre-DM and T2DM. This demands the design and implementation of a new experimental study, forming a large share of the first objective.

The second objective is to select and adapt a minimal-type model requiring both glucose and insulin data. To apply the previously procured datasets to the selected model, two novel adaptations will be proposed: (1) a procedure for model identification from non-fasting conditions will be introduced and (2) a new function for the description of the meal-related appearance of glucose will be proposed. This is necessary because the standard, piecewise-linear description of glucose appearance is highly impractical for describing consecutive meal responses of different durations on the same day. The results of this objective will serve as a basis and validation reference for the subsequent development of glucose-only models.

The third objective sets out to develop novel, glucose-only models, based on the previously selected minimal-type model. This means that the lack of insulin data has to be compensated for by a suitable, mathematical description of the relationship between glucose and insulin concentrations. This description will be informed by examining the relationship between postprandial glucose and insulin levels as well as physiological principles, and lead to the proposal of multiple model candidates.

The fourth objective is to carry out the process of model identification on the models resulting from the second and third objectives using a fully Bayesian approach. The model selected in the second objective will be identified using glucose and insulin data. Subsequently, the developed glucose-only models will be identified using only the glucose data from the same subjects and meal responses. This allows the direct validation of the glucose-only models concerning their ability to provide the same information and will inform on the comparison between model candidates.

The fifth and final objective is to offer fundamental insight for clinicians on the effects of meal composition and timing, sex and status of glycaemic control on postprandial glucose metabolism.

1.4 Thesis structure

Chapter 1 has given an overview of the topic, highlighted the weaknesses of current modelling concepts and outlined the approach taken in this thesis through the formulation of the aim and objectives. Chapter 2 provides the necessary background information on the relevant physiology, measurement principles and will select the most suitable minimal-type model requiring both glucose and insulin data. Chapter 3 introduces the methods used for model development and identification with particular emphasis on parameter estimation techniques and their application to the models used in this thesis. Chapter 4 deals with the adaptation and identification of the model selected in Chapter 2, using the already existing dataset. Chapter 5 introduces, selects and validates a novel function for the description of the meal-related appearance of glucose. Chapter 6 is concerned with the development and validation of glucose-only models from the existing dataset. Chapter 7 provides a description and preliminary analysis of the data collected in the context of this thesis. Chapter 8 then uses this dataset to validate the models developed previously. Chapter 9 concludes this thesis by summarising the most important findings with respect to the aims and objectives described earlier and gives an outlook to future works.

Chapter 2

Background

The following chapter describes the necessary background information on the relevant physiological principles and measurement techniques for glucose and insulin. At the end, the minimal-type glucose-insulin model used as a reference for the development of glucose-only models is selected.

2.1 Physiology

2.1.1 Glucose and insulin metabolism

Glucose is continuously present in the human blood at a normal concentration of around 5 mmol/L, forming a total mass in the bloodstream of circa 4.5 g. In the normal physiological state, glucose levels are tightly regulated by a balance of glucose production, mainly by the liver, and uptake of glucose by the muscles and brain. The efficacy of this control mechanism can be exemplified by considering that the glucose content, say 100 g, of a typical meal, would be enough to increase the blood glucose (BG) levels by more than twentyfold. In actuality, however, the concentration is temporally only approximately doubled before returning to pre-meal levels [28].

One of the main regulators responsible for this tight control mechanism is the hormone insulin. It is constantly synthesised in the pancreas by beta-cells with its secretion rate being highly dependent on glucose levels. The secreted insulin, in turn, acts on the glucose metabolism by two main mechanisms: insulin suppresses glucose production by the liver as well as the release of glucose storages in other tissues and it promotes the uptake of glucose in the liver, skeletal muscle and adipose tissue. This means that insulin has a hypoglycaemic effect, i.e. it leads to a decrease in BG levels and that

almost all tissues need insulin to utilise the glucose in the bloodstream. The exception is the central nervous system, which is capable of utilising glucose independently from insulin and consumes a significant fraction of circulating glucose (circa 120 g per day). Additionally, BG levels alone are also known to affect glucose metabolism [28]. Given the relationship between glucose metabolism and insulin action, it should come as no surprise, that glucose and insulin concentrations are associated, with one of the main drivers of dynamic behaviour being the consumption of carbohydrate (CHO) containing meals. This association is exemplified in Figure 2.1, where glucose and insulin concentrations show similar excursions in response to CHO intake.
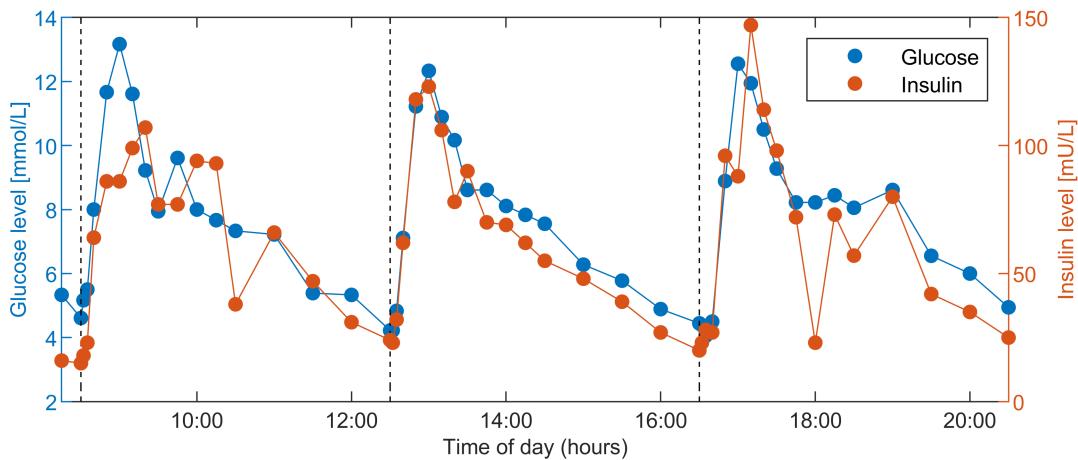
Figure 2.1: Glucose and insulin concentrations in a subject with normal glucose tolerance over the course of 12 hours consuming three identical meals (dashed lines), showing the tight association between glucose and insulin concentrations. The data were taken from a study by Nuttall et al. [29] and are utilised in Chapters 4, 5 and 6.

2.1.2 Diabetes mellitus

Diabetes mellitus - often shortened to just diabetes - is a group of metabolic diseases manifested by chronically elevated glucose concentrations in the blood. The name diabetes mellitus literally means honeyed siphon, which is a graphic description of the disease's main symptom: the passing of large quantities of sweet-tasting urine in order to counteract the elevated glucose levels through renal clearance of excess glucose. This state is called hyperglycaemia and is caused by defects in insulin secretion, action or both, therefore disturbing the regulation of glucose metabolism. Chronic hyperglycaemia is associated with a variety of complications including the destruction of the retina, kidneys and peripheral nerves, as well as heart disease and stroke [1]. The goal for any treatment strategy in diabetes is therefore to maintain BG levels in a healthy

range, which has been shown to significantly reduce the risk of developing the afore-mentioned complications [30].

Diabetes is generally classified into the categories type 1, type 2, gestational and other specific types. The latter refers to a wide range of relatively uncommon diseases causing diabetes-like symptoms by either affecting insulin secretion or action. Gestational diabetes mellitus leads to hyperglycaemia caused by a lack of insulin action first detected during pregnancy and typically resolves after childbirth. Type 1 diabetes mellitus (T1DM) is caused by the autoimmune destruction of beta-cells, leading to an absolute lack of insulin production. It most commonly presents in young children and adolescents and is treated through the lifelong external administration of insulin to regulate BG levels in a healthy range [1].

The main focus of this thesis is type 2 diabetes mellitus (T2DM), by far the most prevalent form of diabetes, accounting for about 85 % of all diabetes cases. It is considered to be one of the most common chronic diseases overall, affecting an increasing amount of people. T2DM is a heterogeneous, progressive disease, caused by the interaction of genetic and environmental factors, such as obesity and old age. In general, however, the deterioration in glycaemic control in T2DM is driven by a decline in beta-cell function as well as impaired insulin sensitivity, i.e. the capacity of the liver, adipose tissue and muscles to respond to the effects of insulin (more details on that are presented in the following section). This means that, in contrast to T1DM patients, a large number of T2DM patients have a significant amount of residual beta-cell function [1]. Studies [31–33] have shown a hyperbolic relationship between insulin sensitivity and beta-cell function, as depicted in Figure 2.2. This means that glucose tolerance can be characterised by a range of high insulin sensitivity and low beta-cell function and low insulin sensitivity and high beta-cell function. Additionally, NGT, Pre-DM and T2DM subjects typically populate three distinct hyperbolas. The figure also demonstrates that the progression of the disease is mainly determined by the ability of beta-cells to react to a decrease in insulin sensitivity [1].

T2DM is typically diagnosed through the measurement of glycated haemoglobin (HbA1c) which represents an average BG level over the previous 2-3 months, therefore indicating the presence of chronic hyperglycaemia. Alternatively, an oral glucose tolerance test (OGTT) can be performed which involves the consumption of 75 g of glucose in liquid solution after an overnight fast. The fasting BG level, as well as the BG level
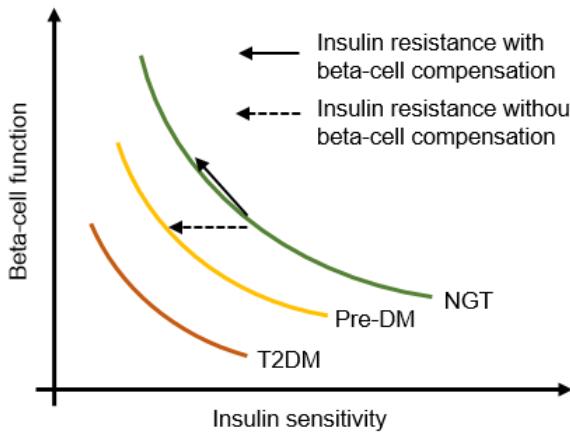
Figure 2.2: Schematic depiction of the hyperbolic relationship between beta-cell function and insulin sensitivity in T2DM, prediabetes (Pre-DM) and normal glucose tolerance (NGT). The arrows indicate possible disease progression routes resulting from a decrease in insulin sensitivity [1].

2 hours after the test, are then used for diagnosis [34] (see Table 2.1). Since there is a large gap between what is considered normal glucose tolerance and T2DM, both in HbA1c and OGTT results, the term prediabetes (Pre-DM) has been introduced. It encompasses several subclinical stages of abnormalities in glucose regulation before the manifestation of T2DM, but does not require immediate clinical intervention. People classified as having Pre-DM have a significantly increased risk of developing T2DM in the future, with about one-third of people eventually progressing to T2DM [1].

Table 2.1: Criteria for the diagnosis of Pre-DM and T2DM based on OGTT results and HbA1c [34]

	NGT	Pre-DM	T2DM
Fasting BG level [mmol/L]	≤ 5.5	5.6 - 6.9	≥ 7
2h OGTT BG level [mmol/L]	≤ 7.7	7.8 - 11	≥ 11.1
HbA1c [mmol/mol]	≤ 38	39 - 47	≥ 48

The treatment for all diabetes types has the goal of maintaining glucose levels in a healthy range to avoid complications associated with chronic hyperglycaemia. In T2DM, these treatments encompass pharmacological interventions using oral antihyperglycaemic drugs and the external administration of insulin, possibly in combination with the drugs. Additionally, all treatment strategies are accompanied by lifestyle modifications in the form of recommendations on diet and physical activity. These lifestyle

intervention strategies are particularly effective in people with Pre-DM, as they can significantly delay or even prevent the progression to T2DM [1–3].

2.1.3 Insulin sensitivity

The concept of insulin sensitivity will play an important role in this thesis, thus warranting a more detailed look into this particular topic. As mentioned in the previous section, the term insulin sensitivity (IS) describes the body's ability to react to the effects of insulin by inhibition of endogenous glucose production and stimulation of glucose utilisation. Measuring these effects separately is difficult, so IS usually describes the net result of these two mechanisms, i.e. the overall hypoglycaemic effect of insulin. This only considers the pure biological effect of insulin and excludes the action of glucose on its own metabolism described in the previous section, called glucose effectiveness. In mathematical terms the insulin sensitivity can, therefore, be expressed by the following relationship:

$$\text{IS} = \frac{\partial}{\partial I}\left[\frac{\partial GCR}{\partial G}\right], \tag{2.1}$$

where I and G denote the insulin and glucose concentrations, respectively and GCR the rate of glucose clearance from the bloodstream. The derivatives account for the fact that IS theoretically can differ depending on the concentration of insulin [35].

The most commonly used direct method for determining IS is an experimental procedure called hyperinsulinemic euglycaemic clamp (HEC) first established in 1979 by DeFronzo et al. [36]. To this day, it is considered to be the gold standard and involves the following procedure: exogenous insulin is infused until an artificially high plateau is reached. To counteract the resulting hypoglycaemia, glucose is infused simultaneously at an adjustable rate until BG levels and glucose/insulin infusion rates are stable. Under these steady-state conditions, the glucose clearance rate is equal to the (known) glucose infusion rate and expression (2.1) can be applied to directly determine IS [35, 36].

Due to the high experimental effort of the HEC procedure, several alternative methods for determining surrogate indices of IS have been put forward. These methods use experimental procedures such as the intravenous injection of glucose, termed an intravenous glucose tolerance test (IVGTT), the OGTT, or only measuring fasting glucose and insulin concentrations. Reviewing these well established methods in detail lies beyond the scope of this thesis and the reader is referred to several existing reviews [35,

37–39]. In general, the correlation of the proposed indices with HEC measurements, as well as amongst each other varies between values of 0.4 and 0.9 dependent on the method used, but also the considered subject population, where NGT subjects typically display the highest agreement.

One commonality of almost all methods of IS determination is that they require the measurements of both glucose and insulin, with the exceptions being the following two methods. The first method proposes the dynamic insulin sensitivity test, which requires the intravenous injection of glucose and insulin to mimic the beginning of an HEC test. Using this method it was found that the glucose levels alone in the first 30 min of the test can be used to predict IS with a correlation of around 0.75 in comparison to HEC results [40]. The second approach proposed by Yates and Watson [41] uses both glucose and insulin and then only glucose data to estimate an IS parameter in the same model proposed by Watson et al. [42], making it similar to the approach used in this thesis. The main difference arises from the fact that a dataset containing IVGTT responses partially collected from rats is utilised, whereas this thesis will utilise postprandial glucose responses collected solely from human subjects.

2.1.4 Meal-related appearance of glucose

Besides insulin sensitivity, the meal-related appearance of glucose will form the second physiological quantity of interest in the modelling process, thus warranting a more detailed look into this particular topic. The postprandial rate of glucose appearance (GA) represents the speed at which glucose appears in the peripheral blood circulation after the consumption of a meal containing CHO and is a major determinant of the postprandial glucose response. A typical GA profile consists of an initial rise commencing as soon as 10 min after meal consumption, reaching a maximum and followed by a gradual decrease thereafter, as depicted in Figure 2.3 [43]. GA can be determined in elaborate experiments involving the simultaneous ingestion and infusion of traced glucose, i.e. molecules of glucose containing isotopes of either carbon (^{13}C) or hydrogen (^{2}H, ^{3}H). Based on the measured concentrations of the differently marked glucose masses in the peripheral veins and underlying models of glucose kinetics, the GA can be calculated [11, 44].

Despite this laborious procedure, GA has been examined by a large number of stud-
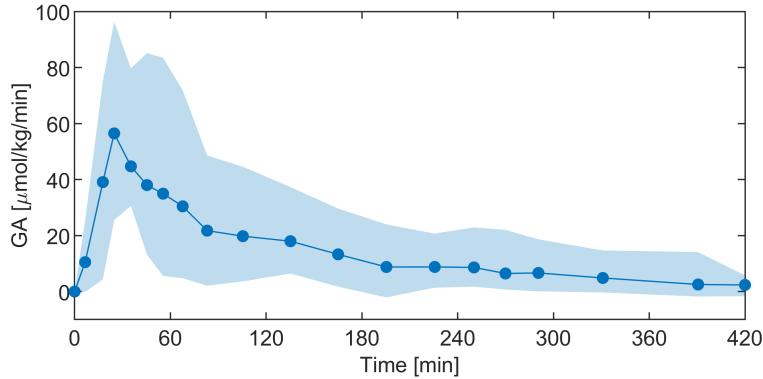
Figure 2.3: Averaged profile and range of variability of postprandial glucose appearance from 88 NGT subjects consuming a normal meal, as measured using traced glucose [45].

ies in a variety of contexts. For example, differences between healthy and subjects with T2DM could not be found [46, 47]. As demonstrated in Figure 2.3, GA profiles can undergo large variability, which could possibly be explained by the variability in gastric emptying [48], i.e. the passing of processed foods from the stomach in the small intestine. A more detailed review of the existing approaches to model GA will be provided in Chapter 5.

A particular feature of the time profile of GA is the existence of a shoulder after the initial peak (see Figure 2.3). A definite physiological cause for this effect has not been established, but it is suspected that it is related to the biphasic nature of gastric emptying [45, 49–51].

2.2 Insulin and glucose measurement

A major part of this thesis is the model-based analysis of insulin and glucose profiles. In this section, the methods for measuring insulin and glucose are reviewed.

2.2.1 Insulin measurement

The hormone insulin was first isolated in 1927 and the first immunoassay for insulin measurement was developed in 1959. Today the measurement is based on the same principle, namely reacting insulin in a blood sample (serum or plasma) with an antibody, producing a measurable signal in response to the binding. The quantity of that signal, e.g. an observable colour change, is then measured and related to the insulin concentration by measuring the same signal from a reference standard of known concentration [15].

Despite long-standing efforts to standardise this measurement technique across methods and laboratories [52], an acceptable level of standardisation has not yet been achieved [15, 53]. This has been demonstrated by studies comparing measurement results across different measurement techniques (assays) detecting a maximum of 2-fold [54] and 1.8-fold [55] difference across assays. Another issue is that even the conversion factors between insulin units (pmol/L and mU/L) are not agreed upon [54, 56, 57]. This leads to the issue that any results involving the use of absolute insulin concentrations, e.g. several surrogate indices for insulin sensitivity, are only comparable within the study cohort, measured with the same insulin assay, a fact that is often ignored [35]. This makes it very difficult to translate and compare results across studies which prevents any meta-analysis or the establishment of standards and diagnostic thresholds for these measures. This explains the fact that the measurement of insulin is currently limited to research purposes and not part of any clinical practice, despite the important role of insulin in the development of diabetes [15, 58].

2.2.2 Glucose measurement

In contrast to the issues in the measurement of insulin, the determination of blood glucose concentrations is established as a crucial tool in the diagnosis and management of diabetes [1]. There are different means for glucose measurement available that mainly vary in the purpose of measurement and therefore accuracy requirements. Three of these methods will be introduced in this section as data from them have been utilised in this thesis. All three methods are based on similar measurement principles and initially involve reacting the glucose in a blood sample with a specific enzyme (e.g. glucose oxidase). Subsequently, the by-products of this reaction, which are proportional to the glucose concentration, are detected. This can be achieved by detecting a colour change, by spectroscopy or more frequently by the measurement of a current in response to a voltage [59].

The most accurate glucose measurements can be obtained from laboratory devices using blood plasma, typically sampled from a peripheral vein (Figure 2.4 (a)). They are currently recommended for the diagnosis of T2DM in the context of an OGTT [58] and are used for research purposes when glucose and insulin are measured simultaneously.

The most common form of blood glucose measurement is conducted using handheld,

point-of-care devices, also known as the self-monitoring of blood glucose (SMBG) or finger-prick devices. As the latter name suggests, the measurement procedure involves the acquisition of a small capillary blood sample through a puncture in the fingertip and the subsequent application to a test strip (Figure 2.4 (b)). These devices provide the result within seconds and are factory calibrated to display the equivalent of venous plasma concentration. They are mainly intended for home use in patients with T1DM or T2DM administering external insulin [58, 60].
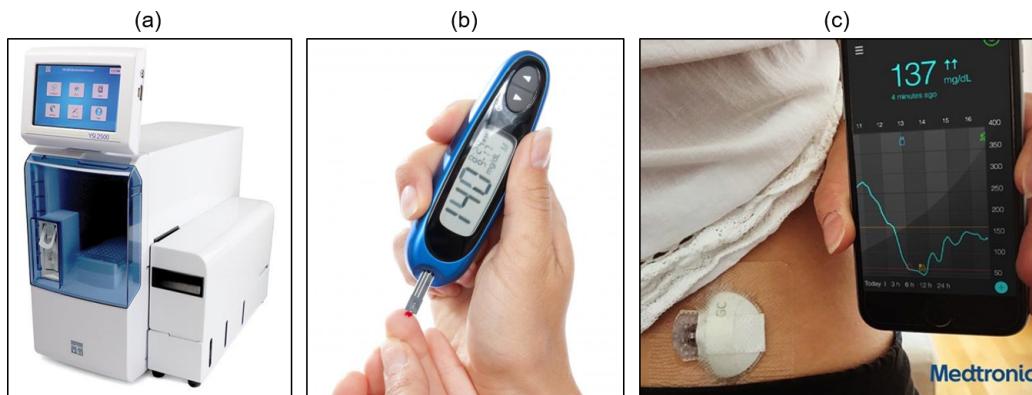
Figure 2.4: Examples of (a) laboratory glucose measurement device[1], (b) self-monitoring of blood glucose (SMBG) device[2], and (c) continuous glucose monitoring (CGM) device coupled with a smartphone[3].

The last means of glucose measurement to be introduced here are devices for continuous glucose monitoring (CGM), commercially available since the early 2000s. These devices automatically provide glucose measurements every 5-15 min, over a period of 7-14 days, both dependent on the device. This is achieved by placing a glucose sensor into the interstitial fluid (ISF) underneath the skin, which is then connected to a small device worn on top of the skin (Figure 2.4 (c)). The actual BG level is then estimated from the ISF glucose level. In most device types, this requires the periodic calibration with SMBG results (2-5 times per day), but the trend is moving toward factory calibrated devices not requiring user calibration at all. CGM devices are used for two main purposes. On the one hand, there are devices capable of displaying results in real-time, for the purposes of immediate therapy adjustment and hypoglycaemia detection. These devices require a secondary handheld device or smartphone to display results (Figure

---

[1]Image source: https://www.ysi.com/2500 (Last access October 2020)

[2]Image source: http://www.wisegeek.net/how-do-i-choose-the-best-flash-glucose-meter.htm (Last access October 2020)

[3]Image source: https://www.diabetesdaily.com/learn-about-diabetes/technology/tbw-how-to-use-a-cgm/all-about-the-medtronic-guardian-connect-continuous-glucose-monitor-cgm/ (Last access October 2020)

2.4 (c)) and are increasingly used in the management of T2DM. On the other hand, CGM devices can be blinded to the patient and be used for retrospective analysis of BG levels in the context of long-term therapy adjustment [16, 18, 61].

The accuracy of CGM systems remains a challenge and is typically assessed using the difference between CGM and SMBG readings, with values ranging from 8 to 15 %. Additional to the measurement error, ISF glucose levels typically lag behind actual BG levels with a delay of between 4 and 27 min, highly dependent on the rate of change of BG levels [61, 62]. Furthermore, it has been suggested that ISF glucose levels are additionally distorted [63], possibly resulting in the attenuation of high-frequency components in the BG signal. Nevertheless, the ongoing improvements in CGM technology have made this method of glucose measurement increasingly favoured in clinical practice and research [17].

Apart from the well established and minimally-invasive CGM technolgy described earlier, there exist several alternative approaches for continuous glucose measurement, e.g. microneedles inserted underneath the skin in the context of a watch type device. Furthermore, non-invasive methods based on fluorescence or spectroscopy are currently under development. However, the majority of these approaches have not been released commercially or their application in practice is very restricted, mainly due to their limited accuracy [64].

2.3 Minimal-type models for the postprandial glucose metabolism

A major part of the second objective formulated in the introduction to this thesis is the selection of an appropriate minimal-type model that will form the basis for the development of glucose-only models. The selected model should

- Contain identifiable parameters from glucose and insulin responses to OGTTs or mixed meals, i.e. meals containing additional macronutrients such as fat and protein besides CHO.

- Provide estimates of quantities that characterise the postprandial glucose metabolism, i.e. insulin sensitivity (IS) and meal-related glucose appearance (GA).

- Be robust so that minor adaptions to the model formulation and identification procedure retain the validity of the model. The model should also be well-established so that the validity of any changes can be assessed by comparison with results from the literature and existing information can be utilised to specify prior distributions.

- Posses minimal complexity to allow the development of glucose-only models.

A common feature of the models fulfilling the first two criteria is that they use the measured glucose concentration as the model output to fit the data against. In contrast, their use of the measured insulin concentrations is different which allows the distinction between two approaches. On the one hand, there are models that contain a description of the plasma insulin concentration dynamics and thus use said dynamics as a model output to fit the measured insulin levels against, analogous to the glucose levels. On the other hand, there are models that use the measured insulin levels as a known input and only fit the model predicted glucose levels against the data. This distinction is important as it influences the possible approaches for the development of glucose-only models.

Several models falling in the former category and fulfilling the first two above named criteria have been proposed [65–69]. This could allow the identification of these models without any modification to the model structure, if all states of the model would be observable and the parameters would be identifiable from glucose data only. This is, however, highly improbable given that these models possess a minimum of five compartments, representing different glucose and insulin sub-compartments and a large number of parameters, some of which are fixed during parameter estimation. It is therefore unfeasible to choose these models as basis for a glucose-only modelling approach due to their highly complex nature.

In contrast, the models proposed by Wilbaux et al. [70] and Dalla Man et al. [71] also fulfil the first two above named criteria, but use the measured insulin concentrations as a known input to fit the model against measured glucose concentrations. In comparison to models that directly describe insulin dynamics, the models [70, 71] require adaptation before the identification from glucose data only. Their advantage, however, is that they have a reduced number of states, parameters and therefore complexity, making them suitable for the glucose-only modelling task in this thesis.

The model proposed by Wilbaux et al. [70] was published only recently and has

therefore not been extensively validated against independent datasets. We will therefore choose the oral minimal model (OMM) published in 2002 by Dalla Man et al. [71] as basis for the development of glucose-only models. The OMM fulfils all of the required criteria because it is sufficiently simple, containing only two states, and uses measured insulin concentrations as a known input to fit the model against measured glucose concentrations. It also provides useful measures for assessing postprandial glucose metabolism in the form of IS and GA. The OMM has been extensively validated against data from experiments using traced glucose [72] as well as traced glucose and HEC measurements [73]. In both studies, it was concluded that the OMM is a reliable tool to estimate both IS and the GA from glucose and insulin responses to OGTTs and mixed meals. This has made the OMM the most popular method for assessing postprandial glucose metabolism [74], as evident by its use in a number of highly influential publications, e.g. [47, 75–78].

These properties make the OMM the most suitable candidate to form the basis for the development of glucose-only models. The datasets used in this thesis, however, demand adaptations that allow the identification of the OMM from non-fasting conditions and the description of meal responses of varying duration. Making these adaptations will be the subject of Chapters 4 and 5, where a detailed discussion of the OMM will be provided.

Chapter 3

Methodology

The following chapter describes the methodology for model development and identification used in this thesis. This process consists of model formulation, structural/practical identifiability analysis, parameter estimation, sensitivity analysis and model comparison.

3.1 Model formulation

The mathematical models utilised and developed in this thesis will be formulated through ordinary differential equations (ODE). These equations describe the evolution of the modelled system over time. The system itself is hereby represented through its state variables, which describe different aspects of the system dynamics and are defined by a system of first-order ordinary differential equations of the form

$$\frac{d\boldsymbol{x(t)}}{dt} = \boldsymbol{F}(\boldsymbol{x(t)}, \boldsymbol{p}, \boldsymbol{u(t)}, t) \quad \boldsymbol{x(0)} = \boldsymbol{x_0}. \tag{3.1}$$

In this thesis letters in bold represent vectors and matrices and t represents time. The n-dimensional vector $\boldsymbol{x(t)} = \{x_1(t), \ldots, x_n(t)\}$ contains all state variables with the associated vector of initial conditions $\boldsymbol{x_0} = \{x_{01}, \ldots, x_{0n}\}$. The vector of functions $\boldsymbol{F} = \{F_1, \ldots, F_n\}$ describes the relationship between the state variables, the fixed-value m-dimensional parameter vector $\boldsymbol{p} = \{p_1, \ldots, p_m\}$ and known external inputs $\boldsymbol{u(t)} = \{u_1(t), \ldots, u_n(t)\}$ [79]. In the context of model identification, the system is observed through a measurement process affected by random noise. This process could theoretically encompass multiple measurements, each comprised of nonlinear combina-

tions of state variables and parameters. In this thesis, however, only the simplified case of one single measurement process directly observing a single state variable without bias or gain is considered. In mathematical terms, the measurement process can be formulated as follows

$$y(t) = x_i(t) + \varepsilon \quad \text{for} \quad i = 1...n \qquad \text{and} \qquad \varepsilon \sim \mathcal{N}(0, \lambda^2). \qquad (3.2)$$

$y(t)$ is the continuous representation of the measurement time series based on a single state variable and is also referred to as model output. The measurement noise ε is assumed to be additive and follows a normal distribution with zero mean and standard deviation λ. More elaborate models of the measurement uncertainty, such as multiplicative noise, are not considered as they make the parameter estimation procedure considerably more complex. Furthermore, as absolute glucose levels, which is the only observed quantity considered in this thesis, are always significantly larger than the measurement error itself, a multiplicative measurement error is not feasible. Additionally, utilising an additive error model is standard practice when glucose assay and CGM data are used for the parameter estimation [8, 80]. The actual measured time series data consisting of T discrete measurements are denoted with $\boldsymbol{y} = \{y_1, \ldots, y_T\}$.

Based on this framework, it is possible to formulate the structure of a model, which essentially means proposing specific mathematical definitions for the functions $F_1, \ldots, F_n$. If these functions are only defined by the linear combinations of one (or multiple) parameters and states, the model is considered to be linear in $\boldsymbol{x(t)}$, if not the model is nonlinear.

3.2 Structural identifiability

3.2.1 Overview

Model (3.1) includes the unknown parameter vector $\boldsymbol{p}$ which contains key information about the underlying system. Any unknown initial conditions are combined with the model parameters to a single vector of unknown parameters $\boldsymbol{\vartheta} = \{\boldsymbol{p}, \boldsymbol{x_0}\}$. These unknown parameters are not measured directly, meaning that the estimation of parameter values can only be approached indirectly by observing the system in response to external stimulation. A prerequisite for this parameter estimation is to determine whether

the model structure allows the unique recovery of parameter values from a continuous and error-free observation, i.e. $\varepsilon = 0$. This is a mathematical property of the model that has to be established before parameter estimation and is referred to as *a priori* structural identifiability [8, 81].

An alternative view of structural identifiability is to ask whether two or more combinations of parameter values could lead to the same model output. This allows the distinction between structural global and local identifiability. A model is said to be structurally globally identifiable if there is only a single combination or unique set of parameter values defining the model output. Structural local identifiability occurs when there is a finite number of parameter value combinations that yield the same observation. Correspondingly, a model is structurally unidentifiable if there exists an infinite number of parameter value combinations defining the model output [8, 81]. This can be exemplified by considering the following simple model

$$\frac{dx(t)}{dt} = -(p_1{}^2 + p_2)x(t), \quad x(0) = x_0, \quad y(t) = x(t). \tag{3.3}$$

The single state variable is denoted with $x(t)$, the observation is $y(t)$ and the unknown parameters are p_1 and p_2. In (3.3) there exists an infinite number of combinations for the values of parameters p_1 and p_2 that lead to the same coefficient of $x(t)$ and, therefore, to the identical observation $y(t)$, even if the initial condition x_0 is known. The model is therefore structurally unidentifiable. If the parameter p_2 is considered to be known, the model is still only structurally locally identifiable, because there exist exactly two values for p_1, i.e. p_1 and $-p_1$, leading to the same model output. To overcome this issue, the parameter p_1 could be restricted to positive values, therefore making it structurally globally identifiable if p_2 is known.

3.2.2 Testing for structural identifiability

In the past decades, several approaches for analysing the structural identifiability of a model have been proposed. These include the Similarity Transform Approach [82], the Taylor series approach [83] and methods based on differential algebra [84], particularly the observability rank criterion (ORC) method [85]. In this thesis, we will utilise the Taylor series and ORC methods which are introduced in more detail.

The Taylor series approach was introduced in 1978 by Pohjanpalo [83] and can be

applied to bilinear and nonlinear models formulated in state-space representation. The approach is based on the Taylor series expansion of the model output around a known time point $t_0 \geq 0$, typically $t_0 = 0$, to give

$$y(t, \boldsymbol{\vartheta}) = y^{(0)}(t_0, \boldsymbol{\vartheta}) + y^{(1)}(t_0, \boldsymbol{\vartheta})\frac{t - t_0}{1!} + \cdots + y^{(k)}(t_0, \boldsymbol{\vartheta})\frac{(t - t_0)^k}{k!} + \cdots , \qquad (3.4)$$

where the $k + 1$ Taylor coefficients are defined by successive derivatives of the model output with respect to time

$$y^{(k)}(t_0, \boldsymbol{\vartheta}) = \frac{d^k}{dt^k}y(t_0, \boldsymbol{\vartheta}), \quad \text{for} \quad k = 0, 1, 2, ... \qquad (3.5)$$

These Taylor series coefficients can theoretically be fully determined by the measured model output $y(t)$. To demonstrate that a given parameter vector $\boldsymbol{\vartheta}$ leads to a unique output, the following system of $k + 1$ simultaneous equations introducing the vector $\overline{\boldsymbol{\vartheta}}$ is defined

$$\begin{aligned} y(t_0, \boldsymbol{\vartheta}) &= y(t_0, \overline{\boldsymbol{\vartheta}}) \\ y^{(1)}(t_0, \boldsymbol{\vartheta}) &= y^{(1)}(t_0, \overline{\boldsymbol{\vartheta}}) \\ &\vdots \\ y^{(k)}(t_0, \boldsymbol{\vartheta}) &= y^{(k)}(t_0, \overline{\boldsymbol{\vartheta}}). \end{aligned} \qquad (3.6)$$

If this system has the single solution $\boldsymbol{\vartheta} = \overline{\boldsymbol{\vartheta}}$, then all Taylor coefficients are uniquely defined by the unknown parameters and the model is structurally globally identifiable. If the system of equations has multiple solutions, it could be the case that not enough Taylor series coefficients have been used or that some parameters are truly structurally locally identifiable. Proving the structural local or unidentifiability of parameters in generalised nonlinear models is, however, very difficult as it would require a strict upper bound on the number of linearly independent Taylor series coefficients. While such upper bounds have been established for certain types of models, e.g. linear, an upper bound for generalised nonlinear models is missing. Additionally, establishing the linear independence of the Taylor series coefficients can be difficult as well [84].

To calculate the Taylor series coefficients and solve the system of simultaneous equations in expression (3.6), it is common to employ symbolic computation software. For that, this thesis will use Mathematica (Wolfram Research, Inc., Champaign, IL, USA). This makes the implementation of the Taylor series method straightforward in compar-

ison to the other previously mentioned methods for structural identifiability analysis. The details of the Mathematica implementation of the Taylor series method are provided in Appendix B. Additional to the difficulties in establishing the structural local or non-identifiability of the parameters with the Taylor series method it is also not always possible to solve system of equations with symbolic computation for any given number of Taylor series coefficients. Whether the computation completes and the structural identifiability of the model can be assessed is therefore highly dependant on the complexity of the model, the number of simultaneous equations, i.e. Taylor series coefficients, and the number of unknown parameters.

Should it be impossible to show the structural global identifiability with the Taylor series method, we will resort to a different approach that can establish the structural local identifiability or non-identifiability of parameters in generalised nonlinear models. It is based on a property of the model called observability, which determines whether the model's internal states can be ascertained from the output measurements in finite time. If the parameters are thereby treated as state variables with zero dynamics, it is possible to determine their structural local identifiability by calculating the rank of a generalised observability-identifiability matrix using results from differential geometry [85]. The disadvantage of this method is that it is not possible to determine the locally identifiable parameter combinations. The method is referred to as the ORC (observability rank criterion) method and is implemented as a freely available MATLAB (The MathWorks, Inc., Natick, MA, USA) toolbox called STRIKE-GOLDD [85, 86].

3.3 Parameter estimation

3.3.1 Overview

In the Introduction, it was mentioned that there are two basic approaches to parameter estimation. Frequentist, also known as Fisherian approaches, assume that unknown parameters are deterministic and can be represented by a single value. This is also known as maximum likelihood estimation because the approach maximises the function $L(\boldsymbol{y}|\boldsymbol{p}, M)$, representing the likelihood of obtaining the data $\boldsymbol{y}$ given the parameters $\boldsymbol{p}$ and the model M to get a single most probable parameter estimate $\hat{\boldsymbol{p}}_{\boldsymbol{ML}}$ using

$$\hat{\boldsymbol{p}}_{\boldsymbol{ML}} = \arg\max_{p} L(\boldsymbol{y}|\boldsymbol{p}, M). \tag{3.7}$$

If the measurement error is Gaussian, the calculation of $\hat{\boldsymbol{p}}_{\boldsymbol{ML}}$ is equivalent to minimising the sum of squared errors between the data and the model output with respect to $\boldsymbol{p}$ [87]. For that, numerical optimisation routines such as the Levenberg-Marquardt algorithm are available. To quantify the associated uncertainty of the parameter estimates, the inverse of the Fisher Information Matrix is often used. This approximation gives a lower bound on the covariance matrix of parameter estimation error by using the sensitivity matrix and covariance matrix of measurement noise. It should be emphasised that the frequentist approach assumes any uncertainties in the parameters to arise from uncertainties in the data and not in the model specification, meaning that the model structure is considered to be true [8].

In contrast to the frequentist approach, the Bayesian approach used in this thesis assigns the model a probability of being true based on the data and formulates a probability density function (PDF) over unknown parameters. All PDFs are denoted by f in this thesis. To estimate the unknown distributions, the Bayesian approach uses both the measured data and information existing before data collection, also known as *a priori* information. Bayes' theorem is applied to formulate the PDF over parameters after data collection $f_{\boldsymbol{p}|\boldsymbol{y},M}(\boldsymbol{p}|\boldsymbol{y}, M)$, known as the posterior distribution, from the PDF over parameters before data collection $f_{\boldsymbol{p}|M}(\boldsymbol{p}|M)$, known as the prior distribution

$$f_{\boldsymbol{p}|\boldsymbol{y},M}(\boldsymbol{p}|\boldsymbol{y}, M) = \frac{L(\boldsymbol{y}|\boldsymbol{p}, M)f_{\boldsymbol{p}|M}(\boldsymbol{p}|M)}{P(\boldsymbol{y}|M)}. \tag{3.8}$$

The posterior distribution $f_{\boldsymbol{p}|\boldsymbol{y},M}$ in expression (3.8) is obtained by updating the prior distribution $f_{\boldsymbol{p}|M}$ based on the previously introduced likelihood function L. The denominator of expression (3.8) is known as the marginal likelihood, or model evidence. It acts as a normalisation constant for the posterior distribution and can be calculated by integrating the numerator with respect to parameters $\boldsymbol{p}$ [87]

$$P(\boldsymbol{y}|M) = \int L(\boldsymbol{y}|\boldsymbol{p}, M)f_{\boldsymbol{p}|M}(\boldsymbol{p}|M)d\boldsymbol{p} = \mathbb{E}[L(\boldsymbol{y}|\boldsymbol{p}, M)]_{f_{\boldsymbol{p}|M}}. \tag{3.9}$$

Here $\mathbb{E}[\cdot]_f$ denotes the expected value with respect to the PDF defined by f. In a fully Bayesian treatment of the parameter estimation procedure, also known as model inversion, this model evidence is calculated as a by-product. It provides a measure for comparing multiple models identified from the same dataset [8, 87]. More details on the model comparison procedure are provided in section 3.5.

Comparing the frequentist and Bayesian approaches, it can be stated that the Bayesian method has the advantage of providing a consistent framework for: (1) including existing knowledge into the parameter estimation via the prior $f_{\boldsymbol{p}|M}(\boldsymbol{p}|M)$, (2) the quantification of uncertainty in the parameters estimates though the calculation of the posterior density $f_{\boldsymbol{p}|\boldsymbol{y},M}(\boldsymbol{p}|\boldsymbol{y},M)$ and (3) the comparison and combination of different models via the model evidence $P(\boldsymbol{y}|M)$. The Bayesian approach will therefore be chosen in this thesis.

The disadvantage of the Bayesian approach is that the complexity of the models formulated in this thesis makes it impossible to directly calculate the posterior distribution of unknown parameters (3.8) and model evidence (3.9). This has led to the development of approximation schemes for Bayesian parameter estimation. These schemes can generally be divided into stochastic and deterministic methods [87].

Stochastic techniques, also known as sampling methods, construct the posterior density through iterative algorithms which are based on drawing random samples of the vector $\boldsymbol{p}$. Given enough computational power and time, this process will converge to the true posterior distribution. Prominent algorithms for this task are the Markov Chain Monte Carlo (MCMC) and Sequential Monte Carlo (SMC) approaches [8, 87]. In the field of glucose dynamics modelling, sampling methods have been applied to several models with increasing prominence in recent years [88–92]. Despite this popularity and guaranteed convergence to the true posterior distribution, stochastic methods have several drawbacks. The main disadvantage is that sampling procedures are computationally expensive, often inefficient and it can be difficult to decide whether the algorithm has converged. Additionally, standard MCMC algorithms only approximate the posterior PDF over parameters and avoid the computation of the model evidence [93].

In contrast to the stochastic sampling methods, deterministic methods approximate the posterior distribution analytically by assuming it has certain properties such as factorising in a specific way or taking a specific parametric form. This means that the true posterior distribution can never be exactly inferred. In return, they are computationally much less expensive in comparison to sampling methods. Additionally, they approximate the model evidence along with the posterior distribution over unknown parameters [87], which makes them particularly useful for the modelling task in this thesis. The utility of such a parameter estimation technique in the field of glucose dy-

namics modelling has been demonstrated by Zhang et al. [25].

Given the drawbacks of the sampling methods previously mentioned, this thesis will employ a deterministic method called variational Bayesian (VB) analysis. This method is computationally more efficient and can provide results within minutes when operated on a conventional PC. This makes the VB approach feasible in a clinical setting for which the models in this thesis are developed for.

Aside from the distinction between deterministic and stochastic methods, parameter estimation techniques can be differentiated in terms of their usage of the data. In this thesis, the time series data y are collected from multiple subjects under the same experimental conditions. This could allow a mixed-effects modelling (MEM) approach, which incorporates the data from all individuals simultaneously for the estimation of the parameters. For that, parameters on the subject level are described as the result of a random fluctuation, known as random effect, about an overall population mean, known as fixed effect. This ties the subjects and their data together by assuming an overall population distribution of each parameter and a shared covariance matrix of the random effects, describing the variability between subjects [94] (Figure 3.1 (a)). The MEM approach has been used in conjunction with both Bayesian [89] and frequentist parameter estimation techniques [42] for models of glucose dynamics and is particularly useful when the data on an individual level are sparse [95].
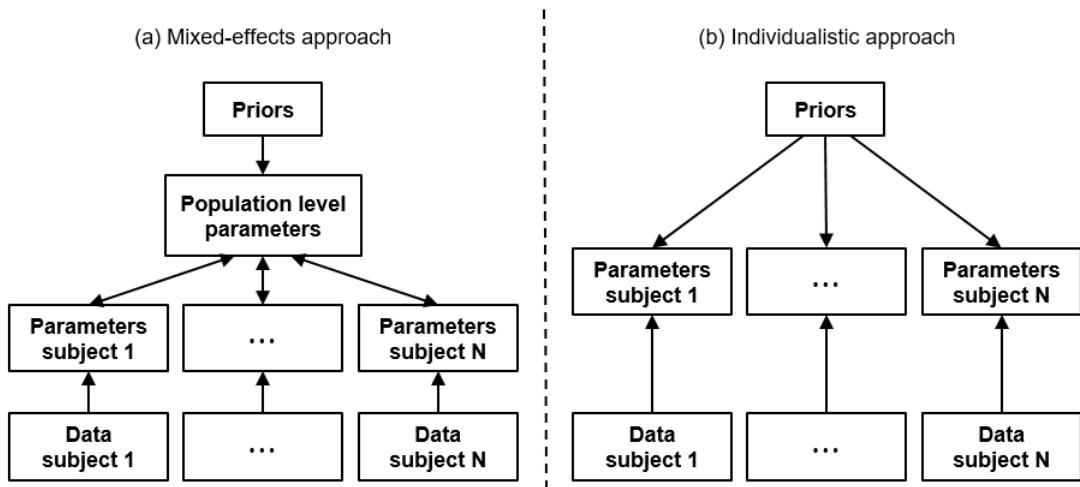
Figure 3.1: Schematic depiction of the (a) mixed-effects and (b) individualistic modelling approaches. The mixed effects modelling approach assumes a population distribution of parameters and allows the flow of information between subjects. In the individualistic approach subjects and are treated independently and only share a common prior distribution.

In contrast to the MEM technique, this thesis will employ a more individualistic approach in which each subject's data are considered separately and the parameter estimation for one subject is completely independent from the data of the other subjects. All unknown parameters in all subjects will however be estimated from the same prior distribution (Figure 3.1 (b)). For the particular modelling task in this thesis, the individualistic approach has two main advantages over the MEM approach and is therefore chosen. Firstly, the individualistic approach requires no assumption of a common population distribution, which could be difficult to specify when a population of subjects with varying degree of glucose tolerance is considered. Secondly, glucose responses to the same food are known do undergo considerable, interpersonal variability [96, 97]. It is therefore preferable to use the individualistic appraoch for the characterisation a person's glucose metabolism. In contrast, the MEM approach focusses on estimating the average behaviour of an individual within a population [94].

3.3.2 The variational Bayesian scheme

The variational Bayesian (VB) scheme for the inversion of nonlinear state-space models was introduced in 2009 by Daunizeau et al. [98] and is based on earlier works by Friston et al. [99–101] and Beal [102]. Its mathematical details are covered elsewhere [93, 98, 103]. For completeness, an brief overview on the underlying theory is provided below. More attention is given to its application to the model formulation considered in this thesis, which is a specific case of a more generic class of models the VB method was developed for. To the author's knowledge, a systematic comparison between the VB method and other Bayesian or frequentist parameter estimation techniques for nonlinear state-space models has not been carried out and lies beyond the scope of this thesis.

3.3.2.1 Theoretical background

As mentioned before, the Bayesian approach treats all unknown parameters as random variables characterised by a PDF. From model (3.1) - (3.2), the unknown quantities are the model parameters $\boldsymbol{p}$, initial conditions $\boldsymbol{x_0}$ and the magnitude of measurement uncertainty, which was specified by the standard deviation λ in expression (3.2). Instead of λ, the VB method uses the precision $\kappa = \lambda^{-2}$ to quantify the measurement uncertainty. A more detailed discussion on the relationship between κ and λ is provided in section 3.3.2.2.

For simplicity, the unknown parameters are described by a single variable $\boldsymbol{\theta} = \{\boldsymbol{\vartheta}, \kappa\}$, where the vector $\boldsymbol{\vartheta}$ is the concatenation of unknown model parameters $\boldsymbol{p}$ and initial conditions $\boldsymbol{x_0}$. The goal of the VB algorithm is to approximate the posterior density $f_{\boldsymbol{\theta}|\boldsymbol{y},M}$ and to quantify the model evidence $P(\boldsymbol{y}|M)$, introduced in (3.8) and (3.9), respectively. For that, the density f_q, approximating the true posterior density is introduced and the Kullback-Leibler divergence between the two densities is formulated as:

$$D_{KL}(f_q \parallel f_{\boldsymbol{\theta}|\boldsymbol{y},M}) = \int f_q(\boldsymbol{\theta}) \log \frac{f_q(\boldsymbol{\theta})}{f_{\boldsymbol{\theta}|\boldsymbol{y},M}(\boldsymbol{\theta}|\boldsymbol{y},M)} d\boldsymbol{\theta}$$

$$= \mathbb{E}\left[\log \frac{f_q(\boldsymbol{\theta})}{f_{\boldsymbol{\theta}|\boldsymbol{y},M}(\boldsymbol{\theta}|\boldsymbol{y},M)}\right]_{f_q},$$

(3.10)

providing a measure for the difference of the two densities. In this thesis, the operator log refers to the logarithm with respect to the base of Euler's number e. Through the replacement of the posterior $f_{\boldsymbol{\theta}|\boldsymbol{y},M}$ with expression (3.8) and subsequent simplification and reformulation, the following expression for the free energy $\mathcal{F}$ can be derived (see Appendix A.1 for the details of the derivation)

$$\underbrace{\mathbb{E}[\log L(\boldsymbol{y}|\boldsymbol{\theta}, M) + \log f_{\boldsymbol{\theta}|M}(\boldsymbol{\theta}|M) - \log f_q(\boldsymbol{\theta})]_{f_q}}_{\mathcal{F}} = \log P(\boldsymbol{y}|M)$$

$$- D_{KL}(f_q \parallel f_{\boldsymbol{\theta}|\boldsymbol{y},M}).$$

(3.11)

D_{KL} is restricted to positive values, meaning that if $D_{KL} = 0$, then f_q and $f_{\boldsymbol{\theta}|\boldsymbol{y},M}$ are identical and the free energy $\mathcal{F}$ is equal to the log of the model evidence $\log P(\boldsymbol{y}|M)$. Maximising the free energy with respect to f_q is thus equivalent to minimising the Kullback-Leibler divergence D_{KL}, therefore simultaneously providing an approximation of the true posterior through f_q and of the lower bound on the model evidence through $\mathcal{F}$.

For this maximisation of the free energy, it is necessary to assume that the approximate joint distribution of f_q, factorises into the densities of individual, unknown parameters, which is known as the mean-field approximation. For the models in this thesis this yields

$$f_q(\boldsymbol{\theta}) = f_{q_{\vartheta}}(\boldsymbol{\vartheta}) f_{q_{\kappa}}(\kappa).$$

(3.12)

Based on this assumption, the maximisation of the free energy can be split into the optimisation of one component of f_q at a time, while keeping the other component fixed.

Since expression (3.11) for $\mathcal{F}$ is a functional, variational calculus is utilised to calculate the optimisation rules for the individual components, giving rise to the name of this method. The overall optimisation is implemented as an iterative process and is repeated until the free energy converges. A schematic depiction of this process in provided in Figure 3.2.
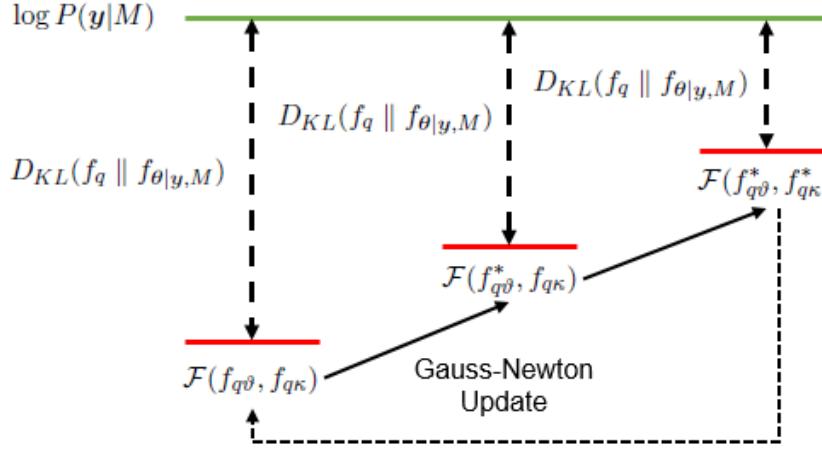
Figure 3.2: Schematic description of the free energy maximisation through the iterative update of individual components of f_q. This simultaneously minimises D_{KL} and brings the free energy $\mathcal{F}$ closer to the log model evidence but leaves a gap depending on the final value of D_{KL}. The mark * indicates that the density has been updated. In the case of $f_{q\vartheta}$, this is achieved through a Gauss-Newton optimisation scheme carried out within the main free energy maximisation [93].

To calculate the iterative update rules for the two approximate densities $f_{q\vartheta}$ and $f_{q\kappa}$, assumptions on the functional forms of their prior distributions have to be made. The measurement uncertainty precision κ is restricted to positive values and its prior PDF is therefore modelled with a Gamma distribution, specified by shape and rate variables a_0 and b_0, referred to as the sufficient statistics of the PDF over κ

$$\kappa \sim \mathcal{G}a(a_0, b_0). \tag{3.13}$$

Choosing a Gamma shaped prior distribution over κ has the additional advantage that it forms a conjugate prior to the approximated Gaussian-shaped likelihood function. This means that $f_{q\kappa}$ also follows a Gamma distribution allowing for the update rules of its sufficient statistics to be directly calculated without the need for further approximation.

In contrast, the unknown model parameters are not restricted and their prior PDF is modelled with a normal distribution specified by the sufficient statistics $\boldsymbol{\mu}_\vartheta^0$ and $\boldsymbol{\Sigma}_\vartheta^0$

so that

$$\boldsymbol{\vartheta} \sim \mathcal{N}(\boldsymbol{\mu}_{\boldsymbol{\vartheta}}^0, \boldsymbol{\Sigma}_{\boldsymbol{\vartheta}}^0). \tag{3.14}$$

Together with nonlinearities in the likelihood function, this leads to a posterior distribution that is not in the conjugate-exponential family. This renders the calculation of the update rules analytically intractable and further approximation is required. For that, the VB approach utilises the Laplace approximation which defines f_{q_ϑ} by its first two moments and matches them to a Gaussian distribution approximating f_{q_ϑ}. To find the mode, i.e. first order moment, the VB approach employs the Gauss-Newton optimisation scheme, i.e. a second iterative process nested within the main update algorithm (see Figure 3.2). After the mode has been found, the variance of the approximated f_{q_ϑ} is derived from the second-order truncation of its Taylor series expansion. The result is a Gaussian PDF over the unknown parameters specified by a mean and covariance matrix [98].

3.3.2.2 Practical considerations

The core of the VB approach is implemented in a freely accessible library of MATLAB functions [104], hereafter referred to as the VB toolbox. Daunizeau et al. [105] have given an overview of its application to models for neurobiological and behavioural data. However, to the author's knowledge, its application to state-space models in metabolic physiology has not been discussed in the literature. This section will thus discuss the most important aspects of its application to the models and data used in this thesis and provide the necessary technical details for future use by independent researchers.

Model specification and ODE solution

Throughout the model inversion process, previously described, the ODEs defining the model have to be solved so that the current model output $y(t)$ can be compared to the available data $\boldsymbol{y}$. For that, the VB toolbox requires the user to specify an update rule to calculate the next value of the state space vector $\boldsymbol{x}_{t+1}$ based on its current value $\boldsymbol{x}_t$ using a fixed, user-specified time step size of Δt. This approximation to the solution of a continuous state-space model using discrete time steps is performed using the Euler

discretisation scheme [105]

$$\boldsymbol{x}_{t+1} = \boldsymbol{x}_t + \boldsymbol{F}(\boldsymbol{x}_t, \boldsymbol{p}, \boldsymbol{u}_t)\Delta t \quad \boldsymbol{x}_{t=0} = \boldsymbol{x}_0. \tag{3.15}$$

The VB toolbox only passes the mean of the model parameters $\boldsymbol{p}$ to the user as a point estimate of the associated PDF. The vector of inputs $\boldsymbol{u_t}$ has to be specified at each time step, where the time itself can be considered as a known input. This procedure allows an adequate approximation of the state trajectories if Δt is significantly smaller than the quickest decay of the system [105], which is the case for the models used in this thesis. Specifically, a step size of 0.1 min was chosen and proved sufficiently small as further reduction of the step size did not lead to a significant change in the results. It should nevertheless be emphasised that the use of Euler's method with a constant step size is not inherently stipulated by the VB method, despite being implemented in the VB toolbox [104, 105]. It is thus theoretically possible to implement more complex ODE solution algorithms with a variable step size.

To update the model parameters during the Gauss-Newton optimisation scheme previously mentioned, it is necessary to calculate a trajectory of the model's sensitivity, i.e. the derivative of the states $\boldsymbol{x}_t$ with respect to the unknown parameters $\boldsymbol{p}$ and initial conditions $\boldsymbol{x_0}$. To our knowledge no detailed information on this procedure is available in the literature, so the mathematical details are provided below. The trajectories for model sensitivity are defined in continuous time by

$$\boldsymbol{S_p}(t) = \frac{d\boldsymbol{x}(t)}{d\boldsymbol{p}} = \begin{bmatrix} \dfrac{dx_1}{dp_1} & \cdots & \dfrac{dx_1}{dp_m} \\ \vdots & \ddots & \vdots \\ \dfrac{dx_n}{dp_1} & \cdots & \dfrac{dx_n}{dp_m} \end{bmatrix} \quad \text{and} \quad \boldsymbol{S_{x_0}}(t) = \frac{d\boldsymbol{x}(t)}{d\boldsymbol{x_0}} = \begin{bmatrix} \dfrac{dx_1}{dx_{01}} & \cdots & \dfrac{dx_1}{dx_{0n}} \\ \vdots & \ddots & \vdots \\ \dfrac{dx_n}{dx_{01}} & \cdots & \dfrac{dx_n}{dx_{0n}} \end{bmatrix},$$
$$\tag{3.16}$$

where $\boldsymbol{S_p}(t)$ is a $n \times m$ matrix and $\boldsymbol{S_{x_0}}(t)$ is a $n \times n$ matrix describing the sensitivities of the n model states with respect to the m parameters and n initial conditions, respectively. Applying the multivariate chain rule to the model (3.1) yields [106]

$$\frac{d\boldsymbol{S_p}(t)}{dt} = \frac{d}{dt}\left(\frac{d\boldsymbol{x}(t)}{d\boldsymbol{p}}\right) = \frac{\partial \boldsymbol{F}}{\partial \boldsymbol{p}} + \frac{\partial \boldsymbol{F}}{\partial \boldsymbol{x}(t)}\frac{d\boldsymbol{x}(t)}{d\boldsymbol{p}}, \qquad \left.\frac{d\boldsymbol{x}(t)}{d\boldsymbol{p}}\right|_{t=0} = 0,$$

$$\tag{3.17}$$

$$\frac{d\boldsymbol{S_{x_0}}(t)}{dt} = \frac{d}{dt}\left(\frac{d\boldsymbol{x}(t)}{d\boldsymbol{x_0}}\right) = \frac{\partial \boldsymbol{F}}{\partial \boldsymbol{x}(t)}\frac{d\boldsymbol{x}(t)}{d\boldsymbol{x_0}}, \qquad \left.\frac{d\boldsymbol{x}(t)}{d\boldsymbol{x_0}}\right|_{t=0} = \boldsymbol{I},$$

where $\boldsymbol{F}$ is defined by the model equations (3.1) and $\boldsymbol{I}$ denotes the identity matrix. The partial derivatives of the model equations $\boldsymbol{F}$ with respect to the states $\boldsymbol{x}(t)$ and model parameters $\boldsymbol{p}$ are provided to the VB toolbox by the user and defined by

$$\boldsymbol{J}(t) = \frac{\partial \boldsymbol{F}}{\partial \boldsymbol{x}(t)} = \begin{bmatrix} \dfrac{dF_1}{dx_1} & \cdots & \dfrac{dF_1}{dx_n} \\ \vdots & \ddots & \vdots \\ \dfrac{dF_n}{dx_1} & \cdots & \dfrac{dF_n}{dx_n} \end{bmatrix} \quad \text{and} \quad \boldsymbol{H}(t) = \frac{\partial \boldsymbol{F}}{\partial \boldsymbol{p}} = \begin{bmatrix} \dfrac{dF_1}{dp_1} & \cdots & \dfrac{dF_1}{dp_m} \\ \vdots & \ddots & \vdots \\ \dfrac{dF_n}{dp_1} & \cdots & \dfrac{dF_n}{dp_m} \end{bmatrix},$$

(3.18)

where $\boldsymbol{J}$ is a $n \times n$ matrix and $\boldsymbol{H}$ is a $n \times m$ matrix which can be analytically calculated using symbolic computation software. Taking into account expressions (3.16) and (3.18), the differential equations (3.17) are reformulated as

$$\frac{d\boldsymbol{S_p}(t)}{dt} = \boldsymbol{H}(t) + \boldsymbol{J}(t)\boldsymbol{S_p}(t) \qquad \boldsymbol{S_p}(0) = 0$$

(3.19)

$$\frac{d\boldsymbol{S_{x_0}}(t)}{dt} = \boldsymbol{J}(t)\boldsymbol{S_{x_0}}(t) \qquad \boldsymbol{S_{x_0}}(0) = \boldsymbol{I}.$$

and solved simultaneously with the ODE itself. For that, we move from continuous to discrete-time notation and utilise Euler's method

$$\boldsymbol{S_{p_{t+1}}} = [\boldsymbol{H}_t + \boldsymbol{J}_t\boldsymbol{S_{p_t}}]\Delta t + \boldsymbol{S_{p_t}} \qquad \boldsymbol{S_{p_{t=0}}} = 0,$$

(3.20)

$$\boldsymbol{S_{x_0{_{t+1}}}} = [\boldsymbol{J}_t\boldsymbol{S_{x_0{_t}}}]\Delta t + \boldsymbol{S_{x_0{_t}}} \qquad \boldsymbol{S_{x_0{_{t=0}}}} = \boldsymbol{I}.$$

Transformation of parameters

In the previous section, it was explained that the VB method assumes certain parametric distributions over the unknown parameters, in particular Gaussian and Gamma distributions. In practice, however, it is often useful to choose a different distribution for the model parameters before parameter estimation. The treatment of three such cases within the VB method is discussed below.

Restriction of parameters to positive values

Assuming the model has a single parameter p, whose PDF is specified with the Gaussian density f_p, mean μ and standard deviation σ, a restriction to positive values can be

achieved by introducing the substitute parameter s and the exponential mapping $s = \exp(p)$. This restriction is common in metabolic modelling, where parameters are often constrained to positive values by the underlying physiology. As far as we are aware, the detailed consequences of this exponential mapping in the context of the VB approach are not discussed in the literature and thus provided below. To determine the density f_s over the substitution for the parameter s from the density f_p using the exponential mapping, the following theorem can be used. If f_x is a PDF over the random variable x and the mapping $y = h(x)$ is introduced, then the PDF over the random variable y is given by [107]

$$f_y(y) = f_x(h^{-1}(y)) \left| \frac{\mathrm{d}h^{-1}(y)}{\mathrm{d}y} \right|. \tag{3.21}$$

Applying this result, the density f_s over s is given by

$$f_s(s|\mu, \sigma) = \frac{1}{s\sqrt{2\pi}\sigma} \exp\left(-\frac{(\log s - \mu)^2}{2\sigma^2}\right), \tag{3.22}$$

which can be recognised as the log-normal distribution. As previously mentioned, the VB toolbox passes the mean μ to the user for model specification. Applying the exponential mapping to μ, i.e. $m = e^\mu$ leads to the fact that the model uses the median m of f_s as q point estimate to solve the model ODEs.

In this work we can generalise this property of μ mapping to the median of f_s to all strictly monotonic mapping functions $s = h(p)$ with the following considerations. It is assumed that a series of random samples of p are mapped to random samples of s by applying the function h. As the number of samples increases, it is expected that half of the samples of p will be smaller than μ and the remaining half larger than μ, because μ is not only the mean, but also the median of f_p. Given the strictly monotonic nature of the function h, it follows that half of the samples of s will be smaller (larger) than $m = h(\mu)$ and the remaining half will be larger (smaller) than $m = h(\mu)$, depending on whether h is strictly monotonically increasing or decreasing. This means that m has to be the median of the distribution f_s.

Returning to the specific case of the exponential mapping function, the uncertainty in the log-normally distributed parameter s can be quantified by its coefficient of variation (CV) and calculated using [108]

$$CV = \sqrt{\exp(\sigma^2) - 1}. \tag{3.23}$$

This means that the CV of f_s is independent of its median, which has the result that its posterior CV is guaranteed to be smaller or equal to its prior CV. Another useful characterisation of the uncertainty in s is the one-sigma range around the median m, which is calculated by [108]

$$\left[\frac{m}{\exp(\sigma)}, m \cdot \exp(\sigma)\right]. \tag{3.24}$$

To specify the prior distribution over p based on the respective prior of s with m_0 and CV_0, the following equations are used

$$\mu_0 = \log m_0 \quad \text{and} \quad \sigma_0 = \sqrt{\log(CV_0{}^2 + 1)}. \tag{3.25}$$

If there are multiple normally distributed parameters described by a vector of means $\boldsymbol{\mu_\vartheta}$ and covariance matrix $\boldsymbol{\Sigma_\vartheta}$ and transformed via the exponential mapping, the resulting correlation coefficient of the *ith* and *jth* log-normally distributed parameters can be calculated by [109]

$$r_{ij} = \frac{\exp(\Sigma_{ij}) - 1}{\sqrt{(\exp(\Sigma_{ii}) - 1)(\exp(\Sigma_{jj}) - 1)}}, \tag{3.26}$$

where Σ_{ij} is the entry of the *ith* row and *jth* column of the covariance matrix $\boldsymbol{\Sigma_\vartheta}$.

Restriction of parameters to values between 0 and 1

Another scenario appearing in this thesis is that a model parameter p needs to be restricted to the interval $(0, 1)$, because it determines the ratio between values A_1 and A_2 that need to be positive and have fixed, known sum A, i.e.

$$A = A_1 + A_2 \quad \text{and} \quad p = \frac{A_1}{A_2}. \tag{3.27}$$

This can be reformulated into

$$A = \underbrace{(1 - p)A}_{A_1} + \underbrace{pA}_{A_2}. \tag{3.28}$$

If p lies in the interval $(0, 1)$, it is guaranteed that the value of A stays constant and A_1 and A_2 remain positive. Restricting a normally distributed parameter p to the interval $(0, 1)$ is achieved by replacing p with the substitute parameter s and a logistic function

$$s = S(p) = \frac{1}{1 + \exp(-p)}. \tag{3.29}$$

The theoretical implications of this mapping in the VB context have been analysed by Daunizeau [110]. The findings of Daunizeau's work are summarised below and their application in this thesis is explained. Assuming that p is normally distributed with mean μ and standard deviation σ, and utilising (3.21), the density f_s over s is given by

$$f_s(s|\mu,\sigma) = \frac{1}{\sqrt{2\pi}\sigma s(1-s)} \exp\left(-\frac{\left[\log\left(\frac{s}{1-s}\right) - \mu\right]^2}{2\sigma^2}\right) \quad \text{for} \quad 0 < s < 1. \quad (3.30)$$

The first and second order moments of this PDF cannot be determined analytically. Daunizeau [110] therefore proposed the following approximation for the mean and variance of f_s, which yields a relative error of less than 2% over a large range of possible values for μ and σ:

$$\mathbb{E}[s]_{f_s} \approx S\left(\frac{\mu}{\sqrt{1+a\sigma}}\right) \quad \text{with} \quad a = \frac{3}{\pi^2}$$

$$(3.31)$$

$$\mathrm{Var}[s]_{f_s} \approx \mathbb{E}[s]_{f_s}(1 - \mathbb{E}[s]_{f_s})\left(1 - \frac{1}{\sqrt{1+a\sigma}}\right).$$

Using this approximation of $\mathbb{E}[s]_{f_s}$ as a point estimate for the parameter s during model specification is not possible because only the mean μ of p is provided by the VB toolbox. In this thesis, we instead propose to use the median m of f_s as point estimate because it is independent of σ and can be calculated using

$$m = \frac{1}{1 + \exp(-\mu)}. \quad (3.32)$$

This expression for the median can be determined with symbolic computation or can be directly deduced from the considerations of the previous section describing the relationship between the mean of a Gaussian variable and the median of a distribution after mapping. Recognising the fact that the function S in (3.29) is a strictly monotonically increasing function, as shown by $dS/dp > 0$, the expression (3.32) can be directly deduced without the need to apply symbolic computation.

To quantify the uncertainty in s with the CV, Daunizeau's formulas from expression (3.31) are used,

$$\mathrm{CV} = \frac{\sqrt{\mathrm{Var}[s]_{f_s}}}{\mathbb{E}[s]_{f_s}}. \quad (3.33)$$

To specify the prior distribution over p based on the respective prior of s, the following

procedure was developed in this thesis. The prior mean μ_0 is calculated from the selected prior median m_0 of s as follows:

$$\mu_0 = -\log\left(\frac{1}{m_0} - 1\right). \tag{3.34}$$

The possible prior values for σ_0 are then varied numerically until the desired prior CV is sufficiently approximated.

To calculate the correlation between logistically and exponentially transformed parameters, there exists, to the author's knowledge, no analytical expression similar to (3.26). A Monte Carlo based approximation approach is therefore adopted. First, one million random samples for each component of the original, multivariate normal distribution specified by $\boldsymbol{\mu_\vartheta}$ and $\boldsymbol{\Sigma_\vartheta}$ are generated. Secondly, the random samples are transformed using the logistic and exponential mapping, respectively, and their sample Pearson correlation coefficients are calculated using standard techniques.

Transformation of noise precision parameter

The VB method assumes a Gamma PDF specified by sufficient statistics a and b for the precision κ of the measurement uncertainty. This PDF is defined by

$$f_\kappa(\kappa|a,b) = \frac{b^a}{\Gamma(a)}\kappa^{a-1}\exp(-\kappa b) \quad \text{for} \quad \kappa, a, b > 0, \tag{3.35}$$

where $\Gamma(\cdot)$ is the Gamma function. The mean and variance of this distribution are given by [107]

$$\mathbb{E}[\kappa]_{f_\kappa} = \frac{a}{b} \quad \text{and} \quad \text{Var}[\kappa]_{f_\kappa} = \frac{a}{b^2}. \tag{3.36}$$

In this thesis, the measurement process is modelled using expression (3.2), where the measurement noise intensity is characterised by the standard deviation λ. The change from κ to λ is necessary because the oral minimal model previously chosen requires the user to specify the measurement uncertainty based on the inter-assay CV of the glucose assay, i.e. a known λ. This requirement extends to a wide range of models used in metabolic physiology, where it is common to characterise the measurement error of the collected data in terms of the standard deviation λ. When applying the VB method to these models, it becomes necessary to specify the prior PDF of κ based on known

values for λ. Additionally, it is useful to be able to interpret the posterior distribution over κ in terms of λ. This thesis, therefore, proposes the following novel method for the forwards and backwards transformation between the PDFs over κ and λ. This method has now been accepted by the development team as an official part of the VB toolbox [104].

Similar to the previous section on exponential and logistic transformations, expression (3.21) and the mapping $\lambda = 1/\sqrt{\kappa}$ are used to formulate the PDF f_λ over λ as

$$f_\lambda(\lambda|a, b) = \frac{2b^a}{\Gamma(a)} \lambda^{-2a-1} \exp\left(-\frac{b}{\lambda^2}\right) \quad \text{for} \quad \kappa, a, b > 0. \tag{3.37}$$

Using symbolic computation, this new PDF can be characterised by the following expression for the mean μ and the standard deviation σ, valid for $a > 1$:

$$\mu = \mathbb{E}[\lambda]_{f_\lambda} = \sqrt{b} \frac{\Gamma(a - \frac{1}{2})}{\Gamma(a)},$$

$$\sigma^2 = \text{Var}[\lambda]_{f_\lambda} = b \left[\frac{1}{a-1} - \frac{\Gamma(a-\frac{1}{2})^2}{\Gamma(a)^2}\right]. \tag{3.38}$$

To facilitate the numerical calculation, the logarithm of the Gamma function $\log\Gamma(\cdot)$ is used instead of the fast growing Gamma function itself. This modifies (3.38) to give

$$\mu = \sqrt{b} \exp\left[\log\Gamma(a - \frac{1}{2}) - \log\Gamma(a)\right],$$

$$\sigma^2 = b \left[\frac{1}{a-1} - \exp\left[\log\Gamma(a - \frac{1}{2})^2 - \log\Gamma(a)^2\right]\right]. \tag{3.39}$$

An example of the PDFs over κ and λ is provided in Figure 3.3, where it is demonstrated that the mean of f_κ does not simply transform into the mean of f_λ by applying the mapping $\lambda = 1/\sqrt{\kappa}$. Furthermore, a transformation of the median of f_κ is not possible because the Gamma PDF has no closed form expression for its median.

To specify the prior distribution over κ based on the chosen prior PDF over λ defined by μ_0 and σ_0, it is necessary to calculate the associated values for a_0 and b_0. For this the following procedure is proposed. We begin by defining the following substitution

$$S(a) = \frac{\Gamma(a - \frac{1}{2})^2}{\Gamma(a)^2} = \exp\left[\log\Gamma(a - \frac{1}{2})^2 - \log\Gamma(a)^2\right]. \tag{3.40}$$
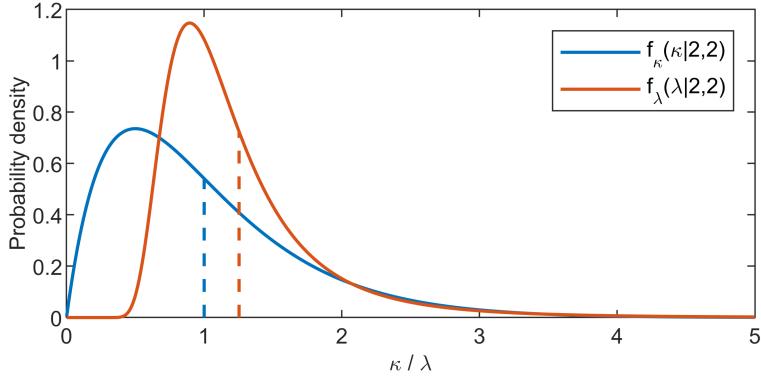
Figure 3.3: Examples of the two PDFs of f_κ and f_λ for $a = b = 2$. The dashed vertical lines display the values of the respective means.

This is followed by the combination and reformulation of the expressions (3.39) into

$$D(a) = \frac{\mu_0{}^2}{S(a)} - \frac{\sigma_0{}^2}{\dfrac{1}{a-1} - S(a)}. \tag{3.41}$$

This eliminates b and makes it possible to find a_0 by solving the equation $D(a_0) = 0$ and subsequently finding b_0 using

$$b_0 = \frac{\mu_0{}^2}{S(a_0)}. \tag{3.42}$$

To find a_0, the expression (3.41) is reformulated into a constrained numerical minimisation task

$$a_0 = \underset{a}{\arg\min} \left(\log \left[D(a)^2 + 1 \right] \right) \quad \text{for} \quad a > 1. \tag{3.43}$$

The square operation and addition of one within the logarithm ensures that the objective function is always positive except for $\log[D(a_0)^2 + 1]$, where the expression is zero. The logarithm facilitates the numerical calculations since the values of only $D(a)^2$ would grow rapidly as a increases. An example of the objective function for different values of μ_0 and σ_0 is given in Figure 3.4, demonstrating a clear minimum of the objective function at a_0.

This minimisation can be solved using an appropriate constrained optimisation technique, e.g. *fminbnd* in MATLAB. Since the expression (3.38) is only valid for $a > 1$ the lower bound is set to 1. To specify an upper bound based on the given values of μ_0 and σ_0 we start by approximating the function $S(a)$ from the expression (3.40) with
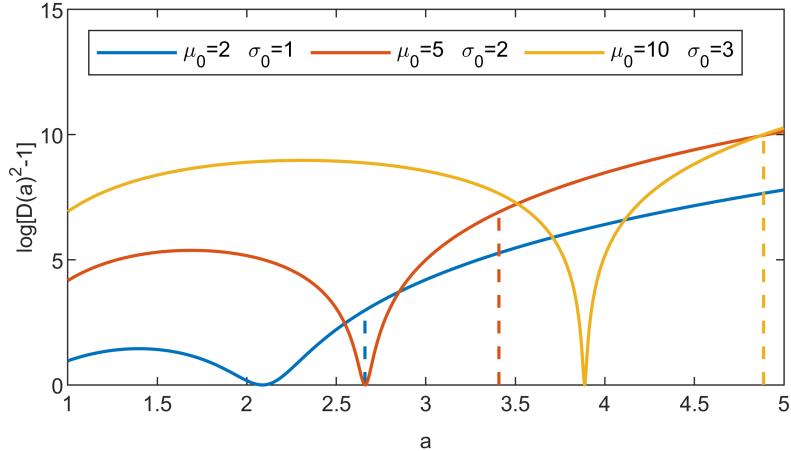
Figure 3.4: Examples of the objective function $\log[D(a)^2 + 1]$ for differing values of of μ_0 and σ_0. The dashed lines give the respective values of the upper bound estimation of $\hat{a}_0$.

the first two terms of its power series expansion for $a \to \infty$, giving

$$\hat{S}(a) = \frac{1}{a} + \frac{3}{4a^2}. \tag{3.44}$$

With this approximation, the minimum $\hat{a}_0$ of $D(a)$ can be found analytically

$$\hat{a}_0 = \frac{1}{8} \left[1 + \sqrt{49 + \frac{\mu_0^4}{\sigma_0^4} + 50\frac{\mu_0^2}{\sigma_0^2}} + \frac{\mu_0^2}{\sigma_0^2} \right], \tag{3.45}$$

which is used as an upper bound (see Figure 3.4). This approach was validated numerically under the following conditions

- $0.005 < \mu_0 < 10^4$

- $0.005\mu_0 < \sigma_0 < 5\mu_0$

It was found that μ_0 and σ_0 can be recovered with an error of less than 1% on both.

Input and output of the VB toolbox

The last practical aspect of the VB method to be discussed is the input and output to the VB toolbox. The implementation of the model and ODE solution routine previously described is passed to the VB toolbox as a separate function. Additionally, it is crucial to specify the prior distributions over the unknown parameters. This is done separately for the model parameters and initial conditions through two vectors of means and two covariance matrices, respectively. The non-diagonal elements are typically set

to zero, indicating no prior covariance, and the user has the option to keep the initial conditions fixed to their prior distribution during model inversion. The same option exists for the measurement noise precision κ, whose prior has to be specified by a_0 and b_0. Throughout this thesis, the priors of all of the unknown parameters are set as informative priors, meaning that preliminary knowledge about the underlying physiology, from the literature and/or the data will be used to specify them, therefore utilising one of the main benefits of a Bayesian parameter estimation approach.

As output, the VB toolbox provides the posterior distributions over the model parameters and initial conditions in the form of separate vectors of means and covariance matrices as well as a single covariance matrix of parameters and initial conditions. This then allows the characterisation of the posterior distribution over potentially transformed parameters using the main diagonal of the covariance matrix to extract the variances of the individual parameters and calculate the posterior CVs. Similarly, the VB toolbox provides the posterior distribution over κ specified by sufficient statistics for a and b, which are utilised to interpret the posterior distribution over λ using the procedure described in the previous section. Lastly, the VB toolbox provides a single value for the free energy $\mathcal{F}$.

3.3.3   Choice of prior distributions

As mentioned in section 3.3.1, one of the benefits of a Bayesian parameter estimation approach is the ability to incorporate existing information about the parameters through the formulation of suitable prior distributions. This approach uses an informative prior and stands in contrast to the use of uninformative priors, which have a flat PDF thus assigning a large portion of possible parameter values an equal, but low probability [87]. An example for such an uninformative prior used with the VB approach in previous works [25] is a normal distribution with zero mean and a variance of 10^4.

Throughout this thesis, the priors of all of the unknown parameters are set as informative priors, meaning that preliminary knowledge about the underlying physiology, from the literature and/or the data, will be used to specify them. The foundation for that has been been established in the previous section through the introduction of several methods for parameter transformations.

3.4 Parameter sensitivity

3.4.1 Practical identifiability

During the structural identifiability analysis described in section 3.2, it is assumed that the observation of the data is continuous and error-free, which cannot be upheld in practice. This could mean that a structurally identifiable parameter may not be estimated with acceptable precision because its effect on the model output is so minor that it cannot be distinguished from the measurement error. Such a parameter is called practically unidentifiable. Practical identifiability analysis therefore examines the estimability and precision of the obtained parameters after estimation [111].

In the context of Bayesian parameter estimation approaches, unknown parameters are inherently treated as random variables and specified by a PDF, meaning that quantifying their uncertainty is an essential part of the Bayesian method. Posterior estimates of this uncertainty thus provide a direct method for assessing practical identifiability [112]. In this thesis, the CV will be used to quantify the uncertainty of the parameters. This is particularly useful for log-normally distributed parameters where the posterior CV is guaranteed to be smaller or equal to the prior CV (see expression (3.23)). The comparison between prior and posterior CV can therefore be used to assess practical identifiability.

3.4.2 Sensitivity analysis

Sensitivity analysis assesses how the uncertainty in the model parameters, specified by the shape of its PDF, affects the model states and its output. This thesis uses this method in three scenarios, (1) to examine the effect of the PDF over a single parameter to assess its practical identifiability prior to model inversion, (2) to assess the output variability of different models to ensure similar variability and set the prior uncertainties accordingly and (3) to examine the uncertainty in the model output and states after model inversion. These analyses will be carried out using two different approaches.

The first approach is completely deterministic, local and implemented in the VB toolbox. It first uses the vector of means of the model parameters $\boldsymbol{\mu_\vartheta}$ to calculate the mean trajectories of model states. Secondly, the trajectories of model sensitivity discussed in section 3.3.2.2 and the covariance matrix of the model parameters and initial conditions $\boldsymbol{\Sigma_{p/x_0}}$ are used to calculate the covariance matrix of the model states

$\boldsymbol{\Sigma_{xt}}$ at each time step using [113]

$$\boldsymbol{\Sigma_{xt}} = \begin{bmatrix} \boldsymbol{S_{p_t}} \\ \boldsymbol{S_{x_0 t}} \end{bmatrix}^T \boldsymbol{\Sigma_{p/x_0}} \begin{bmatrix} \boldsymbol{S_{p_t}} \\ \boldsymbol{S_{x_0 t}} \end{bmatrix}. \tag{3.46}$$

The matrix $\boldsymbol{\Sigma_{xt}}$ can then be used to quantify the uncertainty in the model states and thus output over time. The disadvantage of this approach is that it assumes the model output to be normally distributed which is not necessarily the case.

The second method uses a global Monte Carlo approach and is therefore stochastic. It involves the repeated sampling of individual parameter point estimates from their respective distributions and subsequently simulating the model response over time. This can then be used to characterise the distribution over the model output and its states using suitable summary statistics such as median and interquartile range, without assuming a specific distribution.

An example of the two approaches is given in Figure 3.5. Here, it is demonstrated that the results of the deterministic and stochastic methods are similar for low levels of parameter uncertainty, but diverge in the case of larger uncertainties. This can be explained by the fact the Gaussian approximation assumed by the deterministic methods becomes less accurate for larger values of uncertainty.

3.5 Model comparison and selection

3.5.1 Overview

Throughout this thesis the modelling process will involve the proposal of several model candidates of differing structure and complexity and the subsequent inversion of the model candidates on the same dataset. This makes it necessary to compare the model candidates amongst each other. Bayesian approaches calculate the probability of a certain model M_i being true based on the collected data $\boldsymbol{y}$, using Bayes' theorem

$$p(M_i|\boldsymbol{y}) = \frac{P(\boldsymbol{y}|M_i)p(M_i)}{P(\boldsymbol{y})}, \tag{3.47}$$

where the function $p(\cdot)$ gives a single probability value. It should be pointed out that the in (3.9) defined marginal likelihood, or model evidence $P(\boldsymbol{y}|M_i)$, appears in the numerator and not in the denominator as in expression (3.8). If every model candidate
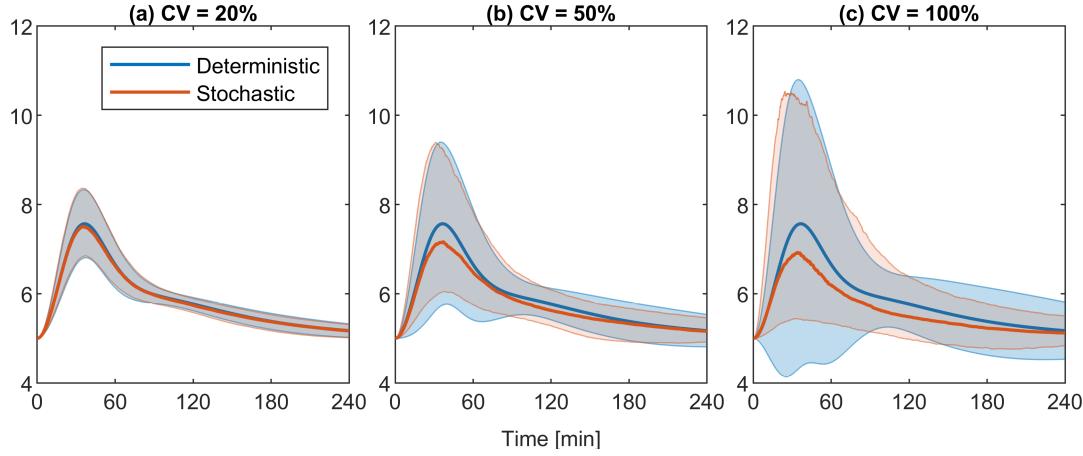
Figure 3.5: Comparison between deterministic and stochastic sensitivity analysis on an example model similar to the ones developed in this thesis with four log-normally distributed model parameters and fixed initial conditions. The three plots represent different levels of uncertainty in the model parameters with a CV of (a) 20 %, (b) 50 % and (c) 100 %. The deterministic analysis (blue) gives the model output from the point estimates of parameters and the standard deviation (shaded area) calculated from the covariance matrix $\boldsymbol{\Sigma}_{\boldsymbol{x}t}$. The results from the stochastic analysis (red) are based on 1000 Monte Carlo simulations summarised with the median and range between the 16th and 84th percentile (shaded area) to approximate the one-sigma range.

has the same prior probability $p(M_i)$, expression (3.47) can be simplified to

$$p(M_i|\boldsymbol{y}) \propto P(\boldsymbol{y}|M_i), \tag{3.48}$$

meaning that the posterior probability $p(M_i|\boldsymbol{y})$ is fully determined by the model evidence $P(\boldsymbol{y}|M_i)$. It thereby complies with the principle of parsimony, which means that it will favour the simplest possible model that fits the data, providing a trade-off between model fit and complexity [87].

In the context of VB model inversion, it was shown that the free energy $\mathcal{F}$ is a lower bound on the log of the model evidence and can, therefore, be used for model comparison [114]. The exact decomposition of the free energy term defined in expression (3.11) is highly complex (see [93, 114] for details) but depends on the sufficient statistics of the prior and posterior distributions as well as the model fit. To compare the free energy values between model candidates, the difference in $\mathcal{F}$ between pairs of models is calculated. A difference greater than three is considered to be strong evidence that the model with the higher free energy is superior. This threshold is related to the log of the Bayes factor, i.e. the ratio of marginal likelihoods of two models and represents a probability of greater than 95 % that the model with the higher free energy is superior [114, 115].

One drawback of using the free energy for model comparison is that the gap between the true model evidence and free energy can be different, depending on the model candidate. This gap is exemplified in Figure 3.2 and arises from fact that the free energy is only a lower bound estimate. For a particular model type known as mixtures of factor analysers model, Beal [102] showed that the gap between true model evidence and free energy is proportional to the number of parameters in the model, meaning that the free energy exhibits a bias towards simpler models in this particular case. Whether this also holds for the class of nonlinear state-space models considered here is unknown. The free energy will therefore only be one of multiple model comparison criteria used in this thesis. These additional criteria are dependent on the specific purpose of modelling approach and will be explained in the corresponding chapters.

Alternative to the free energy, there exist other model selection criteria such as Akaike's Information Criterion and the Bayesian Information Criterion. However, both of them are more course approximations to the log of the model evidence [87] and have been shown to posses a worse model selection ability in comparison to the free energy [114].

3.5.2 Bayesian model averaging

When multiple model candidates are compared, it is often the case neither of the candidates stands out as clearly superior, impeding the selection of a single most suitable model. To overcome this difficulty, this thesis will employ the process of Bayesian model averaging (BMA). This technique omits the need to select a single model and instead averages the inference results of individual models according to their probability of being true. It is not related to the mixed-effects modelling approach described earlier, as the BMA technique averages across different models, independently identified from the data $\boldsymbol{y}$ of a single subject. In this context, the individualistic approach is therefore kept, as no information between the data from different subjects is shared. In formal terms, BMA accounts for the model uncertainty by marginalising over individual models M_i to derive a single posterior density of model parameters

$$f_{\boldsymbol{\theta}|\boldsymbol{y}} = \sum_i p(M_i|\boldsymbol{y}) f_{\boldsymbol{\theta}|\boldsymbol{y}, M_i}, \qquad (3.49)$$

independent of the model, where $p(M_i|\boldsymbol{y})$ is the probability of any given model being true as defined in expression (3.47) and $f_{\boldsymbol{\theta}|\boldsymbol{y},M_i}$ the posterior density of unknown parameters from model M_i [87].

In the context of the VB approach $p(M_i|\boldsymbol{y})$ is determined by the model evidence $P(\boldsymbol{y}|M_i)$ (see expression 3.48) which is in turn approximated by the free energy $\mathcal{F}$. To approximate the probability of any model being true using individually inferred free energy values $\mathcal{F}_i$, the following expression is applied

$$\hat{p}(M_i|\boldsymbol{y}) = \frac{\exp(\mathcal{F}_i)}{\sum_i \exp(\mathcal{F}_i)}, \qquad (3.50)$$

which ensures that the approximated probabilities of individual models $\hat{p}(M_i|\boldsymbol{y})$ sum to one. Note that the exponential of the free energy is taken because $\mathcal{F}$ represents the logarithm of the model evidence, as demonstrated in expression (3.11) [116].

To calculate the sufficient statistics of averaged PDFs of model parameters $f_{\boldsymbol{\theta}|\boldsymbol{y}}$ the unknown parameter vector $\boldsymbol{\theta}$ is split into its components $\boldsymbol{\vartheta}$, i.e. model parameters and initial conditions, and κ, i.e. measurement uncertainty precision. For $\boldsymbol{\vartheta}$ the sufficient statistics $\boldsymbol{\mu_{\vartheta}}$ and $\boldsymbol{\Sigma_{\vartheta}}$ of the Gaussian PDF $f_{\boldsymbol{\vartheta}|\boldsymbol{y}}$ are calculated as follows:

$$\begin{aligned}
\boldsymbol{\mu_{\vartheta}} &= \sum_i \hat{p}(M_i|\boldsymbol{y})\boldsymbol{\mu_{\vartheta}^i} \\
\boldsymbol{\Sigma_{\vartheta}} &= \sum_i \hat{p}(M_i|\boldsymbol{y})([\boldsymbol{\mu_{\vartheta}^i} - \boldsymbol{\mu_{\vartheta}}][\boldsymbol{\mu_{\vartheta}^i} - \boldsymbol{\mu_{\vartheta}}]^T + \boldsymbol{\Sigma_{\vartheta}^i}),
\end{aligned} \qquad (3.51)$$

where $\boldsymbol{\mu_{\vartheta}^i}$ and $\boldsymbol{\Sigma_{\vartheta}^i}$ are the sufficient statistics of the parameter estimates of the individual models.

To calculate the sufficient statistics a and b of the combined Gamma PDF $f_{\kappa|\boldsymbol{y}}$ over κ, the sufficient statistics of the individual estimates of a_i and b_i are first used to calculate mean and variance of the respective PDFs using expression (3.36). Subsequently, expression (3.51) is used to calculate the averaged mean and variance which are then utilised to calculate a and b, defining $f_{\kappa|\boldsymbol{y}}$.

Lastly, the BMA framework makes it possible to combine the individual model states $\boldsymbol{x}_t$ and their uncertainty $\boldsymbol{\Sigma_{\boldsymbol{x}t}}$, as calculated by (3.15) and (3.46) respectively, into a single, averaged trajectory of the model states and uncertainty using expression (3.51) [104].

In order to apply the full BMA approach, i.e. average across all states and parameters, it is necessary for the model candidates to be similar, i.e. to have the same number of parameters and states, and only differ in the mathematical relationship between them. This obviously restricts the flexibility in model specification. Alternatively, when the models are less similar, it is still possible to use BMA and only average across the model output, as described in the previous paragraph, or parameters that have the same physiological interpretation.

3.6   Statistical methods

To evaluate the results of the model identification process, e.g. model parameters, several statistical methods will be employed. The statistical difference between groups of interest will be assessed using the Kruskal-Wallis test. It is a non-parametric test of whether the individual samples forming the groups are drawn from a single distribution [117]. Difference testing between any groups will then be performed using the Wilcoxon rank sum, also known as Mann-Whitney U, test. When multiple tests are performed, Tukey's honestly significant difference procedure will be used [118]. These non-parametric tests are chosen because the normality of the distributions cannot be assumed. As it is common practice in the study of glucose metabolism, the null hypothesis of "no difference between the groups" is tested at the 0.05 significance level (e.g. [47, 75–77]).

Chapter 4

Bayesian oral minimal model identification from mixed meal glucose and insulin responses in NGT subjects

4.1 Introduction

This chapter aims to identify the oral minimal model (OMM) selected in section 2.3 in order to estimate insulin sensitivity and meal-related rate of glucose appearance (GA) using a dataset containing glucose and insulin profiles from normal glucose tolerant (NGT) subjects. These results will subsequently be analysed with respect to the impact of meal composition, time of meal consumption and subject sex on these quantities.

The novelty of this work will be given by (1) adapting the OMM for the identification from non-fasting conditions, i.e incorporate the effects of a previously consumed meal, (2) demonstrating a novel structural identifiability result and (3) utilising the VB approach for parameter estimation. These adaptations are subsequently verified by comparing the results to published studies using the conventional approach for identifying the OMM. Before that, the conventional formulation of the OMM and identification approach is introduced.

4.2 The oral minimal model

The oral minimal model (OMM) of glucose dynamics was proposed in 2002 by Dalla Man et al. [71] and is based on an earlier model often referred to as *the* minimal model, which was developed for the description of glucose excursions during an intravenous glucose tolerance test (IVGTT) [119]. In contrast, the OMM describes OGTT and mixed meal responses and is formulated in a state-space representation with the following equations [71]

$$\frac{dG(t)}{dt} = -G(t)X(t) - p_1[G(t) - G_b] + \frac{Ra_{PL}(t)}{V}, \qquad G(0) = G_b \qquad (4.1)$$

$$\frac{dX(t)}{dt} = -p_2 X(t) + p_3[I(t) - I_b] \qquad\qquad X(0) = 0, \qquad (4.2)$$

with

$$Ra_{PL}(t) = \begin{cases} k_{i-1} + \dfrac{k_i - k_{i-1}}{t_i - t_{i-1}}(t - t_{i-1}) & \text{for} \quad t_{i-1} \le t \le t_i \quad i = 1 \dots n, \\ 0 & \text{for} \quad t > t_n. \end{cases} \qquad (4.3)$$

The glucose concentration and its basal (pre-test) level in mmol/L are represented by $G(t)$ and G_b, respectively. The state $X(t)$ in min^{-1} represents the insulin action in a remote (from plasma) compartment and governs insulin action in both the liver and peripheral tissues. Its initial condition $X(0)$ is assumed to be zero because all meal tests are typically carried out from a fasted state. The parameter p_1 in min^{-1} controls the ability of glucose to affect its own metabolism and is known as glucose effectiveness. This part of the model represents the insulin-independent aspect of glucose metabolism taking place, e.g. in the brain. The nonlinear term $-G(t)X(t)$ in equation (4.1) requires no rate coefficient due to the units of $X(t)$ and represents the insulin and glucose-dependent regulation of glucose. V with units L/kg represents the distribution volume of glucose relative to body weight. The glucose appearance in mmol/kg/min, described by function Ra_{PL}, is the only difference to the IVGTT minimal model and is formulated as a piecewise-linear function (4.3). The n breakpoints are located at times $t_0 - t_n$ in min with adjustable heights of $k_0 - k_n$ in mmol/kg/min [71]. An example of the function Ra_{PL} is provided in Figure 4.1. The specific number and locations of the breakpoints are adapted according to the experimental protocol and will be specified later.
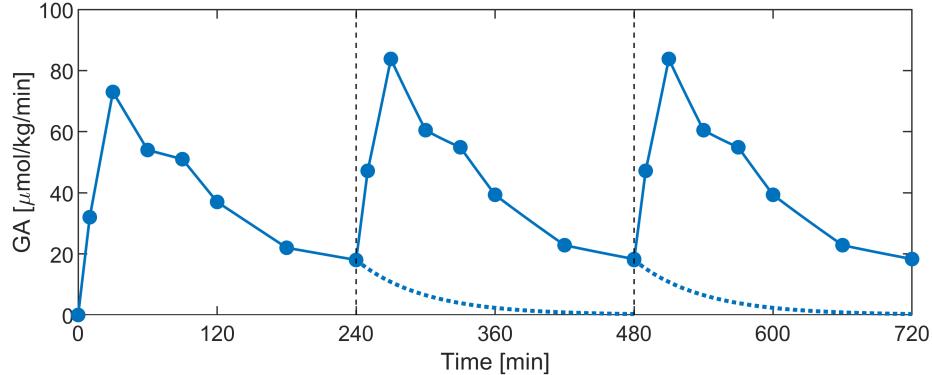
Figure 4.1: Example of the glucose appearance (GA) for three consecutive meals modelled as the sum of functions $Ra_{PL}(t)$ and $Rap(t)$ over the course of the modelled duration. The dotted lines represent the persisting absorption Rap during lunch and dinner. The dotted vertical lines indicate the time of meal consumption.

In order to avoid modelling the dynamics of glucose clearance and insulin secretion simultaneously, which could introduce a bias in insulin sensitivity through errors in model formulation, glucose and insulin systems are partitioned through the "loop cut" principle [7]. In the case of the OMM of glucose dynamics, the insulin concentration $I(t)$ and its basal (pre-test) level I_b in mU/L are considered to be known inputs [71]. This procedure has been criticised as it assumes the measured insulin concentration to be error free as well as disregarding the feedback effects between glucose and insulin levels [13].

In expression (4.2), the parameter p_2 in min^{-1} governs the intrinsic dynamics of the insulin action state $X(t)$. The parameter p_3 in min^{-2} per mU/L determines the amount of plasma insulin $I(t)$ above baseline I_b that contributes to the insulin action $X(t)$ which in turn affects the glucose metabolism in equation (4.1). The insulin sensitivity is subsequently given by the ratio p_3/p_2. This is shown below by using its formal definition from expression (2.1). Here it is assumed that the (negative) rate of change in the glucose concentrations (4.1) can be used as a proxy for the glucose clearance rate (GCR) [119], so that

$$
\begin{aligned}
\frac{\partial}{\partial I}\left[\frac{\partial GCR}{\partial G}\right] &= \frac{\partial}{\partial I(t)}\left[\frac{\partial}{\partial G(t)}\left(-\frac{dG(t)}{dt}\right)\right] = \frac{\partial}{\partial I(t)}\left[X(t)+p_1\right] \\
&= \frac{\partial}{\partial I(t)}\left[-\frac{1}{p_2}\frac{dX(t)}{dt}+\frac{p_3}{p_2}(I(t)-I_b)+p_1\right] = \frac{p_3}{p_2}.
\end{aligned}
\tag{4.4}
$$

In terms of parameter estimation, the IVGTT minimal model, which is identical in structure to the OMM except for expression (4.3), is typically identified with Bayesian

techniques as they have been shown to produce superior results in comparison to frequentist approaches [88–90, 120, 121]. In contrast, the most frequently used method to identify the OMM involves a commercial software package called SAAM II [122] (e.g. [71–73, 77, 123–126]), which employs a maximum likelihood, i.e. frequentist approach [127]. This method, however, gives the option to incorporate prior information and restrict individual parameters using a normal distribution [122]. This is referred to as "maximum a posteriori Bayesian estimation" [71], but cannot be considered to be equivalent to a fully Bayesian approach, where every parameter is modelled and estimated using a PDF. The approach in SAAM II instead gives single value estimates for the unknown parameters, as is common in all frequentist approaches. As mentioned in section 3.3, the associated parameter uncertainties are subsequently approximated from the inverse of the Fisher information matrix [127].

Using this frequentist approach for estimation of parameters in the OMM stands somewhat in contradiction to the full Bayesian methods used for the very similar IVGTT minimal model. To resolve this, this chapter will use the fully Bayesian VB method to estimate the parameters in the OMM.

4.3 Data description

The dataset utilised in this chapter was collected by Ahmed et al. [128] in 1976 and Nuttall et al. [29] in 1985 (collectively referred to as Nuttall dataset). It contains plasma glucose and insulin profiles from 26 young subjects (14 males, 12 females) with NGT, collected over 12 hours in a single day from 08:15 to 20:30. A total of three identical meals each providing 33 % of the total estimated daily calorie requirement were consumed at 08:30 (breakfast), 12:30 (lunch) and 16:30 (dinner), hereafter referred to as daily meals. Subjects took between 20 and 30 minutes to consume the meals. Blood samples were collected at the same time in each subject after meal consumption at 0, 2, 5, 10, 20, 30, 40, 50, 60 min, then every 15 min up to 120 min and then every 30 min up to 240 min. One additional fasting sample was collected before the consumption of breakfast, i.e. at -15 min. The coefficient of variation (CV) of the plasma glucose and insulin assays are given by 1.5 and 13.4 %, respectively [128].

Data from three different meal compositions, referred to as meal types, were used. The meals were consumed by three different subject cohorts assembled from the overall

population (see Table 4.1 for details), leading to a total of 33 glucose and insulin profiles. The first meal type was considered to be a standard diet (STAND) in 1980 according to the National Academy of Sciences of the USA [129]. In comparison, the second meal type is higher in CHO content (HCHO) and the third meal higher in protein content (HPROT). Despite these rather extreme variations in composition, the meals were considered to be "easily attainable by individuals in everyday living" [29]. The details of the meal composition are given in Table 4.1.

Table 4.1: Details on the subject populations and different meal types containing standard (STAND), high carbohydrate (HCHO) and high protein (HPROT) mixtures of macronutrient content. The meal composition is given in percentage of calories contained in the respective macronutrient content. The data are given as mean $\pm$ standard error and were taken from [29]

	STAND	HCHO	HPROT
No. of subjects (females)	12 (5)	10 (4)	11 (5)
Age	23 ± 1	25 ± 3	25 ± 2
Body weight (females) [kg]	76 ± 5 (59 ± 1)	77 ± 4 (59 ± 5)	80 ± 3 (57 ± 3)
Meal composition [% CHO/Fat/Protein]	40/49/11	63/27/10	19/40/41
CHO per meal (females) [g/kg body weight]	1.2 (1.1)	2 (1.8)	0.6 (0.5)
Calories per meal (females) [kcal/kg body weight]	13 (11)	13 (11)	13 (11)

The absolute amount of macronutrients provided was scaled according to the body weight of each individual subject. Additionally, female subjects received 12.5 % fewer calories per body weight to account for the sex differences in average body composition and therefore lean mass [129]. This is justified by the fact that lean mass is the main site of calorie consumption and substrate oxidization [130] and leads to slightly different meal characteristics between male and female subjects (Table 4.1). This adjustment is essential to make the results between male and female subjects comparable.

The Nuttall dataset is displayed in Figure 4.2 where the difference in response according to the meal type is apparent. The dataset fulfils all of the requirements stated in the first objective of this thesis for NGT subjects and will be utilised in Chapters 5

and [6].
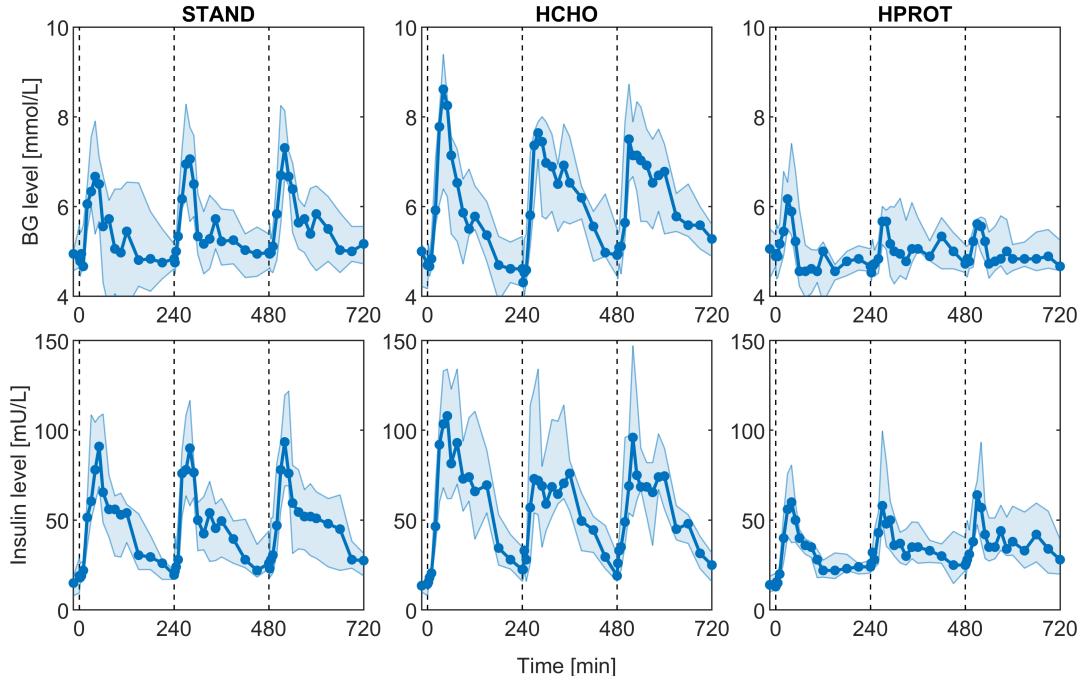
Figure 4.2: Glucose (top) and insulin (bottom) level profiles recorded in the Nuttall dataset for the three meal types. The profiles are given as median and interquartile range. The dashed vertical lines give the times of meal consumption.

4.4 Methods and modelling

4.4.1 Data analysis

In order to ensure the comparability between meal type and sex, a statistical analysis comparing fasting glucose and insulin levels between groups of interest is carried out. Fasting levels are calculated by averaging the results from the -15, 0, 2 and 5 min samples to counteract measurement errors.

4.4.2 Model formulation

In comparison to the conventional formulation of the OMM presented earlier in this chapter, the following adapted formulation is proposed

$$\frac{dG(t)}{dt} = -G(t)X(t) - p_1[G(t) - G_b] + \frac{Ra_{PL}(t) + Rap(t)}{V}, \quad G(0) = G_0, \quad (4.5)$$

$$\frac{dX(t)}{dt} = -p_2\left[X(t) + S_I[I(t) - I_b]\right], \quad X(0) = X_0, \quad (4.6)$$

where

$$Ra_{PL}(t) = \begin{cases} k_{i-1} + \dfrac{k_i - k_{i-1}}{t_i - t_{i-1}}(t - t_{i-1}) & \text{for} \quad t_{i-1} \le t \le t_i \quad i = 1\dots 7, \\ k_7 \exp(-\alpha(t - t_7)) & \text{for} \quad t > t_7. \end{cases} \tag{4.7}$$

The interpretation and units of model states and parameters remains unchanged in comparison to the conventional formulation of the OMM: $G(t)$, $X(t)$ and $I(t)$ represent the glucose concentration, insulin action and (known) insulin concentration, respectively. Parameters p_1, p_2, and V represent the glucose effectiveness, dynamic parameter for $X(t)$ and glucose distribution volume, respectively. The new adaptations are as follows

1. Due to the importance of the insulin sensitivity parameter S_I in min^{-1} per mu/L, it is directly included in the model rather than being the ratio of other parameters. This facilitates the definition and interpretation of the parameter PDF within the VB scheme.

2. To adhere to the experimental protocol of the Nuttall dataset and account for overlapping effects between meals, basal (G_b, I_b) and initial (G_0, X_0) values are characterised by separate, but known, parameters and fixed for every subject individually. G_b and I_b reflect the previously calculated fasting levels and are fixed over the entire duration covered by the dataset (12 hours). A recalculation of basal levels before every daily meal is unfeasible because it cannot be assumed that basal levels are reached before the next meal is consumed. To counteract this, the initial conditions G_0 and X_0 are reset for every meal, where G_0 is calculated as the average of the 0, 2 and 5 min samples. A similar approach for X_0 is not possible as this state is not directly observed, but inferred, by the model. As for the conventional OMM formulation, X_0 is set to 0 before breakfast, assuming no active insulin due to the fasting state of the subjects. For the subsequent meals (lunch and dinner) this assumption cannot be justified, so X_0 is set to the last inferred value from the previous meal, i.e. $X(240)$.

3. To define the piecewise-linear function Ra_{PL} the number and positions of breakpoints in expression (4.7) have to be chosen in accordance with the response duration of 240 min. In this work, Ra_{PL} contains eight fixed breakpoints, located at 0, 10, 30, 60, 90, 120, 180 and 240 minutes, ($t_0 - t_7$), with heights $k_0 - k_7$. The height at time zero, i.e. k_0, is fixed to zero. After the end of the meal period,

i.e. 240 min, the function is modelled by a monoexponential decay with rate α, fixed at 0.017 min^{-1} (equivalent to a half-life of circa 41 minutes) as suggested by Dalla Man et al. (2002) [71] for response durations shorter than 6 hours. This means that, for lunch and dinner, there is a persisting absorption from the previous meal overlapping with the glucose appearance of the current meal (see Figure 4.1). Following that, the total appearance in (4.5) is modelled as the sum of the appearance from the current meal and the remaining appearance from the previous meal $Rap(t)$. This persisting absorption is calculated by extending the absorption from the previous meal beyond the response duration of 240 min, i.e. $Rap(t) = Ra_{PL}(t + 240)$. An example of the modelled glucose appearance, i.e. the function Ra_{PL} is shown in Figure 4.1.

The procedure to account for the overlapping effects between meals is depicted schematically in Figure 4.3.
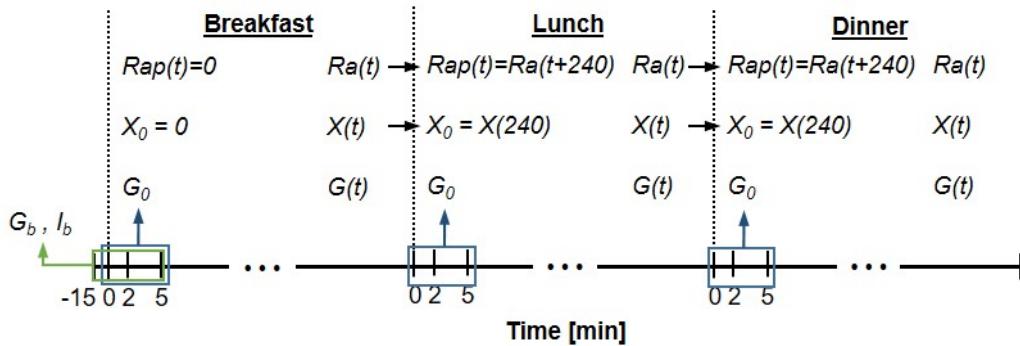
Figure 4.3: Schematic depiction of the procedure to account for the overlapping effects between meals.

Following the general model formulation given in section 3.1, the glucose measurement process is modelled as follows

$$y(t) = G(t) + \varepsilon \qquad \text{with} \qquad \varepsilon \sim \mathcal{N}(0, \lambda^2), \tag{4.8}$$

where $y(t)$ is the observed plasma glucose concentration and ε is the additive, normally distributed measurement error with zero mean and standard deviation λ, the use of which has been justified in section 3.1. Following the conventional approach and due to the well-established, highly accurate glucose measurement process, the measurement error is fixed based CV of the glucose assay not updated during parameter estimation [71]. In order to ensure comparability to the literature a CV of 2 % [71, 72, 77], instead

of the 1.5 % given for the Nuttall dataset, is used. Based on a mean BG level of 5.5 mmol/L across the Nuttal dataset and a measurement error CV of 2 %, the PDF over λ is characterised with a mean of 0.11 mmol/L and a CV of 10 %. This PDF over λ is then transformed into a PDF over the measurement noise precision κ using the procedure described in section 3.3.2.2.

To aid estimation of the GA parameters and include knowledge about the consumed food, Dalla Man et al. (2002) [71] have suggested that the area under the curve (AUC) of glucose absorption A is constrained based on the amount of CHO contained in the meal, and given by the following expression (see Appendix A.2 for the derivation):

$$A = \int_0^\infty Ra_{PL}(t)dt = \frac{1}{2}\sum_{i=1}^{7}(t_i - t_{i-1})(k_i + k_{i-1}) + \frac{k_7}{\alpha} = D \cdot f. \qquad (4.9)$$

where D is the amount of glucose in the meal per kg of body weight, known from the experimental details, and f is the fraction of ingested glucose that enters the peripheral circulation. If the value of f is assumed to be known (see Table 4.2 for the value) as suggested by Dalla Man et al. (2002) [71], one of the height parameters defining Ra_{PL} becomes obsolete. In this work, the height k_6 of the breakpoint at 180 min is chosen to be replaced by the following expression

$$k_6 = \frac{1}{60\alpha}[D \cdot f \cdot \alpha - k_7 - 5\alpha \cdot (3k_1 + 5k_2 + 6k_3 + 6k_4 + 9k_5 + 6k_7)]. \qquad (4.10)$$

This is the result of rearranging expression (4.9) and inserting the specific values for t_0 to t_7. The choice to replace k_6 is based on results reported by Dalla Man et al. (2002) [71], showing that the mean inferred value of GA at 180 min lies linearly between 120 and 240 min, indicating a minor influence on glucose absorption dynamics.

4.4.3 Structural identifiability analysis

In their publication, Dalla Man et al. (2002) [71] presented a structural identifiability analysis using the previously introduced Taylor series approach on the conventional formulation of the OMM provided in section 4.2. Calculating the first three Taylor series coefficients, it was shown that only the ratios k_i/V for all i are identifiable, concluding that the distribution volume V should be fixed to a known value. To evaluate the identifiability of the remaining parameters p_1, p_2 and p_3, three additional Taylor series coefficients were calculated. These could then be reduced to a system of two equations

with three unknown parameters which led to the conclusion that p_1, p_2 and p_3 are only structurally locally identifiable. This issue was resolved by assuming the parameter p_1 to be known, thus making the remaining parameters p_2 and p_3 structurally globally identifiable. This result has been used by all studies utilising the OMM (e.g. [71–73, 77, 123–126]) as well as being explicitly mentioned in the review papers [7, 13, 74] and a textbook [8].

Using a software tool named DAISY, Saccomani et al. [131] give the result that parameters p_1, p_2 and p_3 are all globally identifiable. DAISY utilises differential algebra approach combined with a random number based numerical optimisation to test for global identifiability [132]. Saccomani et al. hypothesised that the discrepancy with the initial result might arise from the fact that the Taylor series expansion was truncated too early [131].

In this thesis, the conjecture formulated by Saccomani et al. [131] can be confirmed by combining the Taylor series approach with symbolic computation. Using one additional Taylor coefficient, i.e. a total of seven, allows for a unique solution for the unknown parameters, therefore showing that the parameters p_1, p_2 and p_3 are all structurally globally identifiable. This disproves the earlier results of Dalla Man et al. (2002) [71]. In this context, it should be mentioned that the corresponding results, i.e. the structural global identifiability of p_1, p_2 and p_3, were obtained for the IVGTT minimal model [133]. Here, Chin et al. [133] also highlighted the fact that the structural identifiability of parameter p_2 is dependant on the knowledge of higher order derivatives of the insulin concentration time profile.

The details of the identifiability analysis are presented in Appendix B.2.1 and B.2.2. In Appendix B.2.1, the OMM is first taken in its conventional form (4.1) - (4.3) and the new structural identifiability results are shown. Appendix B.2.2 confirms these results for the altered formulation of the OMM (4.5) - (4.7) presented in this chapter. The result is that parameters p_1, p_2, S_I, k_1, k_2, k_3, k_4, k_5 and k_7 are all globally identifiable if the distribution volume V is assumed to be known.

4.4.4 Choice of prior distributions

The VB approach requires suitable prior distributions for the unknown parameters, i.e. p_1, p_2, S_I, k_1, k_2, k_3, k_4, k_5 and k_7, which are defined based on existing information.

Additionally, values for the fixed parameters V and f have to be set. For that, the results of a study by Dalla Man et al. (2004) [72] are utilised. This study used additional data from traced glucose to estimate all unknown model parameters of the OMM including p_1, V and f in 88 NGT subjects consuming mixed meals.

The system parameters p_1, p_2 and S_I have to be positive as they would lead to unstable model behaviour otherwise. Similarly, the heights of the input function breakpoints have to be positive because negative GA rates are physiologically implausible. All parameters are thus constrained to be positive through the exponential mapping explained in section 3.3.2.2, making them log-normally distributed. The choice of the prior medians and CVs will be justified in the following sections. For that, the results from the study by Dalla Man et al. (2004) [72], mentioned in the previous paragraph, are used to compare the observed population distributions over parameters p_1, p_2 and S_I, with the respective prior distributions chosen in this thesis. Here, the goal is not to match the population densities exactly, but instead ensure that the chosen prior distributions assign the large majority of parameter values observed in the population a suitable probability density. The details of prior distributions for all inferred parameters are given in Table 4.2, together with the values of the fixed parameters. These fixed parameters were either directly calculated from the information contained in the dataset or are based on recommended values from the literature.

Table 4.2: Details on the unknown model parameters, their prior distributions and fixed values used in the identification of the OMM. The prior distributions are log-normally distributed and specified as median $\pm$ coefficient of variation (CV) in %.

Parameter	Unit	Prior median $\pm$ CV %	Description
p_1	min⁻¹	0.025 $\pm$ [0, 25, 50,100] [72]	Glucose effectiveness
p_2	min⁻¹	0.012 $\pm$ 40 [72]	Rate constant governing the decay of $X(t)$
S_I	10^{-4} min⁻¹ per mU/L	7.1 $\pm$ 100 [72]	Insulin sensitivity
k_1, k_2, k_3, k_4, k_5 and k_7	μmol/kg/min	[3.2, 7.3, 5.4, 5.1, 3.7, 1.8] $\pm$ 50 [72]	Levels of GA at time of break-points. The priors are scaled by $D \cdot f$ to account for the different meal types
V	L/kg	0.145 (fixed) [72]	Glucose distribution volume

λ	mmol/L	0.11 ± 10 (fixed)	Standard deviation of measurement error
t_0 - t_7	min	[0, 10, 30, 60, 90, 120, 180, 240] (fixed) [71]	Times of breakpoints
α	min^{-1}	0.017 (fixed) [71]	Decay rate of Ra_{PL} after 240 min
f	-	0.9 (fixed) [72]	Fraction of ingested glucose that is absorbed
D	mmol/kg	(fixed)	Amount of CHO per kg of body weight (see Table 4.1)

4.4.4.1 Parameter p_1

In light of the novel structural identifiability results obtained regarding the parameter p_1 describing the glucose effectiveness, its impact on the parameter estimation as a whole has to be examined. This is accomplished by repeating the parameter estimation procedure with four different levels of prior uncertainty, i.e. a prior CV of 0 (fixed), 25, 50 and 100 %. The median is kept the same at 0.025 min^{-1} in all cases, representing the recommend fixed value [72]. A comparison between the different prior distributions and the population distribution from [72] is shown in Figure 4.4.
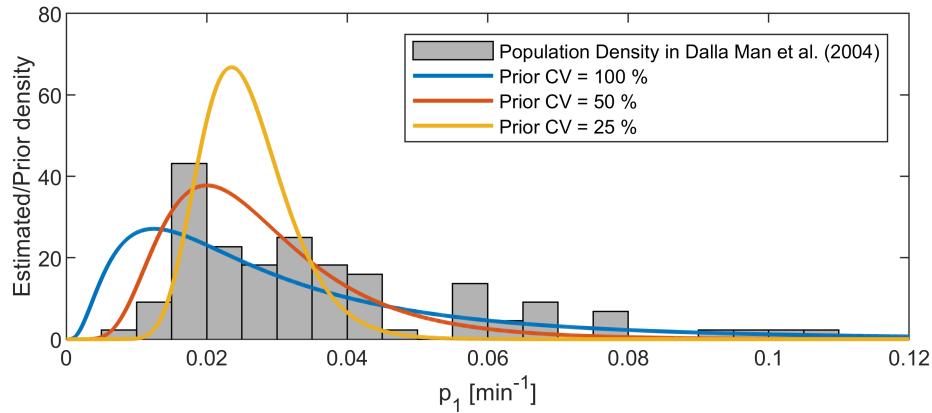
Figure 4.4: Comparison of the observed population distribution for the parameter p_1 by Dalla Man et al. (2004) [72], and the selected prior distributions over p_1 considered in this work.

4.4.4.2 Parameter p_2

The parameter p_2, governing the intrinsic dynamics of the state $X(t)$ is the only parameter constrained by a Gaussian prior in the context of using the previously mentioned

SAAM II software tool. Specifically, it has been suggested to define a prior distribution over the square root of p_2 with a mean of 0.11 min$^{-1/2}$ and small CV of 10 %. This was justified by the fact that, unlike p_2 itself, the square root of p_2 follows a normal population distribution. Additionally, the very narrow prior distribution was justified by the fact that poor posterior precisions were obtained when wider priors were used [72].

Using these values and applying the previously used theorem (3.21) for the transformation of PDFs, it can be shown that the resulting prior distribution over p_2 is rather complex and can be approximated to have mean of 0.012 min^{-1} and a CV of 20 % (see Appendix A.3 for the derivations). We propose to use the more tractable exponential mapping resulting in a log-normal distribution over p_2. Additionally, a larger CV of 40 % is adopted to better reflect the population distribution from [72]. A comparison of the respective distributions is shown in Figure 4.5 .
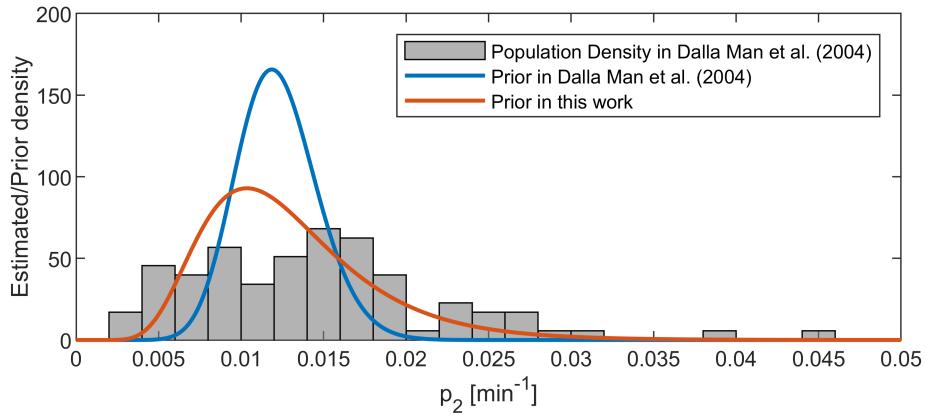
Figure 4.5: Comparison of the observed population distribution for the parameter p_2 by Dalla Man et al. (2004) [72], the subsequently used prior distribution and the prior distribution suggested in this work.

4.4.4.3 Parameter S_I

The median for the prior distribution of S_I, representing insulin sensitivity, is based on the population median of S_I in [72]. Taking the differences in insulin measurement techniques into account, a larger CV of 100 % in comparison to the population CV of 55 % is chosen in this thesis . This can account for any bias caused by the differences in insulin measurement methods. The chosen prior distribution in comparison to the population results in [72] is shown in Figure 4.6
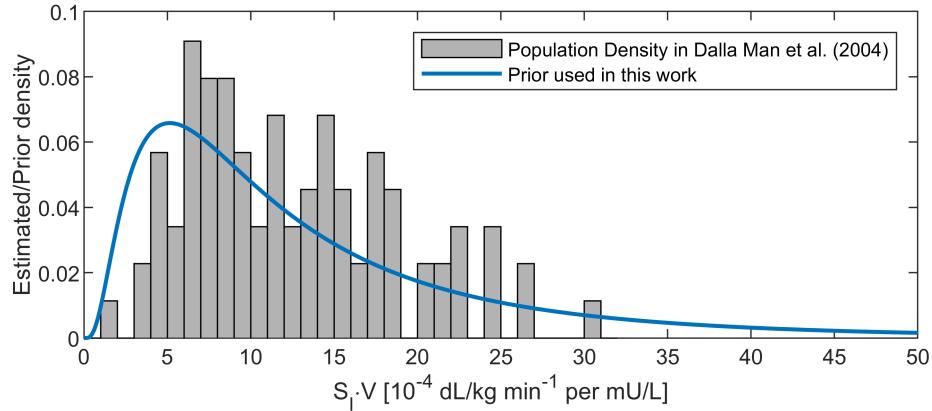
Figure 4.6: Comparison of the observed population distribution of the insulin sensitivity S_I multiplied by the distribution volume V by Dalla Man et al. (2004) [72] and the prior distribution suggested in this work. The prior was scaled to represent a distribution over $S_I \cdot V$ solely to be comparable with the reported results.

4.4.4.4 Parameters k_1 to k_7

The medians for the prior distributions of the input function parameters k_1, k_2, k_3, k_4, k_5 and k_7 are based on the population medians in [72]. The values are scaled according to the glucose content of the meals so that only the shape, but not the AUC, is conserved. The CVs of the prior distributions are set to be 50 % based on the population results in [72]. An example of the prior shape of Ra_{PL} is shown in Figure 4.1.

4.4.4.5 Influence on the model output

In order to demonstrate the influence of the individual parameters and their prior distributions on the model output, several model simulations were carried out. For that, the value of one parameter is varied at a time across the two-sigma range of its prior distribution, while the other parameters are kept fixed at their prior medians. The results are given in Figure 4.7. For the system parameters in plots (a) - (c), it is shown that the parameters p_1 and p_2 have a similar effect on the model output and that the parameter S_I has the greatest effect on the overall model output. Regarding the input parameters in plots (d) - (h), it is demonstrated that the different parameters influence different time periods of the response. Furthermore, the influence of fixing the total AUC of Ra_{PL} is shown by the fact that a change in all input parameters affects the model output after the 180 min because it is the breakpoint height k_6 which is dependant on all other input function parameters as described by expression (4.10).
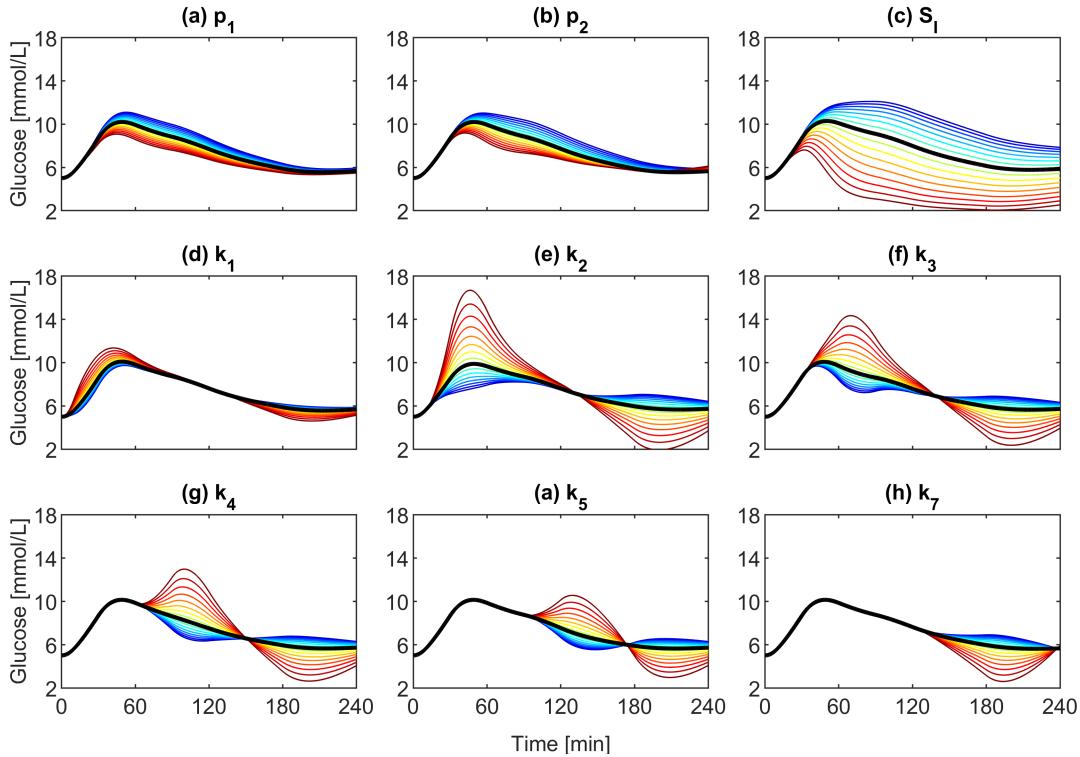
Figure 4.7: Influence of the individual model parameters p_1, p_2, S_I, k_1, k_2, k_3, k_4, k_5 and k_7 (a)-(h) on the model output of the OMM. The value of one parameter is varied at a time across the two-sigma range of its prior distribution, while the other parameters are kept fixed at their prior medians. The colours indicate the increasing parameter values from blue to red and the black lines indicate the responses from the prior medians. A prior CV of 25% was used for parameter p_1 in (a). As the insulin input, the averaged insulin profile from the STAND meal was used.

4.4.5 Parameter estimation procedure

One set of unknown parameters is estimated from every single meal response in the Nuttall dataset using the VB approach. The implementation details of the model and its priors within the VB toolbox are given in Appendix C.1.1. Furthermore, the associated MATLAB code is published online (https://github.com/manueich/VBA-OMM). The model is fully implemented with the piecewise linear definition of the function Ra_{PL}, so that the model equations (4.5) - (4.7) can be solved over the entire response duration and all parameters can be estimated simultaneously. In order to provide the insulin concentration profile as known input, it is linearly interpolated from the measurement time points over the integration time step of 0.1 minutes.

4.4.6 Validation of the parameter estimation procedure

The validation of the parameter estimation procedure is carried out in two steps. In the light of the novel structural identifiability results for parameter p_1, the first step examines the impact of an adjustable parameter p_1 on the estimation results. For that, the estimation procedure is repeated with different prior uncertainties of p_1, i.e. a CV of 0 (fixed), 25, 50 and 100 %, as previously described. The most suitable prior is then selected according the following criteria: (1) the free energy, as it can judge whether the added complexity from including p_1 as a parameter is justified by an improved model fit, (2) the root mean squared error (RMSE) between the model output and the data, and (3) the posterior distributions over the parameters p_1 and S_I, with emphasis on the posterior CVs to assess practical identifiability. This will lead to a choice on the most appropriate prior distribution of p_1.

After the most suitable prior over p_1 is selected, the second step examines the validity of the estimation results as a whole by comparison to the results in the literature. Included are results from studies identifying the OMM under similar conditions, i.e. populations only consisting of NGT subjects and utilising responses from OGTT or mixed meal tolerance tests (MTT). If provided in the selected publications, the following inference results will be compared:

- Inferred values and precisions of the parameter p_2.

- Posterior precision, i.e. the CV, of S_I. Absolute values cannot be compared due to the differences in insulin measurement methods. They are nevertheless included to illustrate the differences in the results.

- Quality of model fit. To allow comparison to the results from the selected publications, the residuals between the model output and the data are weighted by the measurement uncertainty characterised with a CV of 2 % and calculated from each modelled response, with the following expression:

$$W_{RES}^i = \frac{y_i - G_i}{0.02 \cdot y_i},\tag{4.11}$$

where W_{RES}^i is the value of weighted residuals calculated from the measurement point y_i and model output G_i at time point i. Subsequently, the weighted residuals are averaged at each measurement point across all inferred responses to give a time

profile of the averaged weighted residuals. To have a single value for comparison, the absolute value of this time profile is calculated and subsequently characterised by its mean and standard deviation.

4.5 Results and discussion

4.5.1 Fasting glucose and insulin

The results of analysing fasting glucose and insulin levels are displayed in Figure 4.8. The fasting glucose levels are not significantly different between meal types, but significantly different between sexes. This sex difference aligns with the findings from a study examining a very large cohort ($\sim$10 000) of the Australian population [134]. Significant differences in fasting insulin levels are not detected. These results demonstrate that the experimental protocol has not introduced any significant bias and shows that the modelling results can be compared between meal types and sex.
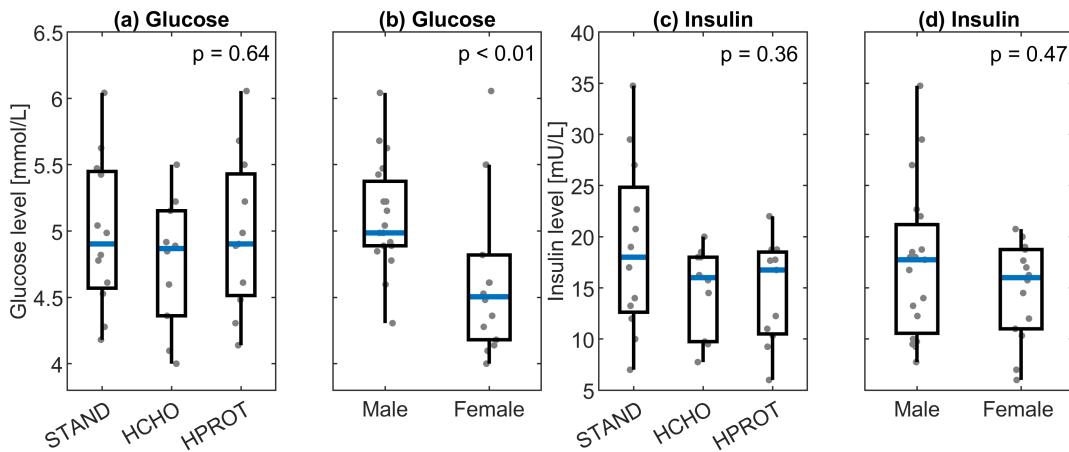
Figure 4.8: Fasting levels of (a)-(b) glucose and (c)-(d) insulin grouped according to meal type and sex. The p-values give the results of the Kruskal-Wallis test (meal types) and the Wilcoxon rank-sum test (sex).

4.5.2 Parameter estimation procedure

4.5.2.1 Impact of the parameter p_1

The results of the first validation step, i.e. repeating the estimation procedure with different levels of prior uncertainty over p_1, are displayed in Figure 4.9. In terms of the mean RMSE displayed in Figure 4.9 (a), there is a minor tendency towards a decreased error with increased prior uncertainty. This can be explained by increased flexibility in

model output and therefore increased model fit. For the posterior results for p_1 displayed in Figure 4.9 (b)-(c), there is an expected increase in the variability of the medians (b) and an increase in the posterior CV (c) along with greater prior uncertainty. In the case of a prior CV of 25 %, there is almost no convergence to a more narrow posterior distribution over p_1, which shows that this parameter cannot be estimated beyond a certain level of precision.
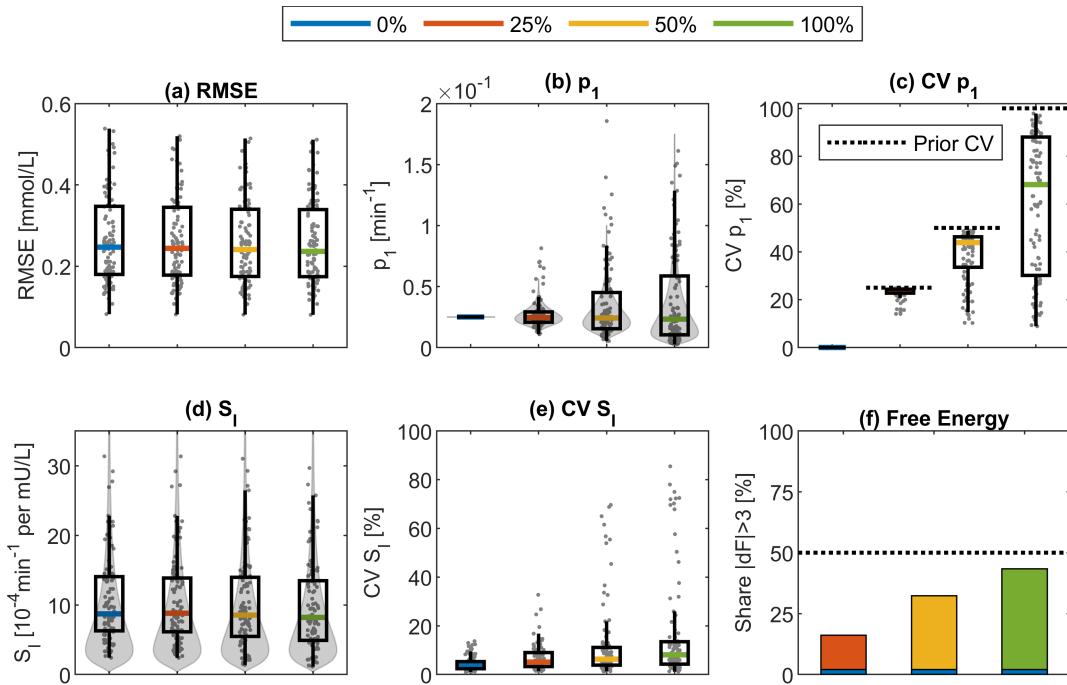
Figure 4.9: Results from identifying the OMM with different levels of prior uncertainties in p_1 indicated by different colours. Displayed are population boxplots of the (a) RMSE, posterior medians and CVs of parameters (b)-(c) p_1 and (d)-(e) S_I. The shaded grey areas in plots (b) and (d) indicate the log-normal prior distributions. Plot (f) shows the share of the responses where the free energy difference between the model with fixed p_1 and the respective models with variable p_1 is greater than three. The red, yellow and green portions of the bars indicate models with variable p_1 to be superior and the blue portion the model with fixed p_1 to be superior.

Regarding the posterior results for S_I displayed in Figure 4.9 (d)-(e), there is only a minor effect on the posterior medians (d), but an increase in the posterior CV (e), along with greater prior uncertainty in p_1. The parameter S_I remains practically identifiable, but the results exemplify how the uncertainty in one parameter can affect another parameter. The results of the free energy analysis displayed Figure 4.9 (f) demonstrate that there is no significant difference in free energy between the model with fixed p_1 and the models with variable p_1 in the majority of cases as indicated by the bars lying below 50 %. When a difference occurs, the models with an adjustable p_1 are superior

to the model with fixed p_1 as indicated by the very small blue bar.

Overall, these results demonstrate that it is difficult to identify the glucose effectiveness parameter p_1 with acceptable precision in practice. This is a general weakness of the OMM because it prohibits the interpretation of the glucose effectiveness with respect to subject and meal characteristics. We nevertheless argue that fixing p_1 to its population median as was done in all previous works using the OMM, is not suitable. The reasons for this are as follows: (1) it would ignore the large population variability in p_1 demonstrated in Figure 4.4, (2) it leads to an underestimation of the uncertainty in S_I demonstrated in Figure 4.9 (e), and (3) the free energy indicates the superiority of models with an adjustable p_1. It is therefore suggested to use an adjustable p_1 with a CV of 25 %. This provides the best trade-off between considering the observed population variability and an acceptable estimation accuracy for the insulin sensitivity S_I.

4.5.2.2 Parameter estimates and correlation

Based on choosing a prior CV of 25 % over the parameter p_1, the results of the parameter estimation procedure as a whole are presented in Figure 4.10. The population distribution of the parameter p_1 in plot (a) follows the prior distribution. Together with the fact that the posterior CVs of p_1 in (b) only marginally decreased from the the prior CV of 25 % implies practical identifiability issues in this parameter, as discussed in the previous section. In the case of the parameter p_2 the population distribution in (a) has shifted with respect to the prior PDF, indicating that the individual posterior densities are informed by the data. The posterior CVs in Figure 4.10 (b), however, show large variability, indicating that the parameter cannot be estimated with adequate precision in a significant number of cases. Given these difficulties in the estimation of parameters p_1 and p_2, an analysis of these parameters with respect to meal time, composition or sex will not be carried out. In contrast, the insulin sensitivity parameter S_I shows excellent convergence to low posterior CVs with very few outliers as indicated in Figure 4.10 (b). The overall median posterior CV of S_I is 5.1 % in comparison to the prior CV of 100 %. This high estimation accuracy could be achieved despite the introduction of additional uncertainties through the adapted priors over p_1 and p_2, therefore justifying the prior choices and demonstrating the aptitude of the VB model inversion approach. A more detailed analysis of the S_I estimates will be presented in section 4.5.3.
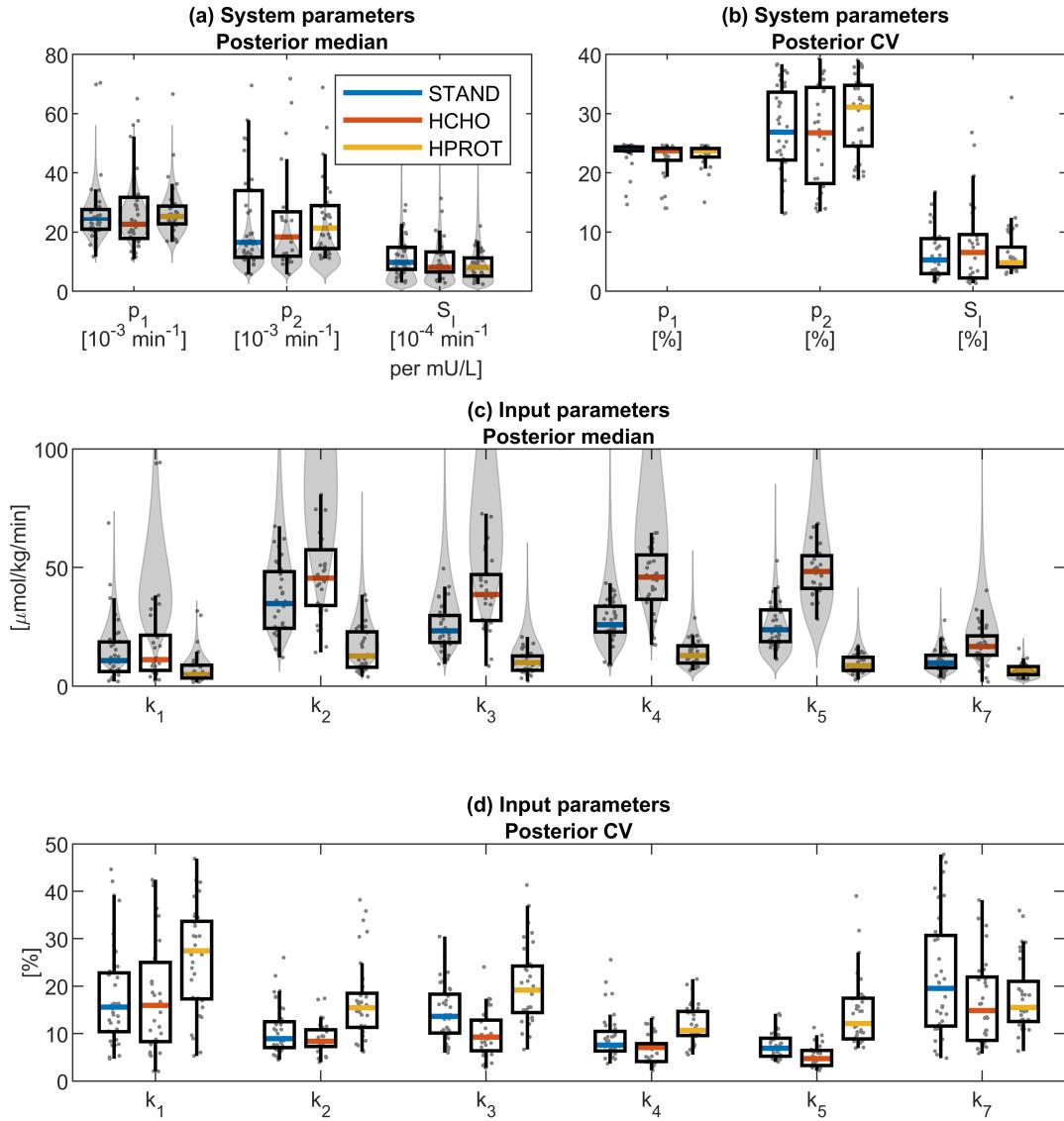
Figure 4.10: Posterior parameter estimates of the OMM. Displayed are the population boxplots of median and CV of the log-normal posterior distributions of (a)-(b) system parameters and (c)-(d) input parameters, grouped according to the meal types of standard (STAND), high CHO (HCHO) and high protein (HPROT) composition. The shaded grey areas indicate the respective prior distributions.

The results of the posterior medians of the input parameters in Figure 4.10 (c) show the expected differences between the meal types due to the differences in the fixed AUCs of Ra_{PL}. The posterior CVs of the input parameters in Figure 4.10 (d) demonstrate satisfactory convergence to more narrow posterior distributions with an overall median of 14.3 % in comparison to the prior CV of 50 %. Of note is that the posterior CVs are increased if the parameter median is decreased, as seen in the HPROT meal. This indicates that it is difficult to estimate low glucose appearance rates with adequate precision.

To investigate the sensitivity of the parameter estimation results with respect to the assumptions made on the fixed values of V and f, i.e. the glucose distribution volume and fractional glucose absorption, the model was inverted with different fixed values of V and f, covering the range of values found in [72]. The results show that parameters p_1 and p_2 are only marginally affected by changes in V and f. In contrast, the insulin sensitivity parameter S_I is highly affected with a proportional relationship to an increase in f and an inverse proportional relationship to an increase in V. As was already concluded by Dalla Man et al. (2004) [72], the fact that population values for V and f have to be assumed impedes the accurate estimation if S_I on an individual level. The details of the results are given in Appendix D.1.

The correlation of the model parameters, assessed through the posterior covariance matrix as described in section 3.3.2.2, is displayed in Figure 4.11. Here, the majority of correlations are small and thus non-significant. Exceptions are the correlations between parameter p_2 and the parameters S_I, k_2, k_3 and k_7 as well as the correlations between k_7 and k_3 and k_4. These correlations can be partially explained by the fact that the associated parameters have a similar effect on the model output, as demonstrated in Figure 4.7, but do not warrant a reparameterisation of the model.
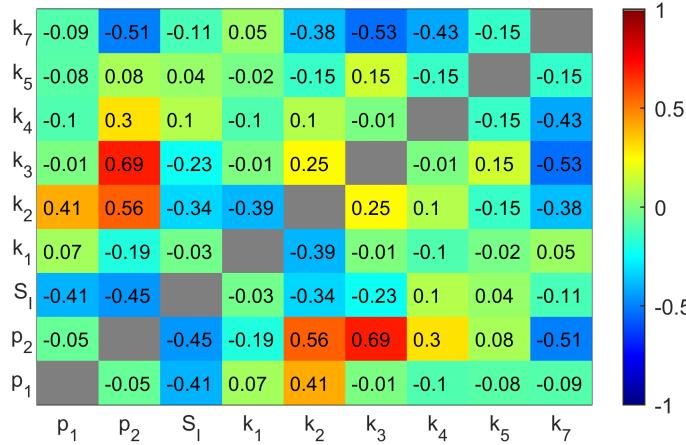
Figure 4.11: Median posterior parameter correlation matrix from the individually estimated parameter correlation matrices of all 99 responses.

4.5.2.3 Model fit

To demonstrate the ability of the novel OMM procedure to describe the data of responses from different meal compositions, the respective time profiles of averaged weighted residuals is displayed in Figure 4.12. Here it is demonstrated that the weighted residuals

are largely contained withing the -1 to +1 range, indicating good model fit. Of note is a bias towards negative residuals within the first 30 min of the response. This is a weakness of the piecewise-linear input function and will be addressed in the following chapter. To further illustrate the model fit, an example of the model output for each meal type is given in Figure 4.13.
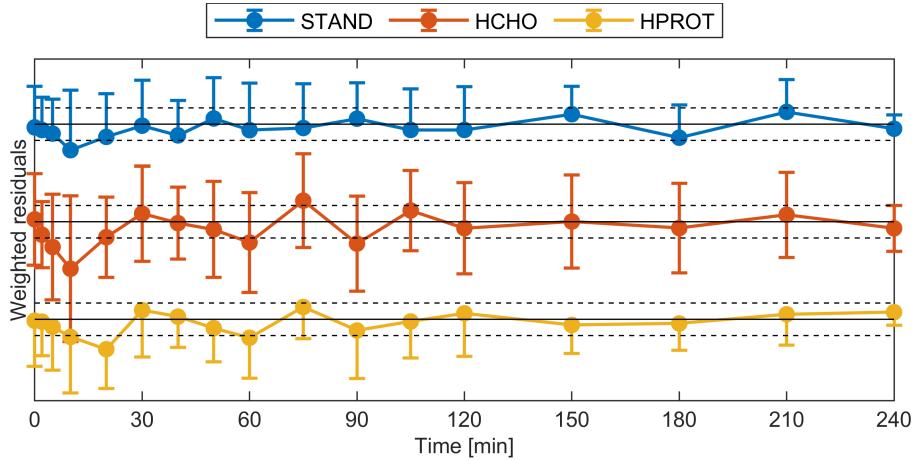
Figure 4.12: Time profile of the mean and standard deviation of the weighted residuals between the model output and data for each meal type. The solid horizontal lines indicated a value of zero and the adjacent dashed lines the -1 to +1 range.
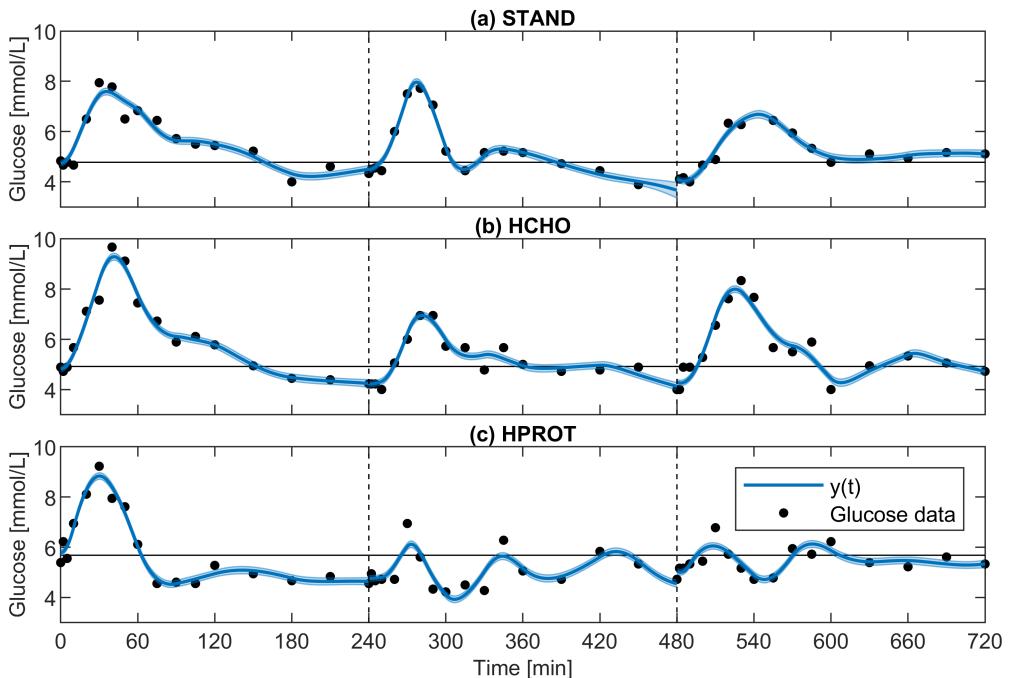
Figure 4.13: Examples of the model output for the three meal types of (a) standard (STAND), (b) high CHO (HCHO) and (c) high protein (HPROT) composition. The shaded area represents the uncertainty (standard deviation) from a deterministic sensitivity analysis and the solid black line provides the basal glucose level G_b.

4.5.2.4 Comparison to the literature

To validate the parameter estimation procedure against the literature, we included six studies matching the inclusion criteria of having a NGT subject population and using data from either mixed meals [71, 72, 77, 123] or OGTT responses [125, 126]. The comparison is provided in Table 4.3.

The number of sampling points and intervals between the Nuttall dataset and literature studies are similar making the overall estimation results comparable. This is an important aspect to consider as the estimation precision of the parameters is typically affected by the number and position of the sampling points. As with the Nuttall dataset, it is common to sample at irregular intervals with a tighter sampling grid at the beginning of the test. Additionally, OGTTs allow for shorter meal durations compared to mixed meals.

In terms of the parameter p_2, only one study provides posterior results. Here, the population standard error of point estimates and the population mean of posterior CVs are lower. This is most likely the consequence of the more narrow prior distribution, of 20 % chosen by Dalla Man et al. (2004) [72], whereas our work utilised a CV of 40 %. Additional to the changes in prior distributions, the bias in population point estimates could additionally be a result of potential biases introduced by the insulin measurement techniques.

The posterior CV of S_I clearly demonstrates that insulin sensitivity can be estimated with a precision comparable to the literature results. The absolute values of S_I are very similar in studies [71, 72, 77, 123] owing to the fact they were conducted by the same research group and used insulin assays from the same manufacturer. When the OMM is utilised by independent groups as it is the case in this thesis and studies [126] and [125], differences in population means are observed, most likely due to differences in insulin measurement methods.

The weighted residuals found in our work are very similar in comparison to the literature results in Table 4.3. This confirms the results of the previous section and indicates that the model fits the data with comparable accuracy.

Table 4.3: Comparison of the results of this work and the literature. If provided, values are given as population mean $\pm$ and population standard error (SE) or standard deviation (SD), to make it comparable with the literature. In the case of an empty cell, the respective results were not reported by the authors of the study.

	Present work	Dalla Man et al. (2002) [71]	Dalla Man et al. (2004) [72]	Dalla Man et al. (2005) [123]	Saad et al. (2012) [77]	Theodorakis et al. (2017) [126]	Geragotou et al. (2016) [125]
Type of Test	MTT	MTT	MTT	MTT	MTT	OGTT	OGTT
No. of samples (Duration [min])	17 (240)	21 (420)	21 (420)	21 (420)	13 (360)	10 (120)	10 (210)
p_2 mean $\pm$ SE [10^{-3} min^{-1}]	25 ± 2	-	11 ± 0.5	-	-	-	-
CV p_2 mean $\pm$ SE [%]	27.7 ± 0.7	-	15 ± 0.7	-	-	-	-
S_I mean $\pm$ SE [10^{-4} min^{-1} per mU/L]	10.5 ± 0.6	6.8 ± 0.7	8.1 ± 0.5	7.9 ± 0.6	6.3 ± 1.1	17.7 ± 1.8	20.3 ± 2.8
CV S_I mean $\pm$ SE [%]	6.9 ± 0.5	2.8 ± 0.3	7 ± 0.3	5	-	17.3	-
$|W_{RES}|$ mean $\pm$ SD	0.49 ± 0.48	0.8 ± 0.77	0.34 ± 0.25	-	0.77 ± 0.72	-	-

4.5.3 Insulin sensitivity

4.5.3.1 Differences between daily meals

To assess the differences in insulin sensitivity between daily meals, i.e. the time of meal consumption, the results are grouped accordingly and displayed in Figure 4.14.
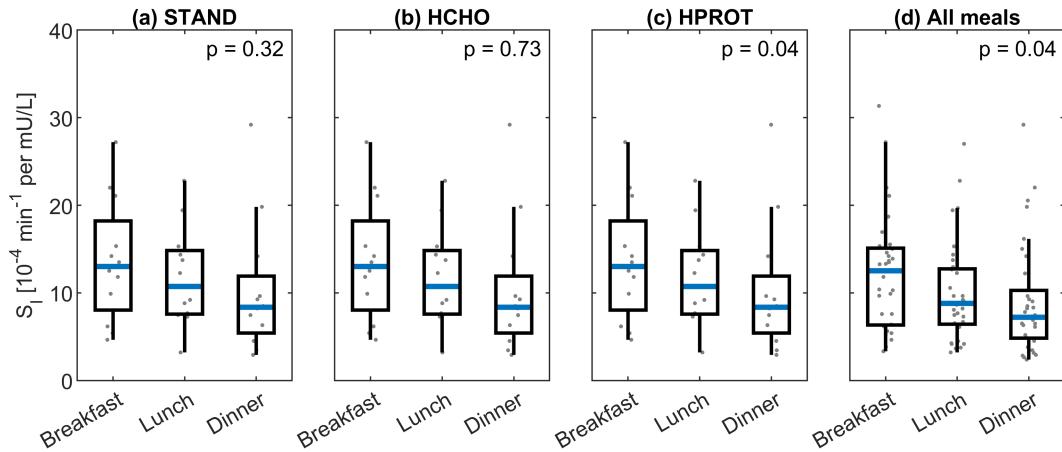
Figure 4.14: Boxplots of insulin sensitivity S_I grouped according to meal time (breakfast, lunch, dinner) for the (a) STAND, (b) HCHO, (c) HPROT meal types as well as (d) all meal types combined. The p-values give the results from the Kruskal-Wallis test.

There is a significant difference in S_I between daily meals ($p = 0.04$ according to the Kruskal-Wallis test), suggesting a decrease in insulin sensitivity over the course of the day. This trend is particularly noticeable in the meal type with high protein (HPROT) and aligns with the findings from the study by Saad et al. [77]. These results demonstrate that the proposed model identification process allows the examination of circadian changes in insulin sensitivity using data collected with a compact protocol on a single day. Applying this procedure to a similar dataset including T2DM subjects could lead to useful information on the treatment of such patients [135].

4.5.3.2 Differences between meal type and sex

The differences in insulin sensitivity between the three meals of standard (STAND), high carbohydrate (HCHO) and high protein (HPROT) as well as sex are analysed and displayed in Figure 4.15.

The results of this analysis reveal that males have a significantly higher insulin sensitivity in response to the HCHO meal and significantly lower insulin sensitivity in the STAND and HPROT meals. Due to the almost identical protein content of the STAND
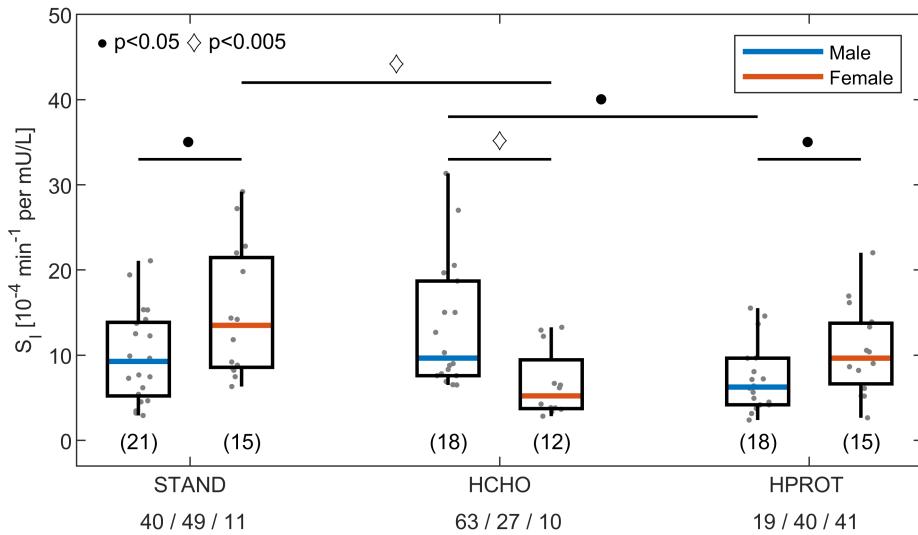
Figure 4.15: Boxplots of insulin sensitivity S_I grouped according to sex and meal type. Differences in sex within the same meal type are assessed using the Wilcoxon rank sum test, whereas differences in meal types within the same sex are assessed using the Kruskal-Wallis test. The bullets ($p < 0.05$) and diamonds ($p < 0.005$) mark significant differences and the numbers in brackets give the number of responses in each group. The numbers below the meal types give the relative meal compositions in % of CHO / fat / protein.

and HCHO meals of around 10 %, this indicates a strong sex difference in response to CHO and/or fat and little difference in response to protein. This is supported by the fact that the HPROT meal reveals a similar sex distribution to the STAND meal despite strongly differing protein contents. The fact that these two meals (STAND and HPROT) additionally have similar fat contents, makes it more likely that the sex differences stem from differences in response to fat rather than CHO content. Following this, it could be concluded that females could benefit from added dietary fat as it increases their glucose tolerance, whereas low-fat meals like the HCHO meal would be more beneficial for males. This information could be very useful in the design of tailored dietary interventions.

These results contradict a study [75] examining sex differences using the OMM in response to a mixed meal very similar to the STAND meal from a similar study population. Here, Basu et al. found a significant decrease in insulin sensitivity estimates scaled by lean body weight in females. A literature review by Magkos et al. [136] found an inconsistent picture of whether there exist sex-related differences in free fatty acid-induced meal insulin resistance, with more recent studies suggesting no difference. However, these studies examined glucose and lipid metabolism under the unrealistic

conditions of clamp experiments [136]. In contrast, the present study was conducted under real-life conditions thus providing more practical relevance. However, it should be emphasised that the low number of subjects in each group as well as the chosen distribution of macronutrient content in the meals limit the explanatory power of the results. A more detailed analysis isolating the effects of specific food contents would require further experiments with additional meal types of different macronutrient content.

4.5.4 Meal-related appearance of glucose

The inferred profiles of GA are grouped according to meal types and time of meal consumption and are displayed in Figure 4.16. A clear pattern in the difference between
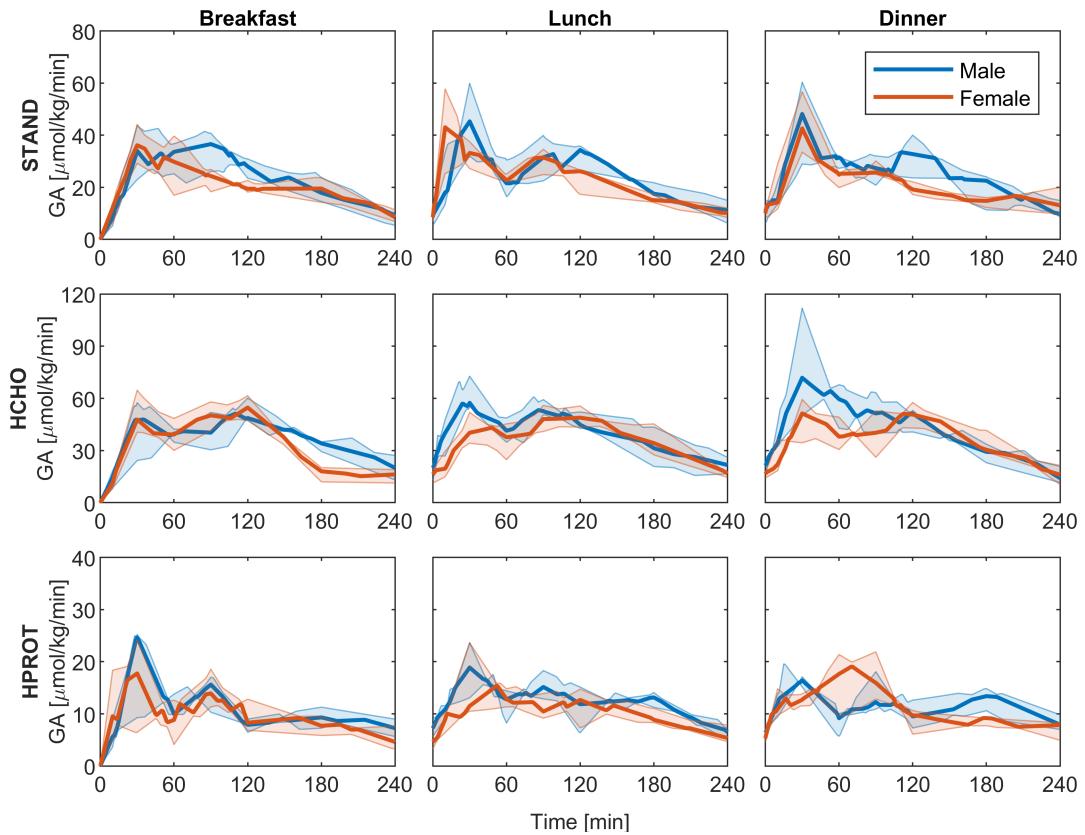
Figure 4.16: Profiles of glucose appearance (GA) grouped according to meal type (rows) and time of meal consumption for each sex. The results are given as median and interquartile range.

sex similar to the insulin sensitivity cannot be observed. Similarly, differences between daily meals, i.e. meal timing, are not apparent. However, in terms of differences between meal types, it can be observed that GA profiles from the meal high in carbohydrate (HCHO) seem to a have a less prominent initial peak within the first 60 min, compared

with the other meal types. This impression is reinforced when the share of glucose, with respect to the total amount of absorbed glucose, appearing within the first 60 min of meal consumption is compared among meal types (Figure 4.17). Although not significant, the HCHO shows a lower share of absorbed glucose compared to the other meals.
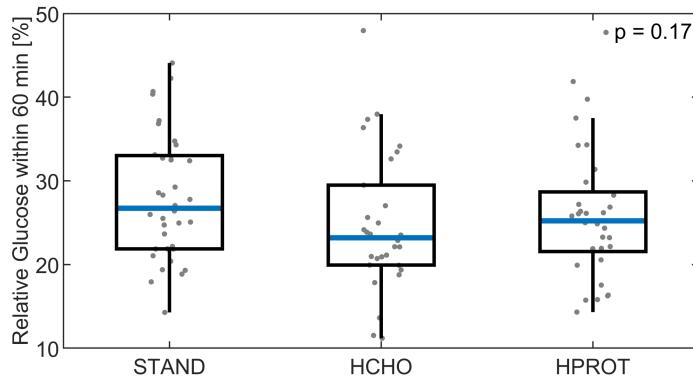
Figure 4.17: Boxplot of the relative amount of glucose absorbed within the first 60 min, grouped according to meal type. The p-value gives the result of the Kruskal-Wallis test.

4.6 Summary and conclusions

This chapter described the identification of a well-established model of postprandial glucose metabolism from consecutive mixed meal responses in healthy subjects during a single day. Compared to the prevalent approach for parameter estimation, a more suitable fully Bayesian method was applied. This required the definition of suitable prior distributions over all unknown parameters, including a parameter previously thought to be unidentifiable. Adaptations to the model formulation were made to account for overlapping effects between consecutive meals, overcoming the need to assume fasting conditions. In comparison to the literature, the estimation results showed similar precision and model fit, demonstrating the validity of the proposed alterations to the model formulation and parameter estimation procedure. This also strengthens the legitimacy of the analysis of insulin sensitivity and meal-related appearance of glucose. Here, it has been shown that there are differences in insulin sensitivity depending on the time of meal consumption, sex and meal composition.

This chapter described the OMM identification procedure in unprecedented detail. Together with the freely available VB toolbox and the publically accessible model-specific code, this chapter allows other research groups the opportunity to easily apply

the OMM to their datasets, without in-depth knowledge on model identification. This follows recent efforts to facilitate the identification of the classical minimal model based on IVGTT data [137].

In the context of this thesis, this chapter provides crucial reference values for the development and validation of glucose-only models. Before this development will be described, the following chapter will propose another adaptation to the OMM. This alteration will address the fact that the piecewise-linear function representing glucose appearance is highly impractical for describing meal responses of varying duration for estimation.

Chapter 5

Development of input functions in the context of the oral minimal modelling approach

5.1 Introduction

In the previous chapter, a novel procedure for identifying an adapted version of the oral minimal model (OMM) from consecutive meal responses has been presented and validated. The proposed adaptations allow identification of the model from non-fasting conditions by accounting for overlapping effects between meals. This was partially made possible because the associated experiments included a fixed duration between meal intakes of four hours. Meals in everyday life, however, are typically consumed at irregular intervals, e.g. perhaps varying the response duration between meals from two to six hours. Applying the OMM to a dataset with such a pattern of meal consumption is highly impractical. This impracticality is rooted in the specific properties of the piecewise-linear input function the OMM uses to describe the meal-related glucose appearance (GA) and can be made clear by the following considerations

- The piecewise-linear function describing GA has eight breakpoints at fixed locations and variable heights. This means that the times and the overall number of breakpoints would have to be set according to the response duration, requiring the adaptation of the function and therefore the model itself for every single meal response. This adaptation will be exemplified in Chapter 8, where a different

dataset is used.

- For response durations shorter than six hours, the remaining appearance overlapping with the following meal is modelled with an exponential decay assuming a fixed half-life. Fixing this decay parameter can no longer be justified for all possible meal response durations and would require individual adjustment as well. It would thus be advantageous to infer the behaviour of GA beyond the response duration during model inversion.

- The AUC of the function, representing the amount of absorbed glucose is fixed by replacing one of the height parameters with an expression based on the remaining parameters and the AUC itself (see section 4.4.2). The choice of the replaced height would again have to be adapted based on the response duration. As it will be demonstrated later in this chapter, this procedure also provides no mechanism for the chosen height to remain positive, which could lead to physiologically implausible absorption rates.

In the light of these issues, the main objective of this chapter is to develop and select an appropriate alternative to the piecewise linear description of GA in the context of modelling consecutive meals of varying response duration using the OMM. This is crucial for the description of glucose dynamics from real-word data and will mainly be achieved by moving from a piecewise to a differentiable, continuous description that is independent of response duration. Several candidates of increasing complexity will be prosed based on models in the literature. Subsequently, the OMM, in combination with the proposed input functions, will be identified using the Nuttall dataset previously analysed. The final selection of the alternative input will then be based on the quality of the model fit and similarity to the conventional piecewise-linear function has in comparison to the results presented in the previous chapter.

5.2 Literature background

Chapter 2 provided general information on meal-related glucose appearance and its measurement. In terms of a model-based description of GA, there are two separate approaches. The first approach involves modelling the physiology of digestion with varying detail. This is most often the case when direct experimental data for GA are

available for model identification or in the context of a maximal modelling approach, i.e. a fine-grained simulation model not identified from data [51]. The second approach is far more suitable for the modelling task in this thesis because it can be used when glucose and insulin data or glucose data only are available. This data-driven approach formulates a direct, parametric description of GA and omits a detailed characterisation of digestion physiology. Within this approach, it is possible to distinguish between the use of discontinuous or non-differentiable functions (see Figure 5.1 (a)), and fully differentiable functions (see Figure 5.1 (b)). The former category contains functions requiring different formulations over the time course of the meal response. The piecewise-linear function used in the OMM [71] falls into this category as well as the stepwise plateau functions proposed in two other studies [65, 138]. While this type of function offers high flexibility, they can cause several problems when consecutive meals of varying response duration are modelled, as explained before.
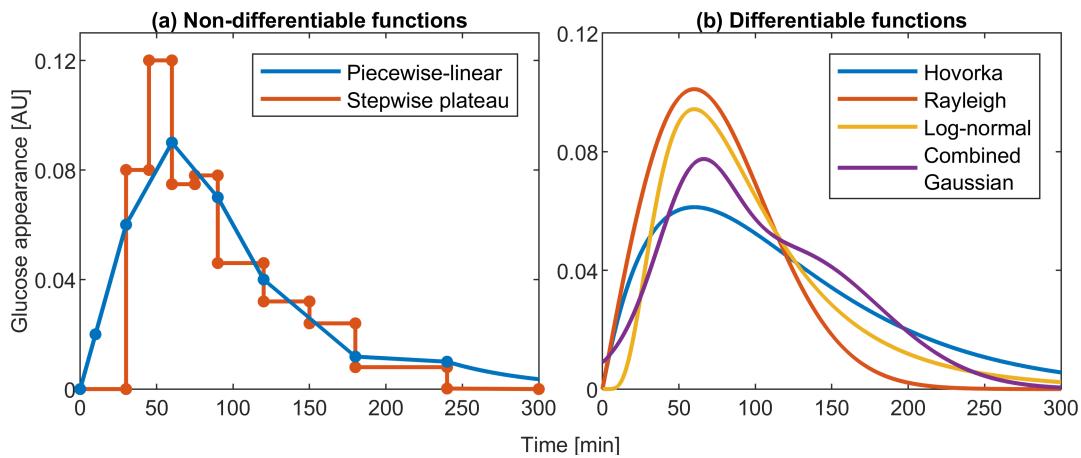
Figure 5.1: Example plots of the (a) non-differentiable and (b) differentiable input functions used in the literature. The stepwise plateau function is based on the results from Choy et al. [138]. For illustrative purposes, the functions peak at the same time of 60 min and are scaled to have the same AUC of 10.

In contrast to the discontinuous or non-differentiable functions, differentiable functions have a single definition over the entire response duration and have thus none of the disadvantages previously mentioned. Additional to being differentiable at all times, these functions must fulfil the following requirements

- High flexibility with a number of parameters smaller or equal to the number of parameters in the piecewise-linear function used by the OMM, i.e. six or less.

- The area under the input function on the time interval $[0, \infty)$ has to be described

by a single parameter that can be related to the carbohydrate (CHO) content of the meal.

- The function has to be restricted to positive values to avoid negative and therefore unphysiological absorption rates.

- The function has to take the value zero at time zero.

From the literature, three function types fulfilling these criteria were identified and are summarised in Table 5.1. Example plots of the functions are provided in Figure 5.1 (b).

Table 5.1: Summary of differentiable functions describing the meal-related appearance of glucose identified from the literature.

Name	Functional form	Description
Hovorka	$\dfrac{t}{T^2} \exp\left(-\dfrac{t}{T}\right)$	The function is defined by a single parameter T, describing the time of peak absorption. It is the impulse response of a linear second-order model of absorption. It was proposed by Hovorka et al. [139] and has since been used in several models [91, 140, 141].
Rayleigh	$\dfrac{t}{T^2} \exp\left(-\dfrac{t^2}{2T^2}\right)$	The function is defined by a single parameter T, describing the time of peak absorption. It is based on the Rayleigh PDF and used in a number of models [26, 142, 143].
Log-normal	$\dfrac{1}{tW} \exp\left(-\dfrac{\left[\log\dfrac{t}{T}\right]^2}{2W^2}\right)$	The function is based on a log-normal distribution and is defined by a timing parameter T and width parameter W [143].

Additional to the functions in Table 5.1, we proposed the combination of two Gaussian-shaped components as an input function to a linear glucose-only model (more details in the following chapter) [144]. It was shown that the proposed input function allows the simple linear model to describe complex, multiphasic glucose responses in NGT subjects. An application of this input function as GA in the context of the OMM is however not suitable, because the Gaussian function does not fulfil the previously specified property of taking the value zero at $t = 0$ as demonstrated in Figure 5.1 (b).

5.3   Methods and modelling

5.3.1   Development of input functions

From Figure 5.1 it is evident that the differentiable functions on their own have a far less flexible shape, compared to the piecewise-linear and the stepwise plateau functions. Experimentally observed GA profiles from mixed meals often display two phases characterised by a secondary hump after the initial peak [45, 50, 51]. It is thus suggested to create a flexible input function shape by superimposing two differentiable functions with different peak times, creating a single function composed of two overlapping components.

The proposed functions are created by combining the Rayleigh and log-normal functions in different variations. Hovorka's function is not considered because it is similar to the Rayleigh function, but shows a slower decay after its peak (see Figure 5.1), making it less suitable when two functional components are superimposed. Overall, a total of three different functions of increasing complexity, as indicated by an increased number of parameters, consisting of the summations of two functions are proposed.

Before the three functions are presented, the individual components are defined. The functional component based on the Rayleigh distribution is formulated as follows

$$F_R(t, T) = \frac{t}{T^2} \exp\left(-\frac{t^2}{2T^2}\right).$$

(5.1)

The variable T describes the peak time and the function is parameterised so that its integral over the time interval $[0, \infty)$ is one. This means that the AUC can be defined with a single coefficient.

The functional component based on a log-normal distribution is formulated as follows:

$$F_{LN}(t, T, W) = \begin{cases} 0 & \text{for } t = 0 \\ \dfrac{1}{t\sqrt{\pi W}} \exp\left(-\dfrac{\left(\log\dfrac{t}{T} - \dfrac{W}{2}\right)^2}{W}\right) & \text{for } t > 0 \end{cases}$$

(5.2)

This formulation is slightly different from Li's original formulation [143]. It was adapted so that the parameter T represents the peak time and the function integrates to one over the time interval $[0, \infty)$. The parameter W has no units and governs the general

width of the function. The details of this derivation are given in Appendix A.4.

It should be mentioned that for both functional forms, the width increases along with the peak time. The log-normal shaped function, however, offers an additional parameter to control the width independently. An important distinction between the two suggested functional components (5.1) and (5.2) is that the log-normal component includes a delay between the time of meal consumption, i.e. at $t = 0$, and the rise of glucose appearance, as exemplified in Figure 5.1. This gives the function more flexibility at the beginning of the response because the time delay can be adapted through the parameters. This is physiologically plausible because it takes time for the ingested CHO to pass through the stomach and gut and appear in the peripheral circulation [51].

Based on the two selected functional components, three different input functions of increasing complexity and fixed AUC are proposed as detailed in Table 5.2 on the next page. Each function consists of two components that both share the total AUC of A. Identical to the approach used in the piecewise-linear function in the previous chapter, A is fixed and calculated from the CHO content of the meal and the known fractional absorption of 0.9. This allows the introduction of the parameter R_H, which controls the relative contributions of the two input function components. As explained in section 3.3.2.2, restricting R_H to the range $(0, 1)$ ensures that all proposed input functions can only take positive values. These functions, therefore, fulfil all the above-named requirements. An example plot of all three functions is provided in Figure 5.2.
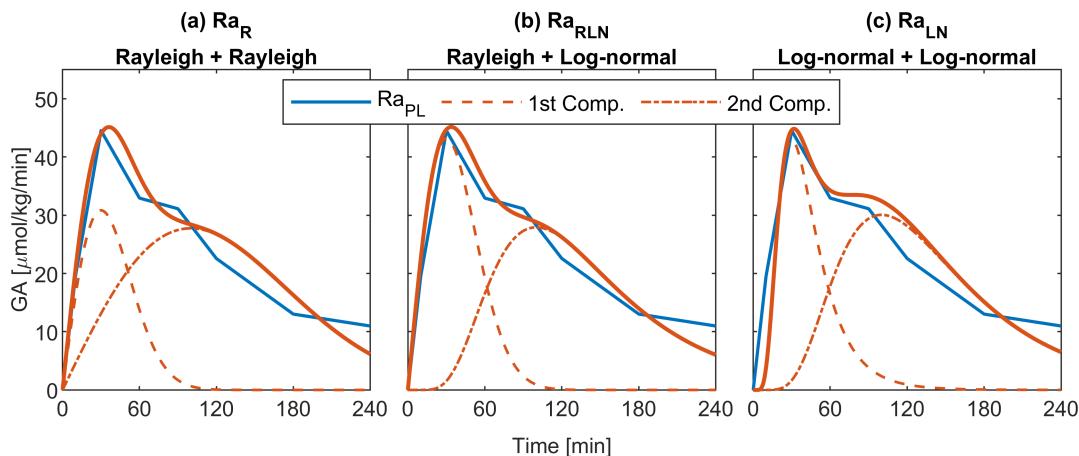
Figure 5.2: Plots of prior shapes for the STAND meal of the three proposed input functions (a) Ra_R, (b) Ra_{RLN} and (c) Ra_{LN}. Included are the two components and the prior shape of the piecewise linear function Ra_{PL} used in Chapter 4

Table 5.2: Proposed input functions based on the Rayleigh and log-normal components. The parameter A describes the total AUC which can be based on the CHO content of the meal and the parameter R_H represents the ratio between the AUCs of the two components. The two functions with a log-normal component are defined to be zero at $t = 0$.

Function	Unknown parameters
Rayleigh + Rayleigh $$Ra_R(t) = A(1 - R_H)F_R^1(t, T_1) + AR_H F_R^2(t, T_2)$$ $$= A(1 - R_H)\frac{t}{T_1^2}\exp\left(-\frac{t^2}{T_1^2}\right)$$ $$+ AR_H\frac{t}{T_2^2}\exp\left(-\frac{t^2}{T_2^2}\right)$$	R_H, T_1, T_2
Rayleigh + Log-normal $$Ra_{RLN}(t) = A(1 - R_H)F_R^1(t, T_1) + AR_H F_{LN}^2(t, T_2, W_2)$$ $$= A(1 - R_H)\frac{t}{T_1^2}\exp\left(-\frac{t^2}{T_1^2}\right)$$ $$+ AR_H\frac{1}{t\sqrt{\pi W_2}}\exp\left(-\frac{\left(\log\frac{t}{T_2} - \frac{W_2}{2}\right)^2}{W_2}\right)$$	R_H, T_1, T_2, W_2
Log-normal + Log-normal $$Ra_{LN}(t) = A(1 - R_H)F_{LN}^1(t, T_1, W_1) + AR_H F_{LN}^2(t, T_2, W_2)$$ $$= A(1 - R_H)\frac{1}{t\sqrt{\pi W_1}}\exp\left(-\frac{\left(\log\frac{t}{T_1} - \frac{W_1}{2}\right)^2}{W_1}\right)$$ $$+ AR_H\frac{1}{t\sqrt{\pi W_2}}\exp\left(-\frac{\left(\log\frac{t}{T_2} - \frac{W_2}{2}\right)^2}{W_2}\right)$$	R_H, T_1, T_2, W_1, W_2

5.3.2 Structural identifiability analysis

To analyse the structural identifiability of the OMM with the new input functions, the Taylor series and the OCR methods described in section 3.2 are used. The model equations of the OMM are as follows

$$\frac{dG(t)}{dt} = -G(t)X(t) - p_1[G(t) - G_b] + \frac{Ra(t) + Rap(t)}{V}, \qquad G(0) = G_0, \qquad (5.3)$$

$$\frac{dX(t)}{dt} = -p_2(X(t) + S_I[I(t) - I_b]), \qquad X(0) = X_0, \qquad (5.4)$$

$$Rap(t) = R_0 \exp(-\alpha t), \qquad (5.5)$$

where the function $Ra(t)$ can be any of the three newly proposed functions in Table 5.2. For all input functions, the parameters V, G_b, G_0, X_0 and I_b are considered to be known. The persisting absorption Rap is defined by known parameters R_0 and α. Subject of the structural identifiability analysis are the system parameters p_1, p_2 and S_I and the parameters of the respective input functions detailed in Table 5.2. To give independent evidence for the validity of the structural identifiability results presented below, the practical identifiability of the input function parameters will be assessed by examining the posterior CVs as explained in section 3.4.

5.3.2.1 Input function Ra_R

For the OMM in combination with the input function Ra_R in Table 5.2, consisting of two Rayleigh components, the Taylor series method is initially used. For that it is assumed that $I(0) = I_b$ and eight Taylor series coefficients are calculated. The resulting system of equations leads to a total of eight solutions, which indicates structural local identifiability in some parameters. The same result is achieved with nine and ten Taylor series coefficients, whereas the symbolic computation no longer completes for a higher number of coefficients. This provides additional evidence for the structural local identifiability of some parameters and is confirmed with the ORC method, where all parameters are determined to be structurally locally identifiable (see Appendix B.2.3.2 for the details).

A more detailed look into the eight solutions of the Taylor series method reveals that the solutions for the system parameters p_1, p_2 and S_I are identical, indicating structural global identifiability. The eight solutions stem from different combinations of input function parameters R_H, T_1 and T_2. These arise from the fact that T_1 and T_2 are

squared giving two solutions each (T_1, $-T_1$ and T_2, $-T_2$) and the two input components are identical, meaning that it is possible to switch the order of the components for the same overall shape. The details of the symbolic computation are given in Appendix B.2.3.1. Restricting parameters T_1 and T_2 to positive values eliminates six possible solutions leaving two locally identifiable parameter combinations. These arise from the symmetry of the input function, i.e. the fact that the order of input components could be switched for the same overall shape, which would be indicated by $T_1 > T_2$.

5.3.2.2 Input functions Ra_{RLN} and Ra_{LN}

For the OMM in combination with the input functions Ra_{RLN} and Ra_{LN}, both including a log-normally shaped component, it is unfeasible to calculate the Taylor series coefficients at $t_0 = 0$ due to the log-normal function being defined as zero at this time (see expression (5.2)). An expansion of the Taylor series around $t_0 = 1$, however, leads, in both input functions, to a system that is intractable with symbolic computation even if the complexity of the system is reduced by assuming that certain parameters are globally identifiable prior to the calculation. This demonstrates that the Taylor series approach in combination with symbolic computation is no longer appropriate when a log-normally shaped component is used in the input function. Other testing methods for structural identifiability, such as the DAISY software tool [132], mentioned in section 4.4.3, or the Exact Arithmetic Rank approach [145, 146] implemented in a Mathematica software package, are also not suitable for this type of function. In contrast, the ORC method can be used for this type of function and shows that all parameters are locally structurally identifiable for both input functions (see Appendix B.2.4 for the details).

Regarding the possible parameter combinations resulting from the local identifiability, two conclusions can be drawn from the results concerning Ra_R previously presented. Firstly, in the function Ra_{RLN} in Table 5.2, combining a Rayleigh and a log-normal component, the parameter T_1 is squared. It is therefore to be expected that there are two possible solutions, T_1 and $-T_1$, which can be resolved by restricting the parameter T_1 to positive values. Secondly, the function Ra_{LN} in Table 5.2, combining two log-normal components, has the same symmetry as the function Ra_R, consisting of two Rayleigh components. This means that there a two possible combinations as the two log-normal input components of Ra_{LN} can be switched for the same overall shape, which would be indicated by $T_1 > T_2$.

5.3.3 Choice of prior distributions

Following the structural identifiability analysis, the developed input functions require the definition of suitable prior PDFs over the peak time parameters T, width parameters W and the relative contribution R_H.

The peak time parameters T_1 and T_2 used in both the Rayleigh and log-normal components are only plausible when positive. They are therefore transformed into log-normally distributed parameters characterised by a median and CV as explained in section 3.3.2.2. This additionally avoids the peak times converging to very small yet positive values which would create a sharp spike in the respective component, making it physiologically implausible. The log-normal form of the PDF helps to avoid this, because it assigns far less probability to values close to zero in comparison to normal distributions, therefore decreasing the likelihood of the input function components taking non-physiological shapes.

Similar to the peak time parameters, the width parameters W_1 and W_2 appearing in the log-normal components are only plausible when positive and are chosen to be log-normally distributed as well. This also avoids non-physiologically spiked components by assigning a low probability to very small, but positive, values of W. As explained in section 5.3.1, the parameter R_H has to lie between zero and one to avoid negative GA rates. For that, the transformation using a logistic mapping, as described in section 3.3.2.2, is applied and the parameter PDF is characterised by median and CV.

To characterise the prior PDFs over the input function parameters, their medians are chosen to approximate the shape of the prior distribution over the piecewise-linear function Ra_{PL}. A plot of the prior function shapes for the STAND meal in comparison to the prior for Ra_{PL} has already been provided in Figure 5.2. In terms of the prior CVs, the prior uncertainty of the input parameters in the piecewise-linear input Ra_{PL} was chosen to be characterised with a CV of 50 %, in the previous chapter. Performing a stochastic sensitivity analysis as described in section 3.4 on the new input functions with a prior CV of 50 % leads to significantly increased functional variability in comparison to Ra_{PL}. It is therefore proposed to reduce the prior CV of the new input function parameters to 30 %, leading to comparable functional variability, as demonstrated in Figure 5.3. This figure also demonstrates one weakness of the piecewise-linear function mentioned previously: the function provides no mechanism for the height of the break-

point at 180 min to remain positive, as indicated by its lower quartile being negative. As explained in section 4.4.2, this is because the height at 180 min is completely determined by the AUC and the remaining parameters. The chosen prior values for the new input functions are summarised in Table 5.3. Similar to Chapter 4 the influence of the individual parameters and their prior distributions on the model output is demonstrated by varying the value of one parameter at a time, while the other parameters are kept fixed at their prior medians. The results are given in Appendix D.2.
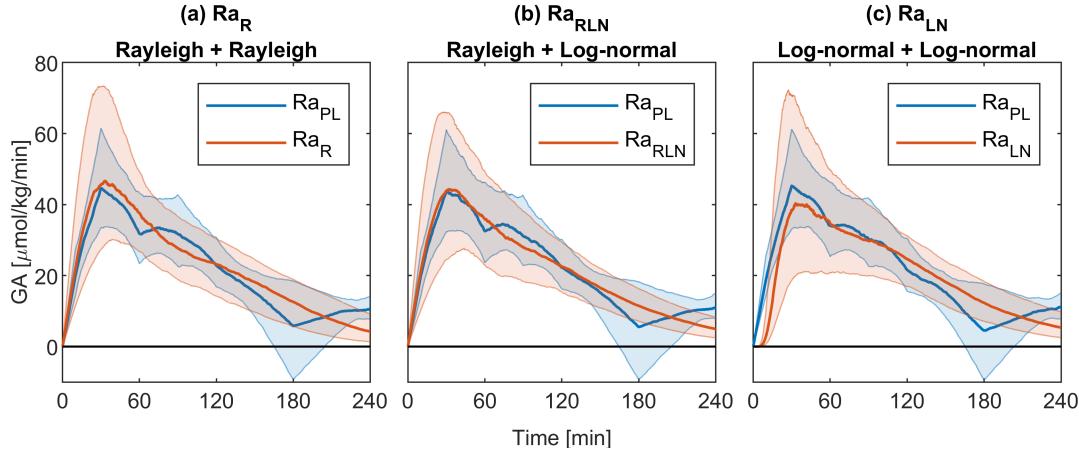
Figure 5.3: Results of the global sensitivity analysis to assess the prior variability of the input functions using 1000 Monte-Carlo simulations for (a) Ra_R, (b) Ra_{RLN} and (c) Ra_{LN}. The solid lines give the median and the shaded area indicates the interquartile range of simulations, respectively.

Table 5.3: Utilised medians of the prior distributions over the input function parameters. All prior CVs were set to 30 %.

Function	Parameter	Distribution	Unit	Prior median
Ra_R	T_1	Log-normal	min	30
	T_2	Log-normal	min	100
	R_H	Logistic	-	0.75
Ra_{RLN}	T_1	Log-normal	min	30
	T_2	Log-normal	min	100
	W_1	Log-normal	-	0.5
	R_H	Logistic	-	0.65
Ra_{LN}	T_1	Log-normal	min	30
	T_2	Log-normal	min	100
	W_1	Log-normal	-	0.5
	W_2	Log-normal	-	0.5
	R_H	Logistic	-	0.7

5.3.4 Parameter estimation procedure

No changes to the parameter estimation procedure described in section 4.4.5 are necessary. Furthermore, the incorporation of the overlapping effects between meals is accomplished using the procedure described previous chapter and depicted in Figure 4.3. This means that the persisting appearance from the previous meal $Rap(t)$ is calculated as $Rap(t) = Ra(t+240)$, where the function $Ra(t)$ can be any of the three newly proposed functions inferred from the previous meal. $Rap(t)$ is thus fully inferred from the data and does not require the fixing of an exponential decay parameter as for the piecewise-linear function. The implementation details of the model and its priors within the VB toolbox are provided in Appendix C.2.

5.3.5 Input function selection

To select the most suitable input function candidate, the proposed functions are compared amongst each other. This is achieved by utilising multiple model selection criteria, where the focus lies on how the individual functions compare against the results using the piecewise linear function. Specifically, the RMSE, free energy and estimated insulin sensitivity S_I are compared. Once the most appropriate function has been chosen, its performance is assessed in more detail.

5.4 Results and discussion

5.4.1 Practical identifiability analysis

The practical identifiability of the input function parameters is assessed by analysing their posterior CVs, as explained in section 3.4. The results are provided in Figure 5.4 and show that the posterior CVs significantly decreased from the prior CV of 30 % in the vast majority of cases for all parameters. These results demonstrate the practical identifiability of the input function parameters in all proposed functions and confirm the results of the structural identifiability analysis. Regarding the local identifiability of the parameters, there are no cases in Ra_R or Ra_{LN} where the respective components are switched as indicated by $T_1 < T_2$ in all responses.
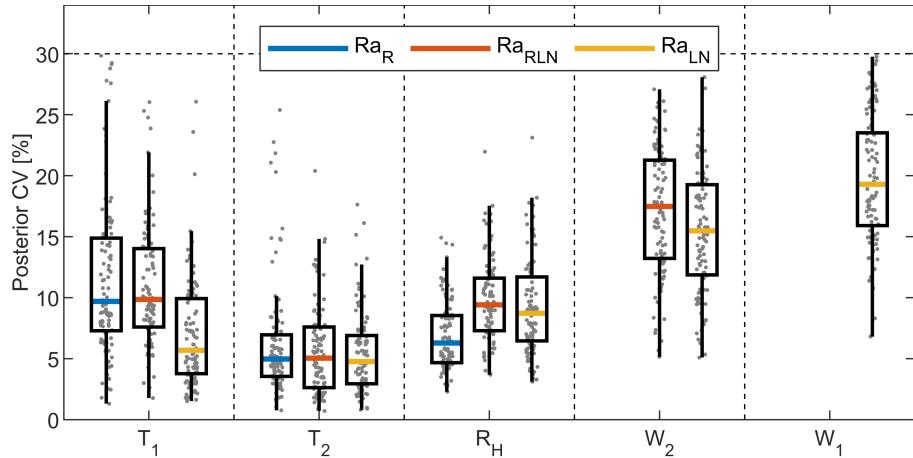
Figure 5.4: Results of the practical identifiability analysis showing boxplots of the posterior parameter CVs. The horizontal dashed line gives the value of the prior CV which was chosen to be 30 % for all parameters.

5.4.2 Input function comparison and selection

The results of the comparison among the different proposed input functions are given in Figure 5.5.
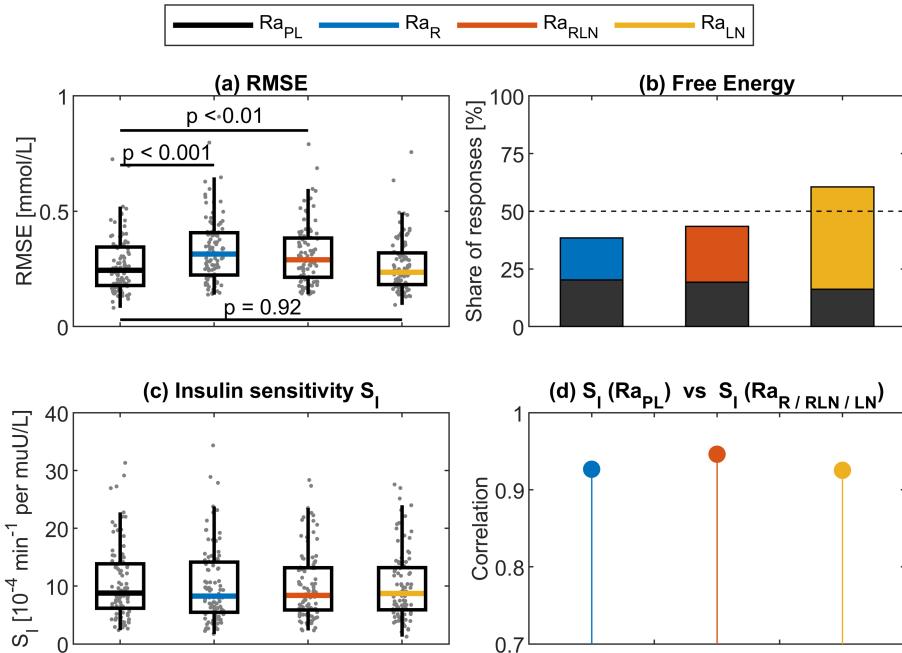
Figure 5.5: Comparison of various metrics between Ra_{PL} and the three proposed input functions Ra_R, Ra_{RLN} and Ra_{LN}. Plot (a) gives a boxplot of the RMSE where the p-values were calculated using the Wilcoxon rank-sum test. Plot (b) shows the share of the responses compared to the OMM using Ra_{PL} in which the models are considered equal (black portion) or superior (blue, red and yellow portion), according to the free energy. Plot (c) gives a boxplot of the estimated insulin sensitivities. Plot (d) gives the Pearson correlation of the insulin sensitivities between the OMM using Ra_{PL} and the three proposed functions.

The differences in RMSE (Figure 5.5 (a)) demonstrate that only function Ra_{LN} yields an equally good fit in comparison to the piecewise-linear function Ra_{PL}, with Ra_R and Ra_{RLN} yielding significantly higher error values ($p < 0.01$). This provides evidence that only Ra_{LN} provides similar flexibility compared to Ra_{PL}. The same conclusion can be drawn from the results of the free energy comparison (Figure 5.5 (b)), where it is demonstrated that only Ra_{LN} is deemed as equal or superior to the piecewise linear function Ra_{PL} in more than 50 % of responses. In contrast, the insulin sensitivity estimation (Figure 5.5 (b)-(c)) does not demonstrate a clear superiority of any of the proposed input functions, with all candidates displaying highly correlated ($r > 0.9$) and statistically equal ($p > 0.6$) insulin sensitivity estimates. Based on the analysis of RMSE and free energy, the function Ra_{LN} consisting of two log-normal components is chosen as the most suitable alternative to the piecewise-linear function Ra_{PL}.

5.4.3 Parameter estimation results

Following the choice of input function Ra_{LN}, consisting of two log-normal components, as the most suitable input function form, the estimation results are examined in more detail and compared to the results from Chapter 4 where the piecewise linear function Ra_{PL} was used.

5.4.3.1 Parameter estimates and correlation

The results of the parameter estimation procedure using Ra_{LN} in comparison to the corresponding results using Ra_{PL} are provided in Figure 5.6. The medians of the system parameters p_1 and p_2 in plot (a) are only weakly correlated with the corresponding estimates using the piecewise linear function Ra_{PL}. Together with the respective results of the posterior CVs in plot (b), this again implies practical identifiability issues in the parameters p_1 and p_2, as already discussed in section 4.5.2.2. The differences in insulin sensitivity estimates will be discussed separately in section 5.4.4.2.

The posterior medians of the input function parameters in Figure 5.6 (c) show no significant differences between meal types ($p > 0.05$ according to the Kruskal-Wallis test). Regarding the posterior CVs of the input function parameters in plot (d), it can be noted that the width parameters W_1 and W_2 show a higher uncertainty than the remaining parameters. This can be explained by the fact that these parameters have the smallest influence on the model output, as shown in the Appendix Figure D.4.
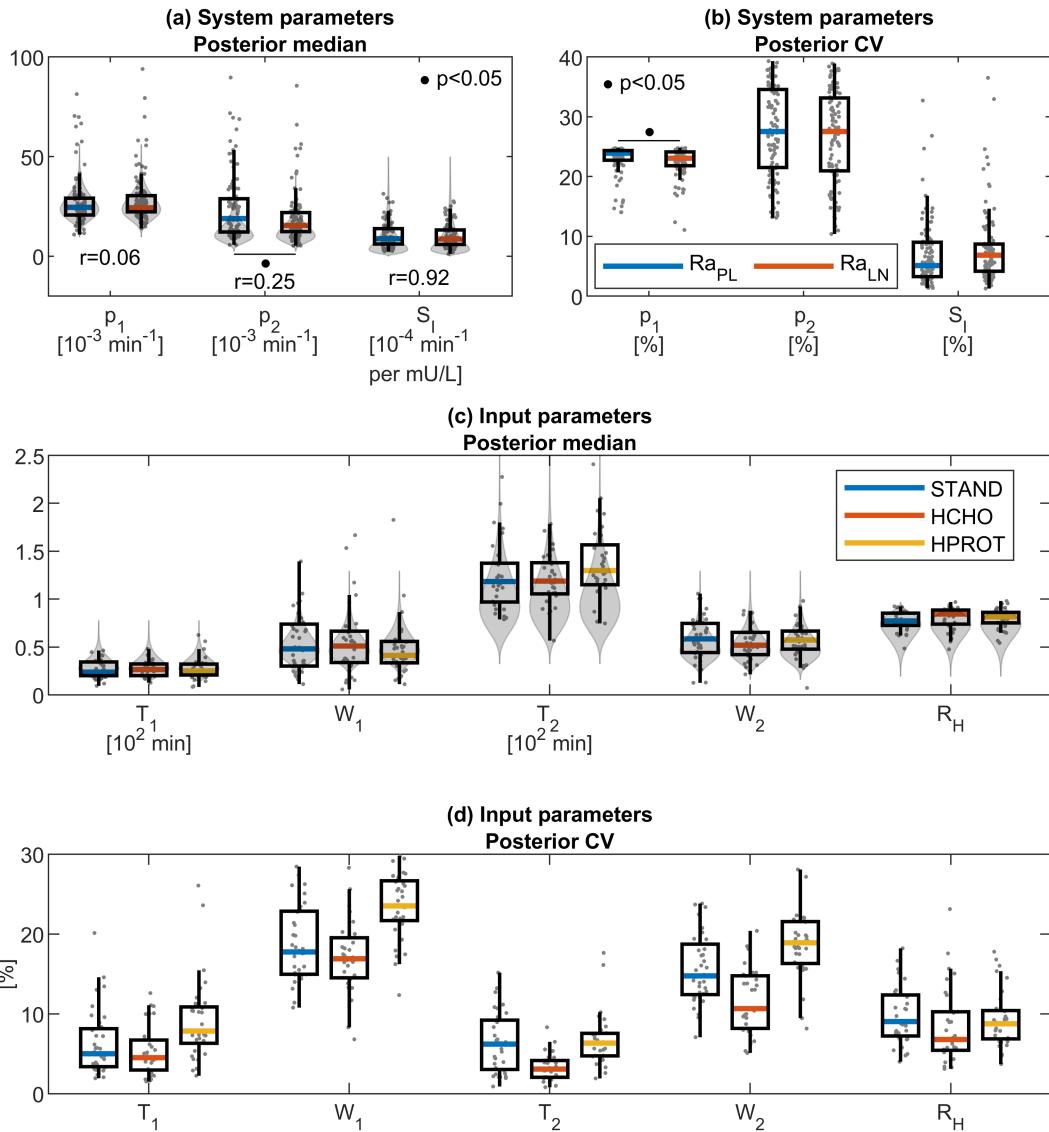
Figure 5.6: Posterior parameter estimates of the OMM using the log-normally based input function Ra_{LN}. Displayed are the population boxplots of median and CV of the posterior distributions. The shaded grey ares indicate the prior PDF. Plots (a)-(b) compare the system parameters to the results using the piecewise linear input Ra_{PL}. Differences were tested using the Wilcoxon ranksum test and the r-values give the Pearson correlation coefficient. Plots (c)-(d) give the input parameters of Ra_{LN}, grouped according to the meal types of standard (STAND), high CHO (HCHO) and high protein (HPROT) composition.

The correlations of the model parameters, assessed through the posterior covariance matrix as described in section 3.3.2.2, are displayed in Figure 5.7 (a). Similar to the OMM using Ra_{PL} in plot (b), the majority of correlations are small and thus non-significant. The exception is input function parameter R_H, which shows correlations to the other input function parameters and p_2. This can be explained by the fact that the

parameter R_H has a significant impact of the model output as shown in the Appendix Figure D.4, which overlaps with the effects of other parameters. A reparameterisation of the input function is, however, not plausible as it was already shown that simpler, less flexible input functions are not suitable.
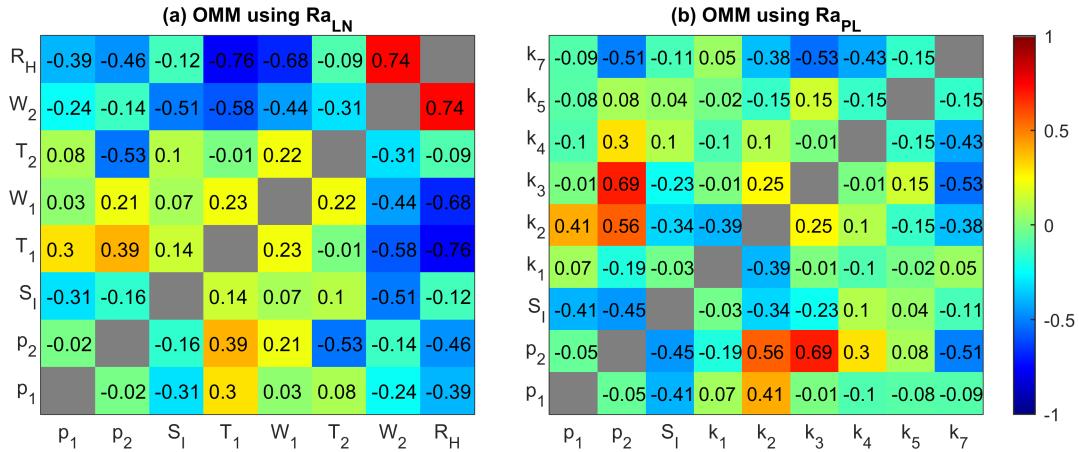
Figure 5.7: Median posterior parameter correlation matrix of the OMM using (a) the log-normally based input function Ra_{LN} and (b) the piecewise linear function Ra_{PL}, from the individually estimated parameter correlation matrices of all 99 responses.

5.4.3.2 Model fit

The residuals between model output and data weighted by the measurement uncertainty were calculated using expression (4.11) and are displayed in Figure 5.8.
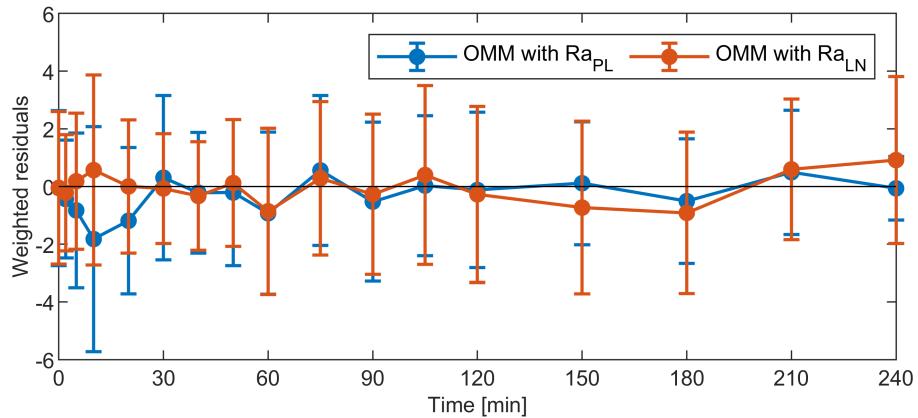
Figure 5.8: Comparison of the weighted residuals between the model output of the OMM with Ra_{PL} and Ra_{LN}, respectively. The values and error bars represent the mean and standard deviation of weighted residuals over all meal responses.

The overall mean and standard deviation of the absolute weighted residuals is 0.40 $\pm$ 0.31 for Ra_{LN} compared to 0.49 $\pm$ 0.48 for Ra_{PL}. This difference is due to the

improved model fit during the first 30 min of the response, as shown in Figure 5.8 and demonstrates the superior flexibility of Ra_{LN} during this period in comparison to Ra_{PL}. In contrast, Ra_{LN} yields slightly more biased residuals with larger variability towards the end of the response. This can be explained by the higher flexibility of Ra_{PL} in the last 90 min of the response. For the remaining part of the response, both input functions produce a similar model fit. To further illustrate model fit epsecially during the first 30 min of the response, an example of the model output for each meal type is given in Figure 5.9.
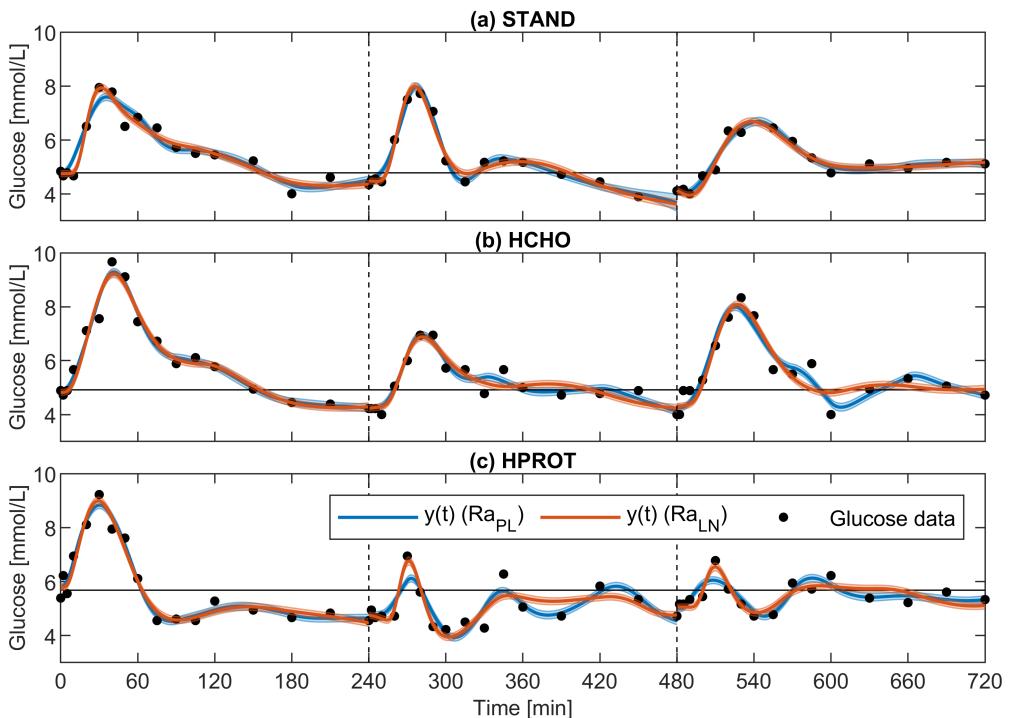
Figure 5.9: Example comparing the model output of the OMM using the piecewise linear input function Ra_{PL} and the log-normally based input function Ra_{LN} for the three meal types of (a) standard (STAND), (b) high CHO (HCHO) and (c) high protein (HPROT) composition. The shaded area represents the uncertainty (standard deviation) from a deterministic sensitivity analysis and the solid black line provides the basal glucose level G_b.

5.4.4 Model validation

5.4.4.1 Comparison of glucose appearance profiles

The difference between glucose appearance profiles is assessed by

$$\delta_{Ra}(t) = \frac{Ra_{PL}(t) - Ra_{LN(t)}}{Ra_{PL}(t)}, \tag{5.6}$$

and the results of this comparison are displayed in Figure 5.10.
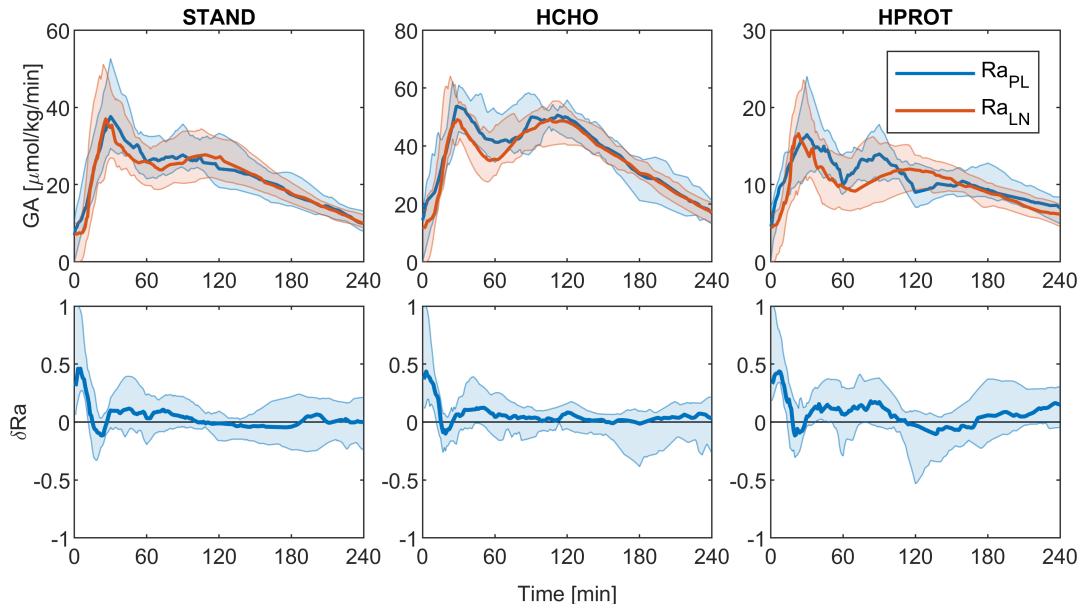
Figure 5.10: Top: Comparison between the inferred appearance profiles of Ra_{PL} and Ra_{LN} for each meal type STAND (left), HCHO (centre), HPROT(right). Bottom: Time course of the relative deviation between Ra_{PL} and Ra_{LN} for each meal type. The solid lines and shaded areas give the median and associated interquartile range.

The comparison demonstrates several differences between the two functional forms. Firstly, it is evident that the first peak in the GA profiles occurs slightly earlier in all meal types when Ra_{LN} is used. This can be considered more realistic because, unlike Ra_{PL}, the proposed function is more flexible over this part of the response and fits the data better, as described in the previous section. This also explains the fairly high values of δ_{Ra} in the first 30 min. Another indication of a more realistic estimation of GA using Ra_{LN} is found in a publication by Dalla Man et al (2004) [72]. Using traced glucose to obtain a reference profile of GA, it was found that the piecewise-linear function overestimates GA in the first 30 min. Since Ra_{LN} infers lower GA rates in comparison to Ra_{PL}, the function Ra_{LN} can thus be considered to provide more realistic results.

For the remaining response time, the inferred profiles in the meals of standard (STAND) and high carbohydrate (HCHO) composition display a similar pattern and low δRa values. This is not the case for the meal with high protein content (HPROT). Here, the piecewise-linear function displays three distinct absorption phases, whereas the new function is, by definition, only capable of producing two phases. Despite this lack of flexibility of Ra_{LN}, a worse model fit in the HPROT meal cannot be detected, as demonstrated by the statistical equivalence of the RMSE values, i.e. Ra_{PL} 0.23 $\pm$

0.1 vs. Ra_{LN} 0.24 ± 0.1 mmol/L, $p = 0.59$. This demonstrates that the choice of two input function components provides a suitable balance between flexibility and model fit.

5.4.4.2 Comparison of insulin sensitivity estimates

The estimation of insulin sensitivity values is compared in Figure 5.11.
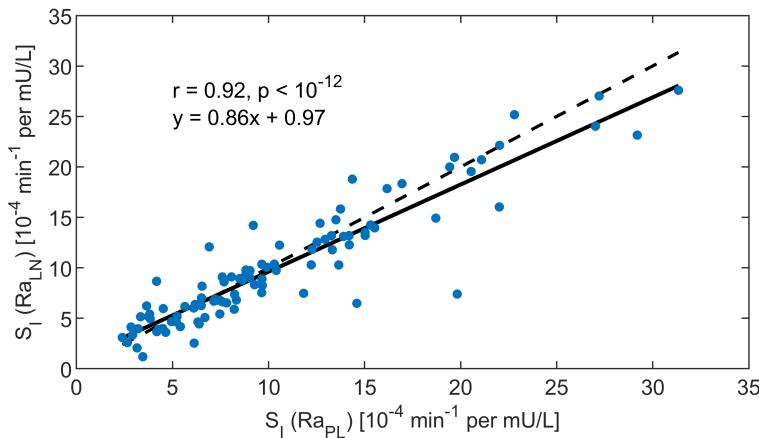
Figure 5.11: Correlation between estimated insulin sensitivity values for the OMM using Ra_{PL} and Ra_{LN}. The black line and equation display the results of the linear regression analysis and the dashed black line displays the line y=x.

The results demonstrate a very strong correlation between the S_I values estimated with Ra_{PL} and Ra_{LN} with very few outliers. Given the well-established nature of the OMM using Ra_{LN}, the respective S_I estimates can be considered to be true and thus indicate a minor underestimation of the S_I values when Ra_{LN} is used. Additionally, the posterior precision of S_I is slightly decreased as indicated by a higher CV, i.e. Ra_{PL} 6.9 ± 5.3 vs. Ra_{LN} 8.5 ± 7.6, $p = 0.06$. It can, therefore, be concluded that the quality of insulin estimation is marginally decreased.

5.5 Summary and conclusions

In this chapter, an alternative formulation to the conventional piecewise-linear input for the OMM was presented and validated. This was motivated by the fact that the piecewise linear function is unsuitable for the description of consecutive meal responses of varying duration. The proposed function is composed of two superimposed, log-normally shaped components, forming a differentiable and continuous function, completely independent from the modelled response duration. This allows the practical description of glucose dynamics if multiple consecutive meals are consumed. For that the procedure

depicted in Figure 4.3 can be adapted for any number of meals with an arbitrary duration in between. In comparison to the piecewise-linear function, it has a reduced number of parameters but shows an equivalent model fit and highly correlated insulin sensitivity estimates with respect to the OMM using the piecewise-linear function. In the meals of standard and high-carbohydrate composition, the inferred appearance profiles display a very similar pattern in comparison to the piecewise-linear function.

These results provide sufficient evidence for utilising the new input function in the glucose-only models which will be developed in the subsequent chapter.

Chapter 6

Minimal modelling of glucose dynamics in NGT subjects using glucose data only

6.1 Introduction

The aim of this chapter is to develop models for the description of postprandial glucose dynamics using glucose data only, referred to as glucose-only models (GOM). This will be achieved by proposing an alternative formulation of the oral minimal model (OMM) that is independent of insulin data. Crucial for this endeavour is the assumption that postprandial glucose dynamics are sufficiently similar to the corresponding insulin dynamics so that it is possible to extract adequate information by only considering glucose dynamics. This chapter will, therefore, present a brief literature review on the relationship between glucose and insulin concentrations and carry out a respective analysis on the Nuttall dataset. Before that, a literature review containing detailed discussions of existing glucose-only models as well as models of glucose-dependant insulin secretion will be presented.

Both, existing modelling approaches and properties of the glucose-insulin relationship will inform the subsequent GOM development. The GOMs will also utilise the novel input function proposed in the previous chapter and will be identified from the glucose measurements of the Nuttall dataset. The performance of the developed GOMs will be validated against the results presented in Chapter 4 where the OMM was applied

to the same dataset. The focus will hereby lie on the ability of the GOMs to fit the data and provide information on insulin sensitivity and meal-related glucose appearance. The goal of the glucose-only modelling task is thus to establish the physiological interpretability of the model parameters by assessing their results in comparison to the associated OMM results obtained from the same dataset. The OMM is thereby considered to be the validation standard.

6.2 Literature background

6.2.1 Minimal modelling using glucose data only

The following section will discuss the small number of published glucose-only models for the description of postprandial glucose dynamics in NGT and non-insulin dependant T2DM.

6.2.1.1 Ackerman's models

The first glucose-only description of OGTT responses was introduced by Ackerman et al. [21] in 1964 with the following model

$$\frac{d^2g(t)}{dt^2} + p_1\frac{dg(t)}{dt} + p_2g(t) = D \cdot \delta(t) \qquad \text{with} \qquad g(0) = 0, \frac{dg(0)}{dt} = 0 \qquad (6.1)$$

where $g(t)$ represents the glucose concentration above basal levels and parameters p_1 and p_2 govern the system dynamics. Note the use of lower case letters to form a distinction to the previously used $G(t)$ representing absolute concentrations. The input $D \cdot \delta(t)$ to the system approximates a quick rise and subsequent slow drop of the actual of glucose appearance (GA) rate, but does not represent GA itself. In order to allow a physiological interpretation of the model and see the similarities to other models of glucose metabolism, expression 6.1 is rewritten as follows

$$\frac{dg(t)}{dt} = -x(t) \qquad\qquad g(0) = 0, \qquad (6.2)$$

$$\frac{dx(t)}{dt} = -p_1x(t) + p_2g(t) - D \cdot \delta(t) \qquad\qquad x(0) = 0, \qquad (6.3)$$

The introduced state $x(t)$, defined as the negative derivative of the glucose concentration $g(t)$, can now be interpreted as a general glucose-lowering effect. The state $g(t)$ couples linearly into the expression (6.2) for the glucose-lowering effect $x(t)$, resulting in

a glucose-dependent increase in $x(t)$ via the parameter p_2. This explains the fact that Ackerman et al. found that the square root of this parameter to be the most different between non-diabetic and T2DM subjects after model identification [21]. Overall, the model (6.1) - (6.2) describes the glucose response to an OGTT as the impulse response of a linear damped harmonic oscillator.

In comparison to the OMM, the impact of Ackerman's model has been modest with comparatively few further applications [22–25, 144, 147]. Khovanova et al. [24, 25] proposed a nonlinear, stochastic extension to the model for the description of postprandial glucose responses in NGT, T2DM and T1DM (without insulin information) subjects. Furthermore, the author of this thesis used the model to propose a novel input function in place of the Dirac impulse [144], as explained in the previous chapter.

Although derived from an earlier physiology-based model proposed by Bolie et al. [10], Ackerman's model and all its subsequent adaptations have no direct physiological interpretation. This is rooted in the simplified description of the state $g(t)$ in (6.1) as well as the fact that the input function does not represent glucose appearance. This makes it difficult to validate the model against physiology-based quantities such as insulin sensitivity and GA and forms the main weakness of Ackerman's model and its adaptations.

6.2.1.2   Goel's model

Another glucose-only model recently proposed by Goel et al. [27] is based on an earlier model by Topp et al. [148] and takes the following form

$$\frac{dG(t)}{dt} = p_0 - p_1 G(t) - S_I G(t) I(t) + F(t), \tag{6.4}$$

$$\frac{dI(t)}{dt} = -p_2 I(t) + I_{max} \frac{G(t)^2}{a + G(t)^2}, \tag{6.5}$$

where $G(t)$, p_0, p_1 and S_I represent the glucose concentration, basal glucose production rate, glucose effectiveness and insulin sensitivity, respectively. The function $F(t)$ represents GA and is described by a second-order model of digestion, resulting in a GA profile similar to Horvorka's function mentioned in Chapter 5 (see Table 5.1). The state $I(t)$ directly represents the insulin concentration with parameters p_2 and I_{max} describing insulin clearance rate and the maximal insulin production rate, respectively.

The glucose-dependant insulin secretion, i.e. second term in (6.5), is described by a Hill equation with parameter a and coefficient $n = 2$. An example of the relationship between glucose levels and insulin secretion is given in Figure 6.1.

Goel's model was identified from isolated "landmark" responses in CGM profiles from only one healthy and one T2DM subject, where parameters p_0, p_2 and a were fixed. This low number of subjects and the fact the modelled responses showed poor fit form the main weakness of the model by Goel et al.
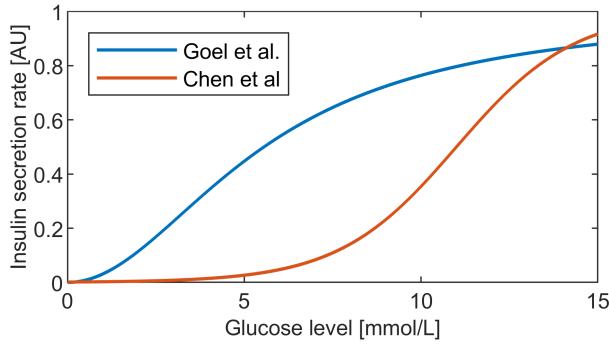
Figure 6.1: Description of glucose-dependent secretion of insulin in the models by Goel et al. [27] and Chen et al. [26].

6.2.1.3 Chen's model

The last glucose-only model to be discussed here was published by Chen et al. [26] and is described by the following equations

$$\frac{dG(t)}{dt} = -f_1(G(t)) + f_2(G(t), I(t - \tau_1)) - S_I f_3(G(t), I(t)) + F(t), \qquad (6.6)$$

$$\frac{dI(t)}{dt} = -p_2 I(t) + p_3 f_4(G(t - \tau_2)). \qquad (6.7)$$

Functions f_1, f_2 and f_3 describe glucose effectiveness, hepatic glucose production and insulin-dependent glucose utilisation, respectively (see Appendix D.3.1 for details). The function $F(t)$ represents GA and is formulated with the Rayleigh PDF introduced in Chapter 5 (see Table 5.1). Of interest is function f_4, which takes a sigmoidal shape to describe the delayed, glucose-dependent insulin secretion. An example of this function is given in Figure 6.1. The main property of the model is the use of delay differential equations as indicated by delay parameters τ_1 and τ_2, giving the model the ability to produce and sustain oscillations in glucose and insulin concentrations.

In contrast to the previously discussed GOMs, Chen's model is considerably more

complex as indicated by the fact that functions f_1 to f_4 are determined by around 25 fixed parameters. The model has nevertheless been identified on CGM profiles from healthy and T2DM subjects. The overall dynamics of the glucose profiles are only roughly approximated and although the authors claim that the parameter values can "identify the patients' conditions of physiological functions", no validation with respect physiology-based measures was carried out.

To conclude this review on existing glucose-only modelling approaches, it can be stated that none of the discussed models have been truly validated with respect to their ability to provide information on the underlying physiology. In contrast, we will develop and validate our models with respect to the well-established and physiology-based OMM, thereby taking a new approach to the development of glucose-only models that ensures physiological interpretability and adequate model fit.

6.2.2   Minimal modelling of insulin secretion

For the purpose of developing GOMs, it is useful to consider models describing the relationship between glucose dynamics and insulin secretion. The main purpose of these models is to quantify beta-cell function through the description of insulin secretion. This is accomplished by modelling the dynamics of insulin concentrations, or more commonly C-peptide concentrations, in response to glucose. C-peptide is a by-product of insulin secretion and is released simultaneously in equimolar amounts by beta-cells. Unlike insulin, C-peptide is not metabolised in the liver and can, therefore, provide a more accurate picture of pre-hepatic insulin concentrations when sampled from a peripheral vein [8].

Regarding the modelling approach in this thesis, only whole-body level models of insulin secretion and dynamics in response to ingested glucose are relevant. This excludes, (1) studies using deconvolution [149, 150] because they do not explicitly describe the effect of glucose concentrations on insulin secretion, (2) models developed for IVGTT responses, and (3) models including detailed descriptions of beta-cell physiology (see reviews [9, 13] for more details on approaches (2) and (3)).

This leaves three approaches by Hovorka and Ruan et al. [151, 152], Ferrannini et al. [153–156] and Breda et al. [157] to be discussed as they fit the mentioned inclusion criteria. These approaches propose a description of the insulin secretion rate $SR(t)$ with

glucose levels as known input. Except for the model by Ruan et al. [152], all approaches discussed below utilise a linear two-compartment model of C-peptide kinetics (Figure 6.2 (a)), whose output is modelled against measured C-peptide levels. This provides a time course of the insulin secretion rate and a dose-response curve relating glucose level to insulin secretion rate (Figure 6.2 (b)).
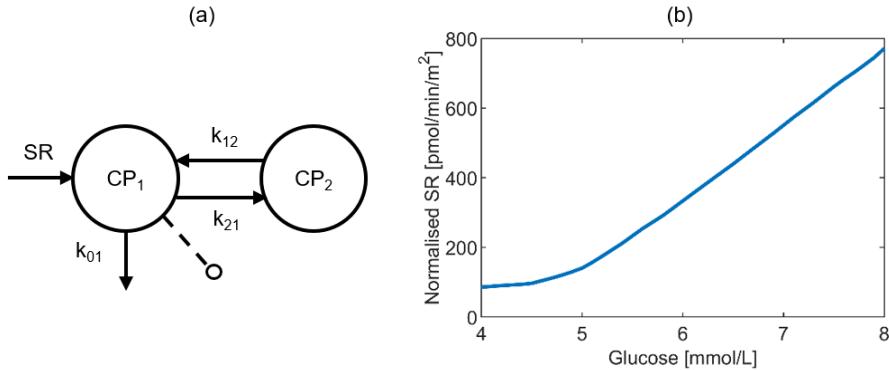
Figure 6.2: (a) Two compartment model of C-peptide kinetics in plasma (CP1) and periphery (CP2) with the secretion rate $SR(t)$ acting as input to the measured compartment CP1 [8]. The parameters k_{01}, k_{12} and k_{21} are determined from the subject characteristics [158]. (b) Example of a dose-response curve. The secretion rate is normalised according to body surface area [155].

6.2.2.1 Hovorka's models

In 1998, Hovorka et al. [151] proposed the following model of insulin secretion featuring a linear relationship between glucose concentration $G(t)$ and insulin secretion rate $SR(t)$

$$SR(t) = \begin{cases} p_1[G(t) - G_b] + p_0 G_b & \text{if} \quad p_1[G(t) - G_b] + p_0 G_b > 0 \\ 0 & \text{otherwise} \end{cases}. \tag{6.8}$$

The parameters p_0 and p_1 are the basal and postprandial sensitivity indices, respectively and G_b is the basal level of glucose concentration. The linear relationship was justified by an earlier study which used deconvolution to determine the dose-response curve during gradual infusion of exogenous glucose [159]. An adaptation of Hovorka's original model was later used by Ruan and Hovorka et al. [152] to directly describe measured post-hepatic insulin concentrations in T2DM subjects. This approach assumed that insulin concentrations are directly proportional to the rate of post-hepatic insulin secretion due to the short half-life of plasma insulin, making the C-peptide kinetics model obsolete. The new model [152] also added a piecewise-linear, glucose-independent se-

cretion term to amplify postprandial insulin secretion, as well as a dynamic secretion term dependent on the rate of glucose change.

6.2.2.2 Ferrannini's models

In the early 2000s, four similar studies by Ferrannini et al. [153–156] were published. Here, the insulin secretion rate was modelled with slightly different formulations in each publication. However, all chosen relationships have at least one parameter governing the basal secretion, one parameter governing the general slope (responsiveness) and one or more parameters governing the shape ranging from quasi-linear to more convex dose-response curves. An example of such a relationship is given in Figure 6.2 (b) and demonstrates a flat but non-zero curve in the hypoglycaemic range below 4 mmol/L representing basal secretion and an approximately linear relationship between glucose levels and insulin secretion above that. Similar to the work by Ruan and Hovorka et al. [152], a dynamic secretion dependent on the rate of glucose change was added. Furthermore, the secretion model included an additional glucose independent, piecewise linear secretion term varying throughout the day.

Ferrannini's studies [153–156] generally found linear dose-response curves in the 5-8 mmol/L range with more flattened shapes below 5 mmol/L (Figure 6.2 (b)). Furthermore, studies [155, 156] found more flattened dose response-curves in obese and T2DM subjects in comparison to NGT subjects.

6.2.2.3 Breda's model

The third and final study to be discussed in this section was published by Breda et al. [157] proposing the oral C-peptide minimal model, which is considered to be the counterpart of the OMM for describing insulin dynamics using glucose profiles as a known input [74]. An important distinction to Hovorka's and Ferrannini's models is that Breda's model only considers C-peptide concentrations above basal levels, omitting the need for a basal secretion component. Furthermore, the secretion rate $SR(t)$ is modelled with a first-order ODE, given by

$$\frac{dSR(t)}{dt} = \frac{1}{T}\left[p_1(G(t) - G_b) - SR(t)\right] \qquad SR(t) = 0. \tag{6.9}$$

Equation (6.9) effectively delays the secretion rate according to the parameter T with respect to the glucose level $G(t)$ above a threshold G_b. The parameter p_1 acts as a linear proportionality factor, relating $G(t)$ above G_b to $SR(t)$. As in all other discussed approaches, the description of secretion is augmented by a dynamic term dependant on the rate of glucose change. A very similar model was proposed by Cretti et al. [160] in the same year. Due to its connection with the OMM, Breda's model had the largest impact out of the three introduced approaches, as indicated by its use in a number of highly influential publications [47, 75–78] to quantify beta-cell function.

To conclude this review on insulin-secretion models, it can be stated that all approaches provide different formulations of the relationship between glucose levels and insulin secretion that have been shown be physiologically plausible. They can thus be used to inform the formulation of glucose-only models.

6.3 Analysis of glucose-insulin relationship

The success of the modelling task in this chapter is partially dependant on the extent to which the dynamics of insulin concentrations can be recovered by only considering the dynamics of glucose levels. A literature search found that only a limited number of studies have been published on this topic. In both publications discussing the Nuttall dataset [29, 128] it was noted that insulin curves paralleled glucose curves in the STAND and HCHO diets, without carrying out a more systematic evaluation. A later study by Robbins et al. [161] took a more systemic approach to a similar dataset and found that around 80 % of glucose peaks coincided with peaks in insulin levels. This was confirmed by other studies [162, 163], where a short sampling period of 4 min allowed the identification of correlated periodic oscillations in postprandial glucose and insulin levels [162]. In order to establish the existence of this similarity in the Nuttall dataset, a systematic evaluation of the glucose-insulin relationship is carried out in the following section.

6.3.1 Correlation analysis

In the OMM, both glucose and insulin concentrations are considered with respect to their (fixed) baseline concentrations G_b and I_b, respectively. As explained in Chapter 4,

the baseline values are calculated for every subject individually by averaging the samples at -15, 0, 2 and 5 min. It is therefore of interest to assess the correlation between the glucose and insulin concentrations above their respective baseline values, the results of which are presented in Figure 6.3.
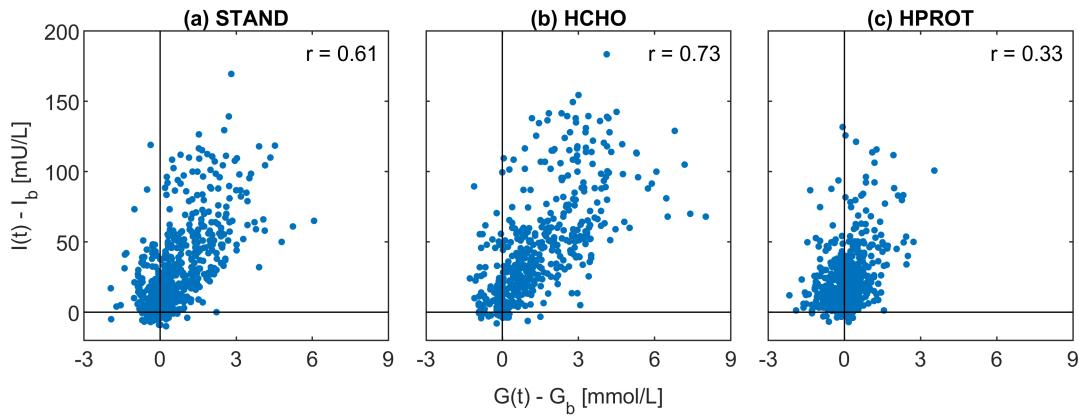
Figure 6.3: Scatter plots of glucose and insulin concentrations above their baseline values G_b and I_b, respectively for the meal types (a) STAND, (b) HCHO and (c) HPROT. The Spearman correlation coefficients are given in top right hand corner of the plots. All correlations are statistically significant with $p < 10^{-12}$.

In comparison to the STAND and HCHO meal types, the HPROT meal type shows a lower but significant correlation between glucose and insulin concentrations above baseline. Of note is that it is far less common for insulin concentrations to fall below baseline in comparison to glucose concentrations, which is especially significant in the HPROT meal. This is an important observation for the subsequent modelling process as it gives crucial information on the relationship between glucose levels and insulin secretion when glucose levels fall below their respective basal values.

6.3.2 Cross-correlation analysis

To assess the temporal relationship between glucose and insulin levels, a cross-correlation analysis is performed. This is carried out on every daily meal response (breakfast, lunch, dinner) separately and subsequently summarised across all responses from the same meal type (STAND, HCHO and HPROT). Due to the large differences in absolute concentrations, glucose and insulin levels above baseline are normalised according to their respective peak value. The resulting correlations are additionally normalised so that the correlation equals one at lag zero. To provide a reference for comparison, the self-similarity of the insulin profiles is assessed using auto-correlation. Should the

cross-correlation profile between glucose and insulin, and the auto-correlation profile of only insulin be similar to each other, it can be assumed that the glucose and insulin levels also have very similar dynamical properties. The comparison of the correlation profiles is depicted in Figure 6.4.
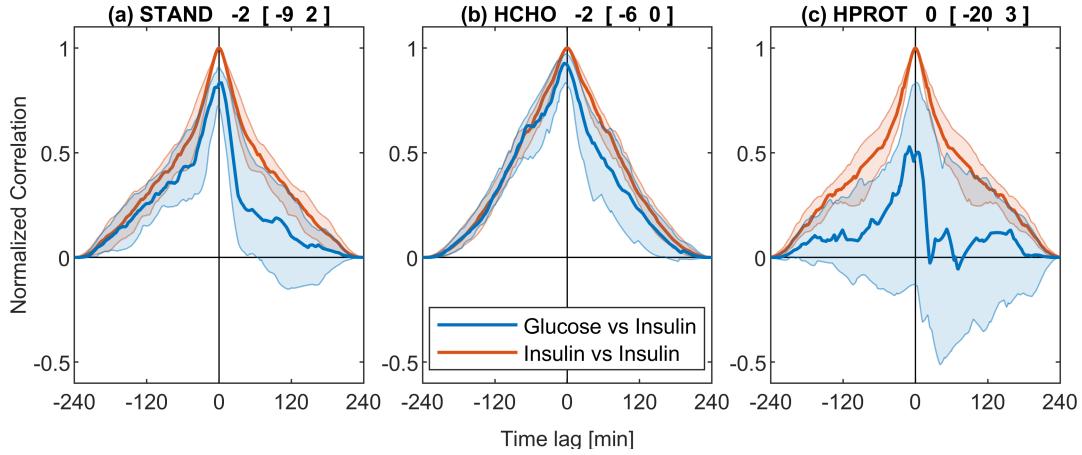
Figure 6.4: Cross-correlation between normalised glucose and insulin levels (blue) and auto-correlation of the insulin levels (red) as reference. The solid lines and shaded areas give the median and interquartile ranges for all meal responses in the (a) STAND, (b) HCHO and (c) HPROT meal types, respectively. The values above the plots give the median and interquartile range of the time lag at the maximum cross-correlation in min.

Comparing cross- and auto-correlation profiles for all meal types, the HCHO meal type shows the greatest similarity with almost identical profiles, followed by the STAND meals and the HPROT meals showing the least amount of similarity. In all meal types, the profiles are most dissimilar between time lags of 0 and 120 min. The time lags at maximum cross-correlation given in the plot headings display a clear bias towards negative values which could imply that the insulin levels lag behind glucose levels.

To conclude this analysis it can be stated that glucose and insulin dynamics show sufficient similarity to fulfil the prerequisite of the modelling task in this chapter.

6.4   Modelling

6.4.1   General model formulation

As noted in the introduction to this chapter, the GOMs proposed here are based on the OMM, where the measured insulin concentrations enter the model as a known input. To make the GOMs independent from this input, i.e. insulin measurements, the following

generalised formulation is proposed

$$\frac{dG(t)}{dt} = -G(t)X(t) - p_1\left[G(t) - G_b\right] + \frac{Ra_{LN}(t) + Rap(t)}{V}, \qquad G(0) = G_0, \quad (6.10)$$

$$\frac{dX(t)}{dt} = -p_2\left[X(t) - S_G Z(t, G_b)\right], \qquad\qquad X(0) = X_0, \quad (6.11)$$

$$Ra_{LN}(t) = A(1 - R_H)\frac{1}{t\sqrt{\pi W_1}}\exp\left(-\frac{\left(\log\frac{t}{T_1} - \frac{W_1}{2}\right)^2}{W_1}\right)$$
$$+ AR_H\frac{1}{t\sqrt{\pi W_2}}\exp\left(-\frac{\left(\log\frac{t}{T_2} - \frac{W_2}{2}\right)^2}{W_2}\right), \qquad (6.12)$$

The interpretation of the variables in expression (6.10) remains unchanged in comparison to the OMM and the glucose appearance is described by the function Ra_{LN} consisting of two superimposed log-normal components, selected in Chapter 5. The persisting GA $Rap(t)$ is known and calculated by extending the inferred GA from the previous meal, if present, beyond the response duration as depicted in Figure 4.3 and described in the previous chapters.

The main change concerning the OMM is the introduction of the function Z in expression (6.11) in place of the measured insulin concentration above baseline. The state $X(t)$ thus no longer represents the active insulin effect, but instead describes a general glucose-lowering effect of identical units min^{-1}, with the parameter p_2 governing its decay dynamics. The introduction of the function Z also means that the parameter S_G replaces the insulin sensitivity parameter S_I in the OMM, as S_G no longer complies with the mathematical definition of insulin sensitivity given by expression (2.1). It is, however, expected that a successful formulation of Z yields a strong correlation between the new parameter S_G and insulin sensitivity S_I inferred by the OMM.

6.4.1.1 Formulation of Z

The function Z couples the current glucose concentration into the description of the state $X(t)$ and replaces the insulin concentrations above baseline in the OMM. In the work by Ruan et al. [152] described in subsection 6.2.2.1, it was assumed that the insulin concentrations are directly proportional to the rate of post-hepatic insulin se-

cretion due to the short half-life of plasma insulin. In this work, the same assumption is made, meaning that Z can be considered similar to the glucose-dependant insulin secretion rate $SR(t)$, for which several modelling approaches were discussed earlier. It should, however, be emphasised that Z only describes a general glucose-lowering effect similar to the state $X(t)$ and a direct connection between Z and actual insulin concentrations cannot be claimed. For the model to be stable and have its steady-state glucose concentration at G_b, the function Z has to be zero at basal glucose level G_b, which is equivalent to the insulin concentration reaching the baseline level I_b in the OMM. The following sections will propose a total of three different formulations for the function Z.

Firstly, similar to Ferrannini's models [153–156], the following relationship is proposed

$$Z_{LOG}(G(t), G_b) = \log \left[\frac{\exp(G(t) - G_b) + \beta}{\beta + 1} \right]. \tag{6.13}$$

The shape of the function Z_{LOG} is similar to the dose-response curve shown earlier in Figure 6.2. However, it is designed to be zero at $G(t) = G_b$. The function is approximately linear in G for $G(t) > G_b$ and flattened at values $G(t) < G_b$ as depicted in Figure 6.5. Here, the influence of the parameter β on the shape of the function is also demonstrated.
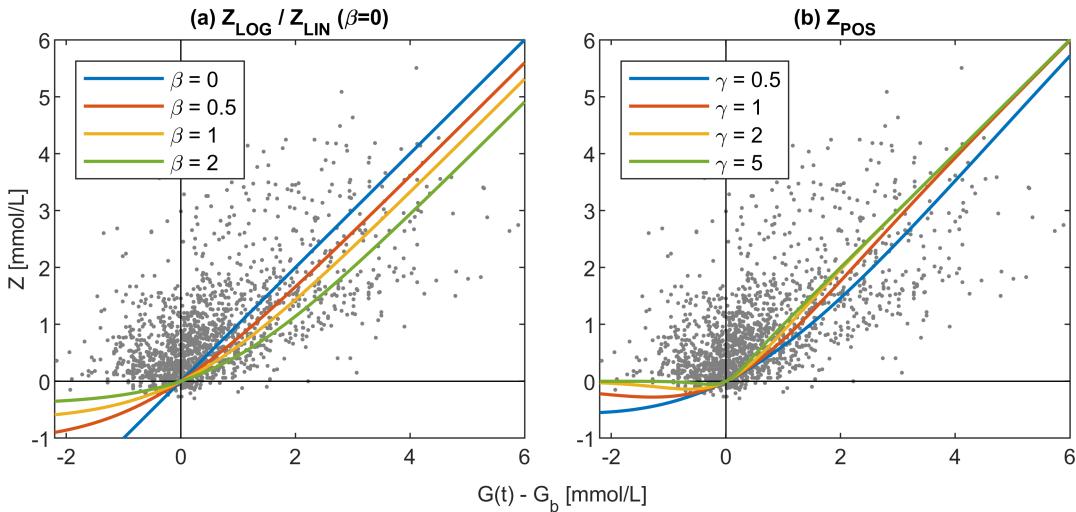
Figure 6.5: Example plots of the functions (a) Z_{LOG} and Z_{LIN} and (b) Z_{POS} for varying values of the shape parameters. For the function Z_{LOG} in (a), it is demonstrated that the function becomes Z_{LIN} for the case of $\beta = 0$. Overlayed in both plots are the scaled data from all meal types already depicted in Figure 6.3.

The function Z_{LOG} is designed so that if $\beta = 0$, it simplifies to

$$Z_{LIN}(G(t), G_b) = G(t) - G_b, \tag{6.14}$$

which forms the second proposed formulation of Z. This linear relationship between glucose and insulin secretion is also used in the models proposed by Hovorka et al. [151, 152] described in section 6.2.2.1. We also proposed model (6.10) - (6.11) in combination with expression (6.14) for the function Z, in a conference publication as a glucose-only alternative to the OMM [164].

In the correlation analysis carried out in section 6.3, it was demonstrated that it is far less common for insulin concentrations to fall below baseline in comparison to glucose concentrations. While this effect is already approximated with the function Z_{LOG} for $\beta > 0$, the function settles on a negative value for values of $G(t) < G_b$. This behaviour, however, cannot be observed in the data as demonstrated in Figure 6.5 (a), where the data are overlayed with the function Z_{LOG}. To better approximate the behaviour of the data for $G(t) < G_b$, the following novel function is proposed as the third alternative

$$Z_{POS}(G(t), G_b) = \frac{G(t) - G_b}{1 + \exp\left[-\gamma(G(t) - G_b)\right]}. \tag{6.15}$$

The function Z_{POS} is designed to be linear in G for $G(t) > G_b$ and to be 0 at $G(t) = G_b$. For $G(t) < G_b$ the function Z_{POS} converges to zero with its shape depending on the parameter γ, as depicted in Figure 6.5 (b).

Initially, it was also considered to formulate Z with a first-order differential equation similar to Breda's model (6.9) to introduce a delay between glucose levels and Z. This, however, gives the model the ability to exhibit significant self-oscillatory behaviour which is physiologically implausible and was thus not considered further in the modelling process. The result of the model formulation in this chapter are three descriptions of Z summarised in Table 6.1. These formulations were partially based on existing ideas for the modelling of glucose-dependent insulin secretion and the relationship between the glucose and insulin levels in the Nuttall dataset examined in section 6.3.

Table 6.1: Summary of the formulations for the function Z proposed in this chapter.

Number	Formulation of $Z(G(t), G_b)$	Parameters
(1)	$Z_{LIN} = G(t) - G_b$	G_b
(2)	$Z_{LOG} = \log\left[\dfrac{\exp(G(t) - G_b) + \beta}{\beta + 1}\right]$	G_b, β
(3)	$Z_{POS} = \dfrac{G(t) - G_b}{1 + \exp[-\gamma(G(t) - G_b)]}$	G_b, γ

6.4.2 Identifiability analysis

6.4.2.1 Sensitivity analysis

Before the structural identifiability analysis was performed, a sensitivity analysis of shape parameters β and γ appearing in the functions Z_{LOG} (2) and Z_{POS} (3), respectively, was carried out. The purpose of this sensitivity analysis was to examine the effect of the parameters β and γ on the model output. The results of this analysis are depicted in Figure 6.6 and imply that β and γ are practically non-identifiable. This is indicated by the fact that, compared to other parameters, they have only a minor influence on the overall shape of the model output, even when sampled from a wide prior PDF with a CV of 200 %. The parameters β and γ are thus fixed and not considered as unknown.
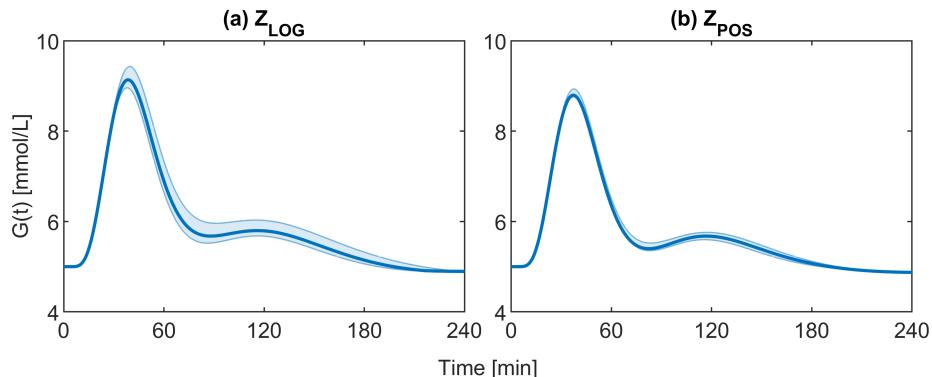
Figure 6.6: Results of the global sensitivity analysis of parameters (a) β and (b) γ for the model using (a) Z_{LOG} and (b) Z_{POS}, respectively. The solid lines and shaded areas show the median and interquartile ranges of the model output over 1000 Monte-Carlo simulations, where all parameters except β and γ were fixed, and the PDFs for both parameters were chosen to be log-normal with medians of one and two for β and γ, respectively and a CV of 200 %.

The chosen values for β and γ are one and two, respectively. This was based on the

results in Figure 6.5, where it is demonstrated that the resulting shapes of functions Z_{LOG} ((a), yellow) and Z_{POS} ((b), yellow), approximate the relationship between glucose and insulin in the Nuttall dataset suitably.

6.4.2.2 Structural identifiability analysis

Based on the results form the previous section, the following parameters are considered for estimation: the system parameters p_1, p_2 and S_G as well as the parameters related to the input function T_1, T_2, W_1, W_2 and R_H. Identical to the previous chapters, it is assumed that both initial conditions G_0 and X_0, as well as G_b, A and V in the model (6.10) - (6.12), are known.

In the previous chapter, it was already mentioned that the Taylor series approach fails in models using the log-normally based input function Ra_{LN}. The ORC method is therefore used, where it can be shown that all unknown parameters in all three proposed model formulations using Z_{LIN}, Z_{LOG} and Z_{POS} are structurally locally identifiable (see Appendix B.3.1 for the details). As the symmetric input function Ra_{LN} is used, the same locally identifiable parameter combinations, mentioned in section 5.3.2.2 exist. These arise from the fact that the two log-normal input components of Ra_{LN} can be switched for the same overall shape, which would be indicated by $T_1 > T_2$.

To give additional evidence for the structural identifiability results of the ORC method, the model (6.10) - (6.11) in combination with Z_{LIN} (1) and the following simplifications is analysed with the Taylor series method

$$Ra_{LN}(t) = k \cdot t, \qquad Rap(t) = R_0 \exp(-t\alpha). \tag{6.16}$$

This assumes a simplified input function with a single unknown parameter k and a known persisting absorption $Rap(t)$, formulated by an exponential decay defined by the known parameters R_0 and α. Here, the Taylor series approach in combination with symbolic computation shows that all parameters, i.e. p_1, p_2, S_G and k are structurally globally identifiable. This could indicate that these parameters are also structurally globally identifiable when the more complex input function Ra_{LN} is used. When the simplifications (6.16) are applied to the GOMs in combination with Z_{LOG} (2) and Z_{POS} (3), the symbolic computation no longer completes unless the parameter k is considered to be known. In this case, the remaining parameters, i.e. p_1, p_2 and S_G are structurally

globally identifiable (see Appendix B.3.2 for the details of the symbolic computation).

Although the structural global identifiability of all parameters in all model candidates cannot be definitively shown, these results provide sufficient evidence to support the numerical identification of the models and do not warrant a reparameterisation. As before, the structural identifiability results are validated with a practical identifiability analysis after parameter estimation.

6.4.3 Choice of prior distributions

The identifiability analysis concluded with the following parameters to be estimated: the system parameters p_1, p_2, S_G and the parameters related to the input function T_1, T_2, W_1, W_2 and R_H. In comparison to the OMM, parameters p_1, p_2, T_1, T_2, W_1, W_2 and R_H have the same interpretation and are thus defined by the respective prior distributions used in the OMM (Table 6.2). This leaves parameter the S_G, requiring the definition of suitable prior distributions. S_G is restrained to positive values as it would cause unstable model behaviour otherwise, so it is transformed into a log-normally distributed parameter as explained in section 3.3.2.2. To define the prior distribution of S_G, a stochastic sensitivity analysis comparing the model output for different prior PDFs to the glucose responses is carried out, as explained in section 3.4. The result is that a prior median of 0.05 min^{-1} per mmol/L and a CV of 50 % is chosen for S_G. The respective model output for all formulations of Z (1)-(3) in comparison to the data is provided in Figure 6.7, where it is demonstrated that the model output approximates the median and variability of the observed data in the case of the STAND meal. Similar results are obtained for the other meals types.
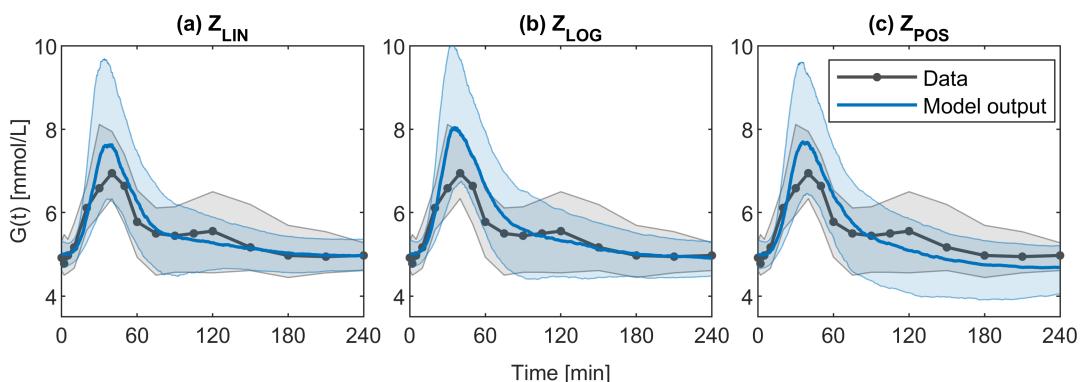
Figure 6.7: Comparison of the data and the median and interquartile range of 1000 Monte-Carlo simulations of the model output of GOMs with (a) Z_{LIN}, (b) Z_{LN} and (c) Z_{POS} using the prior distributions for the STAND meal.

The details of all the prior distributions and constants used for the model identification are summarised in Table 6.2. Similar to the OMM in the previous chapters the influence of the individual parameters and their prior distributions on the output of the GOM candidates is demonstrated by varying the value of one parameter at a time, while the other parameters are kept fixed at their prior medians. The results are given in Appendix D.4.

Table 6.2: Details of the prior distributions and fixed values used for the parameter estimation of the glucose-only models.

Parameter	Unit	Prior median $\pm$ CV %	Description
p_1	min^{-1}	0.025 ± 25	Glucose effectiveness
p_2	min^{-1}	0.012 ± 40	Rate constant governing the decay of $X(t)$
S_G	min^{-1} per mmol/L	0.05 ± 50	Coupling parameter between Z and $X(t)$
T_1, T_2	min	$[30, 100] \pm 30$	Peak times of first and second input function components, respectively
W_1, W_2	-	0.5 ± 30	Width of first and second input function components, respectively
R_H	-	0.7 ± 30	Controls the relative contributions of the two input function components
β	-	1 (fixed)	Shape parameter of Z_{LOG} (2)
γ	-	2 (fixed)	Shape parameter of Z_{POS} (3)
V	L/kg	0.145 (fixed) [72]	Glucose distribution volume
λ	mmol/L	0.11 ± 10 (fixed)	Standard deviation of measurement error
f	-	0.9 (fixed) [72]	Fraction of ingested glucose that is absorbed
D	mmol/kg	(fixed)	Amount of CHO per kg of body weight (see Table 4.1)

6.4.4   Parameter estimation procedure

The parameter estimation procedure is identical to the previous models discussed in Chapters 4 and 5 and uses the VB approach. To incorporate the overlapping effects between meals, the procedure already used for the OMM and depicted in Figure 4.3 is used. This allows the practical description of glucose dynamics if multiple consecutive meals are consumed and would require only minor modifications for any number of meals with an arbitrary duration in between. The details of the model implementation within the VB toolbox are provided in Appendix C.3.

After all three model candidates are identified on every response, the individual results are combined using the Bayesian model averaging (BMA) technique introduced in section 3.5.2. Here, it should be emphasised that this combination is done for each response individually and does not involve results from other responses of the same individual or the population as a whole. This results in a fourth set of results, referred to as the BMA results, for each individual response, additional to the three sets of results of the model with Z_{LIN}, Z_{LOG} and Z_{POS}. The BMA results contain posterior distributions over the unknown parameters as well as the trajectories of the states for each individual response. The application of this technique is possible as the three model candidates are sufficiently similar, i.e. the models are of the same order and have the same number and interpretation of the unknown parameters.

6.4.5   Model comparison and validation

The performance of the three models as well as the combined results using BMA are compared according to four criteria. These criteria consist of the more generic model selection criteria RMSE and free energy as well as criteria specific to the purpose of the developed GOMs, i.e. the extraction of insulin sensitivity and glucose appearance. For three out of the four criteria a reference value for the comparison of the model performance against an independent result is also provided. In detail, the four criteria are as follows

- Model fit, as assessed through the RMSE values. The reference results are provided by the RMSE values of the OMM in Chapter 4 using the piecewise-linear input.

- Free energy, i.e. the model's ability to provide a balance between model fit and

complexity. For that, the following procedure is applied. For each inferred response, a model is considered a "winner" if it has the largest free energy, or the difference of its free energy to the model with the largest free energy is less than 3, i.e. it is considered equal to the model with the largest free energy, as explained in section 3.5. This means that more than one model can be considered a "winner" for each response. To then compare the models with respect to each other, the number of times each model is considered a winner is calculated as a share of the total number of responses across the entire dataset. This criterion can only be applied for the three proposed models and not the BMA results as it does not provide a free energy value. Furthermore, no reference result can be obtained for this criterion.

- Correlation between the parameter S_G and the insulin sensitivity S_I inferred from the OMM in Chapter 4 using the piecewise-linear input. A higher correlation between S_G and S_I means a more accurate and reliable estimation of insulin sensitivity using the respective GOM. To minimise the influence of outliers, the Spearman rank correlation coefficient is utilised. As a reference result, the previously calculated correlation coefficients between the glucose and insulin data are used (see Figure 6.3).

- Similarity between the glucose appearance profile Ra_{LN} estimated with the GOM and the piecewise-linear glucose appearance profile Ra_{PL} inferred with the OMM. To quantify this similarity, we assign to every meal response a single value calculated as the median of the absolute relative difference between the two inferred appearance profiles, as follows

$$m\delta_{Ra} = \text{Median} \left| \frac{Ra_{PL}(t) - Ra_{LN}(t)}{Ra_{PL}(t)} \right|. \tag{6.17}$$

A model with a lower value of $m\delta_{Ra}$ means that the appearance profiles are more similar to the OMM estimated profiles and thus more accurate. The reference values are provided by the $m\delta_{Ra}$ values between the log-normal appearance profiles from Chapter 5 and the piecewise-linear glucose appearance profile Ra_{PL} from Chapter 4 both inferred by the OMM.

The purpose of the model comparison procedure is to assess whether any of the proposed models clearly outperforms the other models across all four criteria. If no

single most suitable model can be determined, it will be assessed to what extent the combined results from the BMA method are comparable to the results of the individual models and whether it is preferable to use the BMA results instead of choosing a single model candidate. To validate the selected results coming from either a single model or BMA, their model fit and ability to extract insulin sensitivity and glucose appearance information with respect to the OMM is examined and judged in more detail.

6.5 Results and discussion

6.5.1 Practical identifiability analysis

The results of the practical identifiability analysis, i.e. posterior CVs of all estimated parameters, are displayed in Figure 6.8.
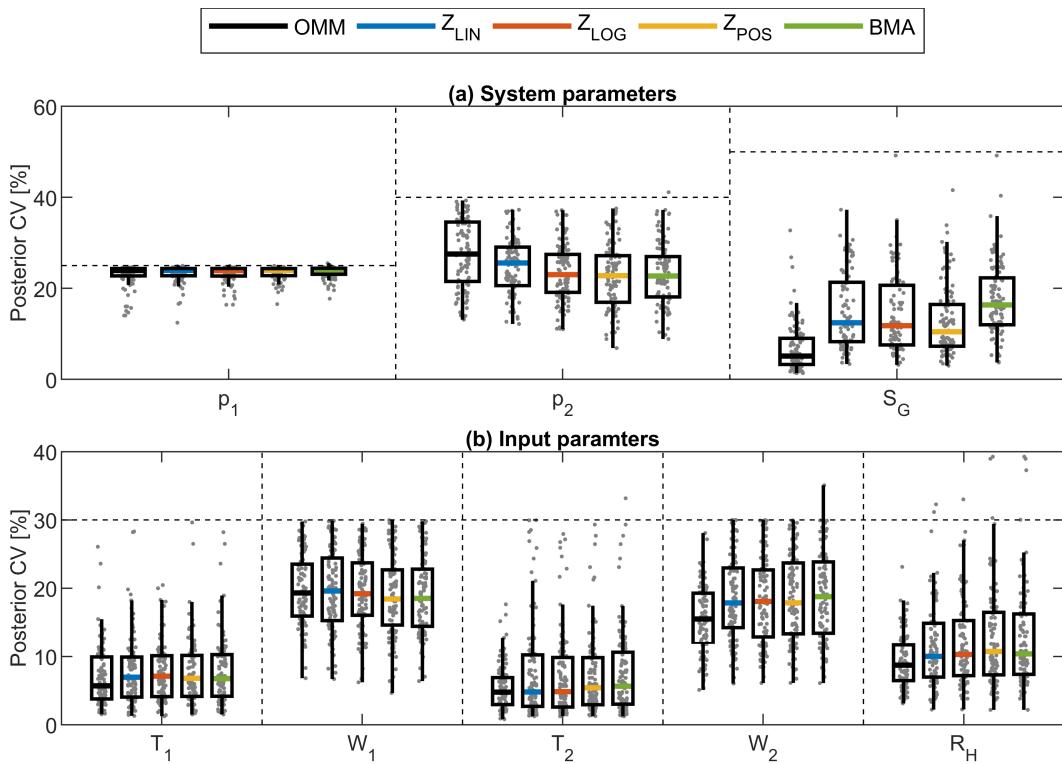
Figure 6.8: Results of the practical identifiability analysis using posterior parameter CVs. The parameters are separated into (a) parameters characterising the system and (b) parameters characterising the input function Ra_{LN}. The results are given as box-plots and individual values with the horizontal dashed lines indicating the prior CV. In (a), the boxplots with the black line represent the posterior CVs of the OMM using the piecewise-linear function Ra_{PL} for p_1, p_2 and S_I (in the S_G column) from Chapter 4. In (b), the boxplots with the black line represent the posterior CVs of the OMM using the new input function Ra_{LN} from Chapter 5.

It is evident that the posterior CVs for the parameter p_1 only marginally decreased from the prior in all of the GOMs considered (see Figure 6.8 (a)) meaning that this parameter cannot be estimated beyond a certain level of precision, similar to the OMM. The parameter p_2 displays minor differences among the considered GOMs with some models yielding a higher posterior precision in comparison to the OMM (black dot). Regarding the new parameter S_G, the results demonstrate the highest posterior precisions of all system parameters and adequate convergence to considerably lower CVs in comparison to the prior. Noteworthy is that the posterior CV of the BMA results (green) is slightly increased during the BMA process. This is a result of the fact that median values of S_G in Z_{LOG} (2) are mildly increased in comparison to Z_{LIN} (1) and Z_{POS} (3), translating into a higher uncertainty in S_G during BMA (see expression (3.51)). Overall, the precision of S_G is lower in comparison to the S_I in the OMM (black), which is most likely the result of omitting the insulin data to describe the state $X(t)$.

The input function parameters in Figure 6.8 (b) show very similar results across all proposed GOMs and the BMA results. In comparison to the OMM using Ra_{LN} (boxplots with black lines), the median values are similar in all parameters but show increased confidence intervals in parameters T_2, W_2 and R_H, indicating the existence of outliers. This means that the estimation accuracy of the parameters of the second, log-normal input function component is impaired in several cases appearing predominantly in the high-protein meal (HPROT). The results nevertheless demonstrate that all input parameters are practically identifiable, which confirms the theoretical results from the structural identifiability analysis.

6.5.2   Model comparison and selection

The results of the model comparison analysis concerning the four model comparison criteria are displayed in Figure 6.9. In terms of the RMSE in Figure 6.9 (a), all three models provide a similar model fit, with only Z_{POS} (yellow) leading to an improved model fit in the meal of standard composition (STAND) and Z_{LIN} (blue) showing a larger variability in the HPROT meal. Regarding the free energy in Figure 6.9 (b), Z_{POS} (yellow) shows the highest winning share across all meal types. Nevertheless, the other model candidates also show winning shares above 50 %, meaning that the other candidates cannot be considered to be clearly inferior according to the free energy. Regarding the correlation analysis in Figure 6.9 (c), the estimated median values

for S_G for all model candidates show very similar and significant ($p < 0.05$) correlations to the insulin sensitivity as estimated by the OMM. As implied by the results of the correlation analysis between glucose and insulin data (shown in black), the correlations are different across meal types with the high CHO meal (HCHO) showing the largest and the high protein meal (HPROT) showing the lowest correlation. In terms of the similarity between the estimated glucose appearance profiles of the GOM candidates and the OMM shown in Figure 6.9 (d), all candidates show significantly ($p < 0.05$) higher $m\delta_{Ra}$ values than the reference provided through the comparison of the new input function to the conventional piecewise-linear function in the OMM. Amongst the model candidates, the $m\delta_{Ra}$ values are similar.
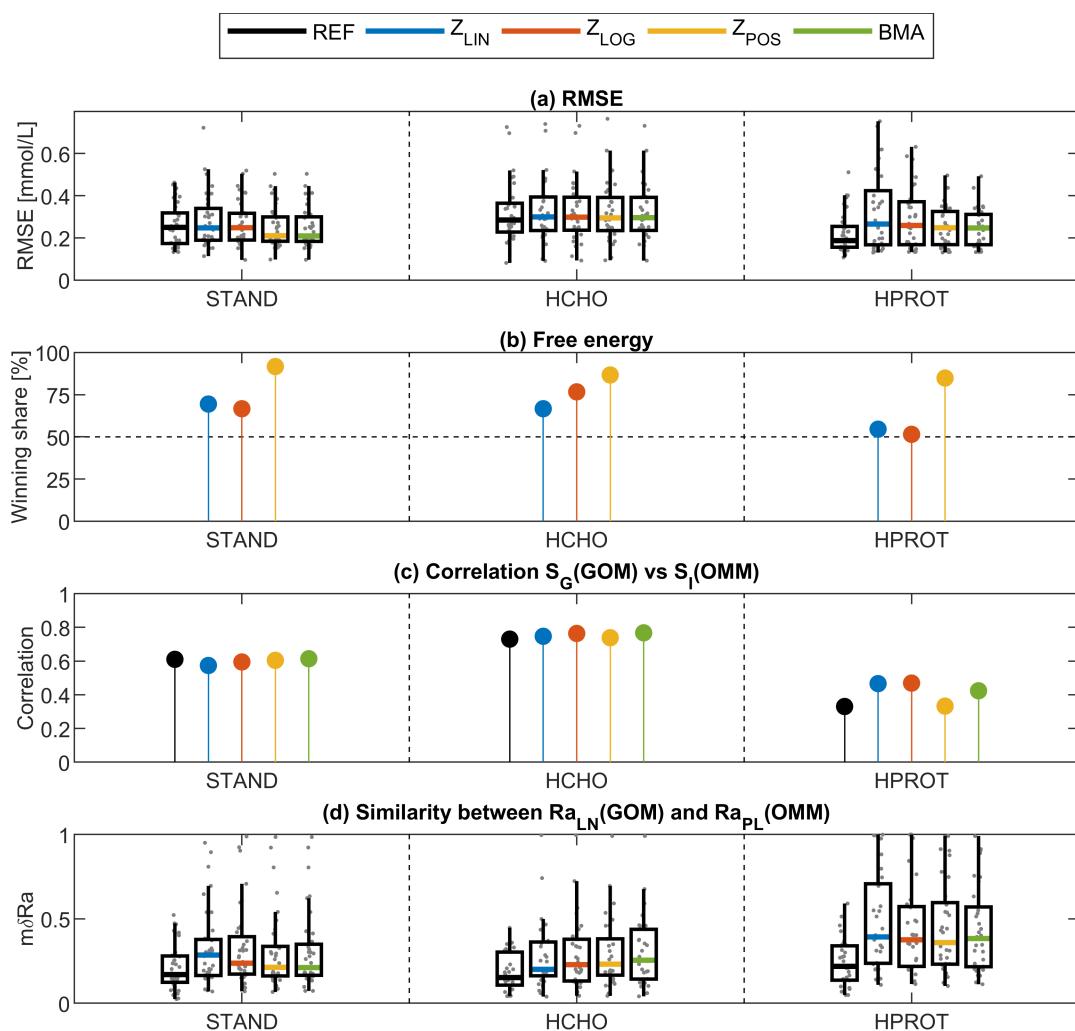
Figure 6.9: Results of the model comparison, concerning the meal types and the four model selection criteria of (a) RMSE, (b) free energy, (c) correlation and (d) the similarity of estimate glucose appearance profiles. In (a) and (d), the distributions are given as boxplots and individual values. The black data indicates the reference results for the respective model fit criteria described in section 6.4.5.

From this comparison, it can be concluded that none of the three proposed models stands out as clearly superior for all of the criteria and all meal types, making it very difficult to select a single model as the most suitable model candidate. This highlights the benefits of using the BMA technique as it allows the combination of estimates from the three model candidates for every response in an objective manner using the free energy criterion. Examining the results of the BMA technique (green) in Figure 6.9 across all criteria, it can be concluded that the BMA method provides results that are very similar to the three proposed candidates. Given this similarity and the difficulties in selecting a single most suitable model candidate, we choose to use the combined BMA results of all the model candidates as the result of the GOM modelling approach.

6.5.3   Parameter estimation results

Based on the choice of using the BMA results, its posterior parameter estimates and ability to fit the data will be examined. They will hereby be referred to as GOM results and include posterior parameter distributions and correlation matrices as well as the model states and corresponding output.

6.5.3.1   Parameter estimates and correlation

The posterior results of the GOM are grouped according to meal type and displayed in Figure 6.10. The system parameters p_1 and p_2 are similar in all meal types and follow their prior distributions. The differences in the posterior medians of S_G with respect to meal type will be discussed in more detail in section 6.5.4.1. With regards to the posterior CVs already discussed in the context of practical identifiability in section 6.5.1, it can be noted that there is a decrease in the posterior precision in the parameters p_2 and especially S_G in the meal of high protein composition (yellow boxplot), which could be explained by the generally decreased glucose excursions in this meal type, making it more difficult to estimate the dynamic parameters.

The posterior medians of the input function parameters in Figure 6.10 (c) show no significant differences between meal types ($p > 0.05$ according to the Kruskal-Wallis test). This result is identical to the OMM using the input function Ra_{PL} displayed in Figure 5.6 in the previous chapter. The same can be said regarding the posterior CVs, where the width parameters W_1 and W_2 show increased values due their minor influence on the model output, as shown in the Appendix Figures D.5 - D.7. Furthermore, the

HPROT meal type generally leads to higher posterior uncertainties which is also similar to the OMM results in Figure 5.6 (d).
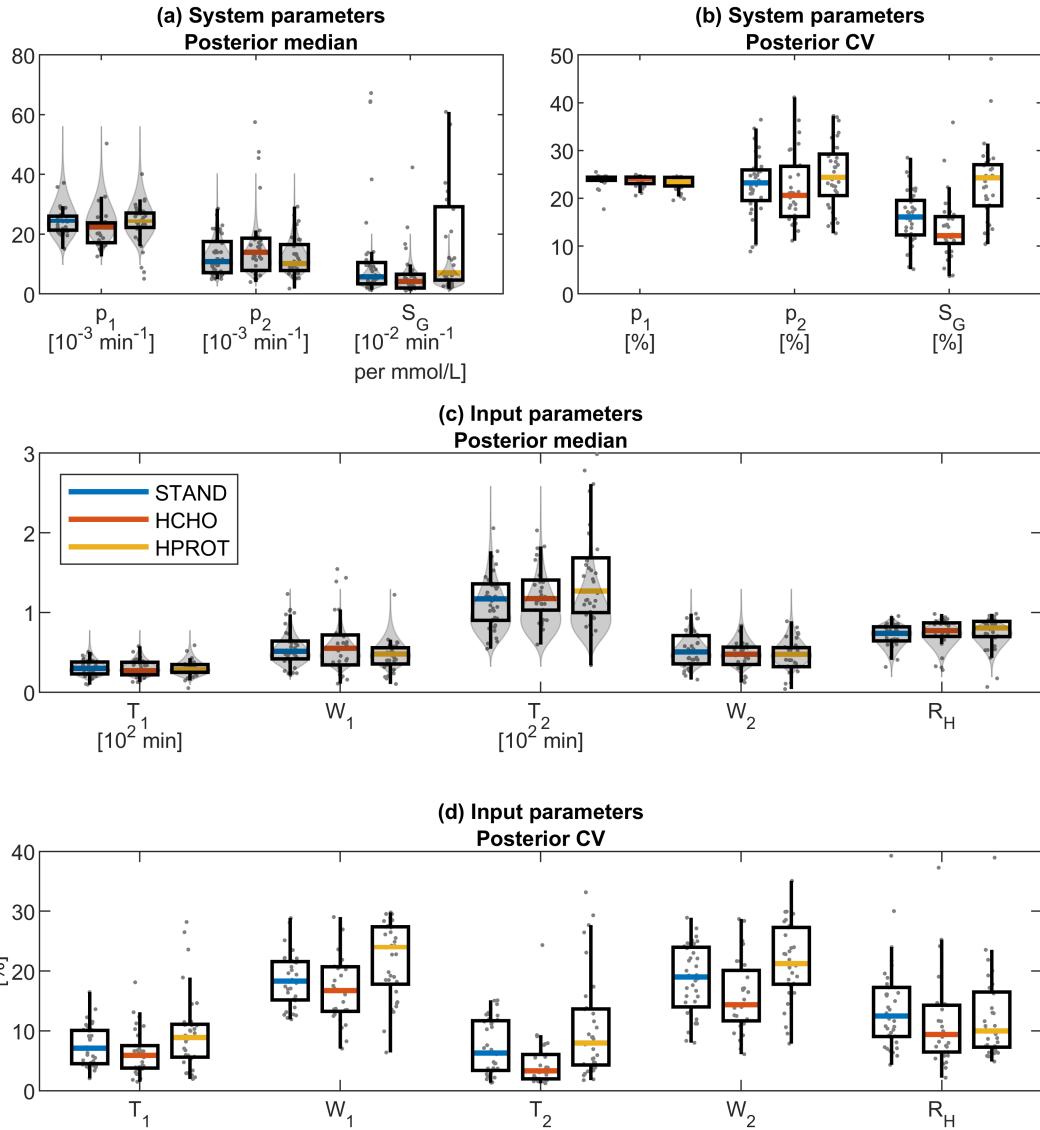
Figure 6.10: Posterior parameter estimates of the GOM. Displayed are the population boxplots of median and CV of the log-normal posterior distributions of (a)-(b) system parameters and (c)-(d) input parameters, grouped according to the meal types of standard (STAND), high CHO (HCHO) and high protein (HPROT) composition. The shaded grey areas indicate the respective prior distributions.

The correlation of the model parameters in the GOMs, assessed through the posterior covariance matrix as described in section 3.3.2.2, is displayed in Figure 6.11 (a). The majority of the correlations are small and thus non-significant. Similar to the corresponding results of the OMM using Ra_{PL} in Figure 6.11 (b), the GOM results also show correlations between R_H and other input function parameters as well as p_2. This can again be explained by the fact that the parameter R_H has a significant impact on

the model output as shown in the Appendix Figure D.4, which overlaps with the effect of other parameters. With respect to the system parameters, there is a minor negative correlation between S_G and p_2, which cannot be seen in the corresponding parameters of the OMM. A reparameterisation of the model is nevertheless not plausible.
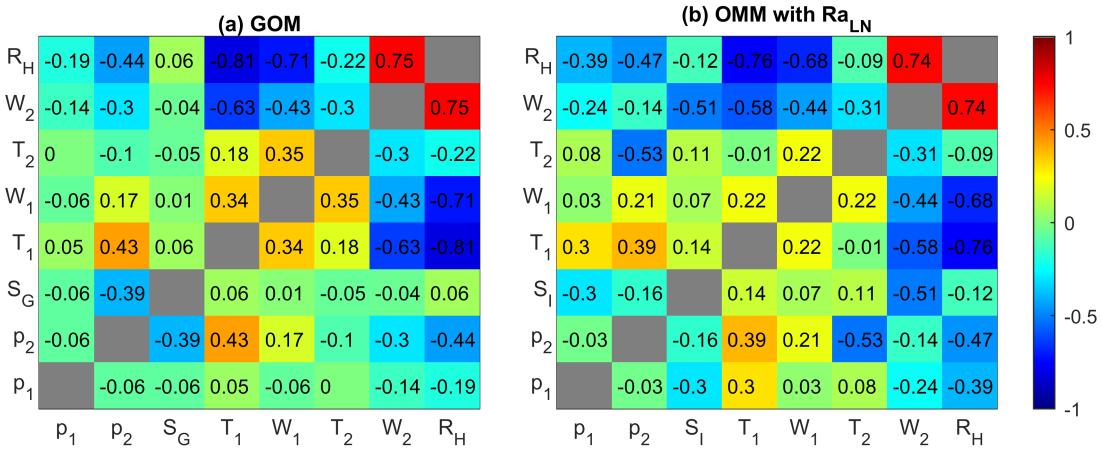
Figure 6.11: Median posterior parameter correlation matrix of (a) the GOM and (b) the OMM using the log-normally based input function Ra_{LN}, from the individually estimated parameter correlation matrices of all 99 responses.

6.5.3.2 Model fit

To provide a more detailed assessment of model fit in comparison to the OMM, the associated profile of weighted residuals is displayed in Figure 6.12.
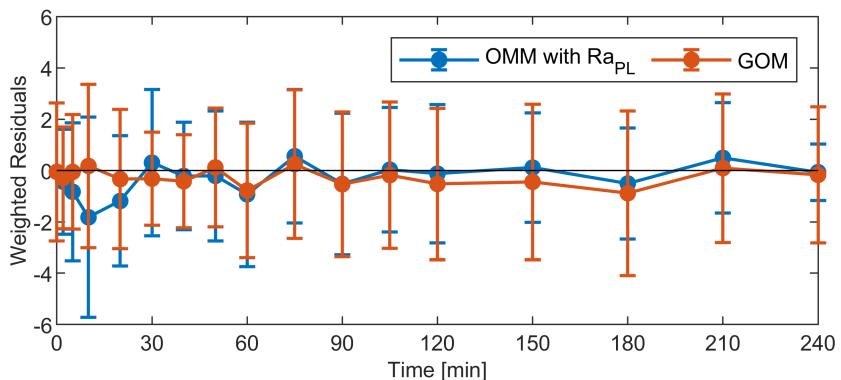
Figure 6.12: Comparison of the weighted residuals between the model output of the OMM and the GOM using Z_{POS}, respectively. The values and error bars represent the mean and standard deviation of the weighted residuals over all meal responses.

The overall mean and standard deviation of the absolute weighted residuals is 0.33 $\pm$ 0.24 for the GOMs compared to 0.49 $\pm$ 0.48 for the OMM using the piecewise-linear input. This difference is due to the improved model fit during the first 30 min of the

response. Overall, the results demonstrate that GOMs fulfil the formulated require-
ments of equal or improved ability to describe the glucose data. To further illustrate
the model fit, an example of the model output for each meal type is given in Figure 6.13.
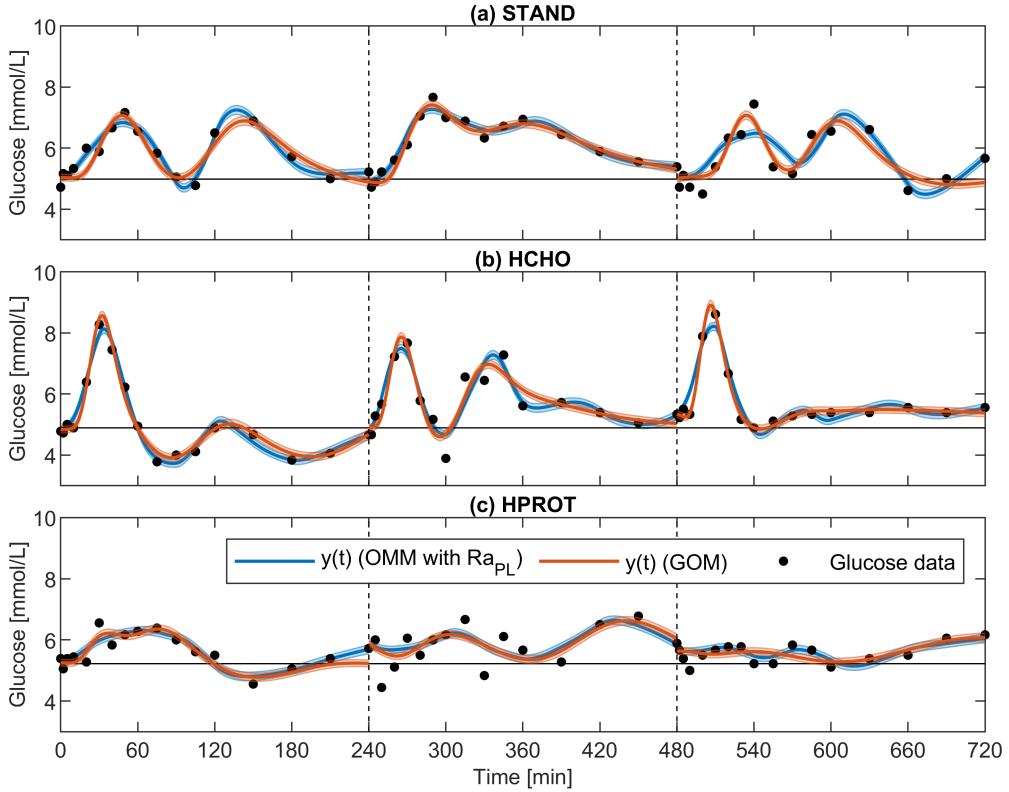
Figure 6.13: Comparison of the model output of the OMM using the piecewise linear
input function Ra_{PL} and the GOMs for the three meal types of (a) standard (STAND),
(b) high CHO (HCHO) and (c) high protein (HPROT) composition. The shaded area
represents the uncertainty (standard deviation) from a deterministic sensitivity analysis
and solid black line provides the basal glucose level G_b.

An example of all model states and GA on an individual level is provided in Figure
6.14. In plot (a), it is demonstrated that both OMM and GOMs describe the glucose
data well and predict similar glucose profiles with very low uncertainty, as indicated by
the small standard deviation. Minor differences occur during the breakfast response,
which stem from the fact that the two models use different input functions. Figure 6.14
(b) exemplifies the differences between the inferred state $X(t)$ in both models. These
differences are due to the fact that, in the OMM, the state $X(t)$ is heavily influenced by
the measured insulin profiles as they enter this state as a known input. This information
is withheld from the GOM and the inferred state $X(t)$ is instead coupled with the state
$G(t)$. The fact that the moderately different profiles of $X(t)$ lead to very similar profiles
of $G(t)$, exemplifies how the description of glucose appearance and the estimation of

the parameter p_1 can compensate for these differences.
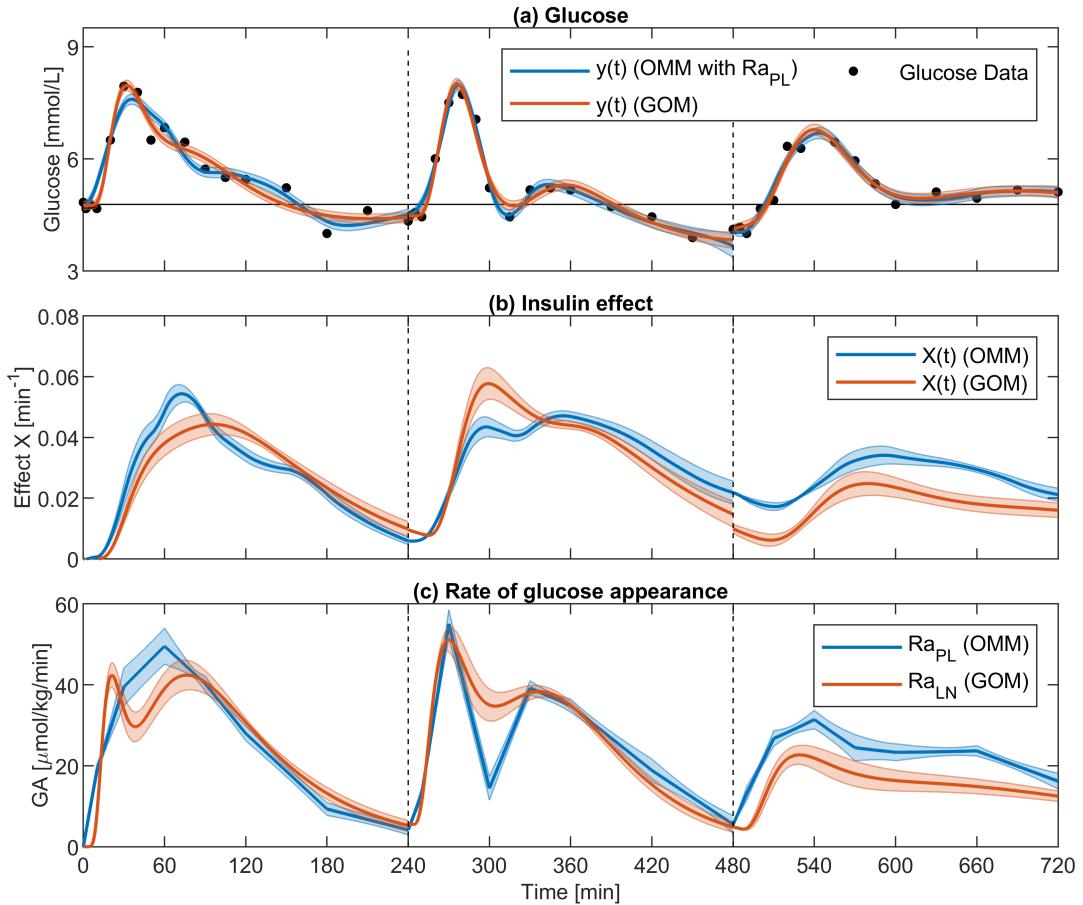
Figure 6.14: Comparison between the OMM (using Ra_{PL}) and the GOM (using Ra_{LN} and BMA) in terms of (a) glucose data against predicted glucose measurements, (b) inferred state X(t) and (c) inferred glucose appearance profiles, on a subject consuming a meal of standard composition. All results are plotted as mean and standard deviation resulting from the deterministic model sensitivity analysis described in section 3.4.

Figure 6.14 (b) also demonstrates, that a resetting of the initial condition to zero for every meal responses would not be plausible. In this context, a minor weakness of the BMA approach can be seen in the transition between lunch and dinner in plot (b): because the results are combined for every response individually, different models may be favoured from one response to the next, leading to discontinuous transitions between responses. In terms of the inferred GA profiles in Figure 6.14 (c), it is demonstrated that the profiles have similar shapes and can be estimated with high precision. The differences are again due to the fact that two different input functions are used and that the GOMs receive no insulin profiles as input.

6.5.4   Model validation

6.5.4.1   Estimation of insulin sensitivity

In terms of the ability of the GOMs to provide information on insulin sensitivity, it has already been shown in Figure 6.9 (c) that the models provide a parameter S_G that is significantly correlated to a validated insulin sensitivity measure derived from the OMM. A more detailed plot of the correlation between S_G and S_I for each meal type is given in Figure 6.15. For comparison with other methods of insulin sensitivity estimation discussed in section 2.1.3, Figure 6.15 also provides the Pearson correlation coefficients and results of a linear regression analysis. For the case of the HCHO meal, a single outlier value of the 30 S_G estimates was removed as the Pearson correlation is highly sensitive to the presence of outliers. Figure 6.15 demonstrates that the slope of the linear trend line and thus the range of S_G values are different for each meal type. Although the GOMs account for different CHO amounts in the meal types through the adjustment of the AUC of the input function, the S_G values are significantly higher ($p < 0.05$) in the HPROT meal type compared to the HCHO meal type, as already shown earlier in Figure 6.10. This difference is not present in the respective S_I results, as demonstrated in Chapter 4, which weakens the interpretability of S_G as insulin sensitivity across different meal types.
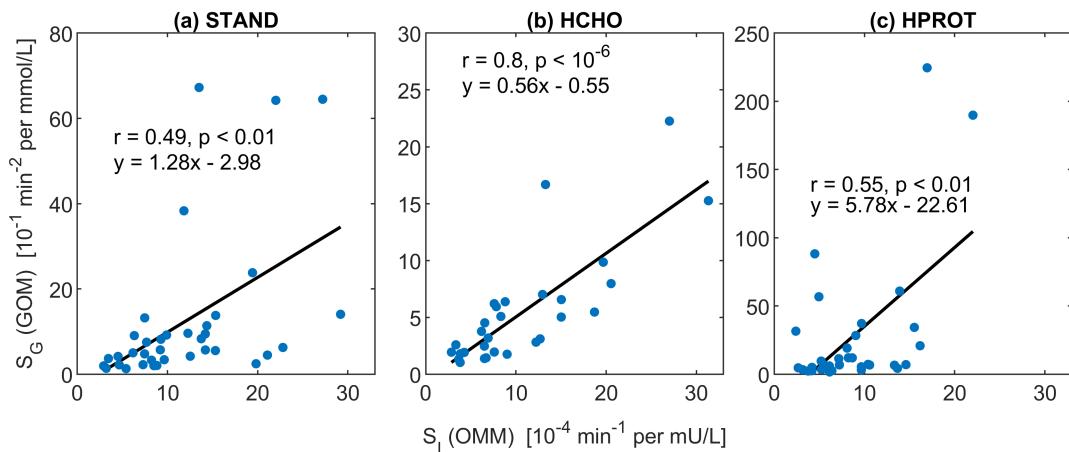
Figure 6.15: Pearson correlation analysis of the GOM parameter S_G against OMM estimated insulin sensitivity S_I for meal types (a) STAND (b) HCHO and (c) HPROT. The black line and equation give the results of a linear regression analysis. It should be mentioned that the y-axis is scaled differently in each plot to fit the respective S_G values.

Taking the meal with high CHO content (HCHO) in Figure 6.15 (b), the Pearson

correlation between S_G and S_I of 0.8 is comparable to results in the literature. Studies using the conventional OMM to estimate insulin sensitivity found correlation coefficients of 0.75 against the IVGTT minimal model [71] and 0.81 against HEC results [123]. In comparison to other indices of insulin sensitivity, such as HOMA-IR ($r = 0.65$ in comparison to HEC results) and the Matsuda index ($r = 0.73$ in comparison to HEC results) [35] the results of the HCHO meal show increased correlation.

There are two inherent limitations in the approach to using only glucose data to assess insulin sensitivity. Firstly, as already shown in the cross-correlation analysis, the dynamic properties of glucose and insulin levels, e.g. peaks, can exhibit very little similarity, especially in meals with low relative CHO content. The second limitation stems from the fact that absolute levels of insulin are not always correlated to absolute glucose levels, even when the dynamical properties of both signals are identical. This means that two subjects could have quantitatively similar glucose profiles but exhibit vastly different absolute insulin levels and thus also have different insulin sensitivities. Detecting this difference using glucose data alone is thus inherently impossible. This reasoning can also explain the differences in S_G values between meal types, mentioned earlier in this section. It could, therefore, be concluded that the correlations between glucose and insulin data give an estimate on the upper bound to the accuracy of insulin sensitivity estimation that can be achieved with GOMs as demonstrated in Figure 6.9 (c).

Based on these results and considerations, the use of the proposed GOMs as a clinical test to measure insulin sensitivity cannot be justified as more elaborate experiments using HEC results would be required. The demonstrated correlations are nevertheless promising and indicate that the models can provide valuable information about insulin sensitivity from glucose data alone.

6.5.4.2   Estimation of glucose appearance

The last requirement for the GOMs developed in this thesis is the ability to estimate the meal-related appearance of glucose. The model comparison results in Figure 6.9 (d) show that the GA profiles of the GOMs have a larger deviation from the reference profiles of the piecewise linear function Ra_{PL} than inferred profiles of Ra_{LN} obtained in the previous chapter. This is also demonstrated in Figure 6.16 where all inferred

GA profiles are compared. Similar to the log-normal input function Ra_{LN} used in the OMM (blue), the function Ra_{LN} as inferred by the GOMs (red) shows a large difference to the piecewise-linear function Ra_{PL} (black) in the first 30 min of the response. This difference stems from the particular properties of Ra_{LN} and was also observed in the previous chapter. Seeing that the model fit is improved during the first 30 min of the response (Figure 6.12), the same arguments already made in the previous chapter for a more realistic estimation using Ra_{LN} can be put forward. This effect is exemplified in Figure 6.14 in the breakfast response.

Another deviation between Ra_{LN} from the GOM (red) and the piecewise-linear function Ra_{PL} (black) is the underestimation of GA in the second half of the GA profile after 120 min. As demonstrated in Figure 6.16, this deviation is not present in the Ra_{LN} profile inferred from the OMM (blue) in the previous chapter. This underestimation of the GA of the GOM in the second half of the response can be explained by the fact that it is common for insulin levels to remain elevated above baseline in the second half of the response when glucose levels have already reached baseline. This means that the OMM infers elevated GA levels to keep the glucose at baseline. Since the GOM does not have the insulin data, it is impossible to account for this effect. An example of this can also be seen in the dinner response in Figure 6.14.
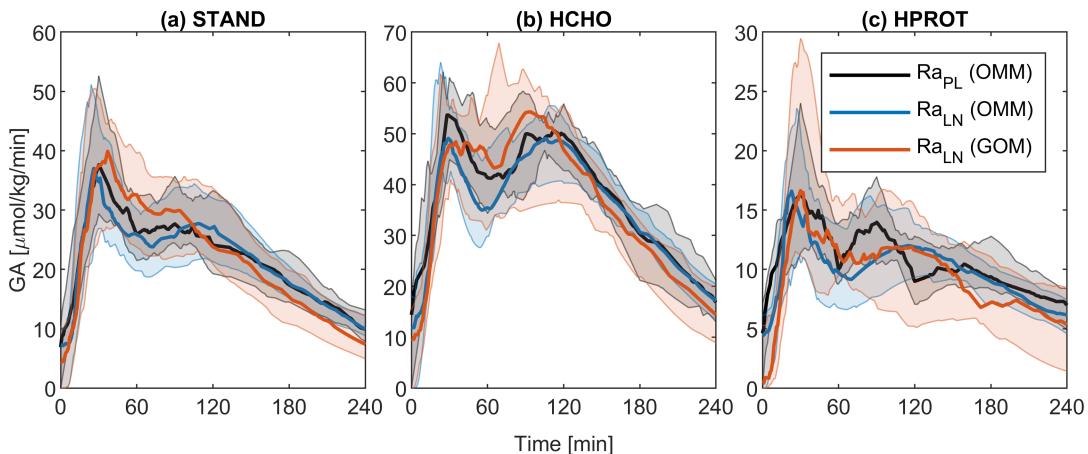
Figure 6.16: Comparison between the inferred glucose appearance profiles for (a) STAND, (b) HCHO and (c) HPROT meal types. The results are given as the median and interquartile range.

Despite these differences, it can be concluded that the GOMs are capable of inferring the general shape of the GA profiles, with evidence of an improved estimation in the first 30 min of the response. This makes it possible to assess differences in GA between

meal types using the GOMs. An example of such an analysis is provided in Figure 6.17, where it is demonstrated that the GA inferred by the GOMs displays the same differences between the STAND and HCHO meal type as the GA inferred by the OMM. In particular, both models reveal that share of glucose absorbed within the first 60 min after meal consumption is reduced in the HCHO meal, as already mentioned in section 4.5.4.
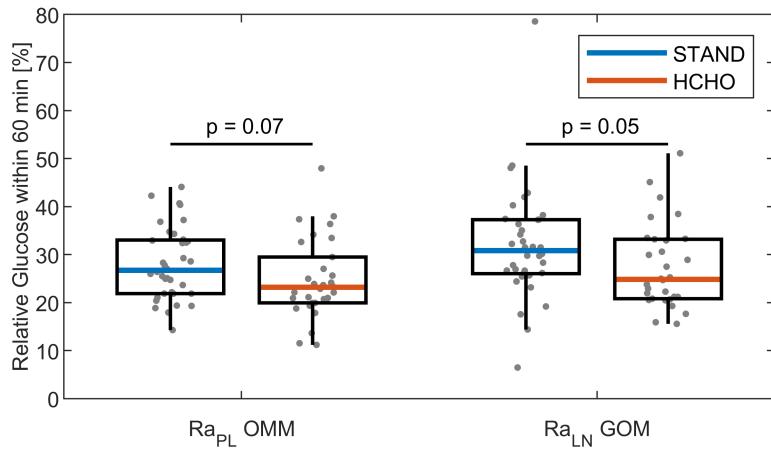
Figure 6.17: Comparison of the share of absorbed glucose within the first 60 min of meal consumption, as inferred by OMM and GOM for the STAND and HCHO meal types. The p-values give the result of a Wilcoxon ranksum test.

6.6   Summary and conclusion

In this chapter, the main aim of this thesis has been reached successfully by developing and subsequently validating glucose-only models for the description of postprandial glucose responses. The proposed models use physiological principles from models of insulin secretion, as well as results from examining the dynamical glucose-insulin relationship. Furthermore, a novel formulation of the meal-related glucose appearance is incorporated. The proposed GOM approach combines the results of three models on an individual level using a Bayesian model averaging (BMA) technique which avoids the need to choose a single model as most suitable in all circumstances. This BMA technique gives the modelling approach the necessary flexibility to be applied to other datasets including other meal types and subjects with varying levels of glycaemic control. The GOM results are validated against the results from the well-established OMM using glucose and insulin data. It has been demonstrated that the GOMs (1) achieve a slightly more accurate description of glucose dynamics (2) contain a newly introduced

parameter that shows a significant correlation to insulin sensitivity estimates from the OMM and (3) enable the inference of GA profiles that are similar to the GA profiles inferred with the OMM, allowing the comparison of GA profiles between meal types.

Shortcomings of the presented work so far stem from the properties of the used dataset and associated experimental protocol, as only NGT subjects and glucose data from venous blood sampling were considered. Additionally, the meals were consumed at regular intervals, not representative of daily life. For successful application, the model has to be useful in conjunction with data from continuous glucose monitoring (CGM) collected on Pre-DM and T2DM subjects. This will be subject of the remaining chapters concerned with the collection of a suitable dataset and validation of the developed GOMs.

Chapter 7

Collection and analysis of experimental data in subjects with varying glucose tolerance under controlled and normal life conditions

7.1 Introduction

All preceding modelling efforts have utilised the Nuttall dataset containing glucose and insulin responses from subjects with normal glucose tolerance (NGT) recorded through frequent venous blood sampling. Meals were additionally consumed under controlled conditions at regular intervals, not representative of daily life. Collecting this type of data in clinical practice is highly infeasible, therefore creating the need to design a study with a more practically oriented data collection process. The main purpose of the described experimental study is to provide an independent pilot dataset to validate the developed models and assess the utility of the experimental techniques. The pilot dataset thereby complements the Nuttall dataset and focuses on:

- Including subjects with Pre-DM and T2DM, as they form the main target group for application of the developed models. NGT subjects will also be recruited as a control group.

- Recording glucose data using continuous glucose monitoring (CGM) over multiple days under controlled and free-living conditions. CGM technology is increasingly used in the management of T2DM [16–18] and can provide a far more detailed picture of BG levels than frequent blood sampling or self-monitoring of blood glucose (SMBG), even outside the hospital.

- Involving a single meal test during which blood sampling for the measurement of glucose and insulin levels is carried out. This provides the necessary data to identify the oral minimal model for comparison with the glucose-only models identified from the CGM data.

- Including controlled exercise periods to examine their effect on glucose dynamics. Besides food intake, exercise has a significant influence on glucose dynamics [165, 166] and it is an important tool for the treatment of Pre-DM and T2DM, thus warranting the examination of its effect on glucose dynamics.

This chapter describes the subject cohort, experimental procedures, presents the collected data and carries out a basic model-free data analysis. The application of the dataset to the models developed previously will be the subject of the following chapter.

7.2 Methods

7.2.1 Subject recruitment

Before the experimental study, ethical approval was given from the National Health Authority Research Ethics Committee, North West - Liverpool East, United Kingdom (ID: 17/NW/0277). This includes compliance with the Ethical Principles for Medical Research on Human Subjects established in the Declaration of Helsinki by the World Medical Association. The study was sponsored by, and conducted at the Human Metabolism Research Unit (HMRU) at the University Hospitals Coventry and Warwickshire NHS Trust. The goal of the recruitment was to enrol participants with NGT, Pre-DM and non-insulin dependant T2DM into the study. Potential subjects were contacted through a number a means including university newsletters, leaflets, public speaking and word of mouth. Prospective participants were considered to have T2DM if they had been diagnosed at least one year prior to the study and taking oral antihyperglycaemic drugs. No diabetes screening was carried out before the study, meaning that the exact glycaemic

status of subjects considered to have NGT and Pre-DM, was only determined during the study. The subjects volunteered for the study and gave written consent which was obtained by a trained and qualified member of staff at the HMRU.

7.2.2 Continuous glucose monitoring

To record blood glucose profiles, subjects were fitted with an abdominal Enlite glucose sensor in conjunction with the Medtronic iPro2 CGM system (Medtronic PLC, Minneapolis, MN, USA). This CGM device provides glucose levels with a sampling period of 5 min and is blinded to the user, i.e. glucose measurements are recorded for retrospective analysis and not shown in real-time, therefore requiring no handheld device. The subjects were instructed to perform four finger-prick calibration measurements per day (after wake-up, before lunch, before dinner and before bed) using the Abbott Freestyle Lite SMBG device (Abbott Laboratories, Abbott Park, IL, USA). After the study, the blood glucose profiles were calculated from interstitial fluid (ISF) glucose levels beneath the skin and SMBG calibrations using the Envision Pro software (Medtronic PLC, Minneapolis, MN, USA). During this calibration process, the ISF glucose levels are shifted forwards by 10 min before the blood glucose profile is calculated to counteract the time delay between ISF and blood glucose levels mentioned in section 2.2. More detailed information on the calibration algorithm is not provided by the manufacturer.

7.2.3 Experimental protocol

In conjunction with the recommended lifetime of the CGM sensors, the study was carried out over a period of six days. Five of the six days were spent under normal living conditions, meaning that the subjects went about their normal daily life while keeping a diary on food intake and exercise. On day one, the experiment was initiated during a short visit to the research site (HMRU). Here, the CGM devices were fitted, the subjects were educated on the calibration routine, their medical history was recorded and basic anthropometric measurements such as height and weight were taken. Additionally, the subject's body composition, i.e. fat and lean weight, was determined through air displacement plethysmography using a BodPod 2000A (Cosmed, Rome, Italy). On the evening of day three, the subjects returned to the HMRU for a 24-hour inpatient monitoring session. This meant that subjects were confined to a small observation room with food and exercise routine being precisely controlled. After the 24-hour inpatient

monitoring session subjects resumed free-living conditions. A detailed schedule of the inpatient monitoring session is provided in Table 7.1. At the end of the experiment, on day six, subjects returned the CGM and SMBG devices as well as their diaries and the experiment was terminated.

Table 7.1: Detailed schedule of the 24-hour inpatient monitoring session at the Human Metabolism Research Unit (HMRU).

Time	Event
19:00	Arrival at HMRU
20:00	Standard meal (dinner)
22:00	Lights out
07:00	Wake-up
08:30	Oral glucose tolerance test (breakfast)
12:00 - 12:30	30 min stepping excercise (80 steps per min)
13:00	Low CHO meal (lunch)
17:30 - 18:00	30 min stepping excercise (120 steps per min)
18:45	Standard meal (dinner)
19:00	Leave HMRU

7.2.3.1 Diet

For the inpatient monitoring session, the diet was as follows:

- Breakfast: Oral Glucose Tolerance Test (OGTT) containing 75 g anhydrous glucose in a liquid solution. To comply with the standard test procedure [34], the size of this meal was not scaled according to body weight or calorie demand.

- Lunch: Low CHO meal containing 20 % CHO, 40 % fat and 40 % protein. The meal was composed of lentil soup, croutons, cheese, natural yoghurt and a milk-based protein shake. The size was scaled to provide 40 % of the estimated daily calorie demand.

- Dinner: Meal of standard composition containing 50% CHO, 35 % fat and 15 % protein. The meal was composed of rice and chicken curry. The size was scaled to provide 40 % of the estimated daily calorie demand.

Water or non-caffeinated herbal teas were provided ad libitum. Subjects were requested to gradually reduce caffeine intake before the experiment, to minimise withdrawal effects. The meal sizes were scaled to provide an isocaloric diet. For that, the resting energy expenditure was calculated based on lean mass using the Katch-McArdle formula [167] and activity multipliers between 1.2 and 1.4 were used to estimate the total daily calorie demand. These activity multipliers were based on recommended values for the mainly sedentary behaviour exhibited by the subjects during the inpatient monitoring session [168].

During normal living conditions, the subjects' diet was not restricted, but recorded via a detailed food log. These diets included mainly standard food items from western/British cuisine such as starchy foods (bread, rice, cereals, potatoes, pasta, etc.), fruit and vegetables (bananas, apples, peas, zucchini, etc.), meat and fish (chicken, cod, sausage, ham, etc.), eggs and dairy products (milk, yoghurt, cheese, etc.) and sweets (cake, biscuits, chocolate, etc.).

7.2.3.2 Exercise

The exercise during the inpatient monitoring session consisted of stepping up and down a standard height exercise step (height 150mm) at varying rates and thus intensities were controlled by a metronome (see Table 7.1). One cycle of stepping up and down consists of four separate steps (two up and two down).

7.2.3.3 Blood sampling

Venous blood samples were collected before (fasted) as well as 15, 30, 60 and 120 min after the OGTT was carried out. For reasons not related to the experiments themselves, the sample analysis was carried out by two different and experienced laboratories. The first laboratory analysed the samples from subjects S2 and S3 (see Table 7.2) and used the Roche Cobas 8000 Enzymatic (Roche Diagnostics, Basel, Switzerland) for glucose measurement and the Mercodia Iso-Insulin enzyme-linked immunosorbent assay (Mercodia, Uppsala, Sweden) for insulin measurement. The samples for the remaining subjects were analysed with the Abbott Alinity glucose and insulin reagent kits (Abbott Laboratories, Abbott Park, IL, USA), respectively. Regarding the comparability of the insulin measurement results between the two laboratories, it can be stated that the Mercodia Iso-Insulin assay has been shown to have a non-significant bias against

the mean of eleven other insulin assays [54]. The Abbott assay used by the second laboratory is new and no comparisons to other assays are published or provided by the manufacturer. Based on the best available information it can thus be concluded that the insulin measurements for the two techniques are comparable.

The fasting blood sample was used to determine HbA1c. Additional to the venous blood sampling, SMBG tests were conducted approximately at -10, 15, 30, 60, 90, 120, 180 and 270 min after the OGTT.

7.2.4 Data analysis

The CGM dataset is analysed from 19:00 on Day 2 to 19:00 on Day 6. This excludes the first 24 hours of data due to inaccuracies in the measurement caused by a localised inflammatory response at the insertion site [169]. In accordance with the protocol of the inpatient monitoring session in Table 7.1, a day is defined as the period between 19:00 on the current day and 19:00 on the following day.

Based on the laboratory glucose and insulin measurements during the OGTT, indices of insulin sensitivity and beta-cell function are calculated. Insulin sensitivity is estimated with the Matsuda index [170], calculated as follows

$$\text{Matsuda index} = \frac{10,000}{\sqrt{G_0 \cdot I_0 \cdot \overline{G} \cdot \overline{I}}}, \tag{7.1}$$

where G_0 and I_0 represent fasting glucose and insulin levels, respectively and $\overline{G}$ and $\overline{I}$ the mean glucose and insulin levels during the OGTT, i.e. at 0, 15, 30, 60 and 120 min, respectively. The Matsuda index has been shown to correlate well with the OMM derived insulin sensitivty in a NGT population [171]. The beta-cell function is estimated with the ratio of glucose and insulin AUCs [172] calculated as follows

$$\text{AUC}_{I/G} = \frac{AUC_I}{AUC_G}, \tag{7.2}$$

where the individual AUCs are calculated using the trapezoidal rule in MATLAB. The choice of these two indices is based on a publication by Retnakaran et al. [33], where it was found that the two indices provide the best hyperbolic relationship between insulin sensitivity and beta-cell function. This relationship describes the fact that different levels of glycaemic control typically form distinct hyperbolas on a plot of beta-cell function

and insulin sensitivity and has been introduced in section 2.1.2. A calculation of these indices for insulin sensitivity and beta-cell function is not possible in the Nuttall dataset as they require the data to be collected during a standard OGTT.

7.3 Results and discussion

7.3.1 Subject population

The recruitment process led to a total number of eight study participants. The relevant details for each subject are given in Table 7.2.

Table 7.2: Details of the subjects included in the experimental study.

Subject ID	Age	Sex	BMI [kg/m^2]	Lean weight [kg]	Glycaemic status	HbA1c [mmol/mol]	Treatment regimen
S1	45	F	23.6	42.5	NGT	29	-
S2	49	M	26.8	65.5	NGT	33	-
S3	46	M	28.5	68.9	NGT	35	-
S4	38	F	34.2	49.3	Pre-DM	38	-
S5	44	F	49.8	59.3	Pre-DM	46	-
S6	52	M	36.1	67.1	T2DM	45	Metformin
S7	57	M	26.0	64.1	T2DM	43	Metformin, Glimepiride
S8	61	M	25.2	55.9	T2DM	76	Metformin, Canagliflozin, Sitagliptin

NGT and Pre-DM subjects were classified into their respective categories by HbA1c, using the criteria presented in section 2.1.2 and repeated in Table 7.3.

Table 7.3: Criteria for the diagnosis of Pre-DM and T2DM based on HbA1c [34].

	NGT	Pre-DM	T2DM
HbA1c [mmol/mol]	≤ 38	39 - 47	≥ 48

Subject S4 is considered to have Pre-DM despite the HbA1c being below the provided

threshold of 39 mmol/mol. This choice was made because this subject had been diagnosed with T2DM, i.e an HbA1c greater than 48 mmol/mol, approximately one year prior to the study, but achieved a significant drop in HbA1c without pharmacological intervention.

7.3.2 Deviations from the experimental protocol

Multiple deviations from the planned experimental protocol occurred during the inpatient monitoring session.

- In the case of subject S1, the inpatient monitoring session had to be aborted approximately 2.5 h after the OGTT due to the subject temporarily feeling unwell. The CGM was continued for the remainder of the study as the subject recovered within hours of leaving the HMRU.

- In subject S4, venous access could not be established and blood sampling could therefore not be carried out, which led to the delayed consumption of the OGTT meal by about 25 min. The HbA1c result was obtained from a routine blood sample taken independently of the experiment about one month prior to the study. The subject was also unable to perform any of the exercise sessions due to fatigue.

- Subject S5 was unable to perform the first exercise session due to knee pain. The second exercise session was thus adapted by instructing the subject to step on the spot at the given frequency of 120 bpm, which could be carried out without pain.

7.3.3 Continuous glucose monitoring

The CGM profiles could be fully recovered in all subjects with no loss of data. The results from the CGM measurements are summarised in Figure 7.1, which demonstrate increased median glucose levels and glucose variability in Pre-DM and T2DM subjects in comparison to NGT subjects. Additionally, subjects with decreased glucose tolerance display a greater individual day-to-day variability. These differences in glycaemic variability align with the findings from a high number of studies with much larger subject populations (see reviews [173–175]). Due to the low number of subjects in our study, further analysis of this particular aspect of the data is not carried out.

A novel result based on the unique design of our study can be obtained from the comparison between the inpatient monitoring session on Day 2 and the remaining days

spent under free-living conditions. Here, subjects S1, S3, S5 and S7 show increased median glucose levels. This could be explained by two possibly overlapping effects, (1) the daily routine, especially the prescribed diet, during the inpatient monitoring session could have been significantly different to the other days and (2) the unfamiliar environment at the research site led to psychological stress which is known to cause hyperglycaemia in T1DM subjects [176]. This effect of increased glucose levels during the inpatient monitoring session demonstrates caution when extrapolating results obtained under controlled conditions to everyday life and highlights the importance of collecting data under both circumstances.
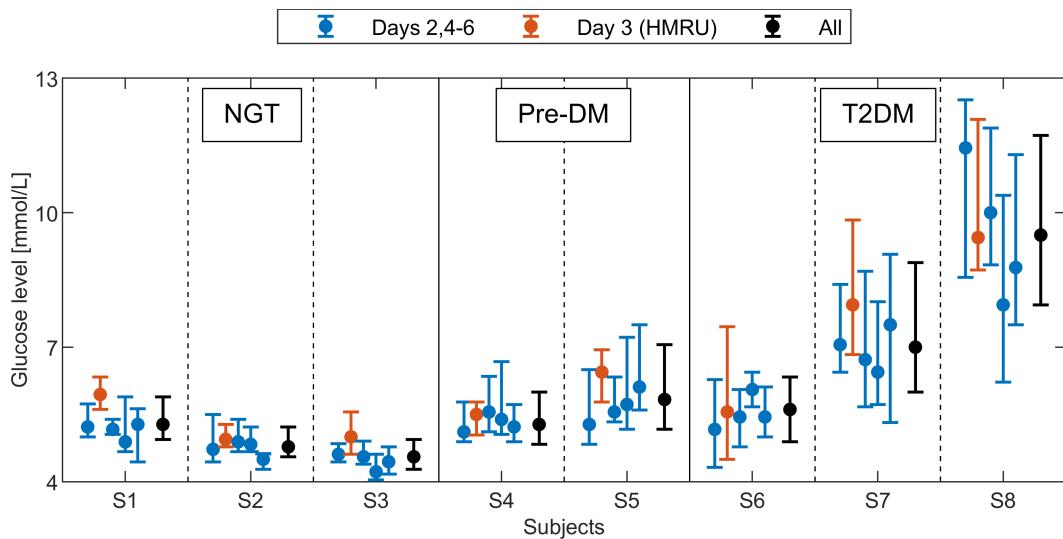
Figure 7.1: Comparison of glucose levels between subjects during the entire study period. Days 2-6 are presented in order with the black datapoint giving the results of all days combined. Day 3 (red) is the period of the inpatient monitoring session at the HMRU. The data are given as the median and interquartile range. In subject S1, day 3 only uses glucose data until 11:00 as this was the time the inpatient monitoring session was aborted.

The CGM profiles of the subjects during the inpatient monitoring session is depicted in Figure 7.2. As expected, the profiles are very different between subject groups, despite all subjects following the same routine. The following dynamical features are of particular interest.

1. Basal glucose behaviour

   The glycaemic behaviour during the night, i.e. under fasted or basal conditions, reveals variabilities in the T2DM group, whereas NGT subjects show almost constant glucose levels. Especially in subjects S5, S6 and S8, there is an upwards trend starting from around 04:00 until subjects were awoken at 07:00. This effect,
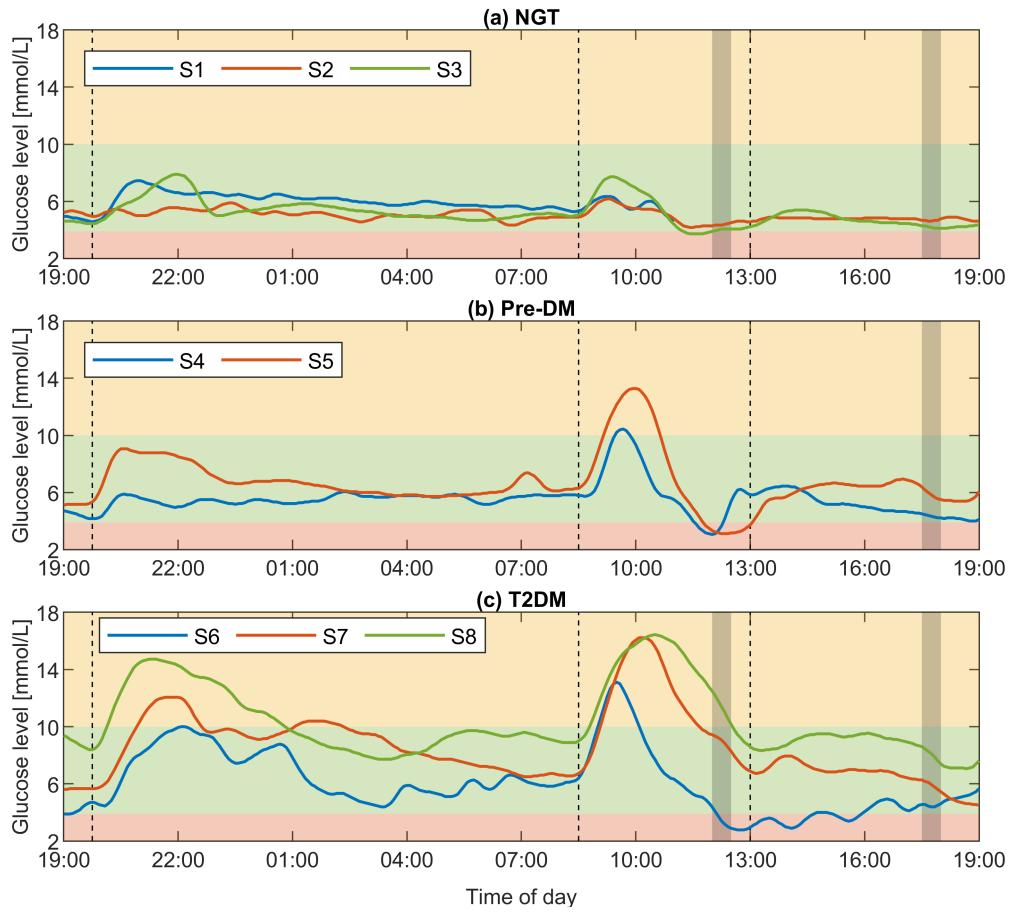
Figure 7.2: CGM profiles of (a) NGT, (b) Pre-DM and (c) T2DM subjects during the inpatient monitoring session. The dashed vertical lines give the approximate times of meal consumption and the grey areas indicate the exercise periods. Since neither of the two Pre-DM subjects carried out the first exercise period, the respective grey area in the centre plot was omitted. The coloured areas give the ranges of hypoglycaemia (red), euglycaemia (green) and hyperglycaemia (yellow).

known as the dawn phenomenon, is common in non-insulin dependant T2DM [177]. A similar drift in basal glucose levels in T2DM could also be present during the day, which has to be considered when making assumptions on the basal glucose levels during modelling.

2. <u>Low CHO meal</u>

The low CHO meal consumed for lunch leads to very small glycaemic excursions, especially apparent in the NGT subjects where almost no excursions are observed, as indicated from 13:00 onwards in Figure 7.2. This is similar to the responses to the meal with high protein composition (HPROT) in the Nutall dataset, which has a similar composition. Pre-DM and T2DM subjects show a more pronounced response, however, their BG levels have not reached steady-state by the time lunch

is consumed, despite a 4.5-hour gap between meals. This means that the persisting effects from the OGTT have a significant influence on the lunch response, which has to be considered during modelling.

3. Exercise

   The effects of the exercise session on BG dynamics are also different among subject groups. NGT subjects show almost no response to either of the two 30-min exercise sessions of different intensity. In contrast to that, Pre-DM and T2DM subjects show a decrease in BG levels in response to exercise. During the first session of lower intensity, the already existing downward trend is accelerated in T2DM subjects. Similarly, during the second exercise session where prior BG levels are more stable, a decrease is observed. In subject S6 the second exercise session leads to deceleration of the existing upward trend. A comparison between the effects of the two exercise sessions is not sensible because the glycaemic conditions before the exercise are not similar enough. The results nevertheless demonstrate the hypoglycaemic and thus beneficial effects of exercise in Pre-DM and T2DM.

The glycaemic behaviour following the OGTT will be examined separately in more detail in the following section.

7.3.4 OGTT and blood sampling

The results of the glucose and insulin measurements during the OGTT are displayed in Figure 7.3. The OGTT glucose responses in Figure 7.3 (a) were recorded by using venous blood sampling, SMBG and CGM allowing the comparison between measurement techniques. CGM and SMBG are not independent because the CGM calibration algorithm uses the SMBG results to calculate its glucose profiles. It is thus expected that the SMBG and CGM measurements agree well with each other as is the case in subjects S4, S5, S6 and S8. In the remaining subjects, especially in S7, the CGM profile lags behind the SMBG results by up to 25 min, although the raw CGM signal is shifted forwards by 10 min before the glucose profile is calculated. This demonstrates that the time lag exhibits inter-subject variability [80, 178]. From a signal processing perspective, the interstitial fluid can be thought of as a low-pass filter attenuating high-frequency changes in BG levels [80, 179, 180]. These changes are particularly prominent

in the excursions of NGT subjects and can explain the fact that CGM profiles show a higher deviation from SMBG values in comparison to the other subject groups. The inclusion of this effect in models using CGM data will be discussed in the next chapter.
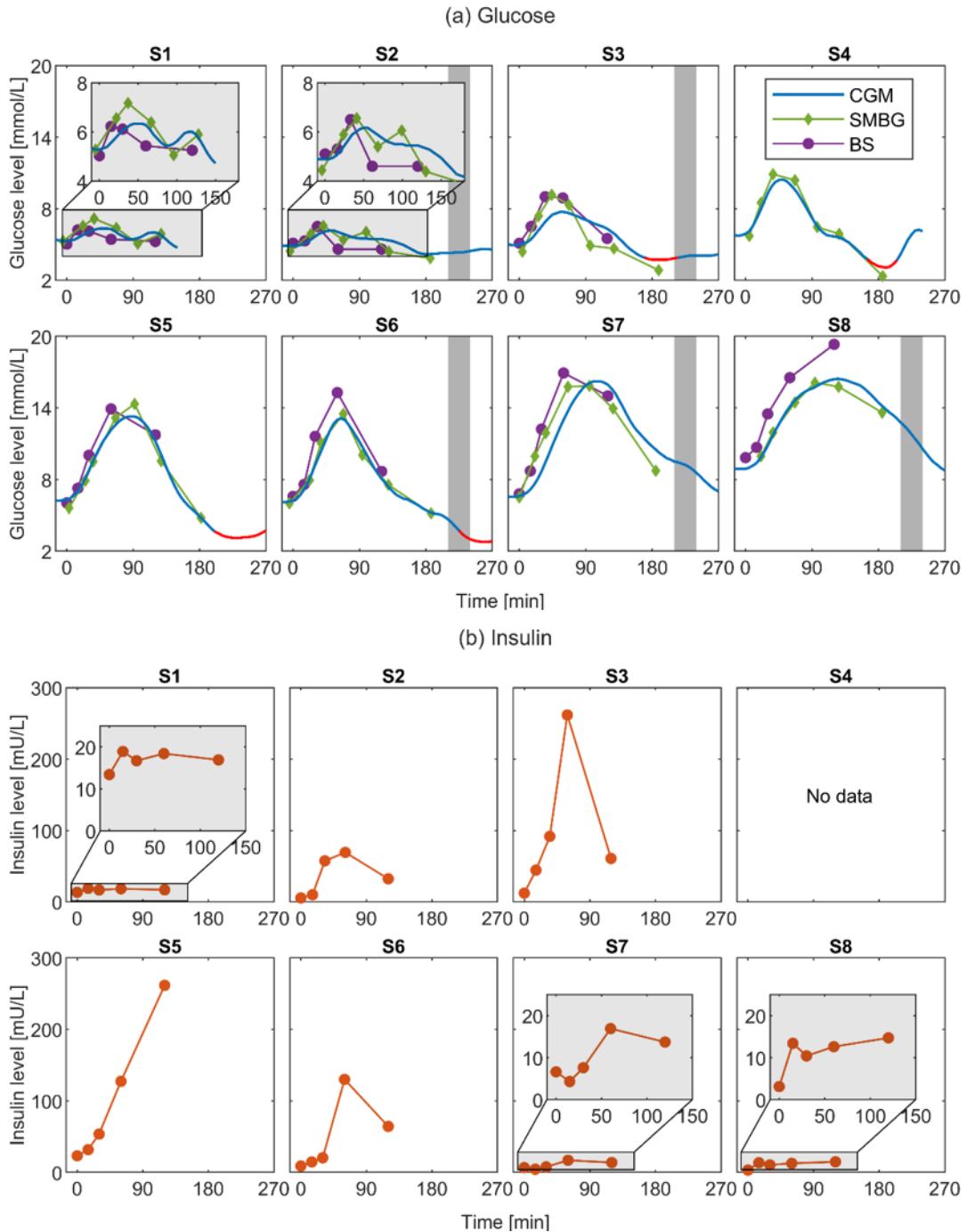
Figure 7.3: (a) Individual plots of glucose levels from CGM, SMBG and blood sampling (BS) during the OGTT. The grey areas indicate the period of exercise in those subjects that performed it and the red sections of the CGM profiles indicate BG levels below the hypoglycaemia threshold of 3.9 mmol/L. (b) Individual plots of insulin levels in response to the OGTT. As explained before, the blood sampling data for subject S4 are missing because venous access could not be acquired.

The blood sampling and SMBG/CGM measurements generally agree well, except for subject S8, where the SMBG results seem to lag behind the venous blood sampling results. This could be a result of that subject's history of peripheral neuropathy impairing blood circulation in the extremities, thus delaying the glucose levels at the finger-tips as measured by the SMBG with respect to venous blood sampled from the inside of the elbow.

The results of the insulin measurements in Figure 7.3 (b) reveal substantial differences between subjects. To interpret these results together with the glucose levels in terms of insulin sensitivity and beta-cell function, the respective indices previously mentioned are calculated and their relationship is displayed in Figure 7.4.
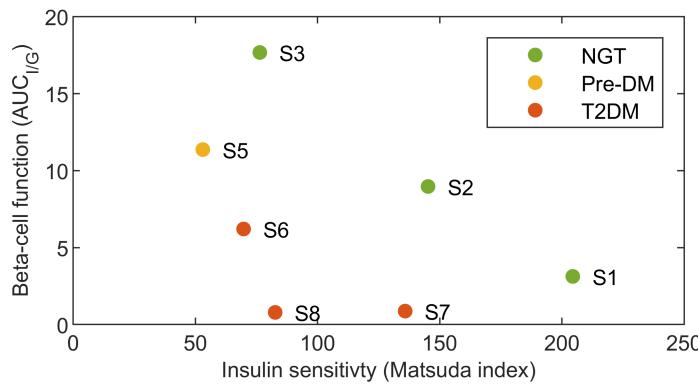
Figure 7.4: Indices of insulin sensitivity and beta-cell function plotted against each other indicating an inverse relationship within subject groups.

Figure 7.4 shows an inverse relationship between insulin sensitivity and beta-cell function. It is additionally indicated that the NGT and T2DM subgroups populate two distinct hyperbolas, as it was explained earlier, with the single Pre-DM subject lying in between. This information is of clinical relevance as it could be used to inform treatment decisions, which can be exemplified in subjects S5 and S7. Both subjects have a similar HbA1c with 45 and 43 mmol/mol respectively, but the results for insulin sensitivity and beta-cell function could have different implications for therapy. Subject S5 has the lowest insulin sensitivity and highest body-mass-index and could thus most benefit from lifestyle interventions such as diet, exercise and weight loss which can increase insulin sensitivity [3]. In contrast, subject S7 already displays good insulin sensitivity, but poor beta-cell function, despite taking the insulin secretagogue Glimepiride (see Table 7.2). This subject could thus potentially benefit from further pharmacological interventions with additional beta-cell stimulants or external insulin.

Examining the relationship between the dynamic properties of the CGM glucose profiles and insulin sensitivity estimates indicates a connection between the two which corroborates the goal of developing glucose-only models for the extraction of insulin sensitivity information taken in this thesis. It also highlights the benefit of using CGM to record glucose responses during an OGTT as it allows the simple identification of relevant glycaemic patterns beyond the typical observation period of 120 min. In particular, the following observation can be made: subjects S3, S5 and S6 with low insulin sensitivity and adequate beta-cell function, exhibit hypoglycaemia approximately 180 min after the OGTT was administered, as displayed by the red sections of the CGM profiles in Figure 7.3 (a). Subjects with higher insulin sensitivity such as S1, S3 and S7 do not display this delayed hypoglycaemia. This can be explained by the fact that subjects with low insulin sensitivity respond to the initial glucose rise with excessive secretion of insulin, leading to delayed hypoglycaemia. Recognising the occurrence of this effect in subject S6, where no insulin data are available, therefore suggests low insulin sensitivity in this subject.

7.4 Summary and conclusions

This chapter described the collection and subsequent model-free analysis of the data in eight subjects with varying glucose tolerance during an inpatient monitoring session and normal daily life. The novelty in the experimental design was given by the use of CGM during both free-living and controlled conditions, as well as recording both glucose and insulin measurements and CGM data during an OGTT. It was revealed that glucose profiles can be different between controlled and free-living conditions, which has implications on the informative value of results obtained under controlled conditions when extended to everyday life. Another important finding was that glucose profiles after the OGTT showed delayed hypoglycaemia in subjects with low insulin sensitivity.

In line with the scope of a PhD project, the experiment included far fewer subjects than the Nuttall dataset and has thus the character of a preliminary study. The results, however, warrant more extensive data collection efforts on additional subjects to reinforce the preliminary findings. Given the problems in executing the exercise routine for some subjects, an alteration to the experimental protocol, e.g. omitting the first exercise session before lunch, should be considered.

Chapter 8

Model-based analysis of experimental data in subjects with varying glucose tolerance

8.1   Introduction

The main purpose of this chapter is to validate the previously introduced contributions to the oral minimal model (OMM) and developed glucose only models (GOM) using the new dataset described in the previous chapter. In particular, the glucose and insulin measurements as well as the CGM recordings during an inpatient monitoring session will be utilised. This provides a unique opportunity to identify the GOMs from CGM data and validate their results by comparison with the results from the OMM identified with blood sampling data.

8.2   Methods and modelling

8.2.1   Identification of oral minimal models

As explained in the previous chapter, the glucose and insulin data required for the identification of the OMM were recorded after an OGTT, conducted during the inpatient monitoring session. Venous blood sampling was carried out fasted (0 min) as well as 15, 30, 60 and 120 min after oral glucose ingestion.

To identify the OMM with the conventional piecewise-linear input function rep-

resenting glucose appearance under these new experimental conditions, the following formulation is used

$$\frac{dG(t)}{dt} = -G(t)X(t) - p_1[G(t) - G_b] + \frac{Ra_{PL}(t)}{V}, \qquad G(0) = G_b, \qquad (8.1)$$

$$\frac{dX(t)}{dt} = -p_2(X(t) + S_I[I(t) - I_b]), \qquad\qquad X(0) = 0, \qquad (8.2)$$

$$Ra_{PL}(t) = \begin{cases} k_{i-1} + \dfrac{k_i - k_{i-1}}{t_i - t_{i-1}}(t - t_{i-1}) & \text{for} \quad t_{i-1} \leq t \leq t_i \quad i = 1 \ldots 4, \\[2mm] k_4 \exp(-\alpha(t - t_4)) & \text{for} \quad t > t_4. \end{cases} \qquad (8.3)$$

In comparison to model formulation (4.5) - (4.7) utilised in Chapter 4, the initial condition for $G(t)$ is set to its baseline G_b and the initial condition of $X(t)$ is set to zero, to reflect fasting conditions. Additionally, the term $Rap(t)$ representing a persisting appearance is removed as only a single response from fasting conditions is described.

Regarding the piecewise-linear input function Ra_{PL} in (8.3), the altered sampling protocol requires adaptations to the number of breakpoints. In Chapter 4, utilising the Nuttall dataset with a tighter and longer sampling schedule, the breakpoints for the piecewise linear function were set at 0, 10, 30, 60, 90, 120, 180 and 240 min, with the height of the breakpoint at 0 min, i.e. k_0 is set to zero. To adhere to the sampling protocol of the new dataset, the breakpoint time points are reduced to $t_0 - t_4$, at 0, 10, 30, 60, 120 min. This eliminates the breakpoints at 180 and 240 min as they lie beyond the duration of the blood sampling. The breakpoint at 90 min is also removed as it would lie between the sampling point at 60 and 120 min, making it difficult to estimate the height of this breakpoint with acceptable precision. Beyond the observation period of 120 min, the function is described by an exponential decay with fixed constant $\alpha = 0.017$ min^{-1}, as recommended in OGTTs with a 120 min response duration [123].

Identical to Chapter 4, the area under the input function curve is restricted during the parameter estimation. For that the height parameter k_4 at 120 min is replaced with the following expression

$$k_4 = \frac{\alpha(D \cdot f - 5(3k_1 + 5k_2 + 9k_3))}{1 + 30\alpha} \qquad (8.4)$$

where D is the amount of glucose in the meal per kg of body weight and f is the fraction of ingested glucose that is absorbed, fixed at 0.9 [123].

To identify the OMM with the newly proposed, differentiable function Ra_{LN}, consisting of two overlapping log-normal components (see Table 5.2), model expressions (8.1) - (8.2) are used. In contrast to the piecewise-linear function, no adaptations to Ra_{LN} are necessary, which demonstrates the practicability of the new input function when applied to new data collected under altered experimental conditions.

The prior distributions over unknown parameters are provided in Table 8.1. The basal levels of glucose and insulin G_b and I_b, respectively, are fixed to the glucose and insulin measurements in the fasting sample. Both models are identified using the VB approach and the details of model implementation in the VB toolbox are provided in Appendix C.1.2.

Table 8.1: Details on the unknown model parameters, their prior distributions and fixed values used in the identification of the OMM.

Parameter	Unit	Prior median $\pm$ CV %	Description
p_1	min^{-1}	0.025 $\pm$ 25 [72]	Glucose effectiveness
p_2	min^{-1}	0.012 $\pm$ 40 [72]	Rate constant governing the decay of $X(t)$
S_I	10^{-4} min^{-1} per mU/L	7.1 $\pm$ 100 [72]	Insulin sensitivity
V	L/kg	0.145 (fixed) [72]	Glucose distribution volume
λ	mmol/L	0.11 $\pm$ 10 (fixed)	Standard deviation of measurement error
f	-	0.9 (fixed) [72]	Fraction of ingested glucose that is absorbed
D	mmol/kg	(fixed)	Amount of CHO per kg of body weight in the OGTT
For Ra_{PL}			
k_1, k_2, k_3	μmol/kg/min	[3.2, 7.3, 5.4] $\pm$ 50 [72]	Levels of GA at time of breakpoints. The priors are scaled by $D \cdot f$
t_0 - t_4	min	[0, 10, 30, 60, 120] (fixed) [71]	Times of breakpoints
α	min^{-1}	0.017 (fixed) [71]	Decay rate of Ra_{PL} after 120 min

<u>For Ra_{LN}</u>

T_1, T_2	min	$[30, 100] \pm 30$	Peak times of first and second components of Ra_{LN}
W_1, W_2	-	0.5 ± 30	Widths of first and second components of Ra_{LN}
R_H	-	0.7 ± 30	Contributions of the AUCs of the individual components to the overall AUC of Ra_{LN}

8.2.2 Identification of glucose-only models

8.2.2.1 Data description

The GOMs are identified from the CGM data recording both OGTT and lunch responses during the inpatient monitoring session. The OGTT response is considered to start at the time of consumption and end when lunch was eaten. Similarly, the lunch response is considered to start when lunch was consumed and end before dinner was consumed. Although the food schedule was controlled during the inpatient monitoring session, the precise time of meal consumption was slightly different for each subject, leading to marginally different response durations. Generally, however, the considered durations for OGTT and lunch responses are 270 min and 345 min, respectively.

8.2.2.2 Model formulation, prior choice and identification procedure

No changes to the formulation of the glucose-only models (6.10) - (6.12) are required, meaning the model equations remain as follows

$$\frac{dG(t)}{dt} = -G(t)X(t) - p_1 \left[G(t) - G_b\right] + \frac{Ra_{LN}(t) + Rap(t)}{V}, \qquad G(0) = G_0, \quad (8.5)$$

$$\frac{dX(t)}{dt} = -p_2 \left[X(t) - S_G Z(t, G_b)\right], \qquad\qquad\qquad X(0) = X_0, \quad (8.6)$$

$$Ra_{LN}(t) = A(1 - R_H)\frac{1}{t\sqrt{\pi W_1}}\exp\left(-\frac{\left(\log\frac{t}{T_1} - \frac{W_1}{2}\right)^2}{W_1}\right)$$
$$+ AR_H\frac{1}{t\sqrt{\pi W_2}}\exp\left(-\frac{\left(\log\frac{t}{T_2} - \frac{W_2}{2}\right)^2}{W_2}\right), \tag{8.7}$$

The three proposed formulations for the functions Z, i.e. Z_{LIN}, Z_{LOG} and Z_{POS} presented in Table 6.1 are also unchanged. The CGM measurement process is described by

$$y(t) = G(t) + \varepsilon, \qquad \varepsilon \sim \mathcal{N}(0, \lambda^2) \tag{8.8}$$

where $y(t)$ is the observed CGM profile and ϵ is the normally distributed measurement error with zero mean and standard deviation λ.

Regarding the choice of priors and model identification procedure, the following changes in comparison to the procedures described in Chapter 6 are made.

- Due to the variability in basal glucose levels in the T2DM subject group, discussed in section 7.3.3, the parameter G_b, describing the baseline glucose levels in expressions (8.5) and (8.6), is considered to be an unknown, normally distributed parameter instead of fixing it to the fasting glucose level. For both OGTT and lunch response, the prior of G_b is determined by the fasting glucose level and a small CV of 2 %, which is calculated as the average BG level in the 30 min prior to the OGTT. The narrow prior distribution does not require a transformation to a log-normal distribution and can keep the baseline level within physiological ranges. It also does not warrant a repetition of the structural identifiability analysis already carried out in Chapter 6.

- The prior median of the parameter S_G, describing the coupling between the function Z and the state $X(t)$ in (8.6) and correlating with insulin sensitivity estimates S_I, is reduced from 0.05 min^{-1} to 0.02 min^{-1}. This change reflects the fact that the study cohort includes subjects with impaired glucose tolerance whose insulin sensitivity and thus S_G values are expected to be reduced.

- The measurement uncertainty defined by the parameter λ is considered to be unknown because the previous chapter revealed inter-subject variability regarding

the accuracy of the CGM profiles. The prior mean for λ for the OGTT response is set to 0.1 mmol/L, as in Chapters 4 to 6 with a large CV of 100 %. For the subsequent lunch response, the prior for λ is defined as the posterior distribution inferred from the OGTT response.

All other prior distributions and techniques of the estimation procedure are identical to Chapter 6. This includes the calculation of the persisting absorption $Rap(t)$ during lunch from the inferred OGTT appearance profile and the determination of the initial conditions as explained in section 6.4.4. As before, the three models, namely Z_{LIN}, Z_{LOG} and Z_{POS} are identified separately on every response and the results are combined using the Bayesian model averaging (BMA) technique.

8.3 Results and discussion

8.3.1 Oral minimal models

8.3.1.1 Model fit

The results of the model inversion of the OMM using both the piecewise-linear input Ra_{PL} and the log-normal input Ra_{LN} are displayed in Figure 8.1. As mentioned in section 7.3.2, no blood sampling data could be collected for subject S4, i.e. the OMM could not be identified in this case.
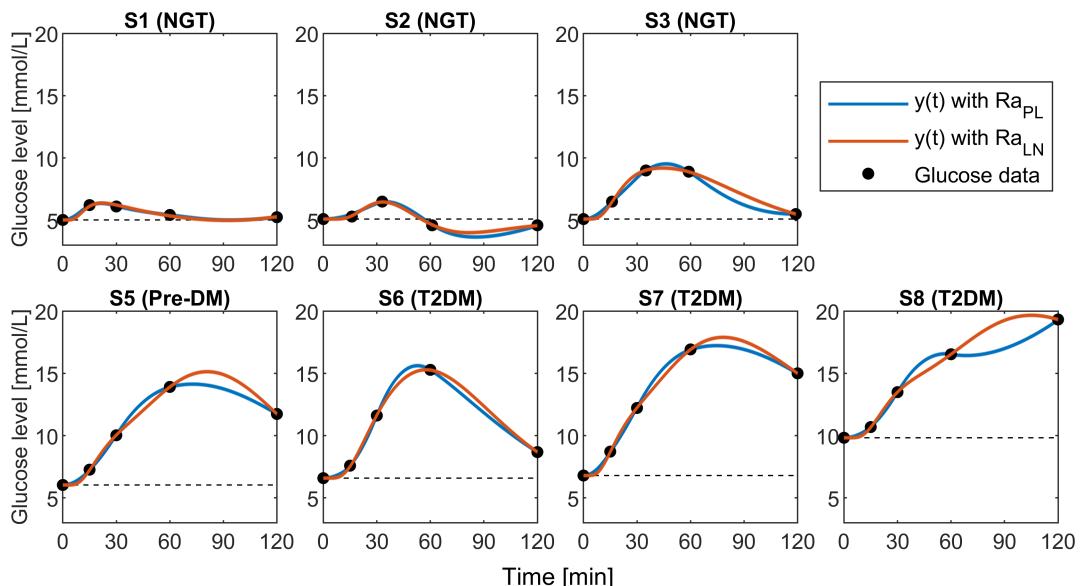
Figure 8.1: Results of the model inversion of the OMM with both input functions Ra_{PL} and Ra_{LN} in terms of the model output. The results are given as mean and standard deviation derived from a deterministic sensitivity analysis as described in section 3.4.

Both forms of the OMM using the two input functions can describe the data well, as demonstrated in Figure 8.1 and also indicated by the low mean and standard deviation of the absolute weighted residuals of 0.09 ± 0.08 for Ra_{PL} and 0.07 ± 0.08 for Ra_{LN}. For comparison, using the Nuttall dataset yielded 0.50 ± 0.48 for Ra_{PL} and 0.37 ± 0.28 for Ra_{LN}.

8.3.1.2 Parameter estimates and correlation

The posterior distributions of the system parameters p_1, p_2 and S_I are displayed in Figure 8.2. Furthermore, the posterior time courses of glucose appearance are displayed in Figure 8.3.
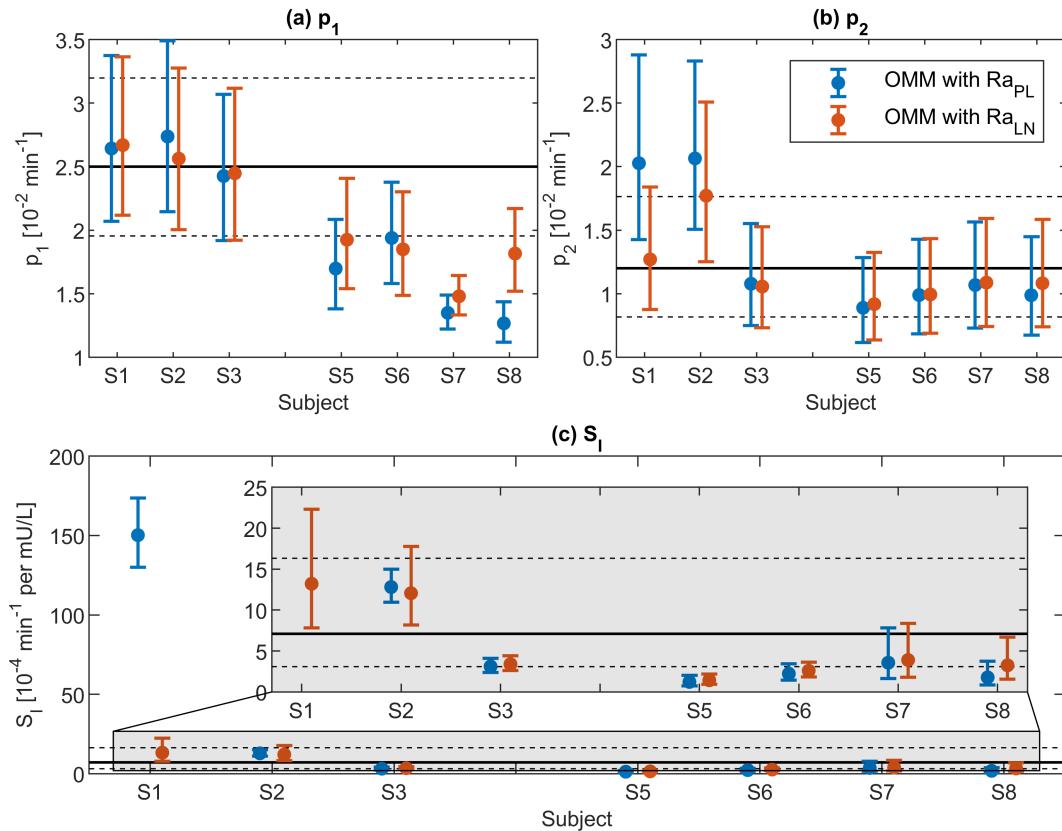
Figure 8.2: Posterior parameter distributions of individual subjects using the OMM and OGTT blood sampling data. The posterior log-normal distributions are given as median and one-sigma range. The bold and dashed horizontal lines indicate the prior median and one-sigma range, respectively.

The estimates of the system parameters and glucose appearances using both input functions generally agree well. The exceptions to that are the results for subjects S1 and S8. In subject S1 the estimates of insulin sensitivity in Figure 8.2 (c) and p_2 in

plot (b) are vastly different between the two input functions. Additionally, two highly different GA profiles are inferred as displayed in Figure 8.3. In contrast, both models lead to a very similar output displayed in Figure 8.1. This indicates the existence of local minima and thus practical identifiability issues caused by the low number of data points available for estimation. Comparing the two estimated median values for S_I in subject S1, it can be concluded that an S_I value of 150 10^{-4} min^{-1} per mU/L as estimated using Ra_{PL} is unrealistic as it more than ten times larger than the estimated S_I value of the other NGT subjects. The S_I value estimated using Ra_{LN} thus appears to be more realistic. This stands in contradiction to the estimated appearance profiles, where the piecewise-linear function Ra_{PL} appears to be physiologically more plausible because the log-normal input Ra_{LN} shows very little appearance at approximately 60 min after meal consumption.

In subject S8, the differences in estimation results, i.e. between parameters S_I and p_1 and the glucose appearance, are less extreme in comparison to subject S1. In contrast, prominent differences in the model output in Figure 8.1 are present. As both models can fit the data very well, practical identifiability issues due to the low number of data points are the most likely cause for the differences in the estimation results in subject S8.
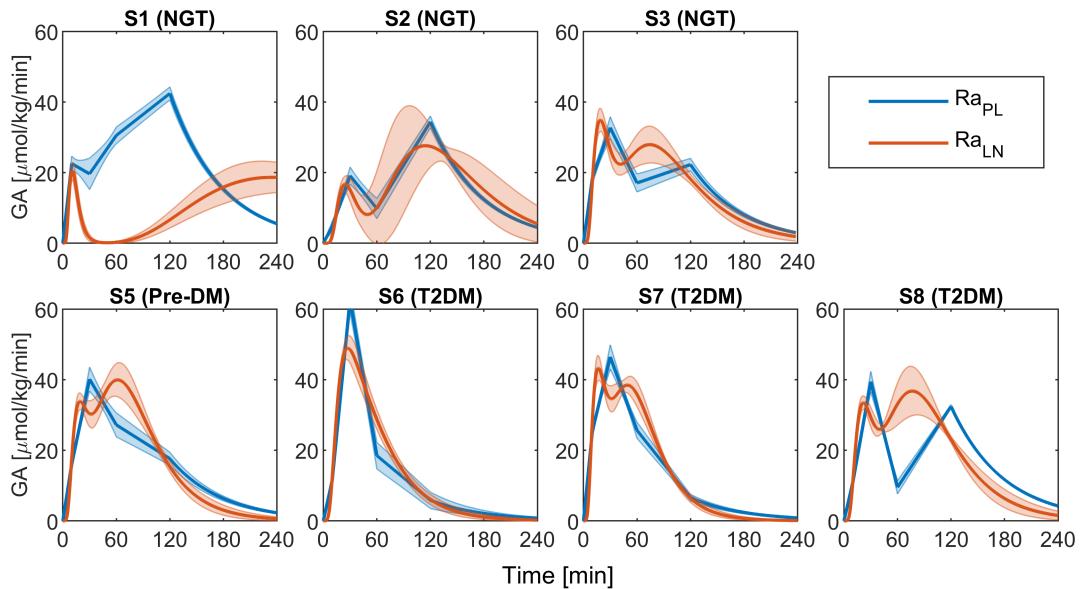
Figure 8.3: Inferred glucose appearance profiles of the OMM using both input functions Ra_{PL} and Ra_{LN}. The results are given as the mean and standard deviation derived from a deterministic sensitivity analysis as described in section 3.4.

In terms of the estimation uncertainty, the log-normal input Ra_{LN} generally leads

to slightly higher posterior uncertainties. This is especially in the case for S_I in Figure 8.2 (c) and the glucose appearance in Figure 8.3 in subjects S2 and S8. This can be explained by the higher number of unknown parameters describing in the model using Ra_{LN} (eight) in comparison to the model using piecewise-linear input Ra_{PL} (six). In comparison to the Nuttall dataset containing much more sampling points, the uncertainty estimates for S_I from the new dataset are increased as demonstrated by the posterior CVs with a mean and standard deviation of 37.1 $\pm$ 32.2 % for Ra_{PL} and 46.8 $\pm$ 29.3 % for Ra_{LN}; for comparison, using the Nuttall dataset yielded 6.9 $\pm$ 5.4 % for Ra_{PL} and 8.5 $\pm$ 7.5 % for Ra_{LN}.

The correlations of the model parameters are displayed in Figure 8.4. In both cases, the correlations are similar to the correlations obtained with the Nuttall dataset presented in 5.7.
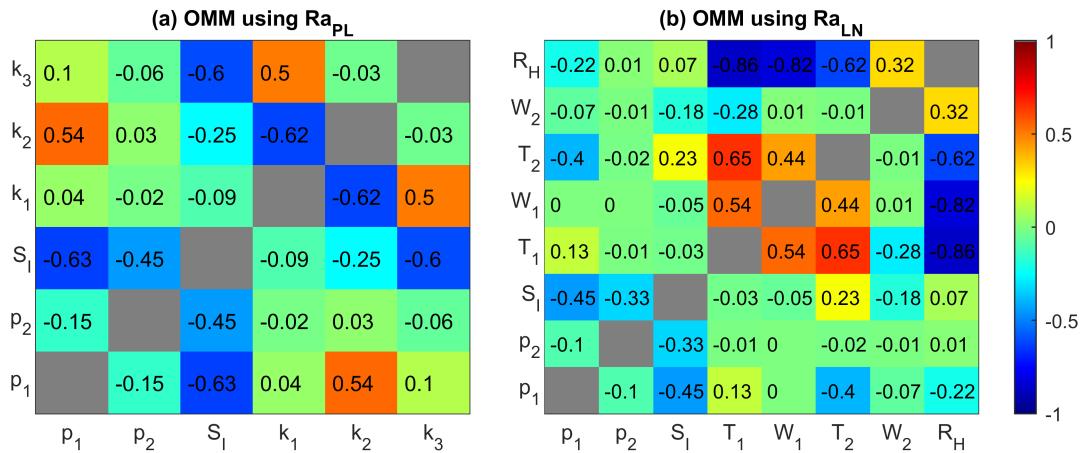
Figure 8.4: Median posterior parameter correlation matrix of the OMM identified from OGTT blood sampling data using (a) Ra_{PL} and (b) Ra_{LN} from the individually estimated parameter correlation matrices of all seven subjects.

8.3.1.3 Conclusion

Comparing the inference results for the two input functions from the new dataset it can be concluded that the piecewise-linear function performs marginally better, most likely due to the reduced number of parameters. It is thus recommended to use the piecewise-linear function when only a small number of data points are available.

With only five data points, this work uses a very low number of sampling points to identify the OMM in comparison to the literature. Dalla Man et al. (2005) [123] used seven sampling points over the same response duration of 120 min. Using the conven-

tional identification procedure explained in section 4.2, led to a CV of 18 % in insulin sensitivity estimates. This increased precision can be explained by the higher number of sampling points and the lower prior uncertainties in parameters p_1 and p_2. Given the high uncertainties in the S_I estimates obtained in this thesis, the use of a higher number of sampling points for identification of the OMM is recommended.

8.3.2 Glucose-only models

8.3.2.1 Model fit and basal glucose level

The BMA technique is utilised to avoid the need the select one of the GOMs using Z_{LIN}, Z_{LOG} or Z_{POS}, similar to Chapter 6. The BMA results for the model output for all subjects are displayed in Figure 8.5.
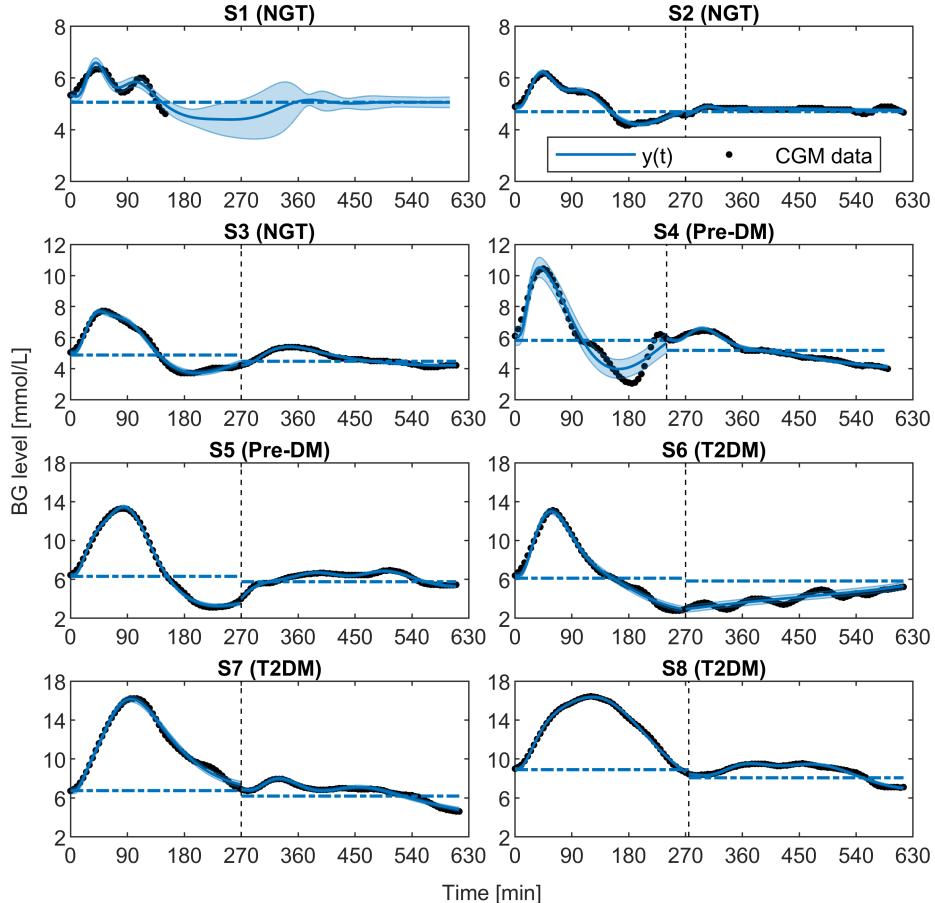
Figure 8.5: Plot of the model output of the GOMs against the CGM data for all subjects. The results are given as the mean and standard deviation derived from a deterministic sensitivity analysis as described in section 3.4. The horizontal dash-dot line gives the inferred baseline glucose level G_b for the OGTT and lunch responses, respectively and the vertical line gives the time lunch was consumed. For subject S1, the model output was simulated for the remainder of the time assuming no food intake.

As mentioned previously, in subject S1 the inpatient monitoring session was aborted approximately 150 min after OGTT consumption and the lunch response could not be recorded. This means that the GOMs were identified from reduced a OGTT response duration, compared to the other subjects, and no identification was carried out for lunch at all.

The GOMs describe the glucose dynamics for both OGTT and lunch generally well. A slightly reduced ability to fit the data can be observed in the second half of the OGTT response from subject S4, where the delayed hypoglycaemia, discussed in the previous chapter, and subsequent rebound of the glucose levels is described with less accuracy. Similarly, the oscillations displayed by subject S6 after lunch are not captured by the model. These model fit issues outline the limitations of the developed GOMs in describing certain dynamic patterns.

In terms of the inferred baseline glucose level G_b displayed by the horizontal dash-dot lines in Figure 8.5, it can be noted that the inferred baseline during lunch lies up to 11 % lower, in comparison to the OGTT baseline for almost all subjects. This trend is generally more pronounced in Pre-DM and T2DM subjects and validates the choice of adaptable glucose baseline parameter. This decrease in G_b could be explained by the hypoglycaemic effects of the exercise period towards the end of the lunch response, mentioned in section 7.3.3.

To analyse the model fit in more detail, the weighted residuals between model output and CGM data are displayed in Figure 8.6.
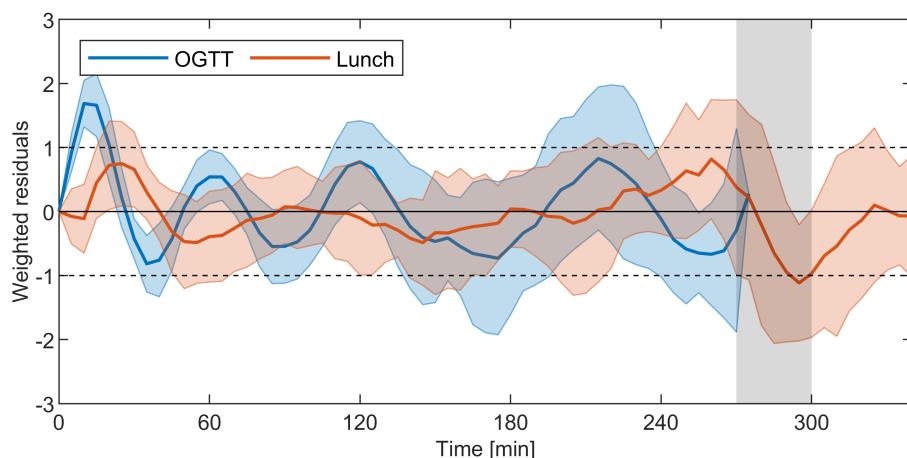
Figure 8.6: Residuals between model output and CGM data weighted by the inferred measurement error. The results are given as the mean and standard deviation. The shaded grey area indicates the period of exercise at the end of the lunch response.

The overall mean absolute weighted residuals for all subjects and meals combined are 0.40 ± 0.32, which indicates a similar model fit as the GOMs in Chapter 6, where a value of 0.33 ± 0.24 was achieved using the Nuttall dataset. Inspecting the time profile of weighted residuals displayed in Figure 8.6 reveals oscillations, especially in the OGTT response. This type of regular pattern in the weighted residuals profile typically indicates a systematic effect in the data that is not described by the model. Given that the oscillations are largely contained within the -1 to +1 range could potentially imply an unmodelled effect in the measurement process. This could mean that assuming a Gaussian measurement error and direct observation of BG levels as described by expression (8.8) is too simplistic and more complex model of the measurement process is required. In fact, several more elaborate models of the CGM data collection have been proposed in the literature [80, 179, 180]. We, however, argue that this would make the GOMs unnecessarily complicated as an adequate model fit is already achieved.

The CGM dataset used for model identification included two exercise periods towards the end of the OGTT and lunch response, respectively, where the second exercise period was carried out with higher intensity. Inspecting the profile of weighted residuals during the second exercise period, indicated by the grey area in Figure 8.6, reveals mostly negative values during and after the exercise which means that the model overestimates the actual glucose level. This demonstrates that the model does not fully capture the glucose dynamics, i.e. immediate reduction of BG levels, caused by the exercise. The fact that the mean of the weighted residuals is largely above the value of -1, however, means that the deviation between the model and the data mainly stays within the range of measurement uncertainty, which does not necessarily warrant the inclusion of the effects of exercise in the model. In fact, at the end of the response, the profile of weighted residuals returns to zero meaning that the overall hypoglycaemic effect of exercise is accounted for, most likely by a decrease in the baseline glucose level G_b during the lunch response. One possibility to explicitly include the effects of the exercise in the model could therefore be to introduce a time dependence in the basal glucose level G_b, allowing short term changes during periods of exercise.

8.3.2.2 Parameter estimates and correlation

The posterior distributions for S_G are displayed in Figure 8.7, corresponding results of the other system parameters p_1 and p_2 are provided in Appendix D.5. Comparing the S_G estimates between the OGTT and lunch, it can be seen that the low-CHO meal, consumed for lunch, leads to higher S_G values in almost all cases. This is consistent with the results from the Nuttall dataset where the S_G values from the high protein meal were significantly higher than the S_G values from the high-CHO meal. In terms of estimation precision for the S_G values, the mean and standard deviation of posterior CVs for all meals is 25.8 ± 6.8 %, which is higher than the 17.7 ± 7.8 % obtained in the Nuttall dataset. Further examinations into this effect lead to the conclusion that the increase in the posterior CV for S_G can be explained by the inclusion of G_b as an unknown parameter.
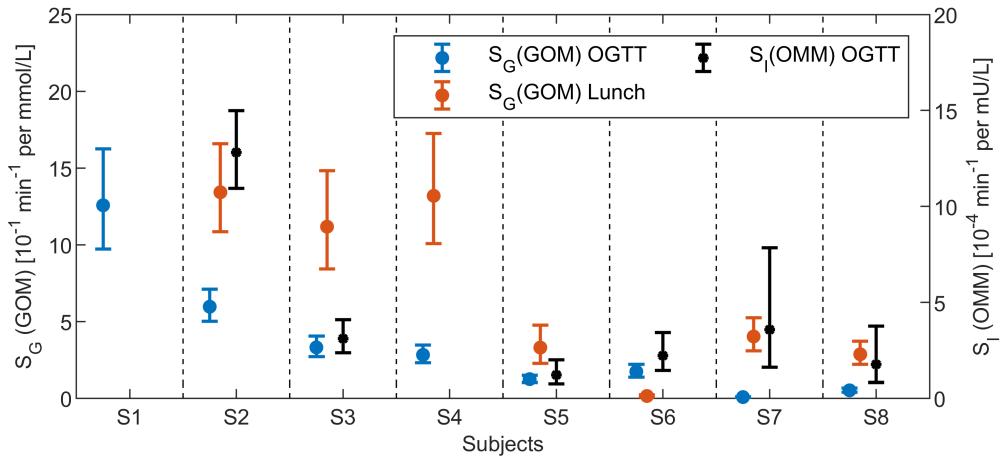
Figure 8.7: Comparison of the results for S_G (left y-axis) of the GOM estimated from the CGM data and S_I (right y-axis) of the OMM with Ra_{PL} estimated from the blood sampling data. The results give the median and one-sigma range for the log-normal posterior distributions. In subject S1, the S_I distribution is not shown as it has a median of 150 10^{-4} min^{-1} per mU/L. Furthermore, no S_G value during lunch is inferred. In subject S4, S_I could not be estimated with the OMM due to missing data.

The correlation of the model parameters, assessed through the posterior covariance matrix as described in section 3.3.2.2, is displayed in Figure 8.8. The correlations are similar to the results using the Nuttall dataset presented in Chapter 6 in Figure 6.11, especially in terms of the input function parameters. Of interest is the positive correlation between S_G and G_b, which further demonstrates the interdependence between these two parameters.

	p_1	p_2	S_G	G_b	T_1	W_1	T_2	W_2	R_H
R_H	-0.17	-0.23	0.13	0.03	-0.84	-0.83	-0.45	0.82	
W_2	-0.25	-0.27	0.11	-0.01	-0.73	-0.51	-0.38		0.82
T_2	-0.14	-0.27	0.18	0.06	0.57	0.5		-0.38	-0.45
W_1	0	0.02	-0.09	-0.03	0.46		0.5	-0.51	-0.83
T_1	0.18	0.16	0.04	0.14		0.46	0.57	-0.73	-0.84
G_b	-0.06	-0.27	0.62		0.14	-0.03	0.06	-0.01	0.03
S_G	0.13	-0.73		0.62	0.04	-0.09	0.18	0.11	0.13
p_2	-0.28		-0.73	-0.27	0.16	0.02	-0.27	-0.27	-0.23
p_1		-0.28	0.13	-0.06	0.18	0	-0.14	-0.25	-0.17
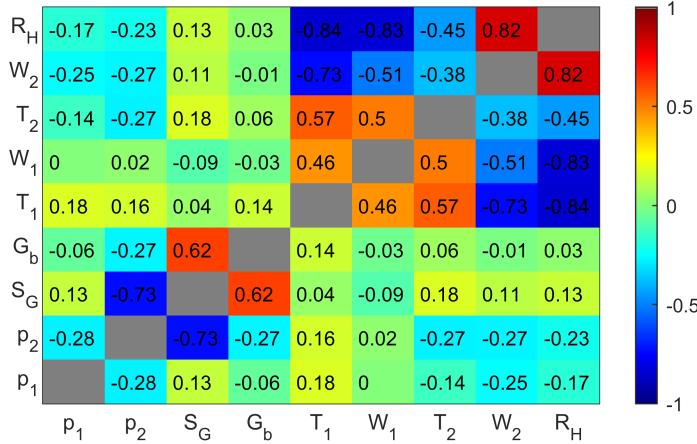
Figure 8.8: Median posterior parameter correlation matrix of the GOM identified from the CGM data from the individually estimated parameter correlation matrices of both meals all subjects.

8.3.2.3 Model validation

Identical to Chapter 6, it is expected that the parameter S_G of the GOMs in expression (8.5) correlates with the insulin sensitivity parameter S_I estimates from the OMM using the piecewise-linear input. The Pearson correlation between S_I and S_G estimated during the OGTT response is 0.92 with $p < 0.005$, demonstrating the significance of the expected correlation. Examining the results for S_G during the OGTT on an individual level in Figure 8.7, it can be seen that the trend for higher S_G values in subjects S1 and S2 and lower values in subjects S3, S5, S6 matches the trend of the S_I values. In subjects S7 and S8, however, the estimated S_G values are lower than in all other subjects which is not the case in the S_I values. Given that these two subjects have low beta-cell function could imply that the GOMs in their current form are not capable of correctly estimating insulin sensitivity in T2DM subjects with low beta-cell function.

The inferred rates of GA by the GOMs are displayed in Figure 8.9. The GA inferred by the GOM and OMM generally follow comparable shapes. Any differences in the profiles can be explained by the fact that the models use different input functions and are identified with very different datasets, i.e. CGM data only for the GOMs and glucose and insulin blood sampling data for the OMM. The general similarity between GA profiles nevertheless demonstrates the GOM's ability to estimate the meal-related appearance of glucose during an OGTT response recorded with CGM. During the lunch response, the inferred appearance rates show a slower rise as well as a prolonged absorption towards the end of the response, which is consistent the high fat/protein and

low CHO composition of the lunch meal. This demonstrates the utility of the GOMs for assessing differences in GA with respect to meal composition. The exception is the inferred GA for lunch in subject S6, where no appearance is estimated. The absence of any GA is physiologically implausible and can be explained by the fact that the entire lunch glucose response lies below the estimated basal glucose level G_b as shown in Figure 8.5. In comparison to the other subjects, this glycaemic behaviour is unusual and makes it difficult for the model to detect the presence of any glucose appearance.
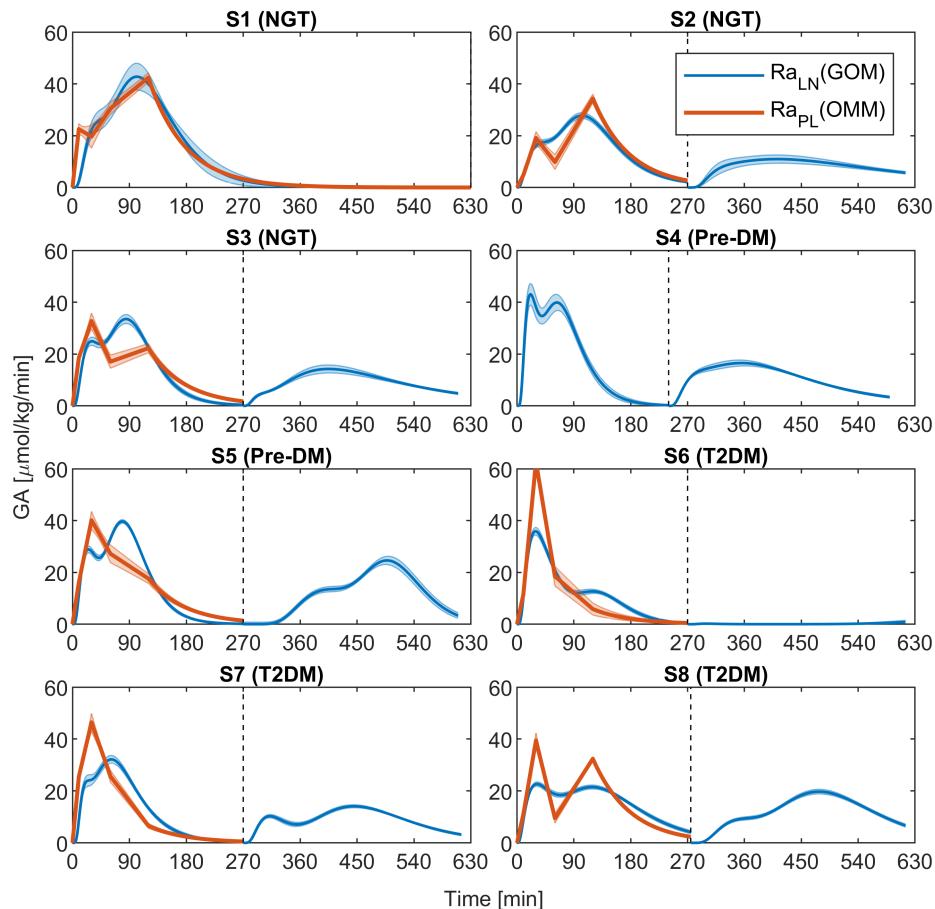
Figure 8.9: Comparison of the glucose appearance (GA) profiles inferred by the OMM (red) and the GOMs (blue) for all subjects. The results are given as the mean and standard deviation derived from a deterministic sensitivity analysis as described in section 3.4. The vertical line indicates the time lunch was consumed.

8.4 Summary and conclusions

This chapter applied the modelling techniques developed in this thesis to data from subjects with varying glucose tolerance. With regard to the OMM, it has been shown that the identification procedure using the VB method reaches its limitations when a low number of data points is available for estimation, as indicated by the existence of local minima and reduced estimation precision of insulin sensitivity. The new input function performs marginally worse in comparison to the conventional piecewise-linear input when only a few data points are utilised.

On the subject of the GOM performance, it has been shown that the developed models can be identified from CGM data and generally describe the observed glucose dynamics well. It has also been demonstrated that the inferred GA profiles are similar to the OMM and that information on insulin sensitivity can be extracted on an individual level.

The preliminary nature of the underlying experimental study, especially the low number of subjects, does not allow any conclusions regarding the applicability of the GOMs in clinical practice and the treatment of Pre-DM and T2DM. The results nevertheless demonstrate the usefulness of CGM as a means of glucose data collection for model identification and warrant the acquisition of similar data on a larger number of subjects.

Chapter 9

Conclusions and future work

The main contribution of this work is the minimal-type models for the description of postprandial glucose profiles that can be identified from glucose data only and provide information on insulin sensitivity and meal-related glucose appearance (GA). This means that it is possible to assess the postprandial glucose metabolism with minimal data collection efforts, which could support healthcare professionals in designing effective treatment strategies for Pre-DM and T2DM. The main aim of this thesis has thus been fulfilled.

The basis for the model development was established by two datasets. The first dataset from voluteers with normal glucose tolerance (NGT), referred to as the Nuttall dataset and described in Chapter 4, was made available for the use of this thesis and played a crucial role in the initial model development. The second dataset, described in Chapter 7, was collected during an experimental study that was fully designed and implemented in the context of this PhD project. This provided the opportunity to complement the Nuttall dataset, mainly through the inclusion of Pre-DM and T2DM subjects and through the use of continuous glucose monitoring (CGM) for glucose data collection. The cohort contained a comparatively small number of subjects giving the conducted study a preliminary nature. This nevertheless provided the opportunity to introduce two novel features to the data collection process.

The first novelty lies in the fact that glucose data were collected both in the highly controlled conditions of an inpatient monitoring session as well as during normal life conditions. Comparing BG levels between these two scenarios revealed increased levels during the inpatient monitoring session in the majority of subjects. This difference

demands caution when extrapolating results obtained under controlled conditions to everyday life and highlights the importance of collecting data under both circumstances. The second novelty lies in the combination of CGM and blood sampling data collection during an oral glucose tolerance test (OGTT). This offered the unique opportunity to validate the modelling results from the CGM data on the results using classical glucose and insulin data from blood sampling. The CGM technique additionally allowed the detection of relevant and interesting dynamical features in the OGTT glucose response beyond the conventional observation duration of 120 min. Specifically, it was observed that delayed hypoglycaemia is common in subjects with reduced insulin sensitivity. Overall, the results of the experimental study warrant more extensive data collection from additional subjects to reinforce the preliminary findings.

Variational Bayesian (VB) inference was used for all parameter estimation tasks in this work. The VB method uses a deterministic and efficient algorithm to approximate the true posterior distribution over unknown parameters, while also providing a lower bound on the model evidence. As the theoretical foundation of this method has been discussed in detail previously [93, 98, 103], this work focussed on describing the practical aspects of applying the VB method in metabolic modelling, thus providing a resource for other researchers using this method to refer back to. In this context, this thesis also developed and implemented a method for the use of existing information to define and interpret the probability density function of the measurement noise uncertainty, which has subsequently been accepted by the development team as an official part of the VB toolbox [104] (Chapter 3).

In order to build a foundation for the development of glucose-only models, the well-established oral minimal model (OMM) was chosen to be identified from the glucose and insulin data. This led to several novel adaptations to the formulation and identification procedure of the OMM, which has been the subject of Chapters 4 and 5. In summary these adaptations are as follows.

- The VB method was used to estimate the parameters in the OMM. This technique allows the probabilistic treatment of the unknown parameters and thus quantification of their uncertainty as well as the inclusion of prior knowledge into the parameter estimation procedure.

- A structural identifiability analysis using the Taylor series method and symbolic

computation revealed that the parameter representing glucose effectiveness is, contrary to previous results [71], structurally globally identifiable. It has, however, also been shown this parameter is difficult to estimate with acceptable precision in practice. This led to the proposal of a suitable prior distribution that provides a trade-off between considering the natural population variability in glucose effectiveness and an acceptable estimation accuracy of the remaining parameters.

- The formulation of the OMM was adapted and a procedure for the identification from non-fasting conditions was developed and implemented. This makes it possible to identify the model from consecutive meal responses allowing the examination of changes to insulin sensitivity and GA throughout the day.

- A novel input function representing the meal-related glucose appearance was introduced. In comparison to the conventional piecewise-linear description, the proposed input consisting of two log-normally shaped functions is fully differentiable and completely independent of the duration of the considered response. This greatly facilitates the application of the OMM to datasets with a varying duration between meals. It was furthermore shown that the new input function leads to an improvement in model fit during the first 30 min of the response, which indicated a more realistic estimation of GA in that period of the response.

A comparison of the inference results with corresponding studies from the literature revealed that the proposed alterations lead to similar results in terms of the model's ability to describe the data and precision of the estimated parameters. This literature-based approach to validation is limited by the fact that it can at most establish the equivalence to the conventional oral minimal modelling approach. Demonstrating that the modifications noted above lead to truly superior results would require additional data from the use of traced glucose and/or clamp experiments.

A weakness of the conventional OMM identification approach is that the commonly used software package SAAM II [122] is only commercially available. In contrast to that, the VB toolbox used in this research is implemented as a freely available library of MATLAB functions. This made it possible to publish the necessary code allowing for independent researchers the opportunity to identify the OMM without in-depth knowledge on model identification. Such efforts are aided by the explanations in Chapter 4, which describe the identification procedure of the OMM in detail. As mentioned previ-

ously, the publishing of the code follows recent efforts to facilitate the identification of the IVGTT minimal model [137]. Furthermore, it increases the impact of this research and promote the use of the VB method in the field of metabolic modelling.

The development of glucose-only models (GOM), described in Chapter 6, used the oral minimal model and Nuttall dataset as a foundation to formulate three different model candidates. As neither of the candidates emerged as clearly superior, a model fusion technique within the VB framework known as Bayesian model averaging was utilised to combine the results of the three candidates according to the model evidence. This gave the modelling framework the necessary flexibility for the application to the new dataset described in Chapter 7. The goal of the glucose-only modelling task was to establish the physiological interpretability of the model parameters by assessing their results in comparison to the associated OMM results obtained from the same dataset. In this context, the combined results of the GOMs have shown that

- In comparison to the conventional OMM, the GOMs show an improved model fit, especially during the first 30 min of the response, as indicated by decreased weighted residuals between model output and data.

- The GOMs can be used to infer information on insulin sensitivity as they contain a parameter highly correlated to the insulin sensitivity inferred from the OMM. Especially in a meal with high carbohydrate content, a correlation coefficient of 0.8, outperforming other surrogate indices of insulin sensitivity, has been achieved.

- The GOM-inferred GA profiles are similar to the GA profiles inferred with the OMM, with evidence of an improved estimation in the first 30 min of the response. This allows the comparison and interpretation of trends using the GOM-inferred appearance profiles with respect to meal composition.

Similar results from the GOMs were obtained utilising CGM profiles from NGT, Pre-DM and T2DM subjects (Chapter 8) from our bespoke dataset.

For the formulation of the GOM candidates, we used physiological principles from models of insulin secretion, as well as results from examining the dynamical glucose-insulin relationship. The latter has proven to provide useful information during model development and has the potential for future improvements. In particular, one aspect of the glucose-insulin relationship, exemplified in Figure 9.1, is not yet included in the

model: after the initial rise, glucose levels decay much faster to their respective baseline than insulin levels. Incorporating this particular behaviour into the GOMs could offer an opportunity for further improvements to the model.
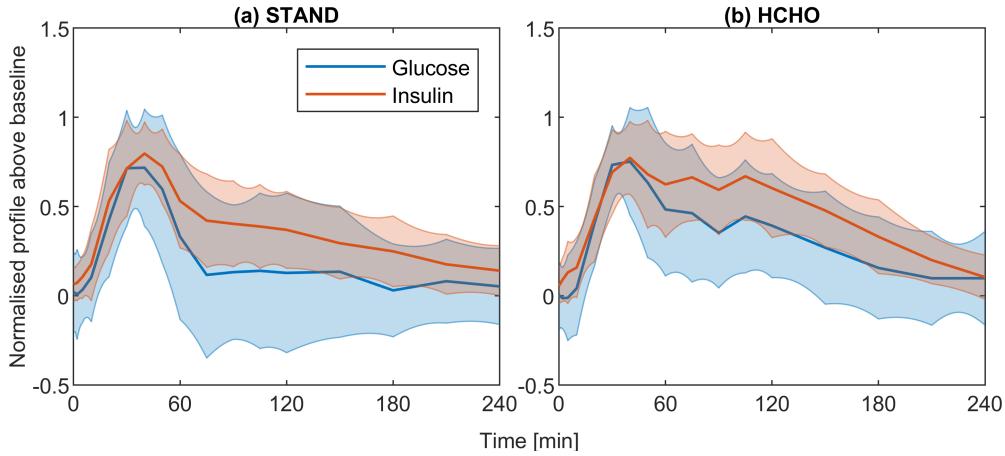
Figure 9.1: Normalised glucose and insulin profiles (with respect to the peak value) above baseline for the (a) STAND and (b) HCHO diet in the Nuttall dataset. The profiles are given as the mean and standard deviation.

Overall, the results of the glucose-only modelling approach are promising and the potential for application purely based on glucose data is large. This is mainly rooted in the already existing glucose data collection in clinical practice and the fact that the GOMs overcome the previously mentioned disadvantages of current insulin measurement techniques.

In order to build upon the modelling work carried out in Chapter 6, a larger dataset similar to Nuttall's data collected on Pre-DM and T2DM subjects would be required. This type of data has already been published [135, 181–183], meaning that it might be more feasible to contact the respective authors instead of designing and conduction separate experimental studies for that purpose. To build on this, additional CGM data from Pre-DM and T2DM subjects would also be required, as mentioned earlier. To continue the modelling work initially, it would be possible to use the data already collected during the study described in Chapter 7, that have not been analysed yet. Here, a minor problem lies in the fact that it is mainly free-living data, meaning that the information on food intake is less reliable. As already mentioned in the context of validating the OMM adaptations, additional data from the use of traced glucose and/or clamp experiments would also be required to further validate the GOMs, e.g. in terms of their ability to estimate insulin sensitivity, before their applicability in clinical practice can be assessed.

With the availability of additional data, especially from single subjects, future work could focus on revisiting the mixed-effects modelling approach for the parameter estimation procedure, explained in section 3.3. However, instead of incorporating data from multiple subjects during parameter estimation, data collected from multiple responses on the same subject could be combined. Such an approach could potentially improve upon the proposed procedure for estimating parameters from multiple, consecutive responses on the same day using the OMM and could also be applied to the description of ambulatory CGM profiles using the GOMs.

Finally, the possible applications of the developed GOMs extend beyond Pre-DM and T2DM to other diabetes types. In particular for gestational diabetes mellitus, i.e. diabetes occurring during pregnancy, which is characterised by a rapid deterioration of glycaemic control, GOMs could be utilised to accurately monitor disease progression. In fact, two projects are currently being undertaken within our research group to continue the work on GOMs in the context of gestational diabetes mellitus.

Bibliography

[1] R. I. G. Holt, C. Cockram, A. Flyvbjerg, and B. J. Goldstein. *Textbook of Diabetes*. Hoboken, UK: John Wiley & Sons, Incorporated, 2017.

[2] T. S. Hannon, S. E. Kahn, K. M. Utzschneider, T. A. Buchanan, K. J. Nadeau, P. S. Zeitler, [...], and K. J. Mather. "Review of methods for measuring beta-cell function: Design considerations from the Restoring Insulin Secretion (RISE) Consortium". In: *Diabetes Obes Metab* 20.1 (2018), pp. 14–24.

[3] N. D. Guess. "Dietary Interventions for the Prevention of Type 2 Diabetes in High-Risk Groups: Current State of Evidence and Future Research Needs". In: *Nutrients* 10.9 (2018), p. 1245.

[4] M. C. Riddle. "Basal Glucose Can Be Controlled, but the Prandial Problem Persists-It's the Next Target!" In: *Diabetes Care* 40.3 (2017), pp. 291–300.

[5] S. Madsbad. "Impact of postprandial glucose control on diabetes-related complications: How is the evidence evolving?" In: *J Diabetes Complications* 30.2 (2016), pp. 374–85.

[6] D. J. Cox, A. G. Taylor, H. Singh, M. Moncrief, A. Diamond, J. Yancy W. S., [...], and A. L. McCall. "Glycemic load, exercise, and monitoring blood glucose (GEM): A paradigm shift in the treatment of type 2 diabetes mellitus". In: *Diabetes Res Clin Pract* 111 (2016), pp. 28–35.

[7] C. Cobelli, C. Dalla Man, M. G. Pedersen, A. Bertoldo, and G. Toffolo. "Advancing our understanding of the glucose system via modeling: a perspective". In: *IEEE Trans Biomed Eng* 61.5 (2014), pp. 1577–92.

[8] E. Carson and C. Cobelli. *Modelling Methodology for Physiology and Medicine*. Waltham, USA: Elsevier Science & Technology, 2014.

[9] I Ajmera, M Swat, C Laibe, N Le Novere, and V Chelliah. "The impact of mathematical modeling on the understanding of diabetes and related complications". In: *CPT: Pharmacometrics & Systems Pharmacology* 2.7 (2013), p. 54.

[10] V. W. Bolie. "Coefficients of normal blood glucose regulation". In: *J Appl Physiol* 16 (1961), pp. 783–8.

[11] R. Basu, B. Di Camillo, G. Toffolo, A. Basu, P. Shah, A. Vella, [...], and C. Cobelli. "Use of a novel triple-tracer approach to assess postprandial glucose metabolism". In: *Am J Physiol Endocrinol Metab* 284.1 (2003), E55–69.

[12] F. A. Nasrallah, G. Pages, P. W. Kuchel, X. Golay, and K. H. Chuang. "Imaging brain deoxyglucose uptake and metabolism by glucoCEST MRI". In: *J Cereb Blood Flow Metab* 33.8 (2013), pp. 1270–8.

[13] P. Palumbo, S. Ditlevsen, A. Bertuzzi, and A. De Gaetano. "Mathematical modeling of the glucose - insulin system: A review". In: *Mathematical Biosciences* 244.2 (2013), pp. 69–81.

[14] S. N. Rathee. "ODE models for the management of diabetes: A review". In: *International Journal of Diabetes in Developing Countries* 37.1 (2017), pp. 4–15.

[15] S. Hoerber, P. Achenbach, E. Schleicher, and A. Peter. "Harmonization of immunoassays for biomarkers in diabetes mellitus". In: *Biotechnology Advances* (2019).

[16] D. J. Cox, A. G. Taylor, M. Moncrief, A. Diamond, J. Yancy W. S., S. Hegde, and A. L. McCall. "Continuous Glucose Monitoring in the Self-management of Type 2 Diabetes: A Paradigm Shift". In: *Diabetes Care* 39.5 (2016), e71–3.

[17] R. Vigersky and M. Shrivastav. "Role of continuous glucose monitoring for type 2 in diabetes management and research". In: *J Diabetes Complications* 31.1 (2017), pp. 280–287.

[18] G. Cappon, M. Vettoretti, G. Sparacino, and A. Facchinetti. "Continuous Glucose Monitoring Sensors for Diabetes Management: A Review of Technologies and Applications". In: *Diabetes Metab J* 43.4 (2019), pp. 383–397.

[19] S. Oviedo, J. Vehi, R. Calm, and J. Armengol. "A review of personalized blood glucose prediction strategies for T1DM patients". In: *Int J Numer Meth Biomed Engng* (2017), e2833.

[20] T. Wilke, A. Groth, A. Fuchs, L. Seitz, J. Kienhofer, R. Lundershausen, and U. Maywald. "Real life treatment of diabetes mellitus type 2 patients: an analysis based on a large sample of 394,828 German patients". In: *Diabetes Res Clin Pract* 106.2 (2014), pp. 275–85.

[21] E. Ackerman, J. W. Rosevear, and W. F. McGuckin. "A Mathematical Model of the Glucose-tolerance test". In: *Physics in Medicine and Biology* 9.2 (1964), p. 203.

[22] H.-i. Wu. "A case study of type 2 diabetes self-management". In: *Biomed Eng Online* 4.1 (2005), pp. 1–9.

[23] K. D. Shiang and F. Kandeel. "A computational model of the human glucose-insulin regulatory system". In: *J Biomed Res* 24.5 (2010), pp. 347–64.

[24] N. Khovanova, Y. Zhang, and T. A. Holt. "Generalised stochastic model for characterisation of subcutaneous glucose time series". In: *IEEE-EMBS International Conference on Biomedical and Health Informatics (BHI)*. 2014, pp. 484–487.

[25] Y. Zhang, T. A. Holt, and N. Khovanova. "A data driven nonlinear stochastic model for blood glucose dynamics". In: *Comput Methods Programs Biomed* 125 (2016), pp. 18–25.

[26] C.-L. Chen and H.-W. Tsai. "Modeling the physiological glucose insulin system on normal and diabetic subjects". In: *Computer Methods and Programs in Biomedicine* 97.2 (2010), pp. 130–140.

[27] P. Goel, D. Parkhi, A. Barua, M. Shah, and S. Ghaskadbi. "A Minimal Model Approach for Analyzing Continuous Glucose Monitoring in Type 2 Diabetes". In: *Front Physiol* 9 (2018), p. 673.

[28] K. N. Frayn and R. D. Evans. *Human metabolism: a regulatory perspective*. 2019.

[29] F. Q. Nuttall, M. C. Gannon, J. L. Wald, and M. Ahmed. "Plasma glucose and insulin profiles in normal subjects ingesting diets of varying carbohydrate, fat, and protein content". In: *J Am Coll Nutr* 4.4 (1985), pp. 437–50.

[30] D. M. Nathan. "The Diabetes Control and Complications Trial/Epidemiology of Diabetes Interventions and Complications Study at 30 Years: Overview". In: *Diabetes Care* 37.1 (2014), pp. 9–16.

[31] S. E. Kahn, R. L. Prigeon, D. K. McCulloch, E. J. Boyko, R. N. Bergman, M. W. Schwartz, [...], and et al. "Quantification of the relationship between insulin sensitivity and beta-cell function in human subjects. Evidence for a hyperbolic function". In: *Diabetes* 42.11 (1993), pp. 1663–72.

[32] B. Ahren and G. Pacini. "Importance of quantifying insulin secretion in relation to insulin sensitivity to accurately assess beta cell function in clinical studies". In: *Eur J Endocrinol* 150.2 (2004), pp. 97–104.

[33] R. Retnakaran, S. Shen, A. J. Hanley, V. Vuksan, J. K. Hamilton, and B. Zinman. "Hyperbolic Relationship Between Insulin Secretion and Sensitivity on Oral Glucose Tolerance Test". In: *Obesity* 16.8 (2008), pp. 1901–1907.

[34] American Diabetes Association. "2. Classification and Diagnosis of Diabetes: Standards of Medical Care in Diabetes-2018". In: *Diabetes Care* 41.Suppl 1 (2018), S13–S27.

[35] R. C. Bonadonna, L. Boselli, A. Dei Cas, and M. Trombetta. "Methods to Assess In Vivo Insulin Sensitivity and Insulin Secretion". In: *Diabetes Epidemiology, Genetics, Pathogenesis, Diagnosis, Prevention, and Treatment.* Ed. by E. Bonora and R. A. DeFronzo. Cham: Springer International Publishing, 2018, pp. 317–367.

[36] R. A. DeFronzo, J. D. Tobin, and R. Andres. "Glucose clamp technique: a method for quantifying insulin secretion and resistance". In: *Am J Physiol* 237.3 (1979), E214–23.

[37] M. Matsuda. "Measuring and estimating insulin resistance in clinical and research settings". In: *Nutrition, Metabolism and Cardiovascular Diseases* 20.2 (2010), pp. 79–86.

[38] J. G. Hattersley and M. O. Weickert. "Practicable Measures and Indices of Insulin Resistance in Nutrition Research". In: *Curr Obes Rep* 2.4 (2013), pp. 285–292.

[39] R. N. Bergman and M. Ader. "Measuring insulin action in vivo". In: *International Textbook of Diabetes Mellitus.* John Wiley & Sons, Ltd, 2015, pp. 234–249.

[40] P. D. Docherty, J. E. Berkeley, T. F. Lotz, L. Te Morenga, L. M. Fisk, G. M. Shaw, [...], and J. G. Chase. "Clinical validation of the quick dynamic insulin sensitivity test". In: *IEEE Trans Biomed Eng* 60.5 (2013), pp. 1266–72.

[41] J. W. T. Yates and E. M. Watson. "Estimating insulin sensitivity from glucose levels only: Use of a non-linear mixed effects approach and maximum a posteriori (MAP) estimation". In: *Computer Methods and Programs in Biomedicine* 109.2 (2013), pp. 134–143.

[42] E. M. Watson, M. J. Chappell, F. Ducrozet, S. M. Poucher, and J. W. T. Yates. "A new general glucose homeostatic model using a proportional-integral-derivative controller". In: *Computer Methods and Programs in Biomedicine* 102.2 (2011), pp. 119–129.

[43] M. Alsahli, M. Z. Shrayyef, and J. E. Gerich. "Normal Glucose Homeostasis". In: *Principles of Diabetes Mellitus*. Ed. by L. Poretsky. Cham: Springer International Publishing, 2017, pp. 23–42.

[44] A. Haidar, D. Elleri, J. M. Allen, J. Harris, K. Kumareswaran, M. Nodale, [...], and R. Hovorka. "Validity of triple- and dual-tracer techniques to estimate glucose appearance". In: *Am J Physiol Endocrinol Metab* 302.12 (2012), E1493–501.

[45] C. Dalla Man, M. Camilleri, and C. Cobelli. "A system model of oral glucose absorption: validation on gold standard data". In: *IEEE Trans Biomed Eng* 53.12 Pt 1 (2006), pp. 2472–8.

[46] E. Ferrannini, D. C. Simonson, L. D. Katz, G. Reichard, S. Bevilacqua, E. J. Barrett, [...], and R. A. DeFronzo. "The disposal of an oral glucose load in patients with non-insulin-dependent diabetes". In: *Metabolism* 37.1 (1988), pp. 79–85.

[47] A. Basu, C. Dalla Man, R. Basu, G. Toffolo, C. Cobelli, and R. A. Rizza. "Effects of type 2 diabetes on insulin secretion, insulin action, glucose effectiveness, and postprandial glucose metabolism". In: *Diabetes Care* 32.5 (2009), pp. 866–72.

[48] S. Lartigue, Y. Bizais, S. B. Des Varannes, A. Murat, B. Pouliquen, and J. P. Galmiche. "Inter- and intrasubject variability of solid and liquid gastric emptying parameters. A scintigraphic study in healthy subjects and diabetic patients". In: *Dig Dis Sci* 39.1 (1994), pp. 109–15.

[49] J. A. Siegel, J. L. Urbain, L. P. Adler, N. D. Charkes, A. H. Maurer, B. Krevsky, [...], and L. S. Malmud. "Biphasic nature of gastric emptying". In: *Gut* 29.1 (1988), pp. 85–89.

[50] E. Ferrannini, O. Bjorkman, G. A. Reichard, A. Pilo, M. Olsson, J. Wahren, and R. A. DeFronzo. "The Disposal of an Oral Glucose Load in Healthy Subjects: A Quantitative Study". In: *Diabetes* 34.6 (1985), pp. 580–588.

[51] E. J. Mansell, P. D. Docherty, and J. G. Chase. "Shedding light on grey noise in diabetes modelling". In: *Biomedical Signal Processing and Control* 31 (2017), pp. 16–30.

[52] S. Marcovina, R. R. Bowsher, W. G. Miller, M. Staten, G. Myers, S. P. Caudill, [...], and M. W. Steffes. "Standardization of insulin immunoassays: report of the American Diabetes Association Workgroup". In: *Clin Chem* 53.4 (2007), pp. 711–6.

[53] M. A. Staten, M. P. Stern, W. G. Miller, M. W. Steffes, S. E. Campbell, and W. for the Insulin Standardization. "Insulin Assay Standardization: Leading to measures of insulin sensitivity and secretion for practical clinical care". In: *Diabetes Care* 33.1 (2010), pp. 205–206.

[54] S. E. Manley, I. M. Stratton, P. M. Clark, and S. D. Luzio. "Comparison of 11 human insulin assays: implications for clinical investigation and research". In: *Clin Chem* 53.5 (2007), pp. 922–32.

[55] M. Tohidi, P. Arbab, and A. Ghasemi. "Assay-dependent variability of serum insulin concentrations: a comparison of eight assays". In: *Scandinavian Journal of Clinical and Laboratory Investigation* 77.2 (2017), pp. 122–129.

[56] M. Takayama, K. Yamauchi, and T. Aizawa. "Quantification of insulin". In: *Diabetic Medicine* 31.3 (2014), pp. 375–376.

[57] J. L. Knopp, L. Holder-Pearson, and J. G. Chase. "Insulin Units and Conversion Factors: A Story of Truth, Boots, and Faster Half-Truths". In: *J Diabetes Sci Technol* 13.3 (2019), pp. 597–600.

[58] D. B. Sacks, M. Arnold, G. L. Bakris, D. E. Bruns, A. R. Horvath, M. S. Kirkman, [...], and D. M. Nathan. "Guidelines and Recommendations for Laboratory Analysis in the Diagnosis and Management of Diabetes Mellitus". In: *Diabetes Care* 34.6 (2011), e61–e99.

[59] N. Moodley, U. Ngxamngxa, M. J. Turzyniecka, and T. S. Pillay. "Historical perspectives in clinical pathology: a history of glucose measurement". In: *J Clin Pathol* 68.4 (2015), pp. 258–64.

[60]   N. Jendrike, A. Baumstark, S. Pleus, C. Liebing, U. Kamecke, C. Haug, and G. Freckmann. "Accuracy of five systems for self-monitoring of blood glucose in the hands of adult lay-users and professionals applying ISO 15197:2013 accuracy criteria and potential insulin dosing errors". In: *Curr Med Res Opin* 35.2 (2019), pp. 301–311.

[61]   D. Olczuk and R. Priefer. "A history of continuous glucose monitors (CGMs) in self-monitoring of diabetes mellitus". In: *Diabetes Metab Syndr* 12.2 (2018), pp. 181–187.

[62]   D. Rodbard. "Continuous Glucose Monitoring: A Review of Successes, Challenges, and Opportunities". In: *Diabetes Technol Ther* 18.Suppl 2 (2016), S2–3–S2–13.

[63]   C. Cobelli, M. Schiavon, C. Dalla Man, A. Basu, and R. Basu. "Interstitial Fluid Glucose Is Not Just a Shifted-In-Time but a Distorted Mirror of Blood Glucose: Insight from an In Silico Study". In: *Diabetes Technol Ther* (2016).

[64]   W. Villena Gonzales, A. T. Mobashsher, and A. Abbosh. "The Progress of Glucose Monitoring-A Review of Invasive to Minimally and Non-Invasive Techniques, Devices and Sensors". In: *Sensors (Basel)* 19.4 (2019).

[65]   H. E. Silber, N. Frey, and M. O. Karlsson. "An integrated glucose-insulin model to describe oral glucose tolerance test data in healthy volunteers". In: *J Clin Pharmacol* 50.3 (2010), pp. 246–56.

[66]   A. De Gaetano, S. Panunzi, A. Matone, A. Samson, J. Vrbikova, B. Bendlova, and G. Pacini. "Routine OGTT: A Robust Model Including Incretin Effect for Precise Identification of Insulin Sensitivity and Secretion in a Single Individual". In: *PLOS ONE* 8.8 (2013), e70875.

[67]   Y. B. Lee, J. H. Lee, E. S. Park, G. Y. Kim, and C. H. Leem. "Personalized metabolic profile estimations using oral glucose tolerance tests". In: *Prog Biophys Mol Biol* 116.1 (2014), pp. 25–32.

[68]   O. Vahidi, K. E. Kwok, R. B. Gopaluni, and F. K. Knop. "A comprehensive compartmental model of blood glucose regulation for healthy and type 2 diabetic subjects". In: *Medical Biological Engineering & Computing* 54.9 (2016), pp. 1383–1398.

[69] Y. J. Rozendaal, A. H. Maas, C. van Pul, E. J. Cottaar, H. R. Haak, P. A. Hilbers, and N. A. van Riel. "Model-based analysis of postprandial glycemic response dynamics for different types of food". In: *Clinical Nutrition Experimental* 19 (2018), pp. 32–45.

[70] M. Wilbaux, B. K. Woelnerhanssen, A. C. Meyer-Gerspach, C. Beglinger, and M. Pfister. "Characterizing the dynamic interaction among gastric emptying, glucose absorption, and glycemic control in nondiabetic obese adults". In: *American Journal of Physiology-Regulatory, Integrative and Comparative Physiology* 312.3 (2017), R314–R323.

[71] C. Dalla Man, A. Caumo, and C. Cobelli. "The oral glucose minimal model: estimation of insulin sensitivity from a meal test". In: *IEEE Trans Biomed Eng* 49.5 (2002), pp. 419–29.

[72] C. Dalla Man, A. Caumo, R. Basu, R. Rizza, G. Toffolo, and C. Cobelli. "Minimal model estimation of glucose absorption and insulin sensitivity from oral test: validation with a tracer method". In: *Am J Physiol Endocrinol Metab* 287.4 (2004), E637–43.

[73] C. Dalla Man, K. E. Yarasheski, A. Caumo, H. Robertson, G. Toffolo, K. S. Polonsky, and C. Cobelli. "Insulin sensitivity by oral glucose minimal models: validation against clamp". In: *Am J Physiol Endocrinol Metab* 289.6 (2005), E954–9.

[74] C. Cobelli, C. Dalla Man, G. Toffolo, R. Basu, A. Vella, and R. Rizza. "The oral minimal model method". In: *Diabetes* 63.4 (2014), pp. 1203–13.

[75] R. Basu, C. Dalla Man, M. Campioni, A. Basu, G. Klee, G. Toffolo, [...], and R. A. Rizza. "Effects of age and sex on postprandial glucose metabolism: differences in glucose turnover, insulin secretion, insulin action, and hepatic insulin extraction". In: *Diabetes* 55.7 (2006), pp. 2001–14.

[76] G. Bock, C. Dalla Man, M. Campioni, E. Chittilapilly, R. Basu, G. Toffolo, [...], and R. Rizza. "Effects of nonglucose nutrients on insulin secretion and action in people with pre-diabetes". In: *Diabetes* 56.4 (2007), pp. 1113–9.

[77] A. Saad, C. Dalla Man, D. K. Nandy, J. A. Levine, A. E. Bharucha, R. A. Rizza, [...], and A. Basu. "Diurnal pattern to insulin secretion and insulin action in healthy individuals". In: *Diabetes* 61.11 (2012), pp. 2691–2700.

[78] L. Hinshaw, C. Dalla Man, D. K. Nandy, A. Saad, A. E. Bharucha, J. A. Levine, [...], and A. Basu. "Diurnal pattern of insulin action in type 1 diabetes: implications for a closed-loop system". In: *Diabetes* 62.7 (2013), pp. 2223–2229.

[79] B. T. Kulakowski, J. F. Gardner, and J. L. Shearer. *Dynamic Modeling and Control of Engineering Systems*. 3rd ed. Cambridge: Cambridge University Press, 2007.

[80] A. Facchinetti, S. Del Favero, G. Sparacino, J. R. Castle, W. K. Ward, and C. Cobelli. "Modeling the glucose sensor error". In: *IEEE Trans Biomed Eng* 61.3 (2014), pp. 620–9.

[81] K. R. Godfrey. "The identifiability of parameters of models used in biomedicine". In: *Mathematical Modelling* 7.9 (1986), pp. 1195–1214.

[82] S. Vajda, K. R. Godfrey, and H. Rabitz. "Similarity transformation approach to identifiability analysis of nonlinear compartmental models". In: *Mathematical Biosciences* 93.2 (1989), pp. 217–248.

[83] H. Pohjanpalo. "System identifiability based on the power series expansion of the solution". In: *Mathematical Biosciences* 41.1 (1978), pp. 21–33.

[84] G. Margaria, E. Riccomagno, M. J. Chappell, and H. P. Wynn. "Differential algebra methods for the study of the structural identifiability of rational function state-space models in the biosciences". In: *Mathematical Biosciences* 174.1 (2001), pp. 1–26.

[85] A. F. Villaverde, A. Barreiro, and A. Papachristodoulou. "Structural Identifiability of Dynamic Systems Biology Models". In: *PLoS Comput Biol* 12.10 (2016), e1005153.

[86] A. F. Villaverde, N. D. Evans, M. J. Chappell, and J. R. Banga. "Input-Dependent Structural Identifiability of Nonlinear Systems". In: *IEEE Control Systems Letters* 3.2 (2019), pp. 272–277.

[87] C. M. Bishop. *Pattern recognition and machine learning*. Information science and statistics. New York: Springer, 2006.

[88] G. Pillonetto, G. Sparacino, P. Magni, R. Bellazzi, and C. Cobelli. "Minimal model S(I)=0 problem in NIDDM subjects: nonzero Bayesian estimates with credible confidence intervals". In: *Am J Physiol Endocrinol Metab* 282.3 (2002), E564–73.

[89]   O. F. Agbaje, S. D. Luzio, A. I. Albarrak, D. J. Lunn, D. R. Owens, and R. Hovorka. "Bayesian hierarchical approach to estimate insulin sensitivity by minimal model". In: *Clin Sci (Lond)* 105.5 (2003), pp. 551–60.

[90]   I. F. Godsland, O. F. Agbaje, and R. Hovorka. "Evaluation of nonlinear regression approaches to estimation of insulin sensitivity by the minimal model with reference to Bayesian hierarchical analysis". In: *Am J Physiol Endocrinol Metab* 291.1 (2006), E167–74.

[91]   Y. Ruan, M. E. Wilinska, H. Thabit, and R. Hovorka. "Modelling Day-to-Day Variability of Glucose-Insulin Regulation over 12-Week Home Use of Closed-Loop Insulin Delivery". In: *IEEE Trans Biomed Eng* (2016).

[92]   G. Cappon, A. Facchinetti, G. Sparacino, and S. D. Favero. "A Bayesian Framework to Identify Type 1 Diabetes Physiological Models Using Easily Accessible Patient Data". In: *Conf Proc IEEE Eng Med Biol Soc* 2019 (2019), pp. 6914–6917.

[93]   Y. Zhang. "Variational Bayesian data driven modelling for biomedical systems". Thesis. University of Warwick, 2016.

[94]   J. Pinheiro and D. Bates. *Mixed-Effects Models in S and S-PLUS*. Springer New York, 2006.

[95]   J. R. Harring and J. Liu. "A Comparison of Estimation Methods for Nonlinear Mixed-Effects Models Under Model Misspecification and Data Sparseness: A Simulation Study". In: *Journal of Modern Applied Statistical Methods* 15.1 (2016).

[96]   D. Zeevi, T. Korem, N. Zmora, D. Israeli, D. Rothschild, A. Weinberger, [...], and E. Segal. "Personalized Nutrition by Prediction of Glycemic Responses". In: *Cell* 163.5 (2015), pp. 1079–1094.

[97]   S. E. Berry, A. M. Valdes, D. A. Drew, F. Asnicar, M. Mazidi, J. Wolf, [...], and T. D. Spector. "Human postprandial responses to food and potential for precision nutrition". In: *Nat Med* (2020).

[98]   J. Daunizeau, K. J. Friston, and S. J. Kiebel. "Variational Bayesian identification and prediction of stochastic nonlinear dynamic causal models". In: *Physica D: Nonlinear Phenomena* 238.21 (2009), pp. 2089–2118.

[99]   K. Friston, J. Mattout, N. Trujillo-Barreto, J. Ashburner, and W. Penny. "Variational free energy and the Laplace approximation". In: *Neuroimage* 34.1 (2007), pp. 220–34.

[100]   K. J. Friston, N. Trujillo-Barreto, and J. Daunizeau. "DEM: a variational treatment of dynamic systems". In: *Neuroimage* 41.3 (2008), pp. 849–85.

[101]   K. J. Friston. "Variational filtering". In: *Neuroimage* 41.3 (2008), pp. 747–66.

[102]   M. Beal. "Variational Algorithms for Approximate Baysian inference". Thesis. University of London, 2003.

[103]   G. T. Dimitris, C. L. Aristidis, and P. G. Nikolaos. "The Variational Approximation for Bayesian Inference". In: *IEEE Signal Processing Magazine* (2008).

[104]   J. Daunizeau and L. Rigoux. "VBA (Variational Bayesian Analysis) Toolbox". In: *http://mbb-team.github.io/VBA-toolbox/* ().

[105]   J. Daunizeau, V. Adam, and L. Rigoux. "VBA: A Probabilistic Treatment of Nonlinear Models for Neurobiological and Behavioural Data". In: *PLoS Comput Biol* 10.1 (2014).

[106]   Y. Bard. *Nonlinear Parameter Estimation.* New York and London: Academic Press, 1974.

[107]   I. Florescu and C. Tudor. *Handbook of Probability.* Wiley, 2014.

[108]   E. L. Crow and K. Shimizu. *Lognormal distributions : theory and applications.* New York: M. Dekker, 1988.

[109]   G. Zhang and Z. Chen. "Inferences on correlation coefficients of bivariate lognormal distributions". In: *Journal of Applied Statistics* 42.3 (2015), pp. 603–613.

[110]   J. Daunizeau. "Semi-analytical approximations to statistical moments of sigmoid and softmax mappings of normal variables". In: *arXiv preprint arXiv:1703.00091* (2017).

[111]   S. Hengl, C. Kreutz, J. Timmer, and T. Maiwald. "Data-based identifiability analysis of non-linear dynamical models". In: *Bioinformatics* 23.19 (2007), pp. 2612–8.

[112]   K. E. Hines, T. R. Middendorf, and R. W. Aldrich. "Determination of parameter identifiability in nonlinear biophysical models: A Bayesian approach". In: *Journal of General Physiology* 143.3 (2014), pp. 401–416.

[113] A. Saltelli, K. Chan, and E. M. Scott. *Sensitivity analysis*. New York: Wiley, 2000.

[114] W. D. Penny. "Comparing dynamic causal models using AIC, BIC and free energy". In: *Neuroimage* 59.1 (2012), pp. 319–30.

[115] R. E. Kass and A. E. Raftery. "Bayes Factors". In: *Journal of the American Statistical Association* 90.430 (1995), pp. 773–795.

[116] W. D. Penny, K. E. Stephan, J. Daunizeau, M. J. Rosa, K. J. Friston, T. M. Schofield, and A. P. Leff. "Comparing Families of Dynamic Causal Models". In: *PLOS Computational Biology* 6.3 (2010), e1000709.

[117] J. Gibbons and S. Chakraborti. *Nonparametric Statistical Inference*. Marcel Dekker Incorporated, 2003.

[118] Y. Hochberg and A. C. Tamhane. *Multiple comparison procedures*. John Wiley & Sons, Inc., 1987.

[119] R. N. Bergman, Y. Z. Ider, C. R. Bowden, and C Cobelli. "Quantitative estimation of insulin sensitivity". In: *Am J Physiol Endocrinol Metab* 236.6 (1979), E667.

[120] G. Pillonetto, G. Sparacino, and C. Cobelli. "Numerical non-identifiability regions of the minimal model of glucose kinetics: superiority of Bayesian estimation". In: *Math Biosci* 184.1 (2003), pp. 53–67.

[121] P. Magni, G. Sparacino, R. Bellazzi, and C. Cobelli. "Reduced sampling schedule for the glucose minimal model: importance of Bayesian estimation". In: *Am J Physiol Endocrinol Metab* 290.1 (2006), E177–E184.

[122] P. H. R. Barrett, B. M. Bell, C. Cobelli, H. Golde, A. Schumitzky, P. Vicini, and D. M. Foster. "SAAM II: Simulation, analysis, and modeling software for tracer and pharmacokinetic studies". In: *Metabolism* 47.4 (1998), pp. 484–492.

[123] C. Dalla Man, M. Campioni, K. S. Polonsky, R. Basu, R. A. Rizza, G. Toffolo, and C. Cobelli. "Two-hour seven-sample oral glucose tolerance test and meal protocol: minimal model assessment of beta-cell responsivity and insulin sensitivity in nondiabetic individuals". In: *Diabetes* 54.11 (2005), pp. 3265–73.

[124]   X. Ma, D. Becker, V. C. Arena, P. Vicini, and C. Greenbaum. "The Effect of Age on Insulin Sensitivity and Insulin Secretion in First-Degree Relatives of Type 1 Diabetic Patients: A Population Analysis". In: *The Journal of Clinical Endocrinology & Metabolism* 94.7 (2009), pp. 2446–2451.

[125]   T. Geragotou, S. Jainandunsing, B. Oezcan, F. W. M. de Rooij, A. Kokkinos, N. Tentolouris, and E. J. G. Sijbrands. "The Relationship of Metabolic Syndrome Traits with Beta-Cell Function and Insulin Sensitivity by Oral Minimal Model Assessment in South Asian and European Families Residing in the Netherlands". In: *Journal of Diabetes Research* 2016 (2016), p. 9.

[126]   M. J. Theodorakis, N. Katsiki, K. Arampatzi, and G. P. Chrousos. "Modeling the oral glucose tolerance test in normal and impaired glucose tolerant states: a population approach". In: *Current Medical Research and Opinion* 33.2 (2017), pp. 305–313.

[127]   B. M. Bell, J. V. Burke, and A. Schumitzky. "A relative weighting method for estimating parameters and variances in multiple data sets". In: *Computational Statistics & Data Analysis* 22.2 (1996), pp. 119–135.

[128]   M. Ahmed, M. C. Gannon, and F. Q. Nuttall. "Postprandial plasma glucose, insulin, glucagon and triglyceride responses to a standard diet in normal subjects". In: *Diabetologia* 12.1 (1976), pp. 61–7.

[129]   National Academy of Sciences. "Recommended Dietary Allowances âĂŤ 1980". In: *Nutrition Reviews* 38.8 (1980), pp. 290–294.

[130]   Z. Wang, S. Heshka, D. Gallagher, C. N. Boozer, D. P. Kotler, and S. B. Heymsfield. "Resting energy expenditure-fat-free mass relationship: new insights provided by body composition modeling". In: *Am J Physiol Endocrinol Metab* 279.3 (2000), E539–45.

[131]   M. P. Saccomani and G. Bellu. "DAISY: An efficient tool to test global identifiability. Some case studies". In: *2008 16th Mediterranean Conference on Control and Automation*. 2008, pp. 1723–1728.

[132]   G. Bellu, M. P. Saccomani, S. Audoly, and L. D'Angio. "DAISY: a new software tool to test global identifiability of biological and physiological systems". In: *Comput Methods Programs Biomed* 88.1 (2007), pp. 52–61.

[133] S. V. Chin and M. J. Chappell. "Structural identifiability and indistinguishability analyses of the minimal model and a euglycemic hyperinsulinemic clamp model for glucose-insulin dynamics". In: *Comput Methods Programs Biomed* 104.2 (2011), pp. 120–34.

[134] R. A. Sicree, P. Z. Zimmet, D. W. Dunstan, A. J. Cameron, T. A. Welborn, and J. E. Shaw. "Differences in height explain gender differences in the response to the oral glucose tolerance testâĂŤ the AusDiab study". In: 25.3 (2008), pp. 296–302.

[135] R. Peter, G. Dunseath, S. D. Luzio, R. Chudleigh, S. Roy Choudhury, and D. R. Owens. "Daytime variability of postprandial glucose tolerance and pancreatic B-cell function using 12-h profiles in persons with Type 2 diabetes". In: *Diabet Med* 27.3 (2010), pp. 266–73.

[136] F. Magkos, X. Wang, and B. Mittendorfer. "Metabolic actions of insulin in men and women". In: *Nutrition* 26.7 (2010), pp. 686–693.

[137] D. Stefanovski, P. J. Moate, N. Frank, G. M. Ward, A. R. Localio, N. M. Punjabi, and R. C. Boston. "Metabolic modeling using Statistical and Spreadsheet Software: Application to the Glucose Minimal Model". In: *Computer Methods and Programs in Biomedicine* (2020), p. 105353.

[138] S. Choy, E. Henin, J.-S. van der Walt, M. C. Kjellsson, and M. O. Karlsson. "Identification of the primary mechanism of action of an insulin secretagogue from meal test data in healthy volunteers based on an integrated glucose-insulin model". In: *Journal of Pharmacokinetics and Pharmacodynamics* 40.1 (2013), pp. 1–10.

[139] R. Hovorka, V. Canonico, L. J. Chassin, U. Haueter, M. Massi-Benedetti, M. Orsini Federici, [...], and M. E. Wilinska. "Nonlinear model predictive control of glucose concentration in subjects with type 1 diabetes". In: *Physiol Meas* 25.4 (2004), pp. 905–20.

[140] A. K. Duun-Henriksen, S. Schmidt, R. M. Roge, J. B. Moller, K. Norgaard, J. B. Jorgensen, and H. Madsen. "Model identification using stochastic differential equation grey-box models in diabetes". In: *J Diabetes Sci Technol* 7.2 (2013), pp. 431–40.

[141] A. Guemes, P. Herrero, J. Bondia, and P. Georgiou. "Modeling the effect of the cephalic phase of insulin secretion on glucose metabolism". In: *Med Biol Eng Comput* 57.6 (2019), pp. 1173–1186.

[142] T. Pearson, J. A. Wattis, J. R. King, I. A. MacDonald, and D. J. Mazzatti. "A mathematical model of the human metabolic system and metabolic flexibility". In: *Bull Math Biol* 76.9 (2014), pp. 2091–121.

[143] Y. Li, C. C. Chow, A. B. Courville, A. E. Sumner, and V. Periwal. "Modeling glucose and free fatty acid kinetics in glucose and meal tolerance test". In: *Theor Biol Med Model* 13 (2016), p. 8.

[144] M. Eichenlaub, N. Khovanova, and J. Hattersley. "A Model Describing the Multiphasic Dynamics of Mixed Meal Glucose Responses in Healthy Subjects". In: *World Congress on Medical Physics and Biomedical Engineering 2018*. Springer Singapore, 2019, pp. 577–581.

[145] J. Karlsson, M. Anguelova, and M. Jirstrand. "An Efficient Method for Structural Identifiability Analysis of Large Dynamic Systems". In: *IFAC Proceedings Volumes* 45.16 (2012), pp. 941–946.

[146] M. Anguelova, J. Karlsson, and M. Jirstrand. "Minimal output sets for identifiability". In: *Mathematical Biosciences* 239.1 (2012), pp. 139–153.

[147] P. Vargas, M. A. Moreles, J. PeÃśa, A. Monroy, and S. Alavez. "Estimation and SVM classification of glucose-insulin model parameters from OGTT data: a comparison with the ADA criteria". In: *International Journal of Diabetes in Developing Countries* (2020).

[148] B. Topp, K. Promislow, G. deVries, R. M. Miura, and D. T. Finegood. "A model of beta-cell mass, insulin, and glucose kinetics: pathways to diabetes". In: *J Theor Biol* 206.4 (2000), pp. 605–19.

[149] R. C. Boston, D. Pei, and P. J. Moate. "A numerical deconvolution method to estimate C-peptide secretion in humans after an intravenous glucose tolerance test". In: *Metabolism* 58.7 (2009), pp. 891–900.

[150] M. C. Laurenti, A. Vella, R. T. Varghese, J. C. Andrews, A. Sharma, N. E. Kittah, [...], and C. Dalla Man. "Assessment of pulsatile insulin secretion derived from peripheral plasma C-peptide concentrations by nonparametric stochastic

deconvolution". In: *American Journal of Physiology-Endocrinology and Metabolism* 316.5 (2019), E687–E694.

[151] R. Hovorka, L. Chassin, S. D. Luzio, R. Playle, and D. R. Owens. "Pancreatic beta-cell responsiveness during meal tolerance test: model assessment in normal subjects and subjects with newly diagnosed noninsulin-dependent diabetes mellitus". In: *J Clin Endocrinol Metab* 83.3 (1998), pp. 744–50.

[152] Y. Ruan, H. Thabit, M. E. Wilinska, and R. Hovorka. "Modelling endogenous insulin concentration in type 2 diabetes during closed-loop insulin delivery". In: *Biomed Eng Online* 14 (2015), p. 19.

[153] A. Mari, S. Camastra, E. Toschi, A. Giancaterini, A. Gastaldelli, G. Mingrone, and E. Ferrannini. "A model for glucose control of insulin secretion during 24 h of free living". In: *Diabetes* 50 Suppl 1 (2001), S164–8.

[154] E. Toschi, S. Camastra, A. Mari, A. Gastaldelli, S. Baldi, A. Masoni, and E. Ferrannini. "A model for assessing insulin secretion and its control under free-living conditions". In: *Diabetes* 50 Suppl 1 (2001), S178–9.

[155] A. Mari, O. Schmitz, A. Gastaldelli, T. Oestergaard, B. Nyholm, and E. Ferrannini. "Meal and oral glucose tests for assessment of Îš-cell function: modeling analysis in normal subjects". In: *Am J Physiol Endocrinol Metab* 283.6 (2002), E1159–E1166.

[156] A. Mari, A. Tura, A. Gastaldelli, and E. Ferrannini. "Assessing insulin secretion by modeling in multiple-meal tests: role of potentiation". In: *Diabetes* 51 Suppl 1 (2002), S221–6.

[157] E. Breda, M. K. Cavaghan, G. Toffolo, K. S. Polonsky, and C. Cobelli. "Oral glucose tolerance test minimal model indexes of beta-cell function and insulin sensitivity". In: *Diabetes* 50.1 (2001), pp. 150–8.

[158] E. Van Cauter, F. Mestrez, J. Sturis, and K. S. Polonsky. "Estimation of insulin secretion rates from C-peptide levels. Comparison of individual and standard kinetic parameters for C-peptide clearance". In: *Diabetes* 41.3 (1992), pp. 368–77.

[159] M. M. Byrne, J. Sturis, and K. S. Polonsky. "Insulin secretion and clearance during low-dose graded glucose infusion". In: *Am J Physiol* 268.1 Pt 1 (1995), E21–7.

[160] A. Cretti, M. Lehtovirta, E. Bonora, B. Brunato, M. G. Zenti, F. Tosi, [...], and R. C. Bonadonna. "Assessment of beta-cell function during the oral glucose tolerance test by a minimal model of insulin secretion". In: *Eur J Clin Invest* 31.5 (2001), pp. 405–16.

[161] D. C. Robbins, J. Jaspan, B. Vasquez, and E. Van Cauter. "Biphasic patterns of peripheral insulin and glucose levels after lunch in normal subjects". In: *Diabetes Care* 10.3 (1987), pp. 293–9.

[162] C. Simon, M. Follenius, and G. Brandenberger. "Postprandial oscillations of plasma glucose, insulin and C-peptide in man". In: *Diabetologia* 30.10 (1987), pp. 769–773.

[163] K. S. Polonsky, B. D. Given, and E. Van Cauter. "Twenty-four-hour profiles and pulsatile patterns of insulin secretion in normal and obese subjects". In: *J Clin Invest* 81.2 (1988), pp. 442–8.

[164] M. M. Eichenlaub, J. G. Hattersley, and N. A. Khovanova. "A Minimal Model Approach for the Description of Postprandial Glucose Responses from Glucose Sensor Data in Diabetes Mellitus". In: *2019 41st Annual International Conference of the IEEE Engineering in Medicine and Biology Society (EMBC)*. 2019, pp. 265–268.

[165] M. Derouich and A. Boutayeb. "The effect of physical exercise on the dynamics of glucose and insulin". In: *J Biomech* 35.7 (2002), pp. 911–7.

[166] C. Zecchin, A. Facchinetti, G. Sparacino, C. Dalla Man, C. Manohar, J. A. Levine, [...], and C. Cobelli. "Physical activity measured by physical activity monitoring system correlates with glucose trends reconstructed from continuous glucose monitoring". In: *Diabetes Technol Ther* 15.10 (2013), pp. 836–44.

[167] W. D. McArdle, F. I. Katch, and V. L. Katch. *Exercise physiology : energy, nutrition, and human performance*. Philadelphia: Lippincott Williams & Wilkins, 2001.

[168] M. Mansoubi, N. Pearson, S. A. Clemes, S. J. Biddle, D. H. Bodicoat, K. Tolfrey, [...], and T. Yates. "Energy expenditure during common sitting and standing tasks: examining the 1.5 MET definition of sedentary behaviour". In: *BMC Public Health* 15 (2015), p. 516.

[169] E. Cengiz and W. V. Tamborlane. "A tale of two compartments: interstitial versus blood glucose monitoring". In: *Diabetes Technol Ther* 11.Suppl 1 (2009), S11–S16.

[170] M. Matsuda and R. A. DeFronzo. "Insulin sensitivity indices obtained from oral glucose tolerance testing: comparison with the euglycemic insulin clamp". In: *Diabetes Care* 22.9 (1999), pp. 1462–70.

[171] M. H. Lim, T. J. Oh, K. Choi, J. C. Lee, Y. M. Cho, and S. Kim. "Application of the Oral Minimal Model to Korean Subjects with Normal Glucose Tolerance and Type 2 Diabetes Mellitus". In: *Diabetes Metab J* 40.4 (2016), pp. 308–17.

[172] R. Levine and D. E. Haft. "Carbohydrate homeostasis". In: *N Engl J Med* 283.5 (1970), pp. 237–46.

[173] S. Suh and J. H. Kim. "Glycemic Variability: How Do We Measure It and Why Is It Important?" In: *Diabetes Metab J* 39.4 (2015), pp. 273–82.

[174] B. Kovatchev and C. Cobelli. "Glucose Variability: Timing, Risk Analysis, and Relationship to Hypoglycemia in Diabetes". In: *Diabetes Care* 39.4 (2016), pp. 502–10.

[175] D. Rodbard. "Glucose Variability: A Review of Clinical Applications and Research Developments". In: *Diabetes Technol Ther* 20.S2 (2018), S25–s215.

[176] L. A. Gonder-Frederick, J. H. Grabman, B. Kovatchev, S. A. Brown, S. Patek, A. Basu, [...], and r. Doyle F. J. "Is Psychological Stress a Factor for Incorporation Into Future Closed-Loop Systems?" In: *J Diabetes Sci Technol* (2016).

[177] L. Monnier, C. Colette, S. Dejager, and D. Owens. "The dawn phenomenon in type 2 diabetes: How to assess it in clinical practice?" In: *Diabetes & Metabolism* 41.2 (2015), pp. 132–137.

[178] A. Facchinetti, S. Del Favero, G. Sparacino, and C. Cobelli. "Model of glucose sensor error components: identification and assessment for new Dexcom G4 generation devices". In: *Med Biol Eng Comput* 53.12 (2015), pp. 1259–69.

[179] A. H. Hansen, A. K. Duun-Henriksen, R. Juhl, S. Schmidt, K. Norgaard, J. B. Jorgensen, and H. Madsen. "Predicting Plasma Glucose From Interstitial Glucose Observations Using Bayesian Methods". In: *J Diabetes Sci Technol* 8.2 (2014), pp. 321–330.

[180]   M. Vettoretti, A. Facchinetti, S. Del Favero, G. Sparacino, and C. Cobelli. "On-line calibration of glucose sensors from the measured current by a time-varying calibration function and Bayesian priors". In: *IEEE Trans Biomed Eng* (2015).

[181]   D. R. Owens, J. Dolben, I. R. Jones, J. Birtwell, and S. D. Luzio. "Hormonal and glycaemic responses to serial meals in newly diagnosed non insulin dependent diabetic patients". In: *Diabete Metab* 15.1 (1989), pp. 1–4.

[182]   F. Q. Nuttall and M. C. Gannon. "Plasma glucose and insulin response to macronutrients in nondiabetic and NIDDM subjects". In: *Diabetes Care* 14.9 (1991), pp. 824–38.

[183]   K. Tsukuda, M. Kikuchi, S. Irie, T. Eto, A. Yamada, K. Matsuguma, [...], and Y. Katayama. "Evaluation of the 24-hour profiles of physiological insulin, glucose, and C-peptide in healthy Japanese volunteers". In: *Diabetes Technol Ther* 11.8 (2009), pp. 499–508.

Appendix A

Mathematical derivations

A.1 Derivation of the expression for free energy

In section 3.3.2.1, expression (3.10) defines the Kullback-Leibler divergence between the approximated distribution f_q and the true posterior $f_{\boldsymbol{\theta}|\boldsymbol{y},M}$ as follows

$$D_{KL}(f_q \parallel f_{\boldsymbol{\theta}|\boldsymbol{y},M}) = \int f_q(\boldsymbol{\theta}) \log \frac{f_q(\boldsymbol{\theta})}{f_{\boldsymbol{\theta}|\boldsymbol{y},M}(\boldsymbol{\theta}|\boldsymbol{y},M)} d\boldsymbol{\theta}$$

$$= \mathbb{E}\left[\log \frac{f_q(\boldsymbol{\theta})}{f_{\boldsymbol{\theta}|\boldsymbol{y},M}(\boldsymbol{\theta}|\boldsymbol{y},M)}\right]_{f_q}.$$

Furthermore the true posterior is defined by expression (3.8) as follows

$$f_{\boldsymbol{\theta}|\boldsymbol{y},M}(\boldsymbol{\theta}|\boldsymbol{y},M) = \frac{L(\boldsymbol{y}|\boldsymbol{\theta},M)f_{\boldsymbol{\theta}|M}(\boldsymbol{\theta}|M)}{P(\boldsymbol{y}|M)}.$$

Substituting this expression for the true posterior in the expression for the Kullback-Leibler divergence leads to

$$D_{KL}(f_q \parallel f_{\boldsymbol{\theta}|\boldsymbol{y},M}) = \mathbb{E}\left[\log \frac{f_q(\boldsymbol{\theta})P(\boldsymbol{y}|M)}{L(\boldsymbol{y}|\boldsymbol{\theta},M)f_{\boldsymbol{\theta}|M}(\boldsymbol{\theta}|M)}\right]_{f_q}.$$

Subsequently expanding the logarithm gives

$$D_{KL}(f_q \parallel f_{\boldsymbol{\theta}|\boldsymbol{y},M}) = \mathbb{E}\left[\log f_q(\boldsymbol{\theta}) + \log P(\boldsymbol{y}|M) - \log L(\boldsymbol{y}|\boldsymbol{\theta},M) - \log f_{\boldsymbol{\theta}|M}(\boldsymbol{\theta}|M)\right]_{f_q}.$$

Since $\log P(\boldsymbol{y}|M)$ is independent of $\boldsymbol{\theta}$, its expected value is itself, i.e.

$$\mathbb{E}\left[\log P(\boldsymbol{y}|M)\right]_{f_q} = \int \log P(\boldsymbol{y}|M)f_q(\boldsymbol{\theta})d\boldsymbol{\theta} = \log P(\boldsymbol{y}|M),$$

meaning that the expression for the Kullback-Leibler divergence can be simplified as follows

$$D_{KL}(f_q \parallel f_{\boldsymbol{\theta}|\boldsymbol{y},M}) = \mathbb{E}\left[\log f_q(\boldsymbol{\theta}) - \log L(\boldsymbol{y}|\boldsymbol{\theta}, M) - \log f_{\boldsymbol{\theta}|M}(\boldsymbol{\theta}|M)\right]_{f_q} + \log P(\boldsymbol{y}|M).$$

Defining the the free energy $\mathcal{F}$ as

$$\mathcal{F} = \mathbb{E}\left[\log L(\boldsymbol{y}|\boldsymbol{\theta}, M) + \log f_{\boldsymbol{\theta}|M}(\boldsymbol{\theta}|M) - \log f_q(\boldsymbol{\theta})\right]_{f_q}.$$

leads to expression (3.11) after reformulation

$$\mathcal{F} = \log P(\boldsymbol{y}|M) - D_{KL}(f_q \parallel f_{\boldsymbol{\theta}|\boldsymbol{y},M}).$$

A.2 Derivation of the AUC of the piecewise-linear function

The piecewise-linear function Ra_{PL} is given as

$$Ra_{PL}(t) = \begin{cases} k_{i-1} + \dfrac{k_i - k_{i-1}}{t_i - t_{i-1}}(t - t_{i-1}) & \text{for} \quad t_{i-1} \le t \le t_i \quad i = 1 \ldots 7, \\ k_7 \exp(-\alpha(t - t_7)) & \text{for} \quad t > t_7. \end{cases}$$

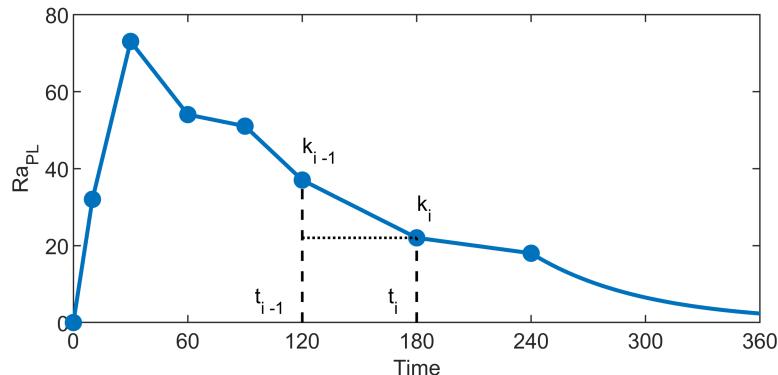An example plot of this function is given in the following Figure.

Figure A.1: Example of the function $Ra_{PL}(t)$.

The area A_i under any linear section is formed by a trapezoid and can be calculated

as follows

$$A_i = (t - t_{i-1})k_i + \frac{1}{2}(t - t_{i-1})(k_{i-1} - k_i)$$
$$= (t - t_{i-1})k_{i-1} + \frac{1}{2}(t - t_{i-1})(k_i - k_{i-1})$$
$$= (t - t_{i-1})\left[k_{i-1} + \frac{1}{2}(k_i - k_{i-1})\right]$$
$$= \frac{1}{2}(t_i - t_{i-1})(k_i + k_{i-1}).$$

The total AUC A of $Ra_{PL}(t)$ can then be calculated as

$$A = \int_0^\infty Ra_{PL}(t)dt = \sum_{i=1}^{7} A_i + \int_{t_7}^\infty k_7 \exp(-\alpha(t - t_7))dt$$
$$= \frac{1}{2}\sum_{i=1}^{7}(t_i - t_{i-1})(k_i + k_{i-1}) + \frac{k_7}{\alpha}.$$

A.3   Transformation of PDF in Dalla Man et al. (2004)

In the publication by Dalla Man et al. (2004) [72], the authors propose to model the square root of a parameter of interest as normally distributed. This can be expressed as taking the normally distributed parameter p with density f_p defined with mean μ and standard deviation σ and mapping it to the parameter s with the function $s = p^2$. Applying theorem (3.21), the density f_s over s is given by

$$f_s(s|\mu, \sigma) = \frac{1}{2\sqrt{2\pi s}\sigma} \exp\left(-\frac{(\mu + \sqrt{s})^2}{2\sigma^2}\right)\left[1 + \exp\left(\frac{2\mu\sqrt{s}}{\sigma^2}\right)\right] \quad \text{for} \quad s > 0.$$

Using symbolic calculation, it can be shown that the density f_s has the following mean and variance

$$\mathbb{E}[s]_{f_s} = \mu^2 + \sigma^2,$$
$$\text{Var}[s]_{f_s} = 2(2\mu^2\sigma^2 + \sigma^4).$$
(A.1)

In Dalla Man et al. (2004) [72], the parameter of interest is p_2 and its square root follows a normal distribution with a mean of 0.11 min$^{-1/2}$ and CV of 10 %. Using expressions (A.1), it can be calculated the actual distribution over p_2, has a mean of 0.012 min^{-1} and a CV of around 20 %.

A.4 Derivation of log-normally shaped input function component

The log-normal distribution is generally defined as follows [108]

$$f_x(t|\mu,\sigma) = \frac{1}{t\sqrt{2\pi}\sigma} \exp\left(-\frac{(\log t - \mu)^2}{2\sigma^2}\right) \qquad \text{for} \qquad t > 0.$$

This parametrisation is based on the associated normal distribution, i.e. $\log t \sim \mathcal{N}(\mu, \sigma^2)$. In order to have a single parameter T defining the peak position of the profile (defined by the mode of the PDF) and another parameter W governing the general width, the following substitutions are made

$$\mu = \log T + \sigma^2,$$
$$\sigma^2 = \frac{W}{2}.$$

This leads to the following parametrisation of the input function component

$$f_{LN}(t, T, W) = \frac{1}{t\sqrt{\pi W}} \exp\left(-\frac{\left[\log\frac{t}{T} - \frac{W}{2}\right]^2}{W}\right).$$

Appendix B

Structural identifiability analysis

B.1 Implementation of Taylor series approach in Mathematica

The details of the structural identifiability analysis using the Taylor series method and symbolic computation can be found below. For that Mathematica code will be presented.

The implemented Mathematica code will be exemplified on the model presented in section 3.2

$$\frac{dx(t)}{dt} = -(p_1{}^2 + p_2)x(t), \quad x(0) = x_0, \quad y(t) = x(t).$$

First, the model equations, initial conditions and output are defined by

```
In[1]:=  (* Model equations *)
         x'[t] = -(p1^2 + p2)*x[t];
         (* Initial condition *)
         x[0] = x0;
         (* Observation *)
         y[t] = x[t];
```

Next, the number of Taylor coefficients `Nt` to be calculated, the time `t0` at which to expand the Taylor series around, the vector of unknown substitution parameters `subst` and the vector `sol` of variables to solve for are defined

```
In[2]:=  Nt = 2;
         t0 = 0;
         subst = {p1 → p1b, p2 → p2b};
         sol = {p1b, p2b}
```

Lastly the following code calculating the Taylor coefficients, creating and solving the system of equations is executed

```
In[3]:= (* Calculates the Taylor coefficients *)
     Cof = {{y[0]}};
     For[i = 2, i <= Nt, i++,
     Cof = Append[Cof, D[y[t], t, i-1] /. t → t0]];
     (* Constructs the system of equations *)
     Eqns = {Cof[[1]] == (Cof[[1]] /. subst)};
     For[i = 2, i <= Nt, i++,
     Eqns = Append[Eqns, Cof[[i]] == (Cof[[i]] /. subst)]];
     (* Solves the system of equations *)
     Solve[Eqns, sol]
```

This yields the result

```
Out[3]= p2b → p1²-p1b²+p2,
```

showing that the model parameters are not identifiable.

In order to determine the number of Taylor coefficients, the value of `Nt` is increased until all parameters have a unique solution, i.e. are structurally globally identifiable, or the system of equations become intractable for the symbolic computation, i.e. the computation no longer completes.

B.2   Oral minimal model

B.2.1   Formulation by Dalla Man et al. (2002)

Dalla Man et al. (2002) [71] formulate the OMM with the following equations described in section 4.2.

$$
\frac{dG(t)}{dt} = -G(t)X(t) - p_1[G(t) - G_b] + \frac{Ra_{PL}(t)}{V}, \qquad G(0) = G_b,
$$
$$
\frac{dX(t)}{dt} = -p_2 X(t) + p_3[I(t) - I_b], \qquad X(0) = 0,
$$

$$
Ra_{PL}(t) = \begin{cases} k_{i-1} + \dfrac{k_i - k_{i-1}}{t_i - t_{i-1}}(t - t_{i-1}) & \text{for} \quad t_{i-1} \le t \le t_i \quad i = 1 \dots n, \\ 0 & \text{for} \quad t > t_n. \end{cases}
$$

The insulin sensitivity S_I is given by p_3/p_2. The model considers the insulin concentration $I(t)$ to be a known input with $I(0) = I_b$. To assess the identifiability using the

Taylor Series approach, the system is initially expanded around $t_0 = 0$. The means that Ra_{PL} takes the following form

$$Ra_{PL}(t) = k_0 + \frac{k_1 - k_0}{t_1 - t_0}(t - t_0) = \frac{k_1}{t_1}t. \tag{B.1}$$

This assumes that $k_0 = 0$ based on fasting state of the subjects.

The model, substitutions and variables to solve for are defined as follows

```
In[4]:= (* Model equations *)
        RaPL[t] = t*(k1/t1);
        G'[t] = -G[t]*X[t] - p1*(G[t] - Gb) + RaPL[t]/V;
        X'[t] = -p2*X[t] + p3*(Ii[t] - Ib);
        (* Initial conditions *)
        G[0] = Gb; X[0] = 0; Ii[0] = Ib;
        (* Observation equation *)
        y[t] = G[t];
        (* Substitutions and unknown parameters to solve for *)
        subst = {p1 → p1b, p2 → p2b, p3 → p3b, k1 → k1b V → Vb};
        sol = {p1b, p2b, p3b, k1b, Vb};
```

Calculating six Taylor coefficients, i.e. Nt=6, as in Dalla Man et al. (2002) [71], the following result using the code in section B.1 is obtained

```
Out[4]= (* Solution 1 *)
                                                    k1Vb
        p1b → p1, p2b → p2, p3b → p3, k1b → ────
                                                     V
        (* Solution 2 *)
        p1b → (6k1³p1Ii'[0]+Gb³p2p3²t1³V³Ii'[0]³+Gb²k1p3t1²V²(-p2²Ii'[0]²
        +2p2Ii'[0]Ii"[0]-Ii"[0]²+p1Ii'[0](p2Ii'[0]+Ii"[0])+Ii'[0]Ii⁽³⁾[0])
        +Gbk1²t1V(6p3Ii'[0]²+p1(p1Ii"[0]+Ii⁽³⁾[0]))) / (6k1³Ii'[0]
        +Gb³p3²t1³V³Ii'[0]³+Gb²k1p3t1²V²Ii'[0](p1Ii'[0]-p2Ii'[0]+2Ii"[0])
        +Gbk1²t1V(p1Ii"[0]+Ii⁽³⁾[0])),
        p2b → (-6k1²Ii'[0]²+Gb²p1p3t1²V²Ii'[0]³+Gbk1t1V(p1²Ii'[0]²
        -p2Ii'[0]Ii"[0]+Ii"[0]²+p1Ii'[0](-p2Ii'[0]+Ii"[0])-Ii'[0]Ii⁽³⁾[0])) ...
        / Gbt1V Ii'[0](Gbp3t1VIi'[0]²+k1(p1Ii'[0]-p2Ii'[0]+Ii"[0])),
        p3b → (Gbp3t1V(Gbp3t1VIi'[0]²+k1(p1Ii'[0]-p2 Ii'[0]+Ii"[0]))²) /
        (Ii'[0](6k1³Ii'[0]+Gb³p3²t1³V³Ii'[0]³+Gb²k1p3t1²V²Ii'[0](p1 Ii'[0]
        -p2Ii'[0]+2Ii"[0])+Gbk1²t1V(p1Ii"[0]+Ii⁽³⁾[0]))),
               k1Vb
        k1b → ────
                V
```

This confirms the results from Dalla Man et al. (2002) [71], namely that only k_1/V is identifiable, and that there are in fact two possible solutions for parameters p_1, p_2 and

p_3, making them only locally identifiable. As mentioned in Chapter 4 the authors then decide to fix p_1 in order to make p_2 and p_2 globally identifiable.

If one additional Taylor coefficient is included, i.e. `Nt=7`, the following result using the code in section B.1 is obtained

```
Out[5]=  p1b → p1, p2b → p2, p3b → p3, k1b → k1Vb/V
```

This result demonstrates the global identifiability of p_1, p_2 and p_3 using the Taylor series approach without the need to assume the knowledge of either one of the parameters. It disproves the statements made by Dalla Man et al. (2002) [71] and confirms the results from Saccomani et al. [131].

To prove the identifiability of the remaining k_i, the model output needs to be expanded around the other breakpoints t_i of the input function. This is the case because the input function takes on a different functional form at each breakpoint. Dalla Man et al. (2002) [71] use the global identifiability of p_1, p_2 and p_3 (achieved through fixing p_1) to prove the identifiability of the remaining k_i.

B.2.2 Formulation presented in this work

In Chapter 4, the OMM is formulated as follows

$$\frac{dG(t)}{dt} = -G(t)X(t) - p_1[G(t) - G_b] + \frac{Ra_{PL}(t) + Rap(t)}{V}, \qquad G(0) = G_0,$$

$$\frac{dX(t)}{dt} = -p_2(X(t) - S_I[I(t) - I_b]), \qquad X(0) = X_0,$$

$$Ra_{PL}(t) = \begin{cases} k_{i-1} + \dfrac{k_i - k_{i-1}}{t_i - t_{i-1}}(t - t_{i-1}) & \text{for} \quad t_{i-1} \le t \le t_i \quad i = 1\ldots 7, \\ k_7 \exp(-\alpha(t - t_7)) & \text{for} \quad t > t_7, \end{cases}$$

$$Rap(t) = R_0 \exp(-\alpha t).$$

The model, substitutions and variables to solve for are defined as follows

```
In[6]:= (* Model equations *)
        RaPL[t] = t*(k1/t1);
        Rap[t] = R0*Exp[-α t]
        G'[t] = -G[t]*X[t] - p1*(G[t] - Gb) + (RaPL[t]+Rap[t])/V;
        X'[t] = -p2*(X[t] - SI*(Ii[t] - Ib));
        (* Initial conditions *)
        G[0] = G0; X[0] = X0; Ii[0] = I0;
```

```
(* Observation *)

y[t] = G[t];

(* Substitutions and unknown parameters to solve for *)

subst = {p1 → p1b, p2 → p2b, p3 → p3b, k1 → k1b};

sol = {p1b, p2b, p3b, k1b};
```

Calculating six Taylor coefficients, i.e. `Nt=6` the following result using the code in section B.1 is obtained

```
Out[6]=  p1b → p1,  p2b → p2,  SIb → SI,  k1b → k1
```

demonstrating the identifiability of of all parameters. It should be pointed out that V is assumed to be known before the analysis. This is necessary because the initial level of $I(t)$, i.e. I_0, could be different from the basal state I_b and has thus to be defined by a separate parameter. This, in turn, makes the second and third Taylor coefficients more complex and the symbolic computation no longer completes. The results confirm the global identifiability of p_1, p_2, S_I and k_1, assuming the knowledge of V. It should be noted, that only six Taylor coefficients were required to obtain this result, most likely through the assumption that V is known prior to the analysis.

Using these results, i.e. p_1, p_2, S_I and k_1 being identifiable, the identifiability of the remaining k_i can be analysed by expanding the Taylor series around $t_0 = t_i$. For the case of $t_0 = t_1$ the function Ra_{PL} takes the following form

$$Ra_{PL}(t) = k_1 + \frac{k_2 - k_1}{t_2 - t_1}(t - t_1).$$

The function Ra_{PL}, substitutions and unknown parameters to solve for are defined as follows

```
In[7]:=  RaPL[t] = k1 + (k2 - k1)/(t2 - t1)*(t - t1);

         subst = {k2 → k2b};

         sol = {k2b};
```

Using three Taylor coefficients, i.e. `Nt=3` and defining `t0=t1`, the following results are obtained

```
Out[7]=  k2b → k2
```

proving the identifiability of k_2. Identical results are obtained for the remaining k_i, therefore demonstrating the global identifiability of all k_i.

B.2.3 Formulation with Ra_R

B.2.3.1 Taylor series method

The OMM in combination with the input function containing two Rayleigh components Ra_R is formulated as follows

$$\frac{dG(t)}{dt} = -G(t)X(t) - p_1[G(t) - G_b] + \frac{Ra_{PL}(t) + Rap(t)}{V}, \qquad G(0) = G_0,$$

$$\frac{dX(t)}{dt} = -p_2(X(t) - S_I[I(t) - I_b]), \qquad\qquad X(0) = X_0,$$

$$Ra_R(t) = (1 - R_H)\frac{t}{T_1^2}\exp\left(-\frac{t^2}{2T_1^2}\right) + R_H\frac{t}{T_2^2}\exp\left(-\frac{t^2}{2T_2^2}\right),$$

$$Rap(t) = R_0\exp(-\alpha t).$$

For simplicity, it is assumed that the AUC under the input function is one and the known persisting absorption is modelled with a monoexponential decay. The model, substitutions and variables to solve for are defined as follows
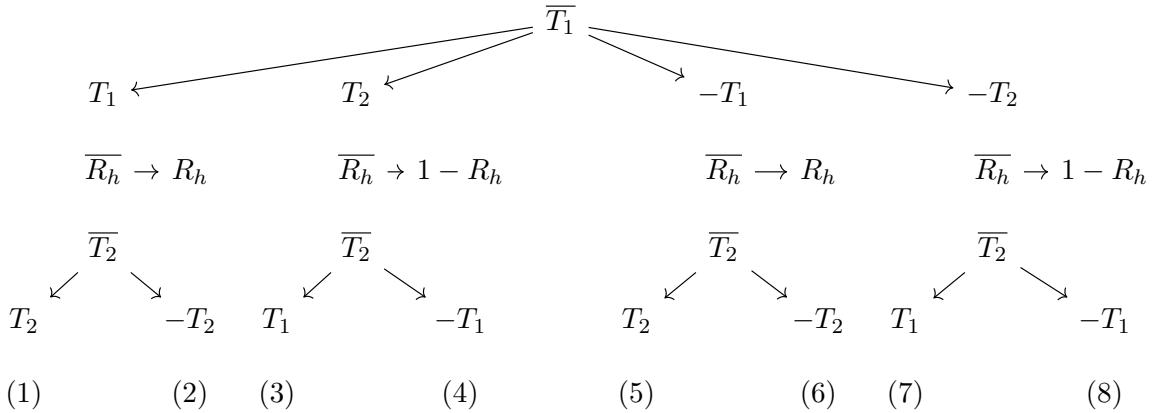
```
In[8]:=  (* Model equations *)
         RaR[t] = (1 - RH)*t^2/T1^2*Exp[-t^2/(2*T1^2)]
         + RH*t^2/T2^2*Exp[-t^2/(2*T2^2)];
         Rap[t] = R0*Exp[-α*t]
         G'[t] = -G[t]*X[t] - p1*(G[t] - Gb) + (RaR[t]+Rap[t])/V;
         X'[t] = -p2*(X[t] + SI*(Ii[t] - Ib));
         (* Initial conditions *)
         G[0] = G0; X[0] = X0; Ii[0] = Ib;
         (* Observation *)
         y[t] = G[t];
         (* Substitutions and unknown parameters to solve for *)
         subst = {p1 → p1b, T1 → T1b, T2 → T2b, RH → RHb}
         sol = {p1b, T1b, T2b, RHb}
```

This assumes that $I(0) = I_b$ and that R_0, α, and V are known. Using eight Taylor coefficients, the following results using the code in section B.1 are obtained
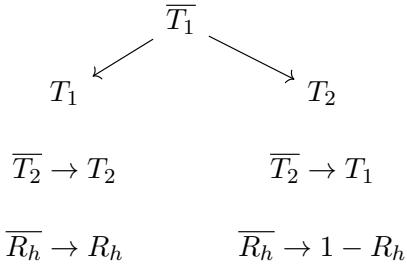
```
Out[8]=  (* Solution 1 *)
         p1b → p1, p2b → p2, SIb → SI,
         T1b → T1, T2b → T2, RHb → RH,
         (* Solution 2 *)
         p1b → p1, p2b → p2, SIb → SI,
         T1b → T1, T2b → -T2, RHb → RH,
         (* Solution 3 *)
```

```
        p1b → p1, p2b → p2, SIb → SI,
        T1b → T2, T2b → T1, RHb → 1-RH,
        (* Solution 4 *)
        p1b → p1, p2b → p2, SIb → SI,
        T1b → T2, T2b → -T1, RHb → 1-RH,
        (* Solution 5 *)
        p1b → p1, p2b → p2, SIb → SI,
        T1b → -T1, T2b → T2, RHb → RH,
        (* Solution 6 *)
        p1b → p1, p2b → p2, SIb → SI,
        T1b → -T1, T2b → -T2, RHb → RH,
        (* Solution 7 *)
        p1b → p1, p2b → p2, SIb → SI,
        T1b → -T2, T2b → T1, RHb → 1-RH,
        (* Solution 8 *)
        p1b → p1, p2b → p2, SIb → SI,
        T1b → -T2, T2b → -T1, RHb → 1-RH
```

The same results are obtained for nine and ten Taylor series coefficients. These results indicate the global identifiability of p_1, p_2 and S_I and the local identifiability of T_1, T_2 and R_H. The solutions with respect to the locally identifiable parameters can be grouped as follows, with the solution number given at the bottom of the graph

Restricting parameters T_1 and T_2 to positive values reduces the solutions to the following two combinations

$$\overline{T_1}$$

$$T_1 \qquad\qquad T_2$$

$$\overline{T_2} \to T_2 \qquad\qquad \overline{T_2} \to T_1$$

$$\overline{R_h} \to R_h \qquad\qquad \overline{R_h} \to 1 - R_h$$

B.2.3.2 ORC method

The ORC method used in this thesis is implemented in the MATLAB toolbox STRIKE-GOLDD v2.2 (https://sites.google.com/site/strikegolddtoolbox/). Here the model is defined as follows

```
% States
syms G X
x = [G; X];
% Inputs
syms I t;
u = [I; t];
% Unknown parameters
syms p1 p2 SI T1 T2 Rh
p =[p1; p2; SI; T1; T2; Rh];
% Output/observation
h = G;
% Initial Conditions
syms G0 X0
ics  = [G0; X0];
known_ics = [1,1];
% Model equations
Ra_R = (1-Rh)*t/T1^2*exp(-t^2/T1^2) + ...
Rh*t/T2^2*exp(-t^2/T2^2);
f = [-X*G - p1*G + Ra_R + exp(-t);
-p2*(X-SI*I)];
```

Here, we assume time to be a known input similar to the insulin concentration. As the toolbox does not allow the definition of known parameters, we had to assume specific values for known parameters, i.e. $I_b = 0$, $G_b = 0$, $V = 1$, $R_0 = 1$, $\alpha = 1$ and $A = 1$. The result is that all parameters are structurally locally identifiable, as demonstrated by the following output:

```
----------------------
>>> RESULTS SUMMARY:
```

```
-----------------------
>>> The model is Fully Input-State-Parameter Observable (FISPO):
    All its states are observable.
    All its parameters are locally structurally identifiable.
    Total execution time: 1.972068e+00
```

B.2.4 Formulation with Ra_{RLN} and Ra_{LN}

To apply the ORC method to the OMM with the input functions Ra_{RLN} and Ra_{LN}, a very similar code as presented in the previous section is used. The differences are the definitions the unknown parameters and input functions. For Ra_{RLN} we have

```
% Unknown parameters
syms p1 p2 SI T1 T2 W2 Rh
p =[p1; p2; SI; T1; T2; W2; Rh];
% Model equations
Ra_RLN = (1-Rh)*t/T1^2*exp(-t^2/T1^2) + ...
Rh/(t*sqrt(pi*W2))*exp(-(log(t/T2) - W2/2)^2/W2);
f = [-X*G - p1*G + Ra_RLN + exp(-t);
-p2*(X-SI*I)];
```

with the following output:

```
 -----------------------
>>> RESULTS SUMMARY:
-----------------------
>>> The model is Fully Input-State-Parameter Observable (FISPO):
    All its states are observable.
    All its parameters are locally structurally identifiable.
    Total execution time: 1.501507e+01
```

For Ra_{LN} we have

```
% Unknown parameters
syms p1 p2 SI T1 T2 W2 W2 Rh
p =[p1; p2; SI; T1; T2; W2; W2; Rh];
% Model equations
Ra_LN = (1-Rh)/(t*sqrt(pi*W1))*exp(-(log(t/T1) - W1/2)^2/W1) + ...
Rh/(t*sqrt(pi*W2))*exp(-(log(t/T2) - W2/2)^2/W2);
f = [-X*G - p1*G + Ra_LN + exp(-t);
-p2*(X-SI*I)];
```

with the following output:

```
-----------------------
>>> RESULTS SUMMARY:
```

```
-----------------------
>>> The model is Fully Input-State-Parameter Observable (FISPO):
    All its states are observable.
    All its parameters are locally structurally identifiable.
    Total execution time: 7.845058e+01
```

confirming the local structural identifiability of all parameters in both cases.

B.3 Glucose-only models

B.3.1 ORC method

As before, the MATLAB toolbox STRIKE-GOLDD v2.2 is used. Here the GOM using Z_{LIN} is defined as follows

```
% States
syms G X
x = [G; X];
% Inputs
syms t;
u = [t];
% Unknown parameters
syms p1 p2 SG T1 W1 T2 W2 Rh
p =[p1; p2; SG; T1; W1; T2; W2; Rh];
% Output/observation
h = G;
% Initial Conditions
syms G0 X0
ics  = [G0; X0];
known_ics = [1,1];
% Model equations
Ra_LN = (1-Rh)/(t*sqrt(pi*W1))*exp(-(log(t/T1) - W1/2)^2/W1) + ...
Rh/(t*sqrt(pi*W2))*exp(-(log(t/T2) - W2/2)^2/W2);
f = [-X*G - p1*G + Ra_LN + exp(-t);
-p2*(X-SG*G)];
```

As the toolbox does not allow the definition of known parameters, we had to assume specific values for known parameters, i.e. $G_b = 0$, $V = 1$, $R_0 = 1$, $\alpha = 1$ and $A = 1$. The result is that all parameters are structurally locally identifiable, as demonstrated by the following output:

```
-----------------------
>>> RESULTS SUMMARY:
```

```
-----------------------
>>> The model is Fully Input-State-Parameter Observable (FISPO):
    All its states are observable.
    All its parameters are locally structurally identifiable.
    Total execution time: 3.822747e+02
```

In the case of the GOM with Z_{LOG} the same code is used, except for defining the model as follows:

```
% Model equations
Ra_LN = (1-Rh)/(t*sqrt(pi*W1))*exp(-(log(t/T1) - W1/2)^2/W1) + ...
Rh/(t*sqrt(pi*W2))*exp(-(log(t/T2) - W2/2)^2/W2);
f = [-X*G - p1*(G) + Ra_LN + exp(-t);
-p2*(X-SG*log((exp(G)+1)/2))];
```

with the following result

```
-----------------------
>>> RESULTS SUMMARY:
-----------------------
>>> The model is Fully Input-State-Parameter Observable (FISPO):
    All its states are observable.
    All its parameters are locally structurally identifiable.
    Total execution time: 9.219956e+03
```

demonstrating the structural local identifiability of all parameters In the case of the GOM with Z_{POS} the model is defined as follows:

```
% Model equations
Ra_LN = (1-Rh)/(t*sqrt(pi*W1))*exp(-(log(t/T1) - W1/2)^2/W1) + ...
Rh/(t*sqrt(pi*W2))*exp(-(log(t/T2) - W2/2)^2/W2);
f = [-X*G - p1*(G) + Ra_LN + exp(-t);
-p2*(X-SG*G/(1+exp(-2*G)))];
```

with the following result

```
-----------------------
>>> RESULTS SUMMARY:
-----------------------
>>> The model is Fully Input-State-Parameter Observable (FISPO):
    All its states are observable.
    All its parameters are locally structurally identifiable.
    Total execution time: 6.725713e+03
```

demonstrating the structural local identifiability of all parameters

B.3.2 Taylor series method

For the identifiability analysis using the Taylor series method, the general glucose-only models are formulated as follows

$$\frac{dG(t)}{dt} = -G(t)X(t) - p_1[G(t) - G_b] + \frac{Ra(t) + Rap(t)}{V}, \qquad G(0) = G_0,$$

$$\frac{dX(t)}{dt} = -p_2(X(t) - S_G Z(t, G_b)), \qquad X(0) = X_0,$$

$$Ra(t) = k \cdot t,$$

$$Rap(t) = R_0 \exp(-\alpha t),$$

where the function Z can take one of the following forms

$$Z_{LIN} = G(t) - G_b,$$

$$Z_{LOG} = \log\left[\frac{\exp(G(t) - G_b) + \beta}{\beta + 1}\right],$$

$$Z_{POS} = \frac{G(t) - G_b}{1 + \exp[-\gamma(G(t) - G_b)]}.$$

The model equations are defined as follows

```
In[9]:=  (* Model equations *)
         Ra[t] = k*t;
         Rap[t] = R0*Exp[-α t]
         G'[t] = -G[t]*X[t] - p1*(G[t] - Gb) + (Ra[t] + Rap[t])/V;
         X'[t] = -p2*(X[t] - SG*Z);
         (* Initial conditions *)
         G[0] = G0; X[0] = X0;
         (* Observation *)
         y[t] = G[t];
```

with the formulations of Z

```
In[10]:=  ZLIN = G[t] - Gb;
          ZLOG = Log[(Exp[G[t] - Gb] + β)/(β+ 1)];
          ZPOS = (G[t] - Gb)/(1 + Exp[-γ*(G[t] - Gb)]);
```

For the case of Z_{LIN}, the following substitutions and unknown parameters to solve for are defined

```
In[11]:=  subst = {p1 → p1b, p2 → p2b, SG → SGb, k → kb};
          sol = {p1b, p2b, SGb, kb};
```

Using six Taylor coefficients and the code in section B.1 the following solution is obtained

```
Out[11]= p1b → p1, p2b → p2, SGb → SG, kb → k
```

demonstrating the global identifiability of the considered parameters.

For the case of Z_{LOG} and Z_{POS}, the following substitutions and unknown parameters to solve for are defined, assuming the knowledge of k

```
In[12]:= subst = {p1 → p1b, p2 → p2b, SG → SGb};

        sol = {p1b, p2b, SGb};
```

Using four Taylor coefficients and the code in section B.1 the following solution is obtained

```
Out[12]= p1b → p1, p2b → p2, SGb → SG
```

demonstrating the global identifiability of the considered parameters. Using the exact same substitutions and number of Taylor coefficients, the same results are obtained for the case of Z_{POS}.

Appendix C

Model formulation in the VB toolbox

C.1 Oral minimal model

C.1.1 Formulation in Chapter 4

Within the context of the VB scheme, the oral minimal model (OMM) using the piecewise-linear input Ra_{PL} is formulated as follows in Chapter 4 to suit the Nuttall dataset. This includes the replacement of the time of breakpoints $t_0 - t_7$ with the chosen values 0, 10, 30, 60, 90, 120, 180 and 240 min, respectively

$$\frac{dG(t)}{dt} = -G(t)X(t) - e^{\theta_1}[G(t) - G_b] + \frac{Ra_{PL}(t) + Rap(t)}{V}, \quad G(0) = G_0, \quad \text{(C.1)}$$

$$\frac{dX(t)}{dt} = -e^{\theta_2}(X(t) - e^{\theta_3}[I(t) - I_b]), \quad X(0) = X_0, \quad \text{(C.2)}$$

$$Ra_{PL}(t) = \begin{cases} \frac{e^{\theta_4}}{10}t & \text{for } 0 \leq t \leq 10 \\ e^{\theta_4} + \frac{e^{\theta_5}-e^{\theta_4}}{20}(t-10) & \text{for } 10 \leq t \leq 30 \\ e^{\theta_5} + \frac{e^{\theta_6}-e^{\theta_5}}{30}(t-30) & \text{for } 30 \leq t \leq 60 \\ e^{\theta_6} + \frac{e^{\theta_7}-e^{\theta_6}}{30}(t-60) & \text{for } 60 \leq t \leq 90 \\ e^{\theta_7} + \frac{e^{\theta_8}-e^{\theta_7}}{30}(t-90) & \text{for } 90 \leq t \leq 120 \\ e^{\theta_8} + \frac{s-e^{\theta_8}}{60}(t-120) & \text{for } 120 \leq t \leq 180 \\ s + \frac{e^{\theta_9}-s}{60}(t-180) & \text{for } 180 \leq t \leq 240 \\ e^{\theta_9}\exp(-\alpha(t-240)) & \text{for } t > 240 \end{cases}$$

$$Rap(t) = R_0 \exp(-\alpha t).$$

The model states are $\{G(t), X(t)\}$. The toolbox parameters $\theta_1 - \theta_9$ are normally distributed and mapped to the log-normally distributed model parameters $p_1, p_2, S_I,$ k_1, k_2, k_3, k_4, k_5 and k_7 via the exponential function as explained in section 3.3.2.2. The variable s replaces the breakpoint at 180 min with the following expression

$$s = \frac{1}{60\alpha}[D \cdot f \cdot \alpha - e^{\theta_9} - 5\alpha \cdot (3e^{\theta_4} + 5e^{\theta_5} + 6e^{\theta_6} + 6e^{\theta_7} + 9e^{\theta_8} + 6e^{\theta_9})]$$

The details of the prior distributions are provided in Table C.1.

Table C.1: Prior values of model parameters and corresponding toolbox parameters

Model parameter	Median	CV [%]	Toolbox parameter	Mean	Variance
p_1	0.025	[25, 50, 100]	θ_1	$\log(0.025)$	$\log(CV^2+1)$
p_2	0.012	40	θ_2	$\log(0.012)$	$\log(0.4^2+1)$
S_I	$7.1{\cdot}10^{-4}$	100	θ_3	$\log(7.1\cdot10^{-4})$	$\log(1^2+1)$
k_1	$3.2{\cdot}10^{-3}A$	50	θ_4	$\log(3.2\cdot10^{-3}A)$	$\log(0.5^2+1)$
k_2	$7.3{\cdot}10^{-3}A$	50	θ_5	$\log(7.3\cdot10^{-3}A)$	$\log(0.5^2+1)$
k_3	$5.4{\cdot}10^{-3}A$	50	θ_6	$\log(5.4\cdot10^{-3}A)$	$\log(0.5^2+1)$
k_4	$5.1{\cdot}10^{-3}A$	50	θ_7	$\log(5.1\cdot10^{-3}A)$	$\log(0.5^2+1)$
k_5	$3.7{\cdot}10^{-3}A$	50	θ_8	$\log(3.7\cdot10^{-3}A)$	$\log(0.5^2+1)$
k_7	$1.8{\cdot}10^{-3}A$	50	θ_9	$\log(1.8\cdot10^{-3}A)$	$\log(0.5^2+1)$

As explained in section 3.3.2.2, the VB toolbox requires the specification of the model sensitivity, i.e. the derivatives of the model equations with respect to the states and parameters. The derivatives of model equations with respect to the model states $\{G(t), X(t)\}$ are as follows

$$\frac{d}{dG(t)}\left(\frac{dG(t)}{dt}\right) = -e^{\theta_1} - X(t) \quad \frac{d}{dX(t)}\left(\frac{dG(t)}{dt}\right) = -G(t)$$

$$\frac{d}{dG(t)}\left(\frac{dX(t)}{dt}\right) = 0 \qquad\qquad \frac{d}{dX(t)}\left(\frac{dX(t)}{dt}\right) = -e^{\theta_2} \tag{C.3}$$

The sensitivity equations with respect to the model parameters $\theta_1 - \theta_9$ are as follows

$$\frac{d}{d\theta_1}\left(\frac{dG(t)}{dt}\right) = -e^{\theta_1}(G(t) - G_b) \quad \frac{d}{d\theta_1}\left(\frac{dX(t)}{dt}\right) = 0$$

$$\frac{d}{d\theta_2}\left(\frac{dG(t)}{dt}\right) = 0 \qquad\qquad \frac{d}{d\theta_2}\left(\frac{dX(t)}{dt}\right) = -e^{\theta_2}(X(t) - e^{\theta_3}[I(t) - I_b]) \tag{C.4}$$

$$\frac{d}{d\theta_3}\left(\frac{dG(t)}{dt}\right) = 0 \qquad\qquad \frac{d}{d\theta_3}\left(\frac{dX(t)}{dt}\right) = e^{\theta_2+\theta_3}[I(t) - I_b]$$

$$\frac{d}{d\theta_4}\left(\frac{dG(t)}{dt}\right) = \begin{cases} \frac{e^{\theta_4}}{10V} & \text{for } 0 \leq t \leq 10 \\[2ex] -\frac{e^{\theta_4}(t-30)}{20V} & \text{for } 10 \leq t \leq 30 \\[2ex] 0 & \text{for } 30 \leq t \leq 120 \\[2ex] -\frac{e^{\theta_4}(t-120)}{240V} & \text{for } 120 \leq t \leq 180 \\[2ex] \frac{e^{\theta_4}(t-240)}{240V} & \text{for } 180 \leq t \leq 240 \end{cases} \qquad \frac{d}{d\theta_4}\left(\frac{dX(t)}{dt}\right) = 0$$

$$\frac{d}{d\theta_5}\left(\frac{dG(t)}{dt}\right) = \begin{cases} 0 & \text{for } 0 \leq t \leq 10 \\[2ex] \frac{e^{\theta_5}(t-10)}{20V} & \text{for } 10 \leq t \leq 30 \\[2ex] -\frac{e^{\theta_5}(t-60)}{30V} & \text{for } 30 \leq t \leq 60 \\[2ex] 0 & \text{for } 60 \leq t \leq 120 \\[2ex] -\frac{e^{\theta_5}(t-120)}{144V} & \text{for } 120 \leq t \leq 180 \\[2ex] \frac{e^{\theta_5}(t-240)}{144V} & \text{for } 180 \leq t \leq 240 \end{cases} \qquad \frac{d}{d\theta_5}\left(\frac{dX(t)}{dt}\right) = 0$$

$$
\frac{d}{d\theta_6}\left(\frac{dG(t)}{dt}\right) = \begin{cases} 0 & \text{for } 0 \le t \le 30 \\[2mm] \frac{e^{\theta_6}(t-30)}{30V} & \text{for } 30 \le t \le 60 \\[2mm] -\frac{e^{\theta_6}(t-90)}{30V} & \text{for } 60 \le t \le 90 \\[2mm] 0 & \text{for } 90 \le t \le 120 \\[2mm] -\frac{e^{\theta_6}(t-120)}{120V} & \text{for } 120 \le t \le 180 \\[2mm] \frac{e^{\theta_6}(t-240)}{120V} & \text{for } 180 \le t \le 240 \end{cases}
\qquad
\frac{d}{d\theta_6}\left(\frac{dX(t)}{dt}\right) = 0
$$

$$
\frac{d}{d\theta_7}\left(\frac{dG(t)}{dt}\right) = \begin{cases} 0 & \text{for } 0 \le t \le 60 \\[2mm] \frac{e^{\theta_7}(t-60)}{30V} & \text{for } 60 \le t \le 90 \\[2mm] -\frac{e^{\theta_7}(t-120)}{30V} & \text{for } 90 \le t \le 120 \\[2mm] -\frac{e^{\theta_7}(t-120)}{120V} & \text{for } 120 \le t \le 180 \\[2mm] \frac{e^{\theta_7}(t-240)}{120V} & \text{for } 180 \le t \le 240 \end{cases}
\qquad
\frac{d}{d\theta_7}\left(\frac{dX(t)}{dt}\right) = 0
$$

$$
\frac{d}{d\theta_8}\left(\frac{dG(t)}{dt}\right) = \begin{cases} 0 & \text{for } 0 \le t \le 90 \\[2mm] \frac{e^{\theta_8}(t-90)}{30V} & \text{for } 90 \le t \le 120 \\[2mm] \frac{e^{\theta_8}(7t-1080)}{240V} & \text{for } 120 \le t \le 180 \\[2mm] \frac{e^{\theta_8}(t-240)}{80V} & \text{for } 180 \le t \le 240 \end{cases}
\qquad
\frac{d}{d\theta_8}\left(\frac{dX(t)}{dt}\right) = 0
$$

$$
\frac{d}{d\theta_9}\left(\frac{dG(t)}{dt}\right) = \begin{cases} 0 & \text{for } 0 \le t \le 120 \\[2mm] -\frac{(1+30\alpha)e^{\theta_9}(t-120)}{3600\alpha V} & \text{for } 120 \le t \le 180 \\[2mm] \frac{e^{\theta_9}(t-240+90\alpha(t-200))}{3600\alpha V} & \text{for } 180 \le t \le 240 \end{cases}
\qquad
\frac{d}{d\theta_9}\left(\frac{dX(t)}{dt}\right) = 0
$$

C.1.2   Formulation in Chapter 8

In Chapter 8 the OMM is formulated differently due to the reduced number of break-points in the piecewise linear input function Ra_{PL}. Replacing the time of breakpoints $t_0 - t_4$ with the chosen values 0, 10, 30, 60 and 120, the following equations are used

$$
\frac{dG(t)}{dt} = -G(t)X(t) - e^{\theta_1}[G(t) - G_b] + \frac{Ra_{PL}(t)}{V}, \qquad\qquad G(0) = G_b,
$$
$$
\frac{dX(t)}{dt} = -e^{\theta_2}(X(t) - e^{\theta_3}[I(t) - I_b]), \qquad\qquad X(0) = 0,
$$

$$Ra_{PL}(t) = \begin{cases} \frac{e^{\theta_4}}{10}t & \text{for } 0 \leq t \leq 10 \\[2ex] e^{\theta_4} + \frac{e^{\theta_5} - e^{\theta_4}}{20}(t - 10) & \text{for } 10 \leq t \leq 30 \\[2ex] e^{\theta_5} + \frac{e^{\theta_6} - e^{\theta_5}}{30}(t - 30) & \text{for } 30 \leq t \leq 60 \\[2ex] e^{\theta_6} + \frac{s - e^{\theta_6}}{30}(t - 60) & \text{for } 60 \leq t \leq 120 \\[2ex] s\exp(-\alpha(t - 120)) & \text{for } t > 120 \end{cases}$$

The model states are again $\{G(t), X(t)\}$ and the toolbox parameters $\theta_1 - \theta_6$ are normally distributed and mapped to the log-normally distributed model parameters p_1, p_2, S_I, k_1, k_2 and k_3 via the exponential mapping. The variable s replaces the breakpoint at 120 min with the following expression

$$s = \frac{\alpha\left(D \cdot f - 5\left(3e^{\theta_4} + 5e^{\theta_5} + 9e^{\theta_6}\right)\right)}{1 + 30\alpha} \tag{C.5}$$

The prior values given in Table C.1 are unchanged and so are the sensitivity equations with respect to the states $\{G(t), X(t)\}$ and system parameters $\theta_1 - \theta_3$ given in (C.3) and (C.4). However, the sensitivity equations with respect to the input function parameters $\theta_4 - \theta_6$ are changed as follows

$$\frac{d}{d\theta_4}\left(\frac{dG(t)}{dt}\right) = \begin{cases} \frac{e^{\theta_4}}{10V} & \text{for } 0 \leq t \leq 10 \\[2ex] -\frac{e^{\theta_4}(t-30)}{20V} & \text{for } 10 \leq t \leq 30 \\[2ex] 0 & \text{for } 30 \leq t \leq 60 \\[2ex] \frac{\alpha e^{\theta_4}(t-60)}{4V(1+30\alpha)} & \text{for } 60 \leq t \leq 120 \end{cases} \qquad \frac{d}{d\theta_4}\left(\frac{dX(t)}{dt}\right) = 0$$

$$\frac{d}{d\theta_5}\left(\frac{dG(t)}{dt}\right) = \begin{cases} 0 & \text{for } 0 \leq t \leq 10 \\[2ex] \frac{e^{\theta_5}(t-10)}{20V} & \text{for } 10 \leq t \leq 30 \\[2ex] -\frac{e^{\theta_5}(t-60)}{30V} & \text{for } 30 \leq t \leq 60 \\[2ex] \frac{5\alpha e^{\theta_5}(t-60)}{12V(1+30\alpha)} & \text{for } 60 \leq t \leq 120 \end{cases} \qquad \frac{d}{d\theta_5}\left(\frac{dX(t)}{dt}\right) = 0$$

$$\frac{d}{d\theta_6}\left(\frac{dG(t)}{dt}\right) = \begin{cases} 0 & \text{for } 0 \le t \le 30 \\ \frac{e^{\theta_6}(t-30)}{30V} & \text{for } 30 \le t \le 60 \\ \frac{e^{\theta_6}(120-t+15\alpha(t+60))}{60V(1+30\alpha)} & \text{for } 60 \le t \le 120 \end{cases} \qquad \frac{d}{d\theta_6}\left(\frac{dX(t)}{dt}\right) = 0$$

C.2 Oral minimal model with novel input functions

The implementation of new input functions within the VB toolbox in Chapter 5 uses model equations (C.1) and (C.2), meaning that sensitivity expressions (C.3) and (C.4) are identical as well. The differences with respect to the new input functions are presented in the sections below for the individual functions.

C.2.1 Function Ra_R

Within the VB toolbox, the proposed input function Ra_R takes the following form

$$Ra_R(t) = \underbrace{A\left(1 - \frac{1}{1+e^{-\theta_6}}\right)\frac{t}{e^{2\theta_4}}\exp\left(-\frac{t^2}{2e^{2\theta_4}}\right)}_{f_R^1} + \underbrace{A\frac{1}{1+e^{-\theta_6}}\frac{t}{e^{2\theta_5}}\exp\left(-\frac{t^2}{2e^{2\theta_5}}\right)}_{f_R^2}.$$

The parameters T_1, T_2, R_H are mapped to the normally distributed toolbox parameters $\theta_4 - \theta_6$. This leads to the prior distributions specified in Table C.2.

Table C.2: Prior values of model parameters and corresponding toolbox parameters

Model parameter	Median	CV [%]	Toolbox parameter	Mean	Variance
T_1	30	30	θ_4	$\log(30)$	$\log(0.3^2+1)$
T_2	100	30	θ_5	$\log(100)$	$\log(0.3^2+1)$
R_H	0.75	30	θ_6	$-\log\left(\frac{1}{0.75}-1\right)$	4

The sensitivity equations with respect to the parameters $\theta_4 - \theta_6$ are defined as follows

$$\frac{d}{d\theta_4}\left(\frac{dG(t)}{dt}\right) = \left[f_R^1\left(e^{-2\theta_4}t^2 - 2\right)\right]\frac{1}{V}$$

$$\frac{d}{d\theta_4}\left(\frac{dX(t)}{dt}\right) = 0$$

$$\frac{d}{d\theta_5}\left(\frac{dG(t)}{dt}\right) = \left[f_R^2\left(e^{-2\theta_5}t^2 - 2\right)\right]\frac{1}{V}$$

$$\frac{d}{d\theta_5}\left(\frac{dX(t)}{dt}\right) = 0$$

$$\frac{d}{d\theta_6}\left(\frac{dG(t)}{dt}\right) = \left[-A\frac{t}{e^{2\theta_4}}\exp\left(-\frac{t^2}{2e^{2\theta_4}}\right)\frac{e^{-\theta_6}}{(1+e^{-\theta_6})^2} + f_R^2\frac{e^{-\theta_6}}{1+e^{-\theta_6}}\right]\frac{1}{V}$$

$$\frac{d}{d\theta_6}\left(\frac{dX(t)}{dt}\right) = 0.$$

C.2.2 Function Ra_{RLN}

Within the VB toolbox, the proposed input function Ra_{RLN} takes the following form

$$Ra_{RLN}(t) = \underbrace{A\left(1 - \frac{1}{1+e^{-\theta_7}}\right)\frac{t}{e^{2\theta_4}}\exp\left(-\frac{t^2}{2e^{2\theta_4}}\right)}_{f_R^1}$$

$$+ \underbrace{A\frac{1}{1+e^{-\theta_7}}\frac{1}{t\sqrt{\pi e^{\theta_6}}}\exp\left(-\frac{\left[\log\frac{t}{e^{\theta_5}} - \frac{e^{\theta_6}}{2}\right]^2}{e^{\theta_6}}\right)}_{f_{LN}^2}.$$

The parameters T_1, T_2, W_1, R_H are mapped to the normally distributed toolbox parameters $\theta_4 - \theta_7$. This leads to the prior distributions specified in Table C.3.

Table C.3: Prior values of model parameters and corresponding toolbox parameters

Model parameter	Median	CV [%]	Toolbox parameter	Mean	Variance
T_1	30	30	θ_4	$\log(30)$	$\log(0.3^2 + 1)$
T_2	100	30	θ_5	$\log(100)$	$\log(0.3^2 + 1)$
W_1	0.5	30	θ_6	$\log(0.5)$	$\log(0.3^2 + 1)$
R_H	0.65	30	θ_7	$-\log\left(\frac{1}{0.65} - 1\right)$	1.3^2

The sensitivity equations with respect to the parameters $\theta_4 - \theta_7$ are defined as follows

$$\frac{d}{d\theta_4}\left(\frac{dG(t)}{dt}\right) = \left[f_R^1\left(e^{-2\theta_4}t^2 - 2\right)\right]\frac{1}{V}$$

$$\frac{d}{d\theta_4}\left(\frac{dX(t)}{dt}\right) = 0$$

$$\frac{d}{d\theta_5}\left(\frac{dG(t)}{dt}\right) = \left[2f_{LN}^2 e^{-\theta_6}\left(\frac{-e^{-\theta_6}}{2} + \log\frac{t}{e^{\theta_5}}\right)\right]\frac{1}{V}$$

$$\frac{d}{d\theta_5}\left(\frac{dX(t)}{dt}\right) = 0$$

$$\frac{d}{d\theta_6}\left(\frac{dG(t)}{dt}\right) = \left[f_{LN}^2\left(-\frac{e^{\theta_6}}{2} + \log\frac{t}{e^{\theta_5}} + e^{-\theta_6}\left(-\frac{e^{\theta_6}}{2} + \log\frac{t}{e^{\theta_5}}\right)^2\right) - \frac{f_{LN}^2}{2}\right]\frac{1}{V}$$

$$\frac{d}{d\theta_6}\left(\frac{dX(t)}{dt}\right) = 0$$

$$\frac{d}{d\theta_7}\left(\frac{dG(t)}{dt}\right) = \left[-A\frac{t}{e^{2\theta_4}}\exp\left(-\frac{t^2}{2e^{2\theta_4}}\right)\frac{e^{-\theta_7}}{(1+e^{-\theta_7})^2} + f_R^2\frac{e^{-\theta_7}}{1+e^{-\theta_7}}\right]\frac{1}{V}$$

$$\frac{d}{d\theta_7}\left(\frac{dX(t)}{dt}\right) = 0.$$

C.2.3 Function Ra_{LN}

Within the VB toolbox, the proposed input function Ra_{LN} takes the following form

$$Ra_{LN}(t) = A\underbrace{\left(1 - \frac{1}{1+e^{-\theta_8}}\right)\frac{1}{t\sqrt{\pi e^{\theta_5}}}\exp\left(-\frac{\left[\log\frac{t}{e^{\theta_4}} - \frac{e^{\theta_5}}{2}\right]^2}{e^{\theta_5}}\right)}_{f_{LN}^1}$$

$$+ A\underbrace{\frac{1}{1+e^{-\theta_8}}\frac{1}{t\sqrt{\pi e^{\theta_7}}}\exp\left(-\frac{\left[\log\frac{t}{e^{\theta_6}} - \frac{e^{\theta_7}}{2}\right]^2}{e^{\theta_7}}\right)}_{f_{LN}^2}$$

The parameters T_1, T_2, W_1, W_2, R_H are mapped to the normally distributed toolbox parameters $\theta_4 - \theta_8$. his leads to the prior distributions specified in Table C.4.

Table C.4: Prior values of model parameters and corresponding toolbox parameters

Model parameter	Median	CV [%]	Toolbox parameter	Mean	Variance
T_1	30	30	θ_4	$\log(30)$	$\log(0.3^2+1)$
W_1	0.5	30	θ_5	$\log(0.5)$	$\log(0.3^2+1)$
T_2	100	30	θ_6	$\log(100)$	$\log(0.3^2+1)$
W_2	0.5	30	θ_7	$\log(0.5)$	$\log(0.3^2+1)$
R_H	0.7	30	θ_8	$-\log\left(\frac{1}{0.7}-1\right)$	1.6^2

The sensitivity equations with respect to the parameters $\theta_4 - \theta_8$ are defined as follows

$$\frac{d}{d\theta_4}\left(\frac{dG(t)}{dt}\right) = \left[2f_{LN}^1 e^{-\theta_5}\left(\frac{-e^{-\theta_5}}{2} + \log\frac{t}{e^{\theta_4}}\right)\right]\frac{1}{V}$$

$$\frac{d}{d\theta_4}\left(\frac{dX(t)}{dt}\right) = 0$$

$$\frac{d}{d\theta_5}\left(\frac{dG(t)}{dt}\right) = \left[f_{LN}^1\left(-\frac{e^{\theta_5}}{2} + \log\frac{t}{e^{\theta_4}} + e^{-\theta_5}\left(-\frac{e^{\theta_5}}{2} + \log\frac{t}{e^{\theta_4}}\right)^2\right) - \frac{f_{LN}^1}{2}\right]\frac{1}{V}$$

$$\frac{d}{d\theta_5}\left(\frac{dX(t)}{dt}\right) = 0$$

$$\frac{d}{d\theta_6}\left(\frac{dG(t)}{dt}\right) = \left[2f_{LN}^2 e^{-\theta_7}\left(\frac{-e^{-\theta_7}}{2} + \log\frac{t}{e^{\theta_6}}\right)\right]\frac{1}{V}$$

$$\frac{d}{d\theta_6}\left(\frac{dX(t)}{dt}\right) = 0$$

$$\frac{d}{d\theta_7}\left(\frac{dG(t)}{dt}\right) = \left[f_{LN}^2\left(-\frac{e^{\theta_7}}{2} + \log\frac{t}{e^{\theta_6}} + e^{-\theta_7}\left(-\frac{e^{\theta_7}}{2} + \log\frac{t}{e^{\theta_6}}\right)^2\right) - \frac{f_{LN}^2}{2}\right]\frac{1}{V}$$

$$\frac{d}{d\theta_7}\left(\frac{dX(t)}{dt}\right) = 0$$

$$\frac{d}{d\theta_8}\left(\frac{dG(t)}{dt}\right) = \left[-A\frac{1}{t\sqrt{\pi e^{\theta_5}}}\exp\left(-\frac{\left[\log\frac{t}{e^{\theta_4}} - \frac{e^{\theta_5}}{2}\right]^2}{e^{\theta_5}}\right)\frac{e^{-\theta_8}}{(1+e^{-\theta_8})^2} + f_{LN}^2\frac{e^{-\theta_8}}{1+e^{-\theta_8}}\right]\frac{1}{V}$$

$$\frac{d}{d\theta_8}\left(\frac{dX(t)}{dt}\right) = 0.$$

C.3 Glucose-only models

The glucose-only models are defined as follows within the VB toolbox

$$\frac{dG(t)}{dt} = -G(t)X(t) - e^{\theta_1}[G(t) - G_b] + \frac{Ra_{LN}(t) + Ra_P(t)}{V}, \qquad G(0) = G_0,$$

$$\frac{dX(t)}{dt} = -e^{\theta_2}(X(t) - e^{\theta_3}Z(t, G(t))), \qquad X(0) = X_0,$$

$$Ra_{LN}(t) = A\left(1 - \frac{1}{1 + e^{-\theta_8}}\right)\frac{1}{t\sqrt{\pi e^{\theta_5}}}\exp\left(-\frac{\left[\log\frac{t}{e^{\theta_4}} - \frac{e^{\theta_5}}{2}\right]^2}{e^{\theta_5}}\right)$$

$$+ A\frac{1}{1 + e^{-\theta_8}}\frac{1}{t\sqrt{\pi e^{\theta_7}}}\exp\left(-\frac{\left[\log\frac{t}{e^{\theta_6}} - \frac{e^{\theta_7}}{2}\right]^2}{e^{\theta_7}}\right)$$

The system parameters p_1, p_2 and S_G are mapped to the normally distributed toolbox parameters $\theta_1 - \theta_3$. Their prior distributions specified in Table C.5. Regarding the input function parameters $\theta_4 - \theta_8$, the priors and sensitivity equations provided in section C.2.3 remain unchanged.

Table C.5: Prior values of model parameters and corresponding toolbox parameters

Model parameter	Median	CV [%]	Toolbox parameter	Mean	Variance
p_1	0.025	25	θ_1	$\log(0.025)$	$\log(0.25^2 + 1)$
p_2	0.012	40	θ_2	$\log(0.012)$	$\log(0.4^2 + 1)$
S_G	0.05	50	θ_3	$\log(0.05)$	$\log(0.5^2 + 1)$

The function Z is described with three different forms Z_{LIN}, Z_{LOG} and Z_{POS} specified in Table 6.1. Irrespective of the chosen formulation of Z, the derivatives of the model equations with respect to parameters $\theta_1 - \theta_3$ are as follows

$$\frac{d}{d\theta_1}\left(\frac{dG(t)}{dt}\right) = -e^{\theta_1}(G(t) - G_b) \qquad \frac{d}{d\theta_1}\left(\frac{dX(t)}{dt}\right) = 0$$

$$\frac{d}{d\theta_2}\left(\frac{dG(t)}{dt}\right) = 0 \qquad \frac{d}{d\theta_2}\left(\frac{dX(t)}{dt}\right) = -e^{\theta_2}(X(t) - e^{\theta_3}Z(t, G(t)))$$

$$\frac{d}{d\theta_3}\left(\frac{dG(t)}{dt}\right) = 0 \qquad \frac{d}{d\theta_3}\left(\frac{dX(t)}{dt}\right) = e^{\theta_2 + \theta_3}Z(t, G(t))$$

For the case of Z_{LIN} the derivatives of the model equations with respect to the states

$\{G(t), X(t)\}$ are as follows

$$\frac{d}{dG(t)}\left(\frac{dG(t)}{dt}\right) = -e^{\theta_1} - X(t) \quad \frac{d}{dX(t)}\left(\frac{dG(t)}{dt}\right) = -G(t)$$

$$\frac{d}{dG(t)}\left(\frac{dX(t)}{dt}\right) = e^{\theta_2+\theta_3} \quad \frac{d}{dX(t)}\left(\frac{dX(t)}{dt}\right) = -e^{\theta_2}$$

For the case of Z_{LOG} the derivative of $dX(t)/dt$ with respect to $G(t)$ changes as follows

$$\frac{d}{dG(t)}\left(\frac{dX(t)}{dt}\right) = \frac{e^{\theta_2+\theta_3+G(t)}}{e^{G(t)} + e^{G_b}\beta}$$

For the case of Z_{POS} the derivative of $dX(t)/dt$ with respect to $G(t)$ changes as follows

$$\frac{d}{dG(t)}\left(\frac{dX(t)}{dt}\right) = \frac{e^{\theta_2+\theta_3+\gamma(G(t)-G_b)}(1 + e^{\gamma(G(t)-G_b)} + \gamma(G(t) - G_b))}{(1 + e^{\gamma(G(t)-G_b)})^2}$$

Appendix D

Additional information

D.1 Chapter 4

The results of inverting the OMM with different fixed values of V and f are provided in Figure D.1.
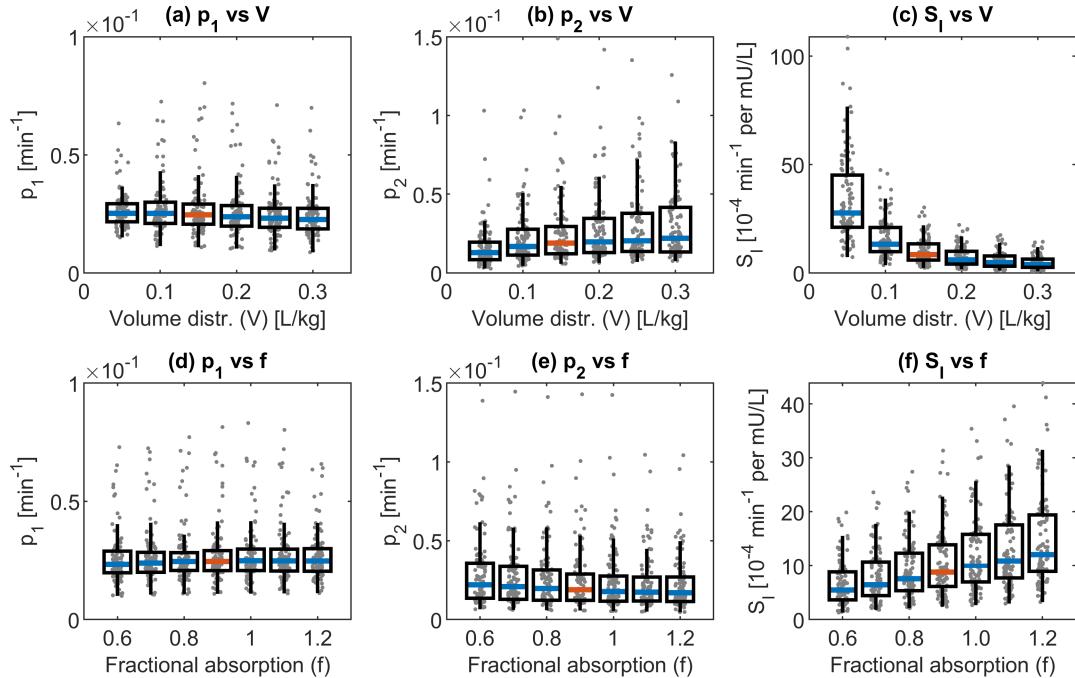
Figure D.1: Influence of inverting the OMM with different fixed values of the distribution Volume V (a)-(c) and fractional absorption f (d)-(f) on model parameters p_1, p_2 and S_I.

D.2   Chapter 5

In order to demonstrate the influence of the individual parameters of the OMM using Ra_R, Ra_{RLN} and Ra_{LN} and their prior distributions on the model output, several model simulations are carried out. Here, the value of one parameter at a time is varied across the two-sigma range of its prior distribution, while the other parameters are kept fixed at their prior medians. The results for the different models are given in Figures D.2 - D.4.
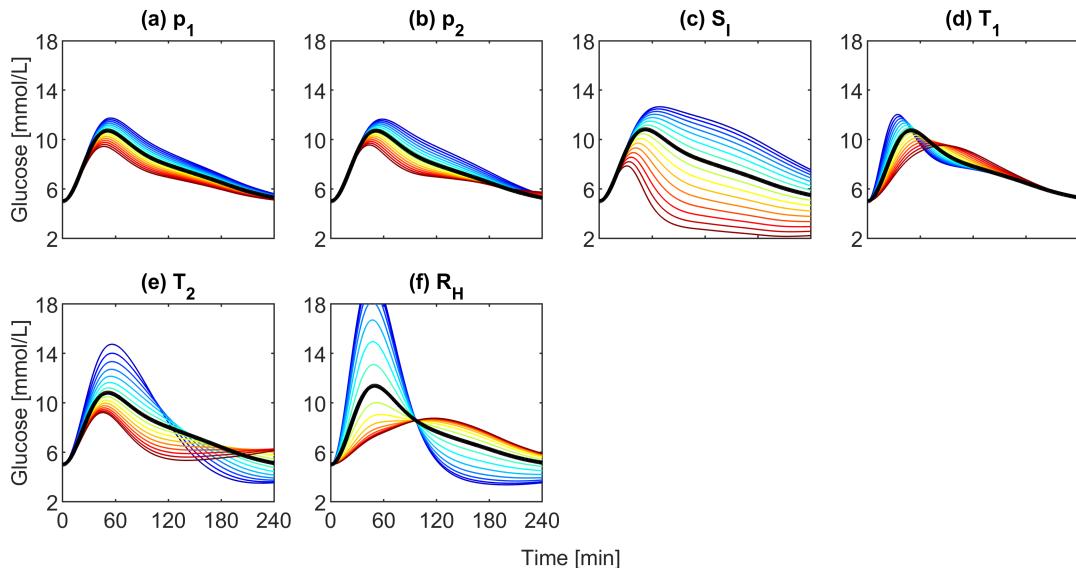
Figure D.2: Influence of individual model parameters on the model output of the OMM using Ra_R. The value of one parameter at a time is varied across the two-sigma range of its prior distribution, while the other parameters are kept fixed at their prior medians. The colours indicate increasing parameter values from blue to red. The black lines indicates the response from the prior median. As insulin input, the averaged insulin profile from the STAND meal was used.
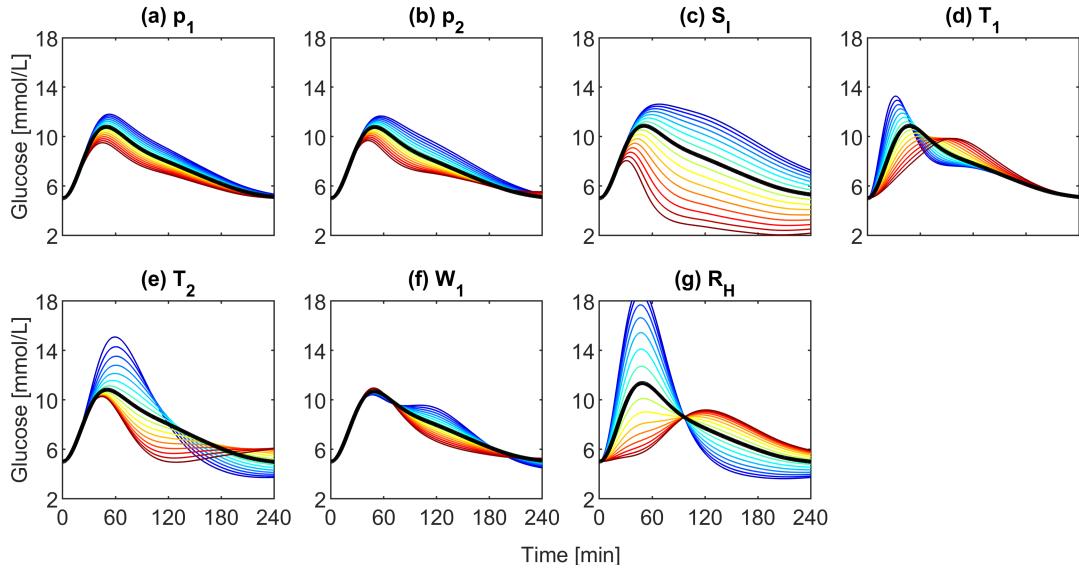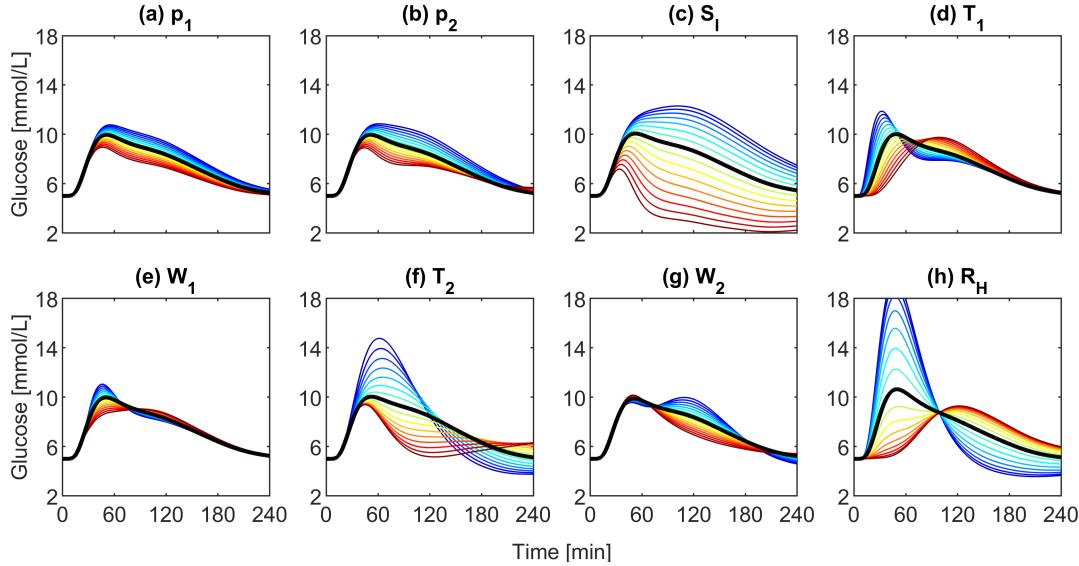
Figure D.3: Influence of individual model parameters on the model output of the OMM using Ra_{RLN}. The value of one parameter at a time is varied across the two-sigma range of its prior distribution, while the other parameters are kept fixed at their prior medians. The colours indicate increasing parameter values from blue to red. The black lines indicates the response from the prior median. As insulin input, the averaged insulin profile from the STAND meal was used.

Figure D.4: Influence of individual model parameters on the model output of the OMM using Ra_R. The value of one parameter at a time is varied across the two-sigma range of its prior distribution, while the other parameters are kept fixed at their prior medians. The colours indicate increasing parameter values from blue to red. The black lines indicates the response from the prior median. As insulin input, the averaged insulin profile from the STAND meal was used.

D.3 Chapter 5

D.3.1 Chen's model

Chen et al. [26] and is described by the following equations

$$\frac{dG(t)}{dt} = -f_1(G(t)) + f_2(G(t), I(t - \tau_1)) - S_I f_3(G(t), I(t)) + F(t), \qquad \text{(D.1)}$$

$$\frac{dI(t)}{dt} = -p_2 I(t) + p_3 f_4(G(t - \tau_2)). \qquad \text{(D.2)}$$

Functions f_1, f_2 and f_3 describe glucose effectiveness, hepatic glucose production and insulin-dependent glucose utilisation, respectively. The details are given in Table D.1

Table D.1: Details of functions f_1 - f_4 in Chen's model

Function	Expression	Description
$f_1(G(t))$	$U_b(1 - \exp(-\frac{G(t)}{c_2 V_g})) +$ $S_b + \dfrac{S_c - S_b}{1 + \exp(\delta(\frac{G(t)-330}{c_3 Vg} - c_7))}$	Insulin-independent glucose utilisation and hyperglycaemic effect
$f_2(G(t), I(t - \tau_1))$	$\dfrac{R_g}{1 + \exp(e_1(\frac{I(t)-\tau_1}{Vp} - c_5))} \times$ $\dfrac{1}{1 + \exp(\gamma(\frac{G(t)}{Vgc_3} - c_6))}$	Hepatic glucose production including a hyperglycaemic effect
$f_3(G(t), I(t))$	$\dfrac{G(t)}{V_g c_3} \times (U_0 +$ $\dfrac{U_c - U_0}{1 + \exp(-\kappa \log(\frac{I(t)}{c_4})(\frac{1}{V_c} + \frac{1}{Et_c}))})$	Hepatic glucose production including a hyperglycaemic effect
$f_4(G(t - \tau_2))$	$\dfrac{R_c}{1 + \exp(\frac{c_1}{e_1} - \frac{G(t)-\tau_2}{V_g e_1})}$	Delayed, glucose-dependant insulin production (sigmoidal shape)

D.4   Parameter influence

In order to demonstrate the influence of the individual parameters of the GOM using Z_{LIN}, Z_{LOG} and Z_{POS} and their prior distributions on the model output, several model simulations are carried out. Here, the value of one parameter at a time is varied across the two-sigma range of its prior distribution, while the other parameters are kept fixed at their prior medians. The results for the different models are given in Figures D.5 - D.6.
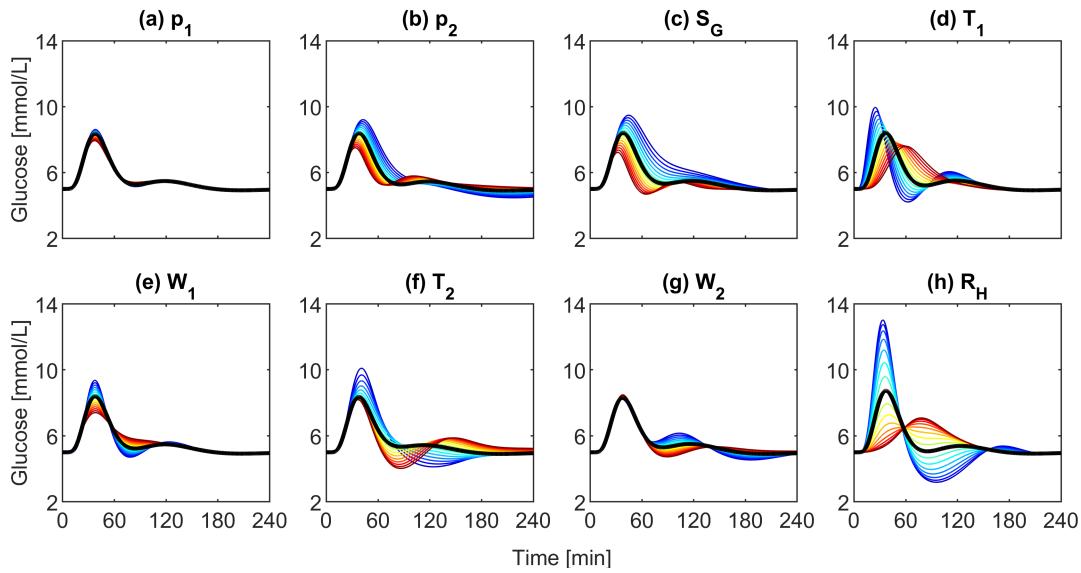

Figure D.5: Influence of individual model parameters on the model output of the the GOM using Z_{LIN}. The value of one parameter at a time is varied across the two-sigma range of its prior distribution, while the other parameters are kept fixed at their prior medians. The colours indicate increasing parameter values from blue to red. The black lines indicates the response from the prior median.
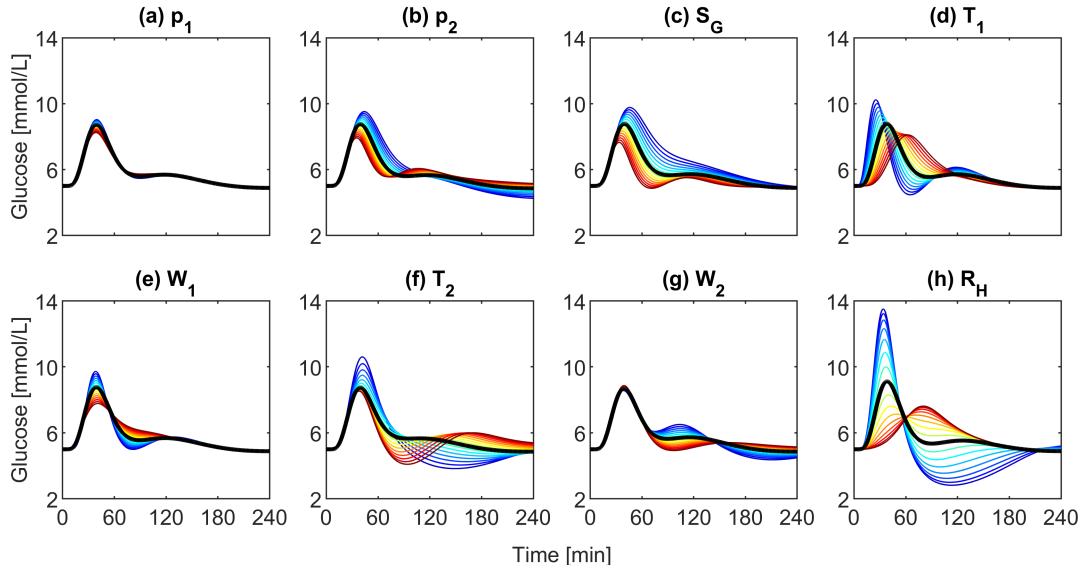
Figure D.6: Influence of individual model parameters on the model output of the the GOM using Z_{LOG}. The value of one parameter at a time is varied across the two-sigma range of its prior distribution, while the other parameters are kept fixed at their prior medians. The colours indicate increasing parameter values from blue to red. The black lines indicates the response from the prior median.
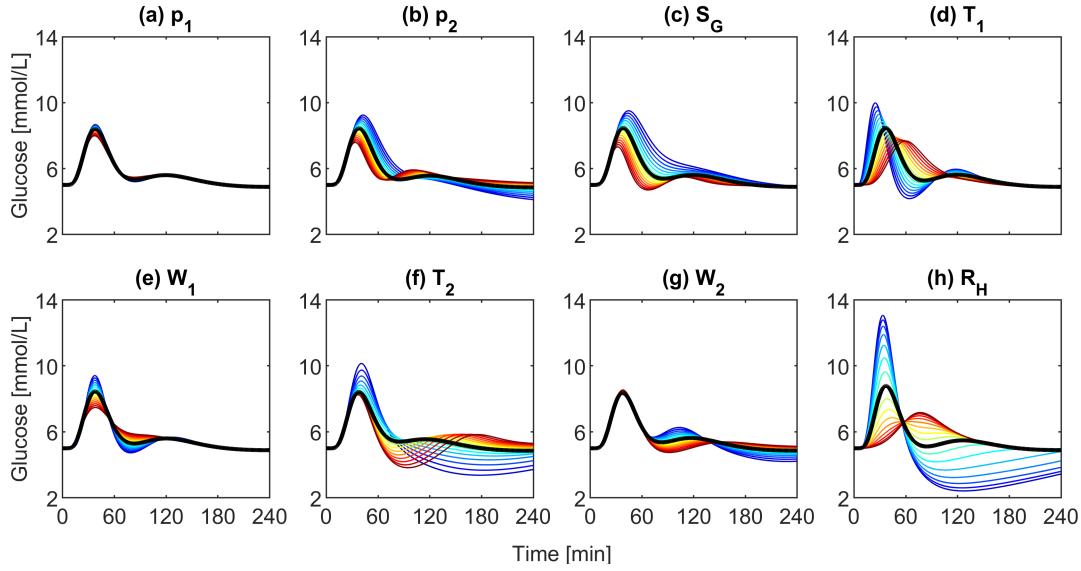

Figure D.7: Influence of individual model parameters on the model output of the the GOM using Z_{POS}. The value of one parameter at a time is varied across the two-sigma range of its prior distribution, while the other parameters are kept fixed at their prior medians. The colours indicate increasing parameter values from blue to red. The black lines indicates the response from the prior median.
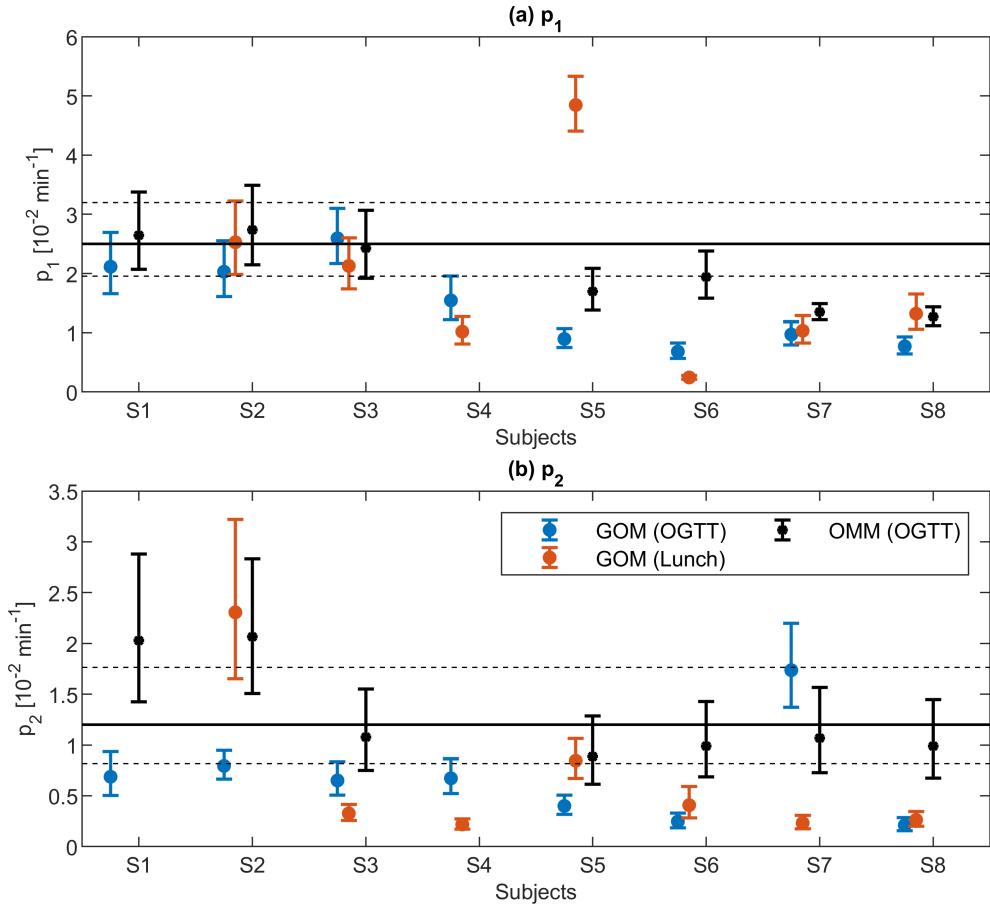
D.5 Chapter 7

Figure D.8: Comparison of the estimation results for (a) p_1 and (b) p_2 of the GOM estimated from the CGM data in comparison to the corresponding results of the OMM estimated from the blood sampling data. The results give the median and one-sigma range of the log-normal posterior distributions. In subject S1 no values are inferred during lunch due to missing data. In subject S4, S_I could not be estimated with the OMM due to missing data.